

$^{87}\text{SR}/^{86}\text{SR}$, CA/SR, AND GE/SI RATIOS AS TRACERS OF SOLUTE SOURCES AT A
TEMPERATE FORESTED, SHALE CATCHMENT IN CENTRAL PENNSYLVANIA

A Thesis

Presented to the Faculty of the Graduate School

of Cornell University

in Partial Fulfillment of the Requirements for the Degree of

Master of Science

by

Katherine Elaine Meek

January 2015

© 2015 Katherine Elaine Meek

ABSTRACT

Weathering processes, governed by dissolution kinetics as well as by the rates and directions of flowing water, are important mechanisms through which solutes are added to watersheds. Flow pathways control the fate and transport of incoming precipitation inputs and consequently, influence water-rock interactions, degrees of weathering, and distributions of solutes in watersheds. Furthermore, plants directly impact the availability of solutes in soil and porewater reservoirs through infiltration, evapotranspiration, decomposition, and preferential discrimination processes. To this end, strontium isotope ratios ($^{87}\text{Sr}/^{86}\text{Sr}$), elemental ratios (Ca/Sr, Ge/Si), and elemental concentrations are used to document sources of solutes at a temperate forested, shale catchment in central Pennsylvania. Spatio-temporal patterns are assessed and inferences are developed using empirical data supplemented by observations on mineral weathering, proposed preferential flow pathways, and plant transport mechanisms at the catchment. In particular, this study entails a comprehensive analysis of calcium, strontium, silicon, and germanium sources in plant leaves and sap waters and in streamwaters, groundwaters, soil porewaters, exchangeable soils, and bedrock in order to investigate hydrological (preferential flow pathways), topographical (hillslope geometry), biological (evapotranspiration, decomposition, and plant preferential discrimination), and mineralogical (dominant weathering inputs) controls on their availability and distribution at the watershed.

For soils and soil porewaters, spatial patterns in chemistry largely reflect lateral and vertical preferential flow processes which influence solute residence times and the transfer of weathering products either in the soil profile or to downslope locations. As such, topographic gradient plays a circumstantial role in lateral subsurface transport processes downslope. Furthermore, biological activities including plant preferential discrimination, decomposition, and

evapotranspiration impact near surface spatial patterns and in particular, temporal patterns in soil and soil porewater chemistry. Although solutes in soils and soil porewaters at ridge top and mid slope locations are largely derived from silicate mineral weathering, influences of carbonate dissolution processes on calcium and strontium are rather significant at valley floor locations where recharge of carbonate affected groundwaters is probable. Strontium isotope ratios in soil reservoirs correspond closely to those in leaves which is consistent with the rapid homogenization of solutes added from weathering and atmospheric sources by biological nutrient cycling processes. Controls on spatio-temporal patterns in leaf and sap water chemistry are predictably similar to those observed for soils and soil porewaters, from which these reservoir components are largely acquiring solutes. However, plant transport mechanisms through the xylem are also important where apoplastic passive transport is suggested for calcium and strontium, while a coexistence of active and passive transport mechanisms either through apoplastic or symplastic pathways is hypothesized for silicon and germanium. As to the site of elemental partitioning, minimal discrepancy between leaf and sap water Ge/Si ratios, where Ge/Si ratios for both are significantly lower than those for soil porewaters, suggests that partitioning between germanium and silicon precedes phytolith formation and occurs in the transport from the endodermal cell layer (and casparian strip) to the xylem stream either during plant uptake or soon thereafter. Conversely, Ca/Sr ratios in sap waters are shown to correspond more closely to those in soil porewaters with elemental partitioning occurring further down the transpiration stream as supported by observations of significantly higher Ca/Sr ratios in leaves compared to soil porewaters.

Groundwater and streamwater chemistry is largely governed by mineralogical processes. In groundwaters and weir streamwaters, carbonate dissolution processes are shown to be rather

important sources of calcium and strontium, while primary weathering of silicate minerals imparts influences on silicon and germanium chemistry. However, stream headwaters are ephemeral and highly responsive to inputs from atmospheric sources for calcium and strontium and to hydrological processes which add silicon and germanium to streamwaters through flushing by infiltrating precipitation of soil porewaters into streamwaters at these locations. Mid streamwaters integrate sources of solutes at weir and stream headwater locations. Diagenetic carbonates at the catchment are reflective of both ankerites and calcites with carbonates at the ridge and valley likely originating from different strata as a result of the heterogeneous lithology of the Rose Hill formation. The rate of carbonate propagation well exceeds those estimated for regolith production and erosion and is consistent with the greater depth inferred for the carbonate weathering front at the catchment. Strontium isotope ratios for silicate fractions of drill core samples suggest that bedrock is, indeed, shale and that calcium and strontium release through weathering is likely from leaching of less radiogenic feldspars at interlayer and adsorption sites of clay minerals. Furthermore, Ge/Si ratios for drill core samples agree to values for shale where silicon and germanium release through primary weathering of silicate minerals is supported by observations of lower Ge/Si ratios, relative to unweathered bedrock, in streamwaters, groundwaters, and soil porewaters unaffected by plant activities.

BIOGRAPHICAL SKETCH

Katherine Meek grew up in the River Oaks neighborhood of Houston, Texas where she attended River Oaks Baptist School and Episcopal High School. After graduating from high school, she attended Smith College in Northampton, Massachusetts where she majored in Chemistry.

Katherine graduated Magna Cum Laude from Smith College and is a member of Phi Beta Kappa, Sigma Xi, and the National Charity League. She has currently been working under the guidance of Professor Louis Derry in the Department of Earth and Atmospheric Sciences at Cornell University. After graduation, Katherine looks forward to using her critical thinking, problem solving, and communication skills to make a positive contribution to society.

I would like to dedicate this thesis to my family. To my parents, Charles and Susan, who have given me every opportunity I could ask for and have been supportive of me in all of my endeavors. And to my siblings, Ryan, Kevin, and Ann who have also been a constant source of support and guidance.

ACKNOWLEDGMENTS

First, I would like to thank Professor Louis Derry for his guidance and encouragement and for giving me the opportunity to learn and grow as a scientist over the past few years. I would also like to thank Professor Larry Cathles for serving on my committee and Professor Jed Sparks for his knowledge and insight on this project.

I would like to express gratitude to fellow graduate students. In particular, Gregg McElwee for his assistance with major element and germanium runs on the ICP-OES and ICP-MS, Ashley Tibbetts for her procedural advice on the TIMS, and Kyle Trostle for his help with general laboratory techniques and procedures.

I also greatly appreciate those who have assisted with field work or contributed to data contained within this thesis: Ashley Cross, John Pollak, Sonia Gregor, Elizabeth Herndon, Katie Gaines, Pamela Sullivan, Jennifer Williams, Susan Brantley, and numerous others. I would also like to thank the National Science Foundation and the Earth and Atmospheric Sciences Department at Cornell University whose financial contributions made this research possible.

Lastly and most importantly, I would like to thank my parents, Charles and Susan, and my siblings, Ryan, Kevin, and Ann for their support and guidance. I truly appreciate all of your advice and encouragement over the years.

TABLE OF CONTENTS

Biographical sketch.....	iii
Dedication.....	iv
Acknowledgements.....	v
Table of Contents.....	vi
List of Figures.....	viii
List of Tables.....	xv
Chapter One: Introduction.....	1
Background.....	1
Site Description.....	4
Objectives of each chapter.....	14
References.....	17
Chapter Two: $^{87}\text{Sr}/^{86}\text{Sr}$ and Ca/Sr ratios as tracers of solute sources at the Susquehanna Shale Hills Critical Zone Observatory.....	25
Introduction.....	25
Procedural methods.....	28
Data analysis methods.....	34
Results and discussion.....	49
Conclusions.....	155
References.....	170
Chapter Three: Ge/Si ratios as tracers of silicon sources at the Susquehanna Shale Hills Critical Zone Observatory.....	183
Introduction.....	183
Procedural and data analysis methods.....	187
Results and discussion.....	190
Conclusions.....	281

References.....	291
Chapter Four: Summary of completed work and potential future work at the Susquehanna Shale Hills Critical Zone Observatory.....	301
Introduction.....	301
Summary of completed work.....	301
Potential future work.....	315
References.....	319
Appendix: Supplementary Data Tables.....	324

LIST OF FIGURES

Figure 1.1 Map of Shavers Creek in relation to the Susquehanna River subbasins.....	9
Figure 1.2 Topographic map of the Susquehanna Shale Hills Critical Zone Observatory displaying sampling locations and soil types	10
Figure 1.3 The spatial distribution of dominant tree species at the Susquehanna Shale Hills Critical Zone Observatory.....	11
Figure 1.4 Topographic map of the Susquehanna Shale Hills Critical Zone Observatory displaying sampling locations and regolith thickness.....	12
Figure 1.5 Schematic diagram of hypothesized hillslope flow pathways at the Susquehanna Shale Hills Critical Zone Observatory.....	13
Figure 2.1 Depth versus $^{87}\text{Sr}/^{86}\text{Sr}$ ratio for southern quadrant ridge top, mid slope, and valley floor exchangeable soils and soil porewaters.....	62
Figure 2.2 Average $^{87}\text{Sr}/^{86}\text{Sr}$ ratios for atmospheric, shale, weathered shale, and carbonate end-members and for southern quadrant ridge top, mid slope, and valley floor exchangeable soils and soil porewaters, sugar maple, chestnut oak, and red oak leaves and sap waters, and groundwaters and streamwaters.....	63
Figure 2.3 Percentage of strontium derived from silicate weathering and atmospheric sources for southern quadrant ridge top and mid slope exchangeable soils and soil porewaters.....	64
Figure 2.4 Ternary plots showing relative proportions of strontium derived from atmospheric, carbonate weathering, and silicate weathering sources for southern quadrant valley floor exchangeable soils and soil porewaters.....	65
Figure 2.5 Soil exchangeable $^{87}\text{Sr}/^{86}\text{Sr}$ ratio versus soil porewater $^{87}\text{Sr}/^{86}\text{Sr}$ ratio for samples collected at similar locations and depths of the southern planar transect.....	66

Figure 2.6 Depth versus average Ca/Sr ratio for southern quadrant ridge top, mid slope, and valley floor exchangeable soils and soil porewaters.....73

Figure 2.7 Ca/Sr ratio as a function of depth for southern quadrant ridge top, mid slope, and valley floor soil porewaters.....74

Figure 2.8 Average Ca/Sr ratios for atmospheric, shale, weathered shale, and carbonate end-members and for southern quadrant ridge top, mid slope, and valley floor exchangeable soils and soil porewaters, sugar maple, chestnut oak, and red oak leaves and sap waters, and groundwaters and streamwaters.....75

Figure 2.9 Soil exchangeable Ca/Sr ratio versus soil porewater Ca/Sr ratio for samples collected at similar locations and depths of the southern planar transect.....76

Figure 2.10 Soil porewater $^{87}\text{Sr}/^{86}\text{Sr}$ ratio of month B versus soil porewater $^{87}\text{Sr}/^{86}\text{Sr}$ ratio of month A for individual porewaters sampled at identical sites and depths.....80

Figure 2.11 Box plots of Ca/Sr ratio for southern planar ridge top, mid slope, and valley floor soil porewaters over the course of the growing season.....81

Figure 2.12 Box plots of Ca/Sr ratio for south swale ridge top, mid slope, and valley floor soil porewaters over the course of the growing season.....82

Figure 2.13 Leaf $^{87}\text{Sr}/^{86}\text{Sr}$ ratio versus sap water $^{87}\text{Sr}/^{86}\text{Sr}$ ratio for samples collected from the same time and individual tree.....91

Figure 2.14 Percentage of strontium derived from silicate weathering and atmospheric sources for leaves and sap waters sampled at mid slope positions in northeastern, southeastern, northwestern, and southwestern quadrants in 2013.....92

Figure 2.15 Percentage of strontium derived from silicate weathering and atmospheric sources for leaves and sap waters sampled at ridge top, mid slope, and valley floor positions of the

northeastern quadrant in 2011.....	93
Figure 2.16 Box plots of Ca/Sr ratio based on sampling location for leaves sampled at mid slope positions in northeastern, southeastern, northwestern, and southwestern quadrants in 2013.....	101
Figure 2.17 Box plots of Ca/Sr ratio based on sampling location for leaves sampled at ridge top, mid slope, and valley floor positions of the northeastern quadrant in 2011.....	102
Figure 2.18 Box plots of Ca/Sr ratio based on sampling year for leaves sampled at mid slope positions of the northeastern quadrant in 2011 and 2013.....	103
Figure 2.19 Leaf $^{87}\text{Sr}/^{86}\text{Sr}$ ratio of month B versus leaf $^{87}\text{Sr}/^{86}\text{Sr}$ ratio of month A for individual leaves sampled from identical trees.....	107
Figure 2.20 Box plots of Ca/Sr ratio for leaves collected over the course of the growing season in 2013.....	108
Figure 2.21 Monthly average calcium and strontium concentrations for leaves sampled at mid slope positions in northeastern, southeastern, northwestern, and southwestern quadrants in 2013.....	109
Figure 2.22 Box plots of Ca/Sr ratio for soil porewaters and sugar maple, chestnut oak, and red oak sapwaters and leaves collected from mid slope positions of the southwestern and southeastern quadrants of the catchment.....	117
Figure 2.23 Box plots of Ca/Sr ratio based on sampling location for sap waters sampled at mid slope positions in northeastern, southeastern, northwestern, and southwestern quadrants.....	124
Figure 2.24 Sap water $^{87}\text{Sr}/^{86}\text{Sr}$ ratio of month B versus sap water $^{87}\text{Sr}/^{86}\text{Sr}$ ratio of month A for individual leaves sampled from identical trees.....	125
Figure 2.25 Box plots of Ca/Sr ratio for sap waters collected over the course of the growing season.....	126

Figure 2.26 Depth versus $^{87}\text{Sr}/^{86}\text{Sr}$ ratio for groundwaters and streamwaters.....132

Figure 2.27 Ternary cation plot for groundwaters and streamwaters.....133

Figure 2.28 Ternary plot depicting relative proportions of strontium derived from atmospheric, carbonate weathering, and silicate weathering sources in groundwaters and streamwaters.....134

Figure 2.29 Depth versus Ca/Sr ratio for groundwaters and streamwaters138

Figure 2.30 Depth versus $^{87}\text{Sr}/^{86}\text{Sr}$ ratio for carbonate and silicate fractions of DC 1 and DC 3 drill core samples.....152

Figure 2.31 Weight percent calcite and ankerite versus $^{87}\text{Sr}/^{86}\text{Sr}$ ratio for DC 1 and DC 3 drill core samples.....153

Figure 2.32 Depth versus Ca/Sr ratio for carbonate and silicate fractions of DC 1 and DC 3 drill core samples.....154

Figure 3.1 Silicon concentration as a function of depth for southern quadrant ridge top, mid slope, and valley floor soil porewaters.....202

Figure 3.2 Depth versus average silicon concentration for southern quadrant ridge top, mid slope, and valley floor soil porewaters.....203

Figure 3.3 Average silicon concentrations for southern quadrant ridge top, mid slope, and valley floor soil porewaters, sugar maple, chestnut oak, and red oak sap waters, and streamwaters and groundwaters.....204

Figure 3.4 Ge/Si ratio as a function of depth for southern quadrant ridge top, mid slope, and valley floor soil porewaters.....210

Figure 3.5 Depth versus average Ge/Si ratio for southern quadrant ridge top, mid slope, and valley floor soil porewaters.....211

Figure 3.6 Average Ge/Si ratios for southern quadrant ridge top, mid slope, and valley floor soil

porewaters, sugar maple, chestnut oak, and red oak leaves and sap waters, and streamwaters, groundwaters, and bedrock.....	212
Figure 3.7 Box plots of silicon concentration for southern planar ridge top, mid slope, and valley floor soil porewaters over the course of the growing season.....	218
Figure 3.8 Box plots of silicon concentration for south swale ridge top, mid slope, and valley floor soil porewaters over the course of the growing season.....	219
Figure 3.9 Box plots of Ge/Si ratio for southern planar ridge top, mid slope, and valley floor soil porewaters over the course of the growing season.....	220
Figure 3.10 Box plots of Ge/Si ratio for south swale ridge top, mid slope, and valley floor soil porewaters over the course of the growing season.....	221
Figure 3.11 Average leaf silicon concentration versus average sap flux.....	231
Figure 3.12 Average leaf silicon concentration versus average diameter at breast height (DBH).....	233
Figure 3.13 Box plots of silicon concentration for leaves sampled at mid slope positions of the northeastern quadrant in 2011 and 2013.....	235
Figure 3.14 Seasonal silicon concentrations for leaves sampled in 2013 at mid slope positions in northeastern, northwestern, southeastern, and southwestern quadrants as well as at all quadrants.....	239
Figure 3.15 Seasonal silicon concentrations for leaves sampled in 2011 at ridge top, mid slope, and valley floor positions of the northeastern quadrant as well as at all positions.....	240
Figure 3.16 Box plots of silicon concentration based on sampling location for leaves sampled at mid slope positions in northeastern, northwestern, southeastern, and southwestern quadrants in 2013.....	241

Figure 3.17 Box plots of silicon concentration based on sampling location for leaves sampled at ridge top, mid slope, and valley floor positions of the northeastern quadrant in 2011.....	242
Figure 3.18 Box plots of Ge/Si ratio based on sampling location for leaves sampled at ridge top, mid slope, and valley floor positions of the northeastern quadrant in 2011.....	250
Figure 3.19 Box plots of Ge/Si ratio based on sampling location for leaves sampled at mid slope positions in northeastern, northwestern, southeastern, and southwestern quadrants in 2013.....	251
Figure 3.20 Seasonal Ge/Si ratios for leaves sampled in 2011 at ridge top, mid slope, and valley floor positions of the northeastern quadrant as well as at all positions.....	256
Figure 3.21 Seasonal Ge/Si ratios for leaves sampled in 2013 at mid slope positions in northeastern, northwestern, southeastern, and southwestern quadrants as well as at all quadrants.....	257
Figure 3.22 Box plots of silicon concentration based on sampling location for sap waters sampled at mid slope positions in northeastern, northwestern, southeastern, and southwestern quadrants.....	265
Figure 3.23 Box plots of seasonal silicon concentration for sap waters sampled at mid slope positions in northeastern, northwestern, southeastern, and southwestern quadrants.....	266
Figure 3.24 Box plots of Ge/Si ratio for soil porewaters and sugar maple, chestnut oak, and red oak sapwaters and leaves collected from mid slope positions of the southwestern and southeastern quadrants.....	270
Figure 3.25 Depth versus silicon concentration for groundwaters and streamwaters.....	276
Figure 3.26 Depth versus Ge/Si ratio for groundwaters and streamwaters	277
Figure 3.27 Ge/Si ratio versus depth for DC 3 valley floor drill core samples.....	280
Figure 4.1 Combined profiles of depth versus Ge/Si and $^{87}\text{Sr}/^{86}\text{Sr}$ ratios for southern planar ridge	

top, mid slope, and valley floor soil porewaters.....313

Figure 4.2 Combined profiles of depth versus Ge/Si and $^{87}\text{Sr}/^{86}\text{Sr}$ ratios for south swale ridge top,
mid slope, and valley floor soil porewaters.....314

LIST OF TABLES

Table 2.1 Strontium and calcium elemental concentrations and Ca/Sr and $^{87}\text{Sr}/^{86}\text{Sr}$ ratios for southern quadrant ridge top, mid slope, and valley floor soil porewaters	59
Table 2.2 Average Ca/Sr and $^{87}\text{Sr}/^{86}\text{Sr}$ ratios for southern quadrant ridge top, mid slope, and valley floor soil porewaters.....	60
Table 2.3 Ca/Sr and $^{87}\text{Sr}/^{86}\text{Sr}$ ratios for southern planar ridge top, mid slope, and valley floor exchangeable soils.....	60
Table 2.4 Weighted average Ca/Sr and $^{87}\text{Sr}/^{86}\text{Sr}$ ratios for southern planar ridge top, mid slope, and valley floor exchangeable soils.....	61
Table 2.5 Weighted average Ca/Sr and $^{87}\text{Sr}/^{86}\text{Sr}$ ratios for southern planar ridge top, mid slope, and valley floor organic and mineral soil exchangeable horizons.....	61
Table 2.6 Average Ca/Sr ratios for southern quadrant ridge top, mid slope, and valley floor soil porewaters sampled from various depths	72
Table 2.7 Seasonal $^{87}\text{Sr}/^{86}\text{Sr}$ ratios for selected southern quadrant mid slope and valley floor soil porewaters.....	79
Table 2.8 Seasonal Ca/Sr ratios for southern quadrant ridge top, mid slope, and valley floor soil porewaters.....	79
Table 2.9 Strontium and calcium elemental concentrations and Ca/Sr and $^{87}\text{Sr}/^{86}\text{Sr}$ ratios for leaves sampled at ridge top, mid slope, and valley floor positions in northeastern, northwestern, southeastern, and southwestern quadrants.....	88
Table 2.10 Average Ca/Sr and $^{87}\text{Sr}/^{86}\text{Sr}$ ratios for sugar maple, chestnut oak, and red oak leaves.....	89
Table 2.11 Average $^{87}\text{Sr}/^{86}\text{Sr}$ ratios for sugar maple, chestnut oak, and red oak leaves sampled at	

mid slope positions in northeastern, northwestern, southeastern, and southwestern quadrants in 2013.....	89
Table 2.12 Average $^{87}\text{Sr}/^{86}\text{Sr}$ and Ca/Sr ratios for sugar maple, chestnut oak, and red oak leaves sampled at ridge top, mid slope, and valley floor positions of the northeastern quadrant in 2011.....	90
Table 2.13 Average Ca/Sr ratios for sugar maple, chestnut oak, and red oak leaves sampled at mid slope positions in northeastern, northwestern, southeastern, and southwestern quadrants in 2013.....	100
Table 2.14 Seasonal $^{87}\text{Sr}/^{86}\text{Sr}$ ratios for selected sugar maple and chestnut oak leaves.....	105
Table 2.15 Seasonal Ca/Sr ratios for leaves collected at mid slope positions in northeastern, northwestern, southeastern, and southwestern quadrants in 2013.....	106
Table 2.16 Strontium and calcium elemental concentrations and Ca/Sr and $^{87}\text{Sr}/^{86}\text{Sr}$ ratios for sap waters collected from sugar maple, chestnut oak, and red oak trees at mid slope positions in northeastern, northwestern, southeastern, and southwestern quadrants in 2013.....	111
Table 2.17 Average Ca/Sr and $^{87}\text{Sr}/^{86}\text{Sr}$ ratios for sugar maple, chestnut oak, and red oak sap waters.....	112
Table 2.18 Average $^{87}\text{Sr}/^{86}\text{Sr}$ ratios for sap waters collected from sugar maple, chestnut oak, and red oak trees at mid slope positions in northeastern, northwestern, southeastern, and southwestern quadrants in 2013.....	114
Table 2.19 Average Ca/Sr ratios for sap waters collected from sugar maple, chestnut oak, and red oak trees at mid slope positions in northeastern, northwestern, southeastern, and southwestern quadrants in 2013.....	116
Table 2.20 Seasonal $^{87}\text{Sr}/^{86}\text{Sr}$ ratios for selected sugar maple, chestnut oak, and red oak sap	

waters.....	123
Table 2.21 Seasonal Ca/Sr ratios for sugar maple, chestnut oak, and red oak sap waters.....	123
Table 2.22 Strontium and calcium elemental concentrations and Ca/Sr and $^{87}\text{Sr}/^{86}\text{Sr}$ ratios for groundwaters and streamwaters.....	131
Table 2.23 Strontium elemental concentrations and $^{87}\text{Sr}/^{86}\text{Sr}$ ratios for the carbonate fraction of DC 1 and DC 3 drill core samples.....	151
Table 2.24 Strontium elemental concentrations and $^{87}\text{Sr}/^{86}\text{Sr}$ ratios for the silicate fraction of DC 1 and DC 3 drill core samples.....	151
Table 3.1 Silicon and germanium concentrations and Ge/Si ratios for southern quadrant ridge top, mid slope, and valley floor soil porewaters	197
Table 3.2 Average silicon concentrations and Ge/Si ratios for southern quadrant ridge top, mid slope, and valley floor soil porewaters	200
Table 3.3 Average silicon and germanium concentrations and Ge/Si ratios for southern quadrant ridge top, mid slope, and valley floor soil porewaters sampled at various depths.....	201
Table 3.4 Seasonal silicon concentrations for southern quadrant ridge top, mid slope, and valley floor soil porewaters.....	216
Table 3.5 Seasonal Ge/Si ratios for southern quadrant ridge top, mid slope, and valley floor soil porewaters.....	216
Table 3.6 Seasonal germanium concentrations for southern quadrant ridge top, mid slope, and valley floor soil porewaters	217
Table 3.7 Silicon and germanium elemental concentrations and Ge/Si ratios for sugar maple, chestnut oak, and red oak leaves sampled at mid slope positions in northeastern, northwestern, southeastern, and southwestern quadrants in 2013.....	225

Table 3.8 Average silicon concentrations and Ge/Si ratios for sugar maple, chestnut oak, and red oak leaves sampled in 2013.....	227
Table 3.9 Silicon and germanium elemental concentrations and Ge/Si ratios for sugar maple, chestnut oak, and red oak leaves sampled at ridge top, mid slope, and valley floor positions of the northeastern quadrant in 2011.....	228
Table 3.10 Average silicon concentrations for sugar maple, chestnut oak, and red oak leaves sampled at ridge top, mid slope, and valley floor positions of the northeastern quadrant in 2011.....	229
Table 3.11 Average silicon concentrations and Ge/Si ratios for sugar maple, chestnut oak, and red oak leaves sampled in 2011.....	230
Table 3.12 Seasonal silicon concentrations for sugar maple, chestnut oak, and red oak leaves sampled at mid slope positions in the northeastern, northwestern, southeastern, and southwestern quadrants in 2013.....	237
Table 3.13 Seasonal silicon concentrations for sugar maple, chestnut oak, and red oak leaves sampled at ridge top, mid slope, and valley floor positions of the northeastern quadrant in 2011.....	238
Table 3.14 Average silicon concentrations for sugar maple, chestnut oak, and red oak leaves sampled at mid slope positions in northeastern, northwestern, southeastern, and southwestern quadrants of the catchment in 2013.....	238
Table 3.15 Average Ge/Si ratios for sugar maple, chestnut oak, and red oak leaves sampled at ridge top, mid slope, and valley floor positions of the northeastern quadrant in 2011.....	248
Table 3.16 Average Ge/Si ratios for sugar maple, chestnut oak, and red oak leaves sampled at	

mid slope positions in northeastern, northwestern, southeastern, and southwestern quadrants in 2013.....	248
Table 3.17 Seasonal Ge/Si ratios for sugar maple, chestnut oak, and red oak leaves sampled at ridge top, mid slope, and valley floor positions of the northeastern quadrant in 2011.....	254
Table 3.18 Seasonal Ge/Si ratios for sugar maple, chestnut oak, and red oak leaves sampled at mid slope positions in northeastern, northwestern, southeastern, and southwestern quadrants in 2013.....	255
Table 3.19 Silicon and germanium elemental concentrations and Ge/Si ratios for sap waters collected from sugar maple, chestnut oak, and red oak trees sampled at mid slope positions in northeastern, northwestern, southeastern, and southwestern locations in 2013.....	260
Table 3.20 Average silicon concentrations and Ge/Si ratios for sugar maple, chestnut oak, and red oak sap waters	262
Table 3.21 Average silicon concentrations for sap waters collected from sugar maple, chestnut oak, and red oak trees sampled at mid slope positions in northeastern, northwestern, southeastern, and southwestern quadrants in 2013.....	263
Table 3.22 Seasonal silicon concentrations for sugar maple, chestnut oak, and red oak sap waters.....	264
Table 3.23 Average Ge/Si concentrations for sap waters collected from sugar maple, chestnut oak, and red oak trees sampled at mid slope positions in northeastern, northwestern, southeastern, and southwestern quadrants in 2013.....	269
Table 3.24 Silicon and germanium elemental concentrations and Ge/Si ratios for groundwaters and streamwaters.....	275

Table 3.25 Ge/Si ratios for DC 3 valley floor drill core samples.....	279
Table A.1 Elemental concentrations and Ca/Sr ratios for southern quadrant soil porewaters....	324
Table A.2 Elemental concentrations and Ca/Sr ratios for sugar maple, chestnut oak, and red oak leaves sampled in 2013.....	328
Table A.3 Elemental concentrations and Ca/Sr ratios for sugar maple and chestnut oak leaves sampled in 2011 where $^{87}\text{Sr}/^{86}\text{Sr}$ ratios were not measured.....	330
Table A.4 Elemental concentrations and Ca/Sr ratios for sugar maple, chestnut oak, and red oak sap waters	331

INTRODUCTION

1. Background

The Critical Zone is a dynamic, near-surface ecosystem extending from the top of the canopy to the base of the water table (Anderson et al., 2008). Existing at the interface of the atmosphere, hydrosphere, and lithosphere, the Critical Zone represents an important system wherein a combination of chemical, physical, geological, and biological processes sustain terrestrial life at the Earth's surface (Brantley et al., 2007). At the Critical Zone, anthropogenic forces combine with climatic and tectonic forces to drive weathering processes which vary over spatial scales ranging from atomic to global and over temporal scales ranging from millennia (e.g. chemical weathering and tectonic activity) to seconds or microseconds (e.g. fluid transport in soil micropores) (Brantley et al., 2007). Accordingly, adequate understanding of intricate feedback and process interactions at the Critical Zone requires research across a multitude of disciplinary fields.

The Susquehanna Shale Hills Critical Zone Observatory (SSHCZO) was established in 2006 to explore questions relating to geochemical, hydrologic, biologic, and geomorphologic processes involved in the formation, evolution, and structure of regolith overlying shale bedrock in a temperate forested ecosystem (Brantley et al., 2006). Geochemical studies at the SSHCZO have focused on understanding weathering processes under varying flow regimes (Jin et al., 2010; Jin and Brantley, 2011), determining regolith production rates and weathering time scales (Ma et al., 2010), investigating deep weathering interactions using nested subsurface reaction fronts (Jin et al., 2011a; Brantley et al., 2013), and identifying mineralogical and slope aspect factors involved in rare earth element release and fractionation during shale weathering (Ma et al., 2011). Preferential flow pathways (Lin, 2006; Lin et al., 2006; Lin and Zhou, 2008, Graham

and Lin, 2011; Takagi and Lin, 2012; Zhang et al., 2014), soil moisture dynamics (Lin et al., 2006), and solute transport (Jin et al., 2010, 2011b, 2014; Andrews et al., 2011; Herndon et al., 2011; Kuntz et al., 2011) have served as the basis of hydrologic studies, while biologic studies have centered on tree species distribution patterns in relation to stem hydraulic traits and soil moisture features (Naithani et al., 2013), above- and belowground controls on tree water use (Meinzer et al., 2013), and metal release from shales in the presence of organic ligands and bacteria (Liermann et al., 2011). Furthermore, geomorphologic studies at the SSHCZO have focused on differential uplift processes involved in regolith formation (Miller et al., 2013) and determining constraints on the timescales of regolith formation (West et al., 2011).

As mentioned previously, an important geochemical process occurring at the Critical Zone is mineral weathering. Over long time scales, mineral weathering controls solute and sediment fluxes from continents to oceans and sequesters atmospheric carbon dioxide (Kurtz et al., 2002), while over shorter time scales, mineral weathering regulates the release of nutrients to ecosystems (Brantley et al., 2007). These nutrients are subject to either uptake by flora and fauna or precipitation in secondary minerals exported from the ecosystem to the ocean through streamwaters via chemical denudation (Balogh-Brunstad et al., 2008). At the Critical Zone, solute transport occurs through both subsurface flowpaths and corresponding reactions occurring at the rock-water interface. Flow rates along preferential flow paths determine if weathering will be transport-limited (e.g. limited by erosion processes) or surface reaction controlled (e.g. limited by chemical weathering reaction rates themselves) (Carson and Kirkby, 1972; Kump et al., 2000). Subsurface flowpaths and water transit times directly affect mineral weathering contributions to reservoir components and are subject to environmental factors such as seasonality (Thomas et al., 2013), climate patterns (Dere et al., 2013), water sources (Jin et al.,

2011b), and biologically-mediated chemical reactions (Liermann et al., 2011). Plants also play an integral role in feedback processes at the Critical Zone. Soil profiles represent an amalgamation of hydrologic, atmospheric, and biotic forces interacting with underlying bedrock and weathered mantle. Consequently, the chemical availability and physical distribution of rock derived nutrients depend on intricate plant-soil feedback relationships. Initially, plant roots extract nutrients from soil solutions for metabolic processes (Marschner, 2012). These nutrients are then provisionally stored in plant tissue and later returned to the soil through litterfall, root decay, and plant decomposition (Marschner, 2012). In upper soil horizons and in the rhizosphere, plant activities facilitate exchange reactions in soils by releasing organic acids which lower a soil's pH (Drever, 1994; Alexandre et al., 1997). Plants also influence the hydrologic cycle by serving as important conduits through which soil water and groundwater can re-enter a watershed (Lucas, 2001; Brooks et al., 2010). Specifically, plants affect soil permeability and the infiltration of precipitation into topsoil (Colin et al., 1992) and produce an additional shallow water reservoir via tap root or hydraulic lift processes which transfer deep groundwater through the influence of roots to dry upper soil layers (Dawson, 1993; Brooks et al., 2010).

Using a combination of strontium isotope ratios ($^{87}\text{Sr}/^{86}\text{Sr}$), elemental ratios (Ca/Sr, Ge/Si), and elemental concentrations, this study employs a multi-tracer approach to document sources of solutes at the SSHCZO. Additionally, spatio-temporal patterns are assessed and inferences are developed using empirical data supplemented by observations on mineral weathering, proposed preferential flow pathways, and plant transport mechanisms at the catchment. Hydrological (preferential flow pathways), topographical (hillslope geometry), biological (plant preferential discrimination), and mineralogical (dominant weathering inputs)

controls on the availability and distribution of calcium, strontium, silicon, and germanium at the SSHCZO are also identified.

2. Site Description

Representing fundamental spatial units with reasonably homogenous geological, ecological, and land use characteristics, small watersheds serve as important mediums in which to explore biogeochemical and geochemical processes (National Research Council, 1997). Located in the ridge and valley region of central Pennsylvania, the Shale Hills Critical Zone Observatory (SSHCZO) encompasses a 7.9 hectare temperate forested V-shaped first-order catchment. The catchment lies within the Shavers Creek watershed of the Juniata River subbasin and drains into the larger Susquehanna River (Figure 1.1). The stream channel is oriented in an east-west direction between narrow ridges (Jin et al., 2010). Mean annual precipitation is 1070 mm yr⁻¹, while mean annual temperature is 10°C (NOAA, 2007). Rainwater is relatively acidic (pH~4.5) and enriched in nitrates and sulfates (NADP, 2013). Elevation varies from 310 meters at the ridge top to 256 meters at the stream outlet (Lin et al., 2006), while slopes within the catchment range from 25-48% (Lin et al., 2006). According to Jin et al. (2010), strike and dip measurements of underlying shale bedrock for the northern ridge top are N54°E and 76°NW, respectively, although shallower dip measurements have been observed at the valley floor (Kuntz et al., 2011).

Four distinct landforms are present at the SSHCZO: a north (south-facing) slope, a south (north-facing) slope, a valley floor, and topographic depressional areas (swales) (Figures 1.2 to 1.4). Deciduous forest and underbrush land cover dominates both the northern (south-facing) and southern (north-facing) slopes while thicker underbrush occurs at the south slope. Western and eastern sides of the valley floor are comprised of evergreen (hemlock) trees and deciduous oak-

hickory forest land cover, respectively. Seven swales with deciduous forest land cover are dispersed throughout the catchment; five are located on the northern slope and two on the southern slope, with each divided by near-planar slopes.

Five soil series (Weikert, Berks, Rushtown, Ernest, and Blairton) (Figure 1.2) have been characterized at the catchment based on depth to bedrock, landform unit, and drainage condition (Lin et al., 2006). The Weikert Series (loamy-skeletal, mixed, active, mesic Lithic Dystrudepts) is the most abundant soil type at the catchment (78.7% area) followed by the Berks (loamy-skeletal, mixed, active, mesic Typic Dystrudepts), Rushtown (loamy-skeletal over fragmental, mixed, mesic Typic Dystrochrepts), Ernest (fine-loamy, mixed, superactive, mesic Aquic Fragiudults), and Blairton Series (fine-loamy, mixed, active, mesic Aquic Hapludults) which occupy 9.8, 6.4, 4.9, and 0.2% of the catchment area, respectively (Figure 1.2) (Lin et al., 2006). Backslopes, shoulders, and summits consist of thin (<50 cm thickness), well drained soils belonging to the Weikert Series, while swale locations are comprised of thicker (50 to >100 cm thickness), well to moderately well drained soils belonging to the Berks (swale sides) and Rushtown (swale bottoms) Series (Figure 1.2). Valley floor locations consist of thick soils (50 to >100 cm thickness) belonging to the Berks (edges of valley floor), Blairton (narrow band at eastern end of valley floor), and Ernest (western end of the valley floor) Series whose drainage conditions range from well drained (Berks) to moderately well drained (Blairton) to somewhat poorly drained (Ernest) (Figure 1.2). Rushtown Series soils occur at the northeastern part of the catchment, while Ernest Series soils are observed at the floodplain (Figure 1.2).

The SSHCZO has 23 tree species within 14 genera (Wubbels, 2010). The current tree stand age is somewhere between 70 and 80 years old with the last tree harvesting event occurring in the 1930s (Wubbels, 2010). Tree species are distributed along distinct soil-depth and soil-

moisture gradients (Wubbels, 2010). Oak species (*Quercus spp.*) dominate deciduous land cover on the drier slope and ridge positions, while smaller populations of hickory (*Carya spp.*), pine (*Pinus spp.*), and maple (*Acer spp.*) are also present (Figure 1.3). Eastern hemlock species (*Tsuga canadensis*) occur at the wetter valley floor positions (Figure 1.3). According to Wubbels (2010), oak, hickory, pine, maple, and eastern hemlock species account for 63, 13, 8, 7 and 8% of the total basal area in the catchment, respectively.

At the SSHCZO, residual shale soils occur on the ridge tops, while mid slope and valley floor soils are formed on a colluvial and alluvial mantle of shale chips (Jin and Brantley, 2011). These soils are underlain by the Silurian-age Rose Hill formation, an oxidized organic-poor marine shale with a few interbedded limestones (Lynch et al., 1976). According to Jin et al. (2010), the shale is comprised predominately of illite (58 wt%), quartz (30 wt%), vermiculitized chlorite (11 wt%), and trace amounts of feldspar (plagioclase and K-feldspar), anatase (TiO₂), Fe-oxides (magnetite and hematite), and zircon, with ankerite and pyrite also present meters below the surface at the northern ridge (Jin et al., 2010) and valley floor near the stream's weir (Brantley et al., 2013). Thin, well drained soils at ridge locations (<50 cm) thicken downslope towards the stream (<300 cm) (Figure 1.4). The convex-upward hillslope of the catchment consists of well drained, oxic soils with a silty loam texture, while valley floor soils are characterized by redoximorphic features indicative of periodic reducing conditions from seasonal soil saturation at these locations (Lin et al., 2006). Throughout the SSHCZO, a 3 to 5 cm thick organic layer (Oe-horizon) is present consisting of decaying leaf litter and other organic materials. Effective rooting depth (i.e. depth to bedrock) ranges from 15 cm on ridge tops to 165 cm at selective slope locations (Figure 1.4).

High soil production rates at ridge locations (~45 m My⁻¹) decrease exponentially

downslope ($\sim 15 \text{ m My}^{-1}$) (Ma et al., 2010). The average catchment-wide erosion rate is estimated to be 15 m My^{-1} based on cosmogenic ^{10}Be dating of sediments (Jin et al., 2010). Furthermore, regolith residence times range from 7 to 40 ky at the SSHCZO and increase from ridge top to valley floor locations (Ma et al., 2010). Swale and valley floor locations have been found to have residence times exceeding that of the last glacial maximum (ca. 15 kyra) (Gardner et al., 1991) and are hypothesized to be accumulating pre-glacial regolith (Ma et al., 2010). Jin et al. (2010, 2011a) and Brantley et al. (2013) predicted the order of mineral reaction fronts occurring at the SSHCZO. The first and deepest reaction front involves oxidative pyrite dissolution at approximately 23 and 9 meters below the ground surface of the ridge and valley floor, respectively (Jin et al., 2010, 2011a; Brantley et al., 2013). Sulfuric acids generated by reactive pyrites and CO_2 charged fluids in the unsaturated zone initiate carbonate dissolution at depths of 22 and 2 meters at ridge and valley floor locations, respectively (Jin et al., 2010, 2011a; Brantley et al., 2013). A shallower reaction front follows involving plagioclase feldspar dissolution at 5 to 6 and 6 to 7 meters below the ground surface of the ridge and valley floor, respectively (Jin et al., 2010, 2011a; Brantley et al., 2013). Above the feldspar reaction front and below the depth of augering refusal, clay weathering transforms primary illite and chlorite minerals into secondary vermiculite, hydroxy-interlayered vermiculite, and kaolinite resulting in a loss of soluble cations and fine particles (Jin et al., 2010, 2011a; Brantley et al., 2013). For planar hillslopes, chemical weathering rates are shown to decrease from ridge top to valley floor locations with elements such as Al and Si accumulating at the valley floor (Jin et al., 2010).

Preferential flow pathways are important transport mechanisms of water and solutes from hillslopes to valley floor and riparian areas in watersheds (Whipkey, 1965; Kirby, 1978; Beven and Germann, 1982; McDonnell, 1990; Jarvis, 2007). Both vertical and lateral preferential flow

pathways have been documented at the Shale Hills Critical Zone Observatory (SSHCZO) (Figure 1.5, Lin, 2006; Lin et al., 2006; Lin and Zhou, 2008; Graham and Lin, 2011; Jin et al., 2011b). Specifically, vertical preferential flow processes have been identified in high-permeability zones and along macropores or fractures due to the hydrophobic nature of organic surface layers (Lin and Zhou, 2008; Graham and Lin, 2011; Jin et al., 2011b), while lateral preferential flow processes have been observed along macropores and in soil horizons/soil-bedrock interfaces (Lin, 2006; Lin et al., 2006; Jin et al., 2011b). Several controls have been identified on preferential flow at the SSHCZO. Drier soils and warmer temperatures at ridge top and planar hillslope positions produce conditions such as soil hydrophobicity and soil cracking which initiate preferential flow at these locations in the late summer (Graham and Lin, 2011). At valley floor, mid slope, and lower swale sites, soil moisture levels and the intensity of precipitation events have been shown to influence preferential flow initiation (Graham and Lin, 2011). Considering that preferential flow has been documented at one or more sites in 90% of all monitored precipitation events (Graham and Lin, 2011), its implications on spatio-temporal patterns in chemistry are considered to be quite significant at the SSHCZO.

Numerous natural and anthropogenic perturbations have affected soil formation at the SSHCZO. Evidence of natural disturbance (e.g. freeze-thaw and stratified slope deposits) corresponds to a periglacial climate present in the region ca. 15 kya (Gardner et al., 1991). Anthropogenic disturbances at the SSHCZO include clear cutting for timber production during colonial times and tree harvesting in the 1930s (Wubbels, 2010). Additionally, Herndon et al. (2011) identified remains of iron furnaces 20 miles from the catchment, a likely source of transported metals to soils within the catchment via the atmospheric deposition of particulates.

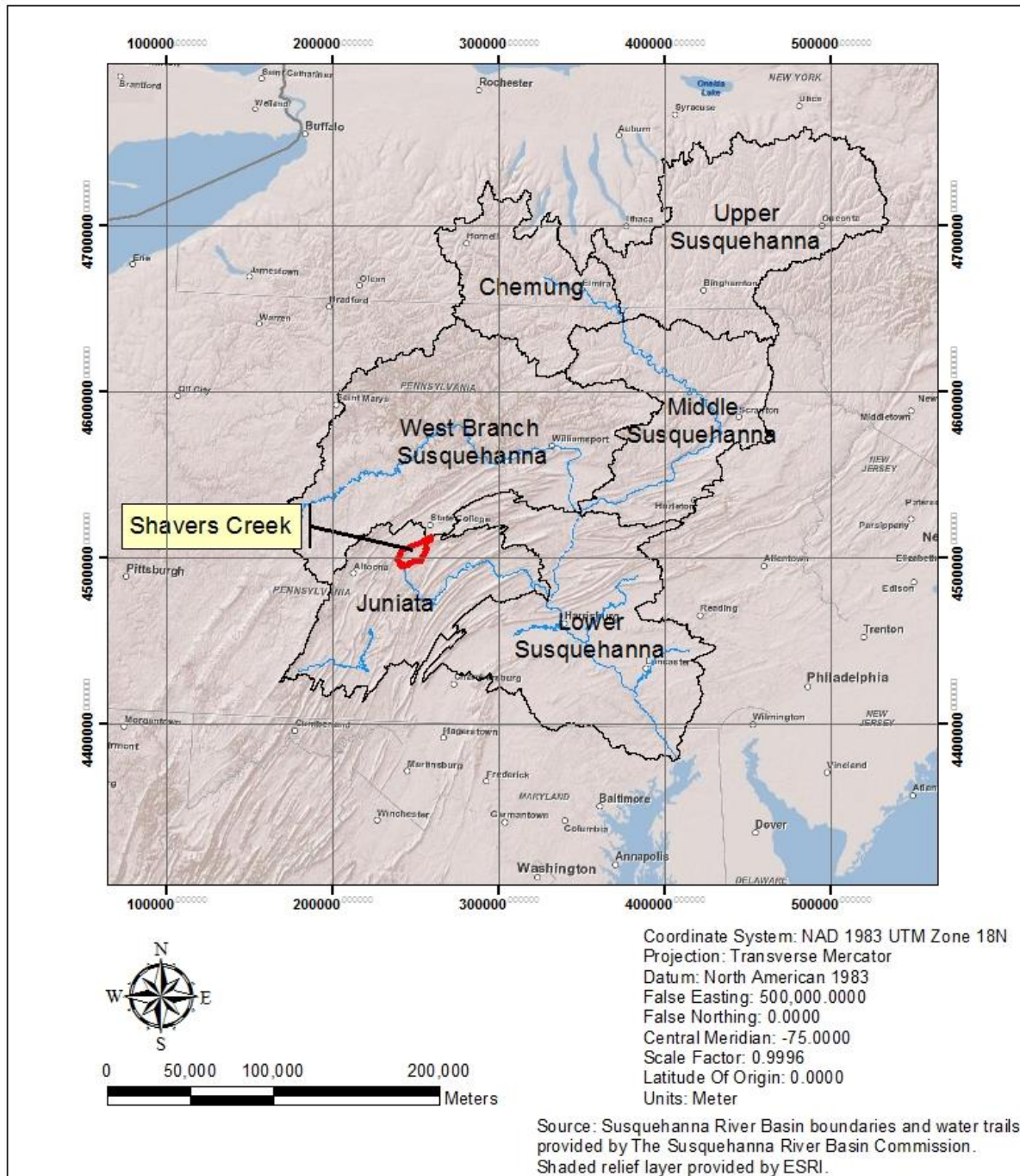


Figure 1.1 Map of the Susquehanna River Subbasins showing the location of Shavers Creek relative to these basins. Shavers Creek drains water from a first-order stream present at the Susquehanna Shale Hills Critical Zone Observatory into the Susquehanna River by means of the Juniata River.

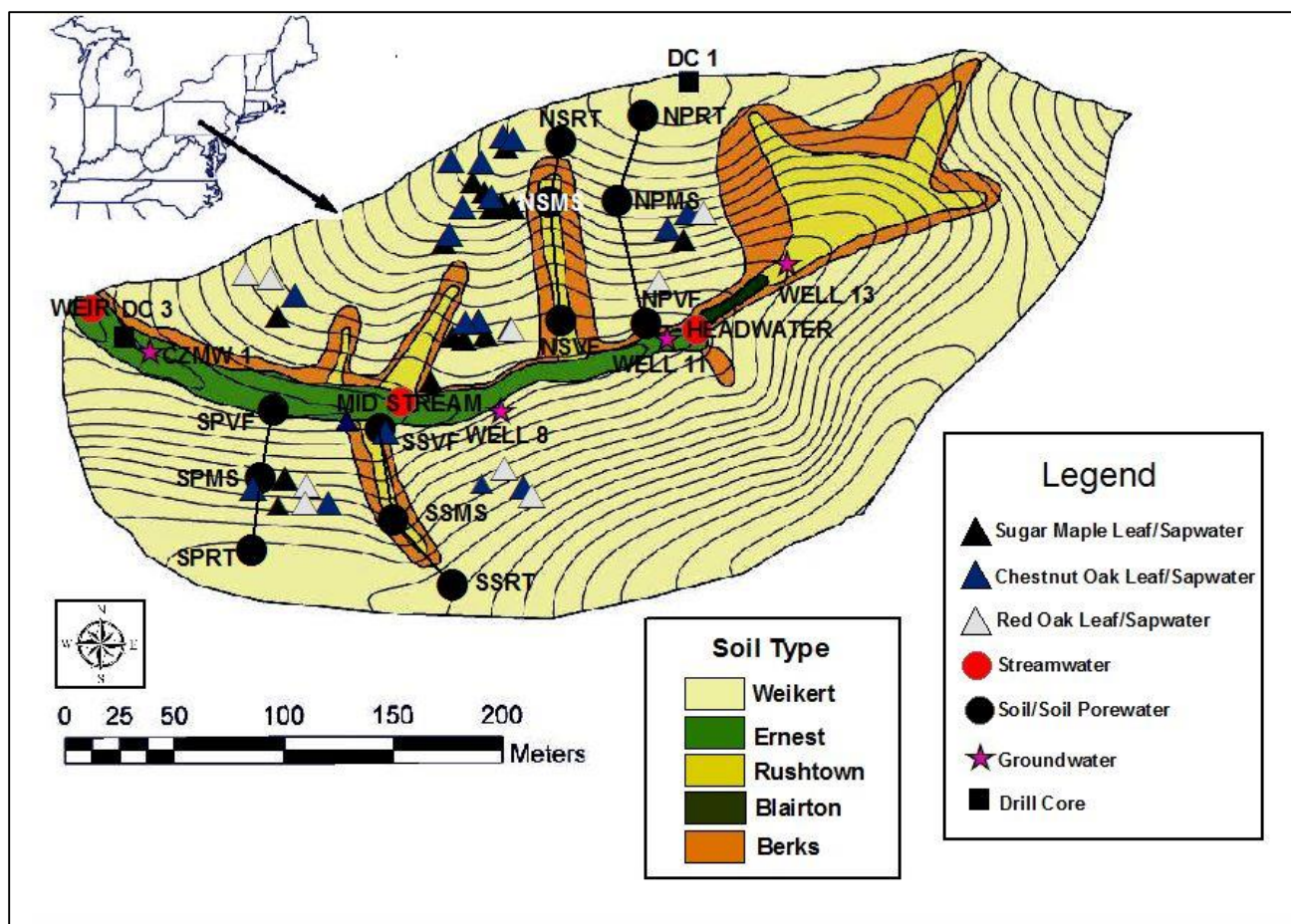


Figure 1.2 Topographic map depicting sampling locations at the Susquehanna Shale Hills Critical Zone Observatory with contour lines shown in black (Figure modified from Thomas, 2013). Colors represent soil type based on field observations (Lin et al., 2006). Leaves and sap waters were collected throughout the observatory from three tree species: sugar maple (black triangles), chestnut oak (blue triangles), and red oak (gray triangles). Soils and soil porewaters (black circles) were sampled from the southern planar (SP) and south swale (SS) ridge top (RT), mid slope (MS), and valley floor (VF) locations. Drill core samples (black squares) were also collected from a northern ridge top borehole (DC 1) and from borehole CZMW 2 near the stream’s weir (DC 3). Streamwaters (red circles) were sampled at the weir and at mid stream and headwater locations. Shallow (CZMW 1) and deep groundwaters (Wells 8, 11, and 13) (pink stars) were also collected. No spatial information was provided for a deep groundwater sample corresponding to sample ID CZMW 6 and, consequently, this sample is not displayed on the figure.

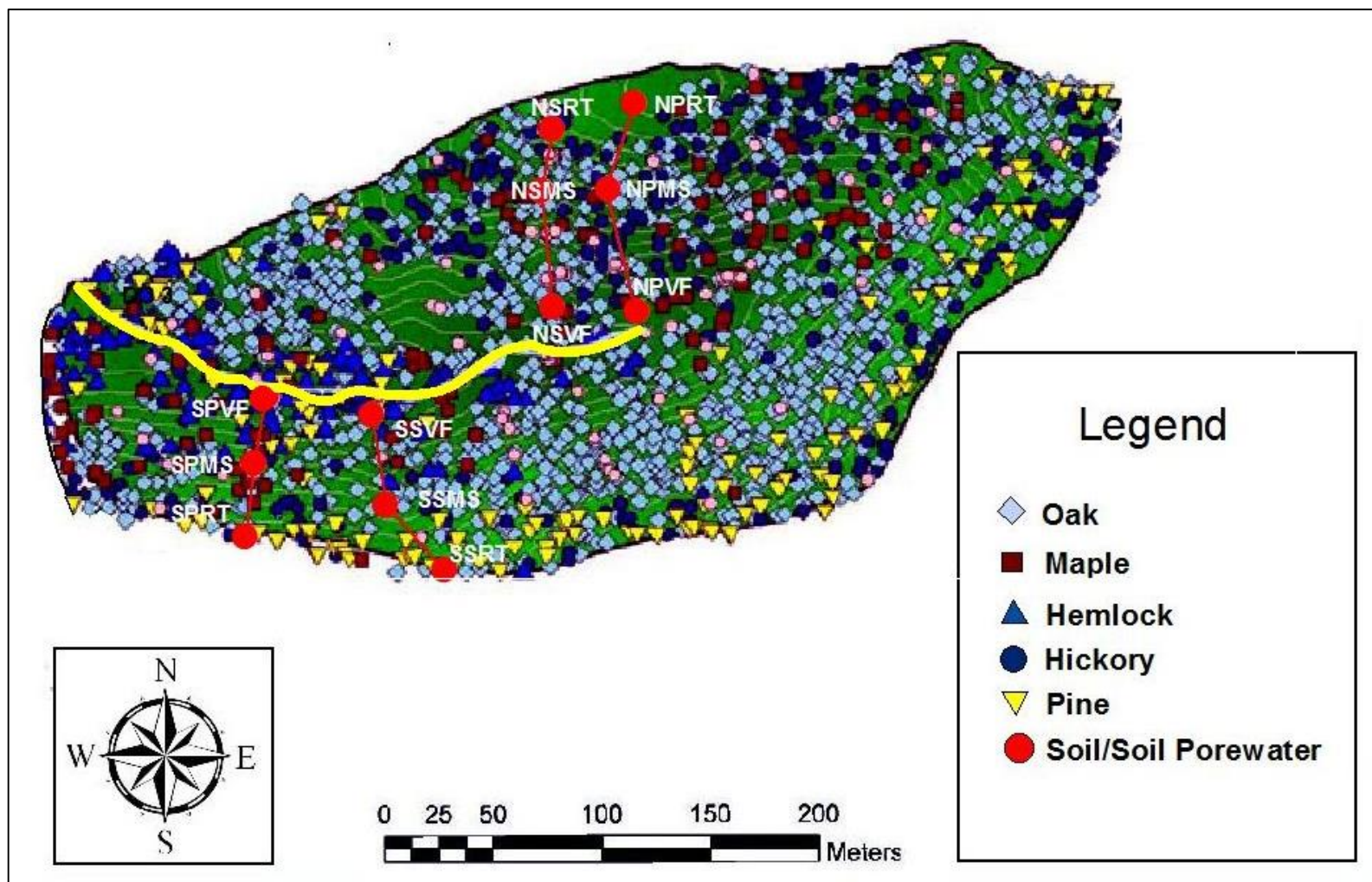


Figure 1.3 The spatial distribution of dominant tree species at the Susquehanna Shale Hills Critical Zone Observatory (Figure modified from Naithani et al., 2013) with contour lines shown in white. Oak (*Quercus spp.*), maple (*Acer spp.*), hemlock (*Tsuga spp.*), hickory (*Carya spp.*), and pine (*Pinus spp.*) species are shown as blue diamonds, red squares, blue triangles, blue circles, and yellow triangles, respectively. Soils and soil porewaters from the northern (NP) and southern planar (SP) and north (NS) and south swale (SS) ridge top (RT), mid slope (MS), and valley floor (VF) locations are shown as red circles, while the first-order catchment stream is outlined in yellow.

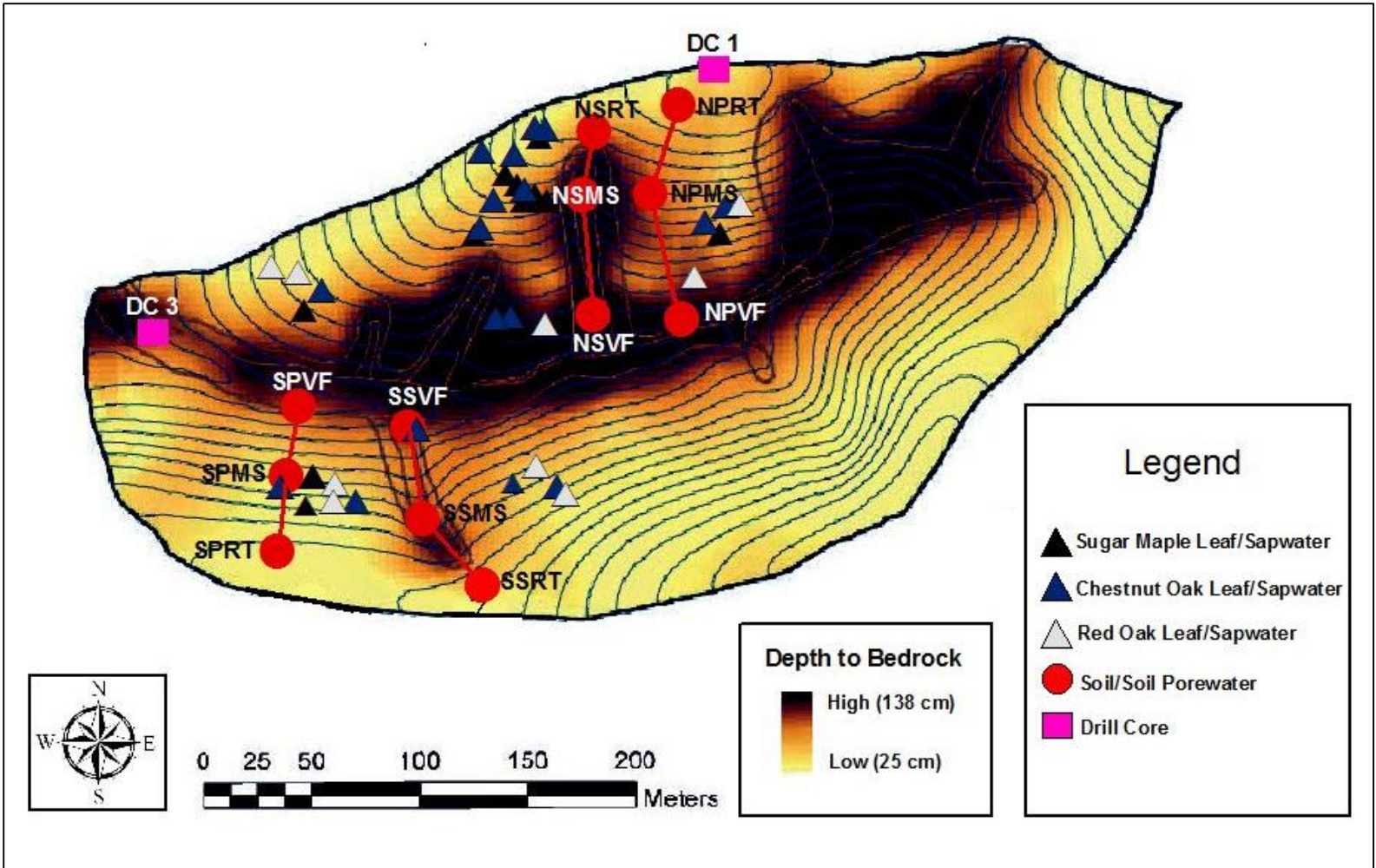


Figure 1.4 Topographic map depicting sampling locations at the Susquehanna Shale Hills Critical Zone Observatory with contour lines shown in blue (Figure modified from Jin et al., 2011a). Colors represent regolith thickness (Jin et al., 2011a). Leaves and sap waters were collected throughout the observatory from three tree species: sugar maple (black triangles), chestnut oak (blue triangles), and red oak (gray triangles). Soils and soil porewaters (red circles) were sampled from southern planar (SP) and south swale (SS) ridge top (RT), mid slope (MS), and valley floor (VF) locations, while drill core samples (pink squares) were also collected from a northern ridge top borehole (DC 1) and from borehole CZMW 2 near the stream’s weir (DC 3).

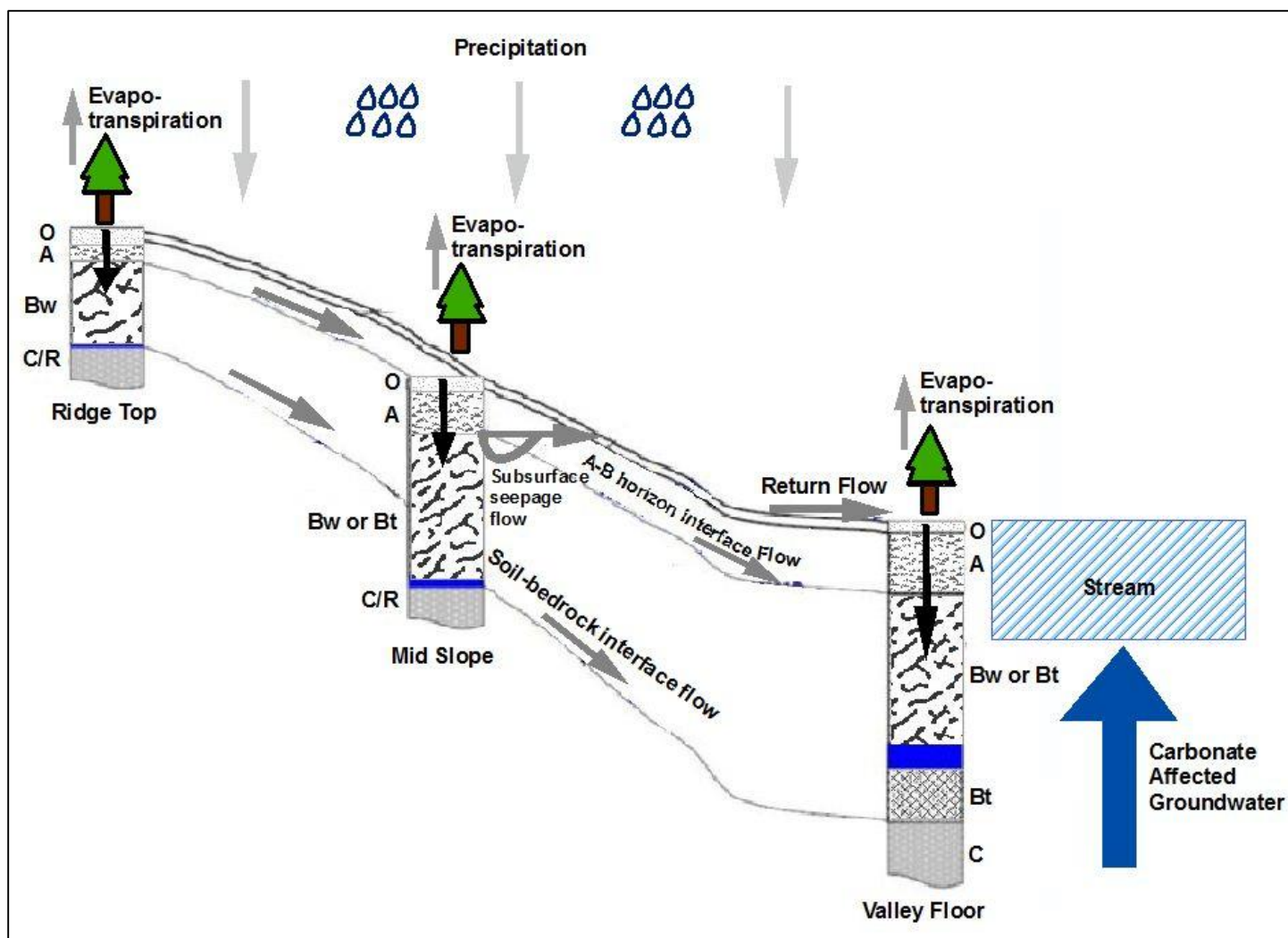


Figure 1.5 Schematic diagram (Figure modified from Lin et al., 2006) showing hillslope flow pathways at the Susquehanna Shale Hills Critical Zone Observatory as hypothesized by Lin et al., 2006. A potential perched/seasonal water table is indicated by the blue regions on the diagram. Arrow sizes on the diagram are irrelevant and do not correspond to magnitudes of reservoir fluxes.

4. Objectives of each chapter

Chapter Two: Ca/Sr and $^{87}\text{Sr}/^{86}\text{Sr}$ ratios as tracers of solute sources at the Susquehanna Shale Hills Critical Zone Observatory

Strontium isotopes are invariant over weathering timescales and do not display fractionation upon biogeochemical processes such as plant uptake, mineral dissolution and precipitation, or evapotranspiration (Stewart et al., 1998). To this end, $^{87}\text{Sr}/^{86}\text{Sr}$ ratios can be used to trace solute sources in reservoirs where relative contributions of end-members in a mixture can be calculated as long as end-members have distinctive $^{87}\text{Sr}/^{86}\text{Sr}$ ratios. Strontium is only a minor constituent of soils, rocks, and plants and is not considered to be an important plant nutrient or weathering product (Capo et al., 1998). However, strontium exhibits similar chemical behavior as calcium (e.g. similar ionic charge, radius, and electron configuration) and, consequently, strontium isotope ratios are oftentimes used in combination with Ca/Sr ratios to study calcium sources in terrestrial systems (Miller et al., 1993; Bailey et al., 1996; Blum et al., 2002; Kennedy et al., 2002; Bullen and Bailey, 2005; Pett-Ridge et al., 2009; Belanger et al., 2012). It should be noted that the extent to which calcium and strontium fractionate in biological systems is not yet fully understood and some studies have challenged the effectiveness of strontium as a proxy for calcium cycling in ecosystems (Poszwa et al., 2000; Watmough and Dillon, 2003).

In this chapter, $^{87}\text{Sr}/^{86}\text{Sr}$ and Ca/Sr ratios are used to identify atmospheric versus weathering derived sources of solutes in exchangeable soils, soil porewaters, leaves, sap waters, groundwaters, and streamwaters at the SSHCZO. Spatio-temporal patterns in Ca/Sr and $^{87}\text{Sr}/^{86}\text{Sr}$ ratios are evaluated and inferences are formulated on the basis of solute source contributions to various reservoirs using compiled data in conjunction with mineralogical observations (Jin et al., 2010; Ma et al., 2010; Jin et al., 2011a, 2011b, 2014; Jin and Brantley, 2011; Ma et al., 2011a,

2011b; Brantley et al., 2013), proposed preferential flow pathways (Lin, 2006; Lin et al., 2006; Lin and Zhou, 2008; Graham and Lin, 2011; Jin et al., 2011b; Takagi and Lin, 2012; Thomas, 2013; Zhang et al., 2014), and calcium transport mechanisms in plants (Clarkson, 1984; McLaughlin and Wimmer, 1999; White, 2001; White and Broadley, 2003; Marschner, 2012) at the catchment.

Chapter Three: Ge/Si ratios as tracers of silicon sources at the Susquehanna Shale Hills Critical Zone Observatory

Existing as a “pseudo-isotope” of silicon, germanium displays several chemical similarities to silicon including its nature as a group IV element, a similar ionic radius and tetrahedral bond length, and an identical outer electron configuration (Shannon, 1976; Martin et al., 1996; Kurtz et al., 2002). Germanium can substitute for silicon at tetrahedral sites of silicate minerals (Goldschmidt, 1958). Additionally, Ge/Si ratios reflect fractionation during weathering and plant uptake processes in terrestrial systems with germanium enriched in secondary minerals (Murnane and Stallard, 1990; Kurtz et al., 2002; Scribner et al., 2006) and depleted in biogenic materials (Derry et al., 2005; Blecker et al., 2007; Delvigne et al., 2009) relative to parent bedrock. Consequently, Ge/Si ratios serve as particularly useful tracers of silicate weathering processes (Murnane and Stallard, 1990; Kurtz et al., 2002; Derry et al., 2006; Scribner et al., 2006; Lugolobi et al., 2010) and silicon pathways in the soil-plant system (Derry et al., 2005; Garvin, 2006; Blecker et al., 2007; Delvigne et al., 2009).

In this chapter, Ge/Si ratios and germanium and silicon elemental concentrations are used to identify silicon sources in soil porewaters, leaves, sap waters, groundwaters, and streamwaters at the Susquehanna Shale Hills Critical Zone Observatory (SSHCZO). Spatio-temporal patterns in silicon concentration and Ge/Si ratio are assessed and inferences are developed as to the sources of silicon in various reservoirs using silicon concentrations and Ge/Si ratios

supplemented by observations on mineral weathering (Jin et al., 2010; Ma et al., 2010; Jin et al., 2011a, 2011b; Jin and Brantley, 2011; Brantley et al., 2013), proposed preferential flow pathways, (Lin, 2006; Lin et al., 2006; Lin and Zhou, 2008; Graham and Lin, 2011; Jin et al., 2011b; Takagi and Lin; 2012; Thomas, 2013; Zhang et al., 2014), and silicon transport mechanisms in plants (Jones and Handreck, 1965; Raven, 1983; Raven, 2003; Mitani and Ma, 2005; Ma and Yamaji, 2006; Ma et al., 2007; Yamaji et al., 2008; Sparks et al., 2010) at the catchment.

Chapter Four: Summary of completed work and potential future work at the Susquehanna Shale Hills Critical Zone Observatory

This chapter outlines the main conclusions of the study as presented in Chapters Two and Three. In particular, a comprehensive evaluation of the impacts of hydrology (preferential flow pathways), topography (hillslope geometry), biology (plant preferential discrimination), and mineralogy (dominant weathering inputs) on the availability and distribution of calcium, strontium, silicon, and germanium in various reservoir components of the watershed is undertaken. Furthermore, facets of drill core chemistry are expounded upon. In any study, sampling, time, and budget constraints limit the scale and scope of questions that can be reasonably addressed. As such, Chapter 4 also offers recommendations for future research at the catchment.

4. References

- Alexandre, A., Meunier, J., Colin, F., and Koud, J., 1997, Plant impact on the biogeochemical cycle of silicon and related weathering processes: *Geochimica et Cosmochimica Acta*, v. 61, p. 677-682.
- Anderson, S., Bales, R., and Duffy, C., 2008, Critical Zone observatories: Building a network to advance interdisciplinary study of Earth surface processes: *Mineralogical Magazine*, v. 72, p. 7–10.
- Andrews, D., Lin, H., Zhu, Q., Jin, L., and Brantley, S., 2011, Hot spots and hot moments of dissolved organic carbon export and soil organic carbon storage in the Shale Hills catchment: *Vadose Zone Journal*, v. 10, p. 943–954.
- Bailey, S., Hornbeck, J., Driscoll, C., and Gaudette, H., 1996, Calcium inputs and transport in a base-poor forest system as interpreted by Sr isotopes: *Water Resources Research*, v. 32, p. 707-719.
- Balogh-Brunstad, A., Keller, C., Borman, B., O'Brien, R., Wang, D., and Hawley, G., 2008, Chemical weathering and chemical denudation dynamics through ecosystem development and disturbance: *Global Biogeochemical Cycles*, v. 22, p. 1-10.
- Belanger, N., Holmden, C., Courchesne, F., Cote, B., and Hendershot, W., 2012, Constraining soil mineral weathering $^{87}\text{Sr}/^{86}\text{Sr}$ for calcium apportionment studies of a deciduous forest growing on soils developed from granitoid igneous rocks: *Geoderma*, v. 185-186, p. 84-96.
- Beven, K., and Germann, P., 1982, Macropores and water flow in soils: *Water Resources Research*, v. 18, p. 1311-1325.
- Blecker, S., King, S., Derry, L., Chadwick, O., Ippolito, J., and Kelly, E., 2007, The ratio of germanium to silicon in plant phytoliths: quantification of biological discrimination under controlled experimental conditions: *Biogeochemistry*, v. 86, p. 189-199.
- Blum, J., Klaue, A., Nezat, C., Driscoll, C., Johnson, C., Siccama, T., Eagar, C., Fahey, T., and Likens, G., 2002, Mycorrhizal weathering of apatite as an important calcium source in base-poor forest ecosystems: *Nature*, v. 417, p. 729-731.
- Brantley, S., White, T., White, A., Sparks, D., Richter, D., Pregitzer, K., Derry, L., Chorover, J., Chadwick, O., April, R., Anderson, S., and Amundson, R., 2006, *Frontiers in exploration of the*

Critical Zone: Report of a workshop sponsored by the National Science Foundation (NSF), October 24-26, 2005, Newark, DE, 30p.

Brantley, S., Goldhaber, M., and Ragnarsdottir, K., 2007, Crossing disciplines and scales to understand the Critical Zone: Elements, v. 3, p. 307–314.

Brantley, S., Holleran, M., Jin, L., and Bazilevskaya, E., 2013, Probing deep weathering in the Shale Hills Critical Zone Observatory, Pennsylvania (USA): The hypothesis of nested chemical fronts in the subsurface: Earth Surface Processes and Landforms, v. 38, p. 1280-1298.

Brooks, J., Barnard, H., Coulombe, R., and McDonnell, J., 2010, Ecohydrologic separation of water between trees and streams in a Mediterranean climate: Nature Geoscience, v. 3, p. 100-104.

Bullen, T., and Bailey, S., 2005, Identifying calcium sources at an acid deposition-impacted spruce forest: A strontium isotope, alkaline earth element multi-tracer approach: Biogeochemistry, v. 75, p. 63-99.

Capo, R., Stewart, B., and Chadwick, O., 1998, Strontium isotopes as tracers of ecosystem processes: theory and methods: Geoderma, v. 82, p. 197-225.

Carson, M., and Kirkby, M., 1972, Hillslope Form and Process, Cambridge University Press: London.

Clarkson, D., 1984, Calcium transport between tissues and its distribution in the plant: Plant, Cell and Environment, v. 7, p. 449-456.

Colin, F., Brimhall, G., Nahon, D., Lewis, C., Barronnet, A., and Danti, K., 1992, Equatorial rainforest lateritic soils: A geomembrane filter: Geology, v. 20, p. 523-526.

Dawson, T., 1993, Hydraulic lift and water use by plants: implications for water balance, performance, and plant-plant interactions: Oecologia, v. 95, p. 565-574.

Delvigne, C., Opfergelt, S., Cardinal, D., Delvaux, B., and Andre, L., 2009, Distinct silicon and germanium pathways in the soil-plant system: Evidence from banana and horsetail: Journal of Geophysical Research, v. 114, p. 1-11.

Dere, A., White, T., April, R., Reynolds, B., Miller, T., Knapp, E., McKay, L., and Brantley, S.,

2013, Climate dependence of feldspar weathering in shale soils along a latitudinal gradient: *Geochimica et Cosmochimica Acta*, v. 122, p. 101-126.

Derry, L., Kurtz, A., Ziegler, K., and Chadwick, O., 2005, Biological control of terrestrial silica cycling and export fluxes to watersheds: *Nature*, v. 433, p. 728-730.

Derry, L., Pett-Ridge, J., Kurtz, A., and Troester, J., 2006, Ge/Si and $^{87}\text{Sr}/^{86}\text{Sr}$ tracers of weathering reactions and hydrologic pathways in a tropical granitoid system: *Journal of Geochemical Exploration*, v. 88, p. 271-274.

Drever, J., 1994, The effect of land plants on weathering rates of silicate minerals: *Geochimica et Cosmochimica Acta*, v. 58, p. 2325-2332.

ESRI, 2012, ESRI Maps and Data –World Shaded Relief Map, Retrieved from <http://www.arcgis.com/home/item.html?id=4cda073db6d444598684805848dae98b>.

Gardner, T., Ritter, J., Shuman, C., Bell, J., Sasowsky, K., and Pinter, N., 1991, A periglacial stratified slope deposit in the valley and ridge province of Central Pennsylvania, USA: sedimentology, stratigraphy, and geomorphic evolution: *Permafrost and Periglacial Processes*, v. 2, p. 141–162.

Garvin, C., 2006, An exploratory study of the terrestrial biogeochemical silicon cycle at a forested watershed in northern Vermont: Master's Thesis, 128 p.

Goldschmidt, V., 1958, *Geochemistry*, Oxford University Press: London.

Graham, C., and Lin, H., 2011, Controls and frequency of preferential flow occurrence: A 175-event analysis: *Vadose Zone Journal*, v. 10, p. 816-831.

Herndon E., Jin, L., and Brantley S., 2011, Soils reveal widespread manganese enrichment from industrial inputs: *Environmental Science & Technology*, v. 45, p. 241–247.

Jarvis, N., 2007, A review of non-equilibrium water flow and solute transport in soil macropores: principles, controlling factors and consequences for water quality: *European Journal of Soil Science*, v. 58, p. 523-546.

Jin L., Ravella R., Ketchum B., Bierman P., Heaney P., White T., and Brantley S., 2010, Mineral weathering and elemental transport during hillslope evolution at the Susquehanna/Shale

Hills Critical Zone Observatory: *Geochimica et Cosmochimica Acta*, v. 74, p. 3669–3691.

Jin, L., Rother, G., Cole, D., Mildner, D., Duffy, C., and Brantley, S., 2011a, Characterization of deep weathering and nanoporosity development in shale – A neutron study: *American Mineralogist*, v. 96, p. 498-512.

Jin L., Andrews, D., Holmes, G., Lin, H., and Brantley, S., 2011b, Opening the “Black Box”: Water Chemistry Reveals Hydrological Controls on Weathering in the Susquehanna Shale Hills Critical Zone Observatory: *Vadose Zone Journal*, v. 10, p. 928-942.

Jin, L., Ogrinc, N., Yesavage, T., Hasenmueller, E., Ma, L., Sullivan, P., Kaye, J., Duffy, C., Brantley, S., 2014, The CO₂ consumption potential during gray shale weathering: Insights from the evolution of carbon isotopes in the Susquehanna Shale Hills critical zone observatory: *Geochimica et Cosmochimica Acta*, v. 142, p. 260-280.

Jin L., and Brantley S., 2011, Soil chemistry and shale weathering on a hillslope influenced by convergent hydrologic flow regime at the Susquehanna/Shale Hills Critical Zone Observatory: *Applied Geochemistry*, v. 26, p. S51–S56.

Jones, L., and Handreck, K., 1965, Studies of silica in the oat plant. III. Uptake of silica from soils by plant: *Plant and Soil*, v. 23, p. 79-96.

Kennedy, M., Hedin, L., and Derry, L., 2002, Decoupling of unpolluted temperate forests from rock nutrient sources revealed by natural ⁸⁷Sr/⁸⁶Sr and ⁸⁴Sr tracer addition: *PNAS*, v. 15, p. 9639-9644.

Kirby, M., 1978, *Hillslope Hydrology*: John Wiley and Sons, Chichester, UK.

Kump, L., Brantley, S., and Arthur, M., 2000, Chemical weathering, atmospheric CO₂, and climate: *Annual Review of Earth and Planetary Sciences*, v. 28, p. 611-667.

Kuntz, B., Rubin, S., Berkowitz, B., and Singha, K., 2011, Quantifying solute transport at the

Shale Hills Critical Zone Observatory: *Vadose Zone Journal*, v. 10, p. 843–857.

Kurtz, A., Derry, L., and Chadwick, O., 2002, Germanium-silicon fractionation in the weathering environment: *Geochimica et Cosmochimica Acta*, v. 66, p. 1525-1537.

Liermann, L., Mathur, R., Wasylenki, L., Nuester, J., Anbar, A., and Brantley, S., 2011, Extent and isotopic composition of Fe and Mo release from two Pennsylvania shales in the presence of organic ligands and bacteria: *Chemical Geology*, v. 281, p. 167-180.

Lin, H., 2006, Temporal stability of soil moisture spatial pattern and subsurface preferential flow pathways in the Shale Hills catchment: *Vadose Zone Journal*, v. 5, p. 317-340.

Lin, H., Kogelmann, W., Walker, C., and Bruns, M., 2006, Soil moisture patterns in a forested catchment: A hydrogeological perspective: *Geoderma*, v. 131, p. 345-368.

Lin, H., and Zhou X., 2008, Evidence of subsurface preferential flow using soil hydrologic monitoring in the Shale Hills catchment: *European Journal of Soil Science*, v. 59, p. 34-49.

Lucas, Y., 2001, The role of plants in controlling rates and products of weathering: Importance of biological pumping: *Annual Review of Earth and Planetary Sciences*, v. 29, p. 135-163.

Lugolobi, F., Kurtz, A., and Derry, L., 2010, Germanium-silicon fractionation in a tropical, granitic weathering environment: *Geochimica et Cosmochimica Acta*, v. 74, p. 1294-1308.

Lynch, J., 1976, Effects of antecedent soil moisture on storm hydrographs: Dissertation, The Pennsylvania State University, 141 p.

Ma, J., and Yamaji, N., 2006, Silicon uptake and accumulation in higher plants: *Trends in Plant Science*, v. 11, p. 392-397.

Ma, J., Yamaji, N., Mitani, N., Tamai, K., Konishi, S., Fujiwara, T., Katsuhara, M., and Yano, M., 2007, An efflux transporter of silicon in rice: *Nature*, v. 448, p. 209-212.

Ma, L., Chabaux, F., Pelt, E., Blaes, E., Jin, L., and Brantley, S., 2010, Regolith production rates calculated with uranium-series isotopes at Susquehanna/Shale Hills Critical Zone Observatory: *Earth and Planetary Science Letters*, v. 297, p. 211-225.

Ma, L., Jin, L., and Brantley, S., 2011a, Geochemical behaviors of different element groups during shale weathering at the Susquehanna/Shale Hills Critical Zone Observatory: *Applied Geochemistry*, v. 26, p. S89-S93.

Ma, L., Jin, L., and Brantley, S., 2011b, How mineralogy and slope aspect affect REE release and fractionation during shale weathering in the Susquehanna/Shale Hills Critical Zone

Observatory: Chemical Geology, v. 290, p. 31-49.

Martin, F., Ildefonse, P., Hazemann, J., Petit, S., Grauby, O., and Decarreau, A., 1996, Random distribution of Ge and Si in synthetic talc: an EXAFS and FTIR study: *European Journal of Mineralogy*, v. 8, p. 289-299.

Marschner, P., 2012, *Mineral Nutrition of Higher Plants*, 3rd Edition: Academic Press, London.

McDonnell, J., 1990, A rationale for old water discharge through macropores in a steep, humid catchment: *Water Resources Research*, v. 26, p. 2821-2832.

McLaughlin, S., and Wimmer, R., 1999, Calcium physiology and terrestrial ecosystem processes: *New Phytologist*, v. 142, p. 373-417.

Meinzer, F., Woodruff, D., Eissenstat, D., Lin, H., Adams, T., and McCulloh, K., 2013, Above- and belowground controls on water use by trees of different wood types in an eastern US deciduous forest: *Tree Physiology*, v. 33, p. 345-356.

Miller, E., Blum, J., and Friedland, A., 1993, Determination of soil exchangeable cation loss and weathering rates using Sr isotopes: *Nature*, v. 362, p. 438-441.

Miller, S., Sak, R., Kirby, E., and Bierman, P., 2013, Neogene rejuvenation of central Appalachian topography: Evidence for differential rock uplift from stream profiles and erosion rates: *Earth and Planetary Science Letters*, v. 369, p. 1-12.

Mitani, N., and Ma, J., 2005, Uptake system of silicon in different plant species: *Journal of Experimental Botany*, v. 56, p. 1255-1261.

Murnane, R., and Stallard, R., 1990, Germanium and silicon in rivers of the Orinoco drainage basin: *Nature*, v. 344, p. 749-752.

Naithani, K., Baldwin, D., Gaines, K., Lin, H., and Eissenstat, D., 2013, Spatial distribution of tree species governs the spatio-temporal interaction of leaf area index and soil moisture across a forested landscape: *PLoS ONE*, v. 8, p. 1-12.

National Atmospheric Deposition Program (NADP), 2013, Seasonal Precipitation-Weighted Mean Concentrations for PA-15. Retrieved from <http://nadp.sws.uiuc.edu>.

National Oceanographic and Atmospheric Administration (NOAA), 2007, U.S. divisional and station climatic data and normals: Asheville, North Carolina, U.S. Department of Commerce, National Oceanic and Atmospheric Administration, National Environmental Satellite Data and Information Service, National Climatic Data Center. Retrieved from <http://cdo.ncdc.noaa.gov/CDO/cdo>.

National Research Council, 1997, *Watershed Research in the U.S. Geological Survey*, The National Academies Press: Washington.

Pett-Ridge, J., Derry, L., and Barrows, J., 2009, Ca/Sr and $^{87}\text{Sr}/^{86}\text{Sr}$ ratios as tracers of Ca and Sr cycling in the Rio Icacos watershed, Luquillo Mountains, Puerto Rico: *Chemical Geology*, v.267, p. 32-45.

Poszwa, A., Dambrine, E., Pollier, B., and Atteia, O., 2000, A comparison between Ca and Sr cycling in forest ecosystems: *Plant and Soil*, v. 225, p. 299-310.

Raven, J., 1983, The transport and function of silicon in plants: *Biological Reviews*, v. 58, p. 179-207.

Raven, J., 2003, Cycling silicon – the role of accumulation in plants: *New Phytologist*, v. 158, p. 419-421.

Scribner, A., Kurtz, A., and Chadwick, O., 2006, Germanium sequestration by soil: Targeting the roles of secondary clays and Fe-oxyhydroxides: *Earth and Planetary Science Letters*, v. 243, p. 760-770.

Shannon, R., 1976, Revised effective ionic radii and systematic studies of interatomic distances in halides and chalcogenides: *Acta Crystallographica Section A*, v. 32, p. 751-767.

Sparks, J., Chandra, S., Derry, L., Parthasarathy, M. Daugherty, C., and Griffin, R., 2010, Subcellular localization of silicon and germanium in grass root and leaf tissues by SIMS: evidence for differential and active transport: *Biogeochemistry*, v. 104, p. 237-249.

Stewart, B., Capo, R., and Chadwick, O., 1998, Quantitative strontium isotope models for weathering, pedogenesis, and biogeochemical cycling: *Geoderma*, v. 82, p. 173-195.

Susquehanna River Basin Commission, 2006, The Pennsylvania Geospatial Data Clearinghouse – Subbasins of the Susquehanna River Basin. Retrieved from <http://www.pasda.psu.edu/uci/MapService.aspx?Dataset=512>.

Takagi, K., and Lin, H., 2012, Changing controls of soil moisture spatial organization in the Shale Hills Catchment: *Geoderma*, v. 173-174, p. 289-302.

Thomas, E., Lin, H., Duffy, C., Sullivan, P., Holmes, G., Brantley, S., Jin, L., 2013, Spatiotemporal patterns of water stable isotope compositions at the Shale Hills Critical Zone Observatory: Linkages to subsurface hydrologic processes: *Vadose Zone Journal*, v. 12, p. 1-16.

Thomas, E., 2013, Spatial and temporal patterns of water stable isotope compositions at the Susquehanna-Shale Hills Critical Zone Observatory: Master's Thesis, The Pennsylvania State University, 104 p.

Watmough, A., and Dillon, P., 2003, Calcium losses from a forested catchment in South-Central Ontario, Canada: *Environmental Science and Technology*, v. 37, p. 3085-3089.

West, N., Kirby, E., Bierman, P., Rood, D., 2011, Preliminary estimates of regolith generation and mobility in the Susquehanna Shale Hills Critical Zone Observatory, Pennsylvania, using meteoric ^{10}Be : *Applied Geochemistry*, v. 26, p. S146-S148.

Whipkey, R., 1965, Subsurface stormwater from forested slopes: *Bulletin of the International Association of Hydrological Sciences*, v. 10, p. 74-85.

White, P., 2001, The pathways of calcium movement to the xylem: *Journal of Experimental Botany*, v. 52, p. 891-899.

White, P., and Broadley, M., 2003, Calcium in plants: *Annals of Botany*, v. 92, p. 487-511.

Wubbels, J., 2010, Tree species distribution in relation to stem hydraulic traits and soil moisture in a mixed hardwood forest in central Pennsylvania: Master's Thesis, The Pennsylvania State University, 39 p.

Yamaji, N., Mitani, N., and Ma, J., 2008, A transporter regulating silicon distribution in rice shoots: *Plant Cell*, v. 20, p. 1381-1389.

Zhang, J, Lin, H., and Doolittle, J., 2014, Soil layering and preferential flow impacts on seasonal changes of GPR signals in two contrasting soils: *Geoderma*, v. 213, p. 560-569.

CHAPTER TWO

⁸⁷SR/⁸⁶SR AND CA/SR RATIOS AS TRACERS OF SOLUTE SOURCES AT THE SUSQUEHANNA SHALE HILLS CRITICAL ZONE OBSERVATORY

1. Introduction

Strontium isotopes have widely been used as tracers in catchment studies involving weathering and solute transport (Aberg et al., 1989; Clow et al., 1997; Jacobson et al., 2002; Derry et al., 2006; Shand et al., 2009; Chadwick et al., 2009). Four natural isotopes of strontium exist: the non-radiogenic ⁸⁴Sr, ⁸⁶Sr, and ⁸⁸Sr isotopes occur in relatively constant proportions, while the radiogenic ⁸⁷Sr isotope is added to reservoirs over geologic time through the radioactive decay of ⁸⁷Rb (Stewart et al., 1998). In general, Rb-rich rocks such as shales have relatively high ⁸⁷Sr/⁸⁶Sr ratios, while Rb-poor rocks such as carbonates display significantly lower strontium isotope signatures (Capo et al., 1998). Unlike major elements, strontium isotopes exhibit negligible fractionation during biogeochemical processes (e.g. mineral dissolution and precipitation, evapotranspiration, biological uptake, etc.) which make them conservative tracers for the investigation of solute source materials, flow pathways, and mixing processes in watersheds (Bain and Bacon, 1994; Aberg, 1995; Kennedy et al., 1998; Hogan and Blum, 2002; Shand et al., 2007). In fact, mass dependent fractionation is eliminated by normalizing the radiogenic ⁸⁷Sr/⁸⁶Sr ratio to the non-radiogenic ⁸⁶Sr/⁸⁸Sr ratio of 0.1194 (Capo et al, 1998). Consequently, strontium isotope ratios can provide an indication of source contributions to various reservoirs within a catchment with each source displaying a distinctive ⁸⁷Sr/⁸⁶Sr ratio to a high degree of analytical precision.

The ⁸⁷Sr/⁸⁶Sr ratios of reservoir components reveal sources of strontium available during their formation. Relative proportions of strontium in various reservoirs can be determined

through mixing calculations provided that the isotope compositions for selected end-members (e.g. atmospheric or weathering) are distinct and measured isotope compositions of the mixture are contained within the bounds established by these end-members. Exchangeable soil and soil porewater $^{87}\text{Sr}/^{86}\text{Sr}$ ratios reflect a mixture of atmospheric and mineral weathering sources (Miller et al., 1993; Vitousek et al., 1999; Drouet et al., 2005; Pett-Ridge et al., 2009; Chadwick et al., 2009). Likewise, strontium isotope compositions of vegetation reflect a mixture of these sources as solutes in vegetation are generally extracted from soil exchange pool and soil porewater sources (Bailey et al., 1996; Blum et al., 2002; Kennedy et al., 2002; Poszwa et al., 2004; Belanger et al., 2012). A groundwater's $^{87}\text{Sr}/^{86}\text{Sr}$ ratio will closely resemble isotope compositions in underlying rocks or soil minerals and is dependent upon their relative abundances, weathering rates, and strontium concentrations (Aberg et al., 1989; Hogan et al., 2000; Negrel and Lachassagne, 2000; Negrel et al., 2004; Shand et al., 2009). Furthermore, streamwaters integrate atmospheric deposition, mineral weathering, throughfall, and groundwater strontium sources with stream discharge playing a significant role in determining which source or mixture of sources will largely influence a streamwater's isotope signature (Bain et al., 1998; Land et al., 2000; McNutt et al., 2000; Aubert et al., 2002; Hogan and Blum, 2002). The strontium isotope ratio of atmospheric deposition is largely reflective of ocean water but is oftentimes altered by contributions from biological materials or dust derived from geological sources (Graustein and Armstrong, 1983; Andersson et al., 1990; Bailey et al., 1996; Negrel and Roy, 1998).

Calcium is an essential macronutrient involved in several important plant functions including cell wall stabilization, stomatal regulation, and intercellular signaling (McLaughlin and Wimmer, 1999; White and Broadley, 2003; Marschner, 2012). Calcium transport through the

xylem largely occurs via passive mechanisms through apoplastic (e.g. through cell walls and intercellular spaces) or symplastic (e.g. through the plasmodesmata) pathways which have been shown to be heavily influenced by levels of plant transpiration (Clarkson, 1984; McLaughlin and Wimmer, 1999; White, 2001; White et al., 2002; White and Broadley, 2003; Marschner, 2012). As an immobile element, calcium cannot be retranslocated to other plant tissues once it has been assimilated into leaf tissue (McLaughlin and Wimmer, 1999; Marschner, 2012). In route through the xylem from root to leaf tissues, divalent cations (e.g. calcium and strontium) are involved in cation exchange reactions at negatively charged sites on cell walls of xylem vessels and surrounding tissues (Marschner, 2012). Strontium is oftentimes retained by cation exchange sites to a greater degree than calcium where increased translocation of calcium relative to strontium is observed in foliage (Veresoglou et al., 1996; Poszwa et al., 2000; Dasch et al., 2006; Blum et al., 2008, 2012; Pett-Ridge, 2009; Funk and Amantangelo, 2013). However, heterogeneity in the distribution and availability of calcium in forest floor (Bullen and Bailey, 2005) and/or soil reservoirs (Dasch et al., 2006) may be affecting the access of calcium to plants at the catchment. Consequently, passive tracers such as strontium isotopes can provide an indication of sources from which plants are acquiring strontium (and by inference, calcium). In particular, similar chemical properties such as ionic radius ($r_{Sr}/r_{Ca} = 1.13$), charge, and electron configuration enable the use of strontium as a proxy for calcium in watershed studies (Elias et al., 1982; Jacks et al., 1989). It should be noted that, although several studies have employed the use of strontium as a tracer for calcium, others have suggested that calcium and strontium cycling may differ in soils and plants (Poszwa et al., 2000; Watmough and Dillon, 2003). As a consequence, recent studies (Dasch et al., 2006; Drouet and Herbauts, 2008; Blum et al., 2012; Lucash et al., 2012; Watmough, 2014) have incorporated discrimination factors into budget estimates where

elemental ratios of calcium and strontium are adjusted between soil components and plant tissues across tree species.

In this chapter, $^{87}\text{Sr}/^{86}\text{Sr}$ and Ca/Sr ratios are used to identify atmospheric versus weathering derived sources of solutes in exchangeable soils, soil porewaters, leaves, sap waters, groundwaters, and streamwaters at the Susquehanna Shale Hills Critical Zone Observatory (SSHCZO). Spatio-temporal patterns in Ca/Sr and $^{87}\text{Sr}/^{86}\text{Sr}$ ratios are assessed and inferences are developed on solute source contributions to various reservoirs using compiled data in conjunction with mineralogical observations (Jin et al., 2010; Ma et al., 2010; Jin et al., 2011a, 2011b, 2014; Jin and Brantley, 2011; Ma et al., 2011a, 2011b; Brantley et al., 2013), proposed preferential flow pathways (Lin, 2006; Lin et al., 2006; Lin and Zhou, 2008; Graham and Lin, 2011; Jin et al., 2011b; Takagi and Lin, 2012; Thomas, 2013; Zhang et al., 2014), and calcium transport mechanisms in plants (Clarkson, 1984; McLaughlin and Wimmer, 1999; White, 2001; White et al., 2002; White and Broadley, 2003; Marschner, 2012) at the catchment.

2. Procedural Methods

2.1 Waters

Soil porewaters (n=159) were sampled from nested suction cup lysimeters installed at southern planar and south swale ridge top, mid slope, and valley floor locations of the SSHCZO in May to July of 2013 (Figure 1.2). At southern planar and south swale ridge top locations, soil porewaters were sampled in 10 cm intervals from depths ranging from 10 to 30 cm. Southern planar mid slope soil porewaters were sampled at depths of 10, 40, and 50 cm, while south swale mid slope soil porewaters were sampled at depths of 10, 20, 40, 60, 80, 100, 120, 140, and 160 cm. For southern planar and south swale valley floor sites, soil porewaters were sampled in 10 cm depth intervals ranging from 20 to 60 cm and from 10 to 90 cm, respectively.

Streamwater grab samples were collected from weir, mid stream, and stream headwater locations in October of 2013 (Figure 1.2). Groundwaters were also sampled at this time from boreholes at depths of 91 (CZMW 1) and 849 cm (CZMW 6) from the top of the casing to the water table and from wells at depths of 230 (Well 8), 478 (Well 11), and 276 cm (Well 13) from the top of the casing to the water table (Figure 1.2).

Xylem sap waters (n=61) were derived from three tree species (*Acer saccharum*, ACSA–sugar maple; *Quercus prinus*, QUPR – chestnut oak; and *Quercus rubra*, QURU– red oak) representing 50% of all surveyed trees at the SSHCZO (Wubbels, 2010). Xylem sap water was collected in July to September of 2013 from sugar maple, chestnut oak, and red oak trees at mid slope positions in northeastern, southeastern, northwestern, and southwestern quadrants of the catchment (Figure 1.2). Specifically, sap water was extracted by means of a PMS pressure chamber. Small leafy branches were placed inside the pressure chamber with only the cut end protruding from the chamber. Pressure was increased inside the chamber using nitrogen gas (N₂) which forced sap water out of the cut end of the branch. To dissolve organic matter, sap water was treated with hydrogen peroxide (H₂O₂, 30%) in a 5:1 ratio (e.g. 5 mL sap water to 1 mL H₂O₂) and gently heated.

Soil porewater, streamwater, groundwater, and sap water samples were filtered using 0.45 µm Nylon syringe filters and acidified with a few drops of ultra pure concentrated nitric acid (HNO₃). Calcium (Ca) and strontium (Sr) concentrations were measured on a SPECTROBLUE inductively coupled plasma optical emission spectrometer (ICP-OES) with typical analytical uncertainties of 5% or less.

For Sr isotope analyses, filtered and acidified soil porewater, streamwater, and groundwater sample aliquots containing volumes ranging from 20 to 50 mL were evaporated to

between 2 and 5 mL, respectively. For all water samples, approximately 1 mL of sample was passed through 0.1 g of Eichrom Sr-Spec resin, rinsed with HNO₃ (3N) and eluted with quartz distilled (QD) water. The eluted volume was evaporated until dry and redissolved in 5 μL of hydrochloric acid (HCl, 2.5N) with 1 μL of sample placed on a tungsten filament containing 1 μL of tantalum fluoride (TaF₅). Sr isotope ratios were measured on a VG Sector 54 thermal ionization mass spectrometer (TIMS) and Sr isotopic compositions were corrected for mass fractionation where $^{86}\text{Sr}/^{88}\text{Sr} = 0.1194$. Analyses of NBS-987 standard yielded an average $^{87}\text{Sr}/^{86}\text{Sr} = 0.71023$. The 2σ uncertainties for the isotopic data based on repeat analyses of standards ranged between 0.00002 and 0.00005.

2.2 Soils

Soil samples (n=19) derived from ridge top, mid slope, and valley floor sites of the southern planar transect were hand augered until the point of refusal (e.g. depth at which hand augering is no longer physically possible) in October of 2011 (Figure 1.2). Soil samples were collected from each horizon at all southern planar sites, sealed in Ziploc bags, and stored at field moisture conditions of 4°C until analysis. Zero depth was defined as the bottom of the organic layer or, alternatively, the top of the mineral soil. The organic horizon was collected by hand from the surface of the soil. Mid points of depth ranges were used to describe average soil depths for each horizon interval.

Exchangeable cations were extracted from soil samples by combining approximately 10 grams of air dried soil pulverized to pass through a #10 mesh sieve (<2 mm) with 50 mL of 0.5 M ammonium acetate (NH₄OAc). The resultant mixture was equilibrated for ~30 minutes on a shaker table and then centrifuged at 3000 rpm for ~10 minutes. Supernatant was collected and filtered using 0.45 μm Nylon syringe filters. Sodium hydroxide (NaOH) was added in 1 mL

increments to supernatant in order to increase the solution pH to 9. The solution was then heated for ~30 minutes to drive off ammonia (NH₃). HNO₃ (3N) was subsequently added and the solution was heated again until it was nearly dry. A 5:1 mixture of HNO₃ (3N) and H₂O₂ (30%) was added to the solution where it was reheated until it was completely dry and then redissolved in HNO₃ (2%) for major element and Sr isotope analyses. Elemental Ca and Sr analyses were performed on the ICP-OES with typical analytical uncertainties of 5% or less. For Sr isotope analyses, the Sr separation and loading procedure described earlier for waters was applied to the exchangeable soil solutions. Sr isotope ratios were measured through TIMS and Sr isotopic compositions were corrected for mass fractionation where $^{86}\text{Sr}/^{88}\text{Sr} = 0.1194$. Analyses of NBS-987 standard yielded an average $^{87}\text{Sr}/^{86}\text{Sr} = 0.71023$. The 2σ uncertainties for the isotopic data based on repeat analyses of standards ranged between 0.00002 and 0.00005.

2.3 Leaves

Upper canopy leaves (n=72) were sampled from sugar maple, chestnut oak, and red oak trees at ridge top, mid slope, and valley floor sites in the northeastern quadrant of the catchment from June to September of 2011 (Figure 1.2). Upper canopy leaves from the same three tree species were resampled at mid slope positions in northeastern, southeastern, northwestern, and southwestern quadrants of the catchment from June to September of 2013 (Figure 1.2). Leaves were obtained by rope climbing trees and using a pole cutter to remove a section of the tree branch. The leaves were subsequently placed in coin envelopes, transferred to the laboratory, and immediately air-dried to prevent decomposition.

Air-dried leaves were powdered using a coffee grinder. A leaf digestion method modified from Parr et al. (2001) was utilized where HNO₃ (3N) and H₂O₂ (30%) were added in a 9:1 ratio to between 0.42998 and 0.50664 grams of powdered leaf weighed inside a Teflon reaction

vessel. Vessels were left uncovered for approximately 10 minutes until bubbling from the reaction had ended and then recapped before being placed into the Milestone Ethos microwave digestion system. The digestion program was set to ramp the solution temperature to 180°C within each vessel over a period of five minutes, remaining at this temperature for another ten minutes to complete the digestion. After cooling to 21°C, vessel contents were transferred into vials for future analyses. Samples were diluted by a factor of 5 to 10 with HNO₃ (2%) for elemental Ca and Sr analyses which were performed on the ICP-OES with typical analytical uncertainties of 5% or less. For Sr isotope analyses, the Sr separation and loading procedure described earlier for waters was applied to the diluted samples. Sr isotope ratios were measured through TIMS and Sr isotopic compositions were corrected for mass fractionation where $^{86}\text{Sr}/^{88}\text{Sr} = 0.1194$. Analyses of NBS-987 standard yielded an average $^{87}\text{Sr}/^{86}\text{Sr} = 0.71023$. The 2σ uncertainties for the isotopic data based on repeat analyses of standards ranged between 0.00002 and 0.00005.

2.4 Drill Core

Rock chips and powders (n=12) were derived from a ridge top borehole in the northern quadrant of the catchment (DC 1) and from the CZMW 2 borehole near the stream's weir (DC 3) (Figure 1.2) in May of 2014. Boreholes were drilled using a direct rotary air drill to depths of 25 m at DC 1 (Jin et al., 2010) and 16 m at DC 3 (Kuntz et al., 2011). Bulk samples consisting of rock fragments and granular powder were pulverized to pass through a 100 mesh sieve (<150 μm) and further ground to a fine powder using a mortar and pestle.

Carbonate and silicate fractions of borehole powders were extracted using a buffered ammonium acetate (NaOAc)/acetic acid (HOAc) leach and a hydrofluoric acid (HF)/nitric acid (HNO₃) digestion, respectively. Specifically, the carbonate fraction was extracted by combining

between 2.00047 and 2.01546 g of borehole powder with 20 mL of buffered NaOAc/HOAc solution. The resultant mixture was allowed to equilibrate overnight. To complete the dissolution, glacial acetic acid was added in 1 mL increments to each solution until bubbling from the reaction had ended. The resultant mixture was buffered to a pH between 4 and 5 with the NaOAc/HOAc solution, then equilibrated for approximately 5 minutes on a shaker table, and finally centrifuged at 3000 rpm for 20 minutes. Supernatant was collected and filtered using 0.45 μm Nylon syringe filters. To remove colloidal material, 1 mL of NaOAc (0.5 M) was added to samples which were subsequently centrifuged at 3000 rpm for 20 minutes. Supernatant was then collected and filtered using 0.45 μm Nylon syringe filters. Samples were dried completely and redissolved in HNO_3 (2%) for major element and strontium isotope analyses. Following the NaOAc/HOAc leach, samples were dried in an oven set at 130 $^\circ\text{C}$ and then ashed for 30 minutes at 600 $^\circ\text{C}$ in a muffle furnace to further oxidize any organic material. Subsamples (0.09101 to 0.09997 g) were digested in a 3 to 1 ratio of concentrated HF to concentrated HNO_3 with a few drops of perchloric acid (HClO_4) added to remove any residual fluorides. The subsamples were dried completely and redissolved in HNO_3 (2%) and hydrochloric acid (HCl , 2.5 N) for major element and strontium isotope analyses, respectively.

Elemental Ca and Sr analyses were performed on the ICP-OES with typical analytical uncertainties of 5% or less. For Sr isotope analyses, the Sr separation procedure described earlier for waters was applied to the carbonate fraction. For the silicate fraction, approximately 1 mL of sample was passed through AG-50-X8 resin, prewashed with HCl (6N) and backwashed, conditioned, and eluted with HCl (2.5N). The eluted volume was evaporated until dry. The Sr loading procedure described earlier for waters was applied to both carbonate and silicate fractions of drill core samples. Sr isotope ratios were measured through TIMS and Sr isotopic

compositions were corrected for mass fractionation where $^{86}\text{Sr}/^{88}\text{Sr} = 0.1194$. Analyses of NBS-987 standard yielded an average $^{87}\text{Sr}/^{86}\text{Sr} = 0.71023$. The 2σ uncertainties for the isotopic data based on repeat analyses of standards ranged between 0.00002 and 0.00005.

3. Data Analysis Methods

3.1 Strontium Mixing Calculations

Ridge Top and Mid Slope Exchangeable Soils and Soil Porewaters

Proportions of strontium derived from atmospheric and silicate mineral weathering end-members in ridge top and mid slope exchangeable soils and soil porewaters were calculated using a two-component mixing equation (Capo et al., 1998) where $X(\text{Sr})_{\text{Atmosphere}}$ reflects the mass fraction of strontium derived from the atmosphere as shown below in Equation 1:

$$X(\text{Sr})_{\text{Atmosphere}} = \frac{\left(\frac{^{87}\text{Sr}}{^{86}\text{Sr}}\right)_{\text{Exchangeable Soil or Soil Porewater}} - \left(\frac{^{87}\text{Sr}}{^{86}\text{Sr}}\right)_{\text{Silicate Weathering}}}{\left(\frac{^{87}\text{Sr}}{^{86}\text{Sr}}\right)_{\text{Atmosphere}} - \left(\frac{^{87}\text{Sr}}{^{86}\text{Sr}}\right)_{\text{Silicate Weathering}}} \quad (\text{Equation 1})$$

The carbonate weathering front at the ridge is hypothesized to initiate at a depth of ~2200 cm (Jin et al., 2010; Jin et al., 2011a; Brantley et al., 2013). This depth lies well below those of deep southern planar and south swale ridge top exchangeable soils and soil porewaters (30 cm), deep southern planar mid slope exchangeable soils and soil porewaters (60 cm), and deep south swale mid slope soil porewaters (160 cm) sampled at the catchment. Consequently, effects of carbonate dissolution processes on strontium concentrations and strontium isotope compositions in ridge top and mid slope exchangeable soils and soil porewaters are expected to be minimal and these reservoir components were modeled through two component mixing using atmospheric and silicate weathering end-members.

The average $^{87}\text{Sr}/^{86}\text{Sr}$ ratio for bulk precipitation at Penn State ($^{87}\text{Sr}/^{86}\text{Sr} = 0.71054$, Kim, 2005) was chosen as the atmospheric end-member. This value is similar to those reported by

other researchers for precipitation in the northeastern United States (Dasch, 1969; Miller et al., 1993; Bailey et al., 1996; Dijkstra et al., 2003) where the strontium isotope composition in precipitation has been shown to be relatively uniform over time. The $^{87}\text{Sr}/^{86}\text{Sr}$ ratio in bulk precipitation is slightly higher than the ratio reported for ocean water with deviation likely reflecting minor contributions to precipitation from soluble mineral dust and biological materials. In a silicate dominated terrain such as Shale Hills, the solubility of biological materials in dust is greater than that of minerals with the consequence that biological materials significantly influence atmospheric strontium concentrations and strontium isotope compositions (Bailey et al., 1996). Additionally, as will be discussed in detail later, results from mixing calculations (Figures 2.14 and 2.15) suggest that leaf and sap water strontium isotope compositions were greatly affected by underlying geological substrate. Accordingly, strontium contributions to precipitation from biomass and dust derived from geological sources are expected to be rather similar. Consequently, if bulk precipitation is modeled using a two-component mixing calculation with average $^{87}\text{Sr}/^{86}\text{Sr}$ ratios for ocean water ($^{87}\text{Sr}/^{86}\text{Sr} = 0.7092$, Hess et al., 1986) and leaves and sap waters ($^{87}\text{Sr}/^{86}\text{Sr} = 0.72311$, Tables 2.9 and 2.16) as end-members, then a 10% strontium contribution from biological materials is determined in bulk precipitation.

Traditionally, the weathering end-member is defined by the strontium isotope composition of minerals in rocks and soils, with each mineral displaying a distinctive weathering rate and $^{87}\text{Sr}/^{86}\text{Sr}$ ratio. Spatial variability in the mineralogical composition of the weathered substrate and temporal variability in the weathering rates of individual minerals both directly affect the strontium isotope composition in exchangeable soils and soil porewaters. In this study, the fine grain nature of shales (Jin et al., 2006) and soils (Lin et al., 2006) at the catchment precluded identification of strontium isotope compositions for mineral separates in rocks and

soils. Instead, the average $^{87}\text{Sr}/^{86}\text{Sr}$ ratio for “weathered shale” ($^{87}\text{Sr}/^{86}\text{Sr} = 0.72967$, Table 2.23) was chosen as the silicate weathering end-member. This value was taken as the average value from the carbonate fraction of “carbonate free” DC 1 drill core samples (DC 1-21 to DC 1-36, Table 2.23) where the mild leach procedure applied to extract carbonates should simulate weathering of shale in these samples. Although spatial distance exists between the DC 1 drill core and exchangeable soil and soil porewater sites sampled in the southern quadrant of the catchment (Figure 1.2), Jin et al. (2010) found average compositions of deep, unweathered soils derived from soil cores across the catchment to resemble those of DC 1 drill core samples where standard deviations for major elements ranged from 0.01 to 0.38 weight percent. Furthermore, bulk densities of the deepest soils in soil cores resembled those of shallow DC 1 drill core samples (Jin et al., 2010). Based on these observations, use of “carbonate free” DC 1 drill core $^{87}\text{Sr}/^{86}\text{Sr}$ ratios for determination of the “weathered shale” end-member value seems reasonable. According to the empirical range of $^{87}\text{Sr}/^{86}\text{Sr}$ ratios (Tables 2.1 and 2.3) measured for southern planar ridge top (0.72276 to 0.72494) and mid slope (0.72118 to 0.72493) exchangeable soils and soil porewaters and south swale ridge top (0.72400 to 0.72648) and mid slope (0.72411 to 0.72599) soil porewaters at the catchment, the $^{87}\text{Sr}/^{86}\text{Sr}$ ratio of “weathered shale” ($^{87}\text{Sr}/^{86}\text{Sr} = 0.72967$, Table 2.23) was deemed as a more appropriate choice for the silicate weathering end-member than the average value determined for shale ($^{87}\text{Sr}/^{86}\text{Sr} = 0.74558$, Table 2.24). Lending support for use of “weathered shale” rather than shale as the silicate weathering end-member for ridge top and mid slope exchangeable soils and soil porewaters are observations of their high total chemical weathering rates as calculated based on average soil chemistry, soil density, and soil thickness (Jin et al., 2010), low cation exchange capacities relative to parent drill cores (Jin et al., 2010), and high weathering advance rates as determined through U-series isotopes (Ma et

al., 2010).

As mineral separates were not analyzed in this study, it is difficult to assess the relative contributions of specific minerals to the strontium isotope signature of the “weathered shale” end-member. However, hypotheses can be made based on mineralogical observations established in previous studies at Shale Hills. Major, trace, and rare earth element studies (Jin et al., 2010; Jin and Brantley, 2011; Ma et al., 2011a; Ma et al., 2011b) have interpreted calcium and strontium loss from parent material and bulk soils as the result of feldspar (e.g. plagioclase) dissolution processes. Chips collected from southern quadrant ridge top and mid slope soil cores show depletion relative to drill core shale chips with respect to sodium and calcium (Jin et al., 2010). However, no such depletion was observed for potassium, magnesium, aluminum, and iron (Jin et al., 2010), suggestive of the procession of feldspar dissolution before clay mineral weathering. Significantly positive europium (Eu) anomalies observed in natural waters ($(Eu/Eu^*)_N$ as high as 1.71) and exchangeable pools ($(Eu/Eu^*)_N$ as high as 2.52) at Shale Hills (Ma et al., 2011a; Ma et al., 2011b) also lend support to this hypothesis as Eu-enriched minerals such as plagioclase feldspars are known to preferentially dissolve during chemical weathering (McLennan, 1989; Leybourne and Johannesson, 2008). Despite low feldspar contents present in bulk soils at the catchment (between 1.2 and 6.6 wt%, Jin et al., 2010), preferential weathering during soil forming processes of calcium and strontium enriched minerals with low $^{87}Sr/^{86}Sr$ ratios (e.g. plagioclase feldspar) has been shown to be important in determining a soil’s strontium isotope composition (Aberg et al. 1989; Bain and Bacon, 1994; Bailey et al., 1996; Drouet et al., 2005). In general, feldspars are less radiogenic than illites and bulk shales (Faure and Mensing, 2005). Removal of feldspar through weathering would, therefore, be expected to increase the strontium isotope composition of the “weathered shale” end-member relative to the

shale end-member which was not observed in this study. Thus, it is hypothesized that the lower $^{87}\text{Sr}/^{86}\text{Sr}$ ratio of the “weathered shale” end-member compared to the shale end-member is the result of leaching of less radiogenic strontium from feldspar dissolution processes at interlayer and adsorption sites of clay minerals (e.g. illites and chlorites) which are known to dominate the mineralogy of shales at the catchment according to quantitative x-ray diffraction (XRD) patterns (69 wt %, Jin et al., 2010). To this end, the less radiogenic isotope signature of feldspar would be incorporated into the “weathered shale” end-member through exchange reactions with more radiogenic clay minerals at interlayer and adsorption sites. Additionally, as mentioned previously, the “weathered shale” end-member was determined using $^{87}\text{Sr}/^{86}\text{Sr}$ ratios from the carbonate fraction of “carbonate free” DC 1 drill core samples. As discussed in the Procedural Methods section, the carbonate fraction of drill core samples was extracted by means of a combined NaOAc/HOAc leach. This procedure releases carbonates as well as exchangeable cations into solution and, thus, the “weathered shale” end-member should be reflective of the weathering processes described earlier.

Leaves and Sap Waters

Proportions of strontium derived from atmospheric and silicate mineral weathering end-members in leaves sampled at ridge top, mid slope, and valley floor positions of the northeastern quadrant in 2011 and in leaves and sap waters sampled at mid slope positions in all quadrants in 2013 were modeled through two-component mixing (Equation 1). According to Jin et al. (2011b), average rooting depth at Shale Hills is approximately 20 cm; however, trees at valley floor locations of the catchment have been observed to tap water sources at depths of up to 100 cm (Gaines, unpublished data). Additionally, average xylem stem water $\delta^{18}\text{O}$ values (Gregor, unpublished data) for sugar maple ($\delta^{18}\text{O} = -7.59 \text{ ‰}$) and oak ($\delta^{18}\text{O} = -7.65 \text{ ‰}$) trees were found

to more closely resemble underlying shallow soils (Average $\delta^{18}\text{O} = -6.47 \text{ ‰}$ and -6.57 ‰ for shallow soils underlying sugar maple and oak species, respectively, Gregor, unpublished data) than groundwaters (Average $\delta^{18}\text{O} = -8.82 \text{ ‰}$, Thomas, 2013) at the catchment. These observations suggest that the trees analyzed in this study are largely acquiring water (and hence, nutrients) from shallow soil exchange pool and porewater sources. Consequently, leaves and sap waters should be relatively unaffected by carbonate dissolution processes which are hypothesized to initiate at depths of $\sim 2200 \text{ cm}$ and $\sim 200 \text{ cm}$ at ridge top and valley floor locations of the catchment, respectively (Jin et al., 2010; Brantley et al., 2013).

Considering plants are largely deriving solutes from shallow soil exchange pool and soil porewater sources, the same end-members used to calculate atmospheric and weathering derived proportions of strontium in exchangeable soils and soil porewaters were incorporated into mixing calculations for leaves and sap waters. Thus, bulk precipitation ($^{87}\text{Sr}/^{86}\text{Sr} = 0.71054$, Kim, 2005) and “weathered shale” ($^{87}\text{Sr}/^{86}\text{Sr} = 0.72967$, Table 2.23) were used as atmospheric and silicate weathering end-members, respectively. It should be noted that average $^{87}\text{Sr}/^{86}\text{Sr}$ ratios for sugar maple and oak leaves collected at valley floor positions (0.72483 ± 0.00032 and 0.72436 ± 0.00025 , respectively) closely resembled those sampled at ridge top (0.72345 ± 0.00023 and 0.72314 ± 0.00044 , respectively) and mid slope positions (0.72393 ± 0.00016 and 0.72354 ± 0.00023 , respectively) in the northeastern quadrant. Strontium isotope ratios were not measured for north swale valley floor soil porewaters where northeastern leaves were collected. However, strontium isotope ratios for sugar maple and chestnut oak leaves sampled at valley floor positions of this quadrant suggest that the carbonate source affecting chemistry in southern quadrant valley floor exchangeable soils and soil porewaters and in groundwaters and streamwaters is unlikely influencing chemistry in north swale valley floor exchangeable soils or soil porewaters.

According to the topographic map of the SSHCZO (Figure 1.2), north swale valley floor porewaters are located further from the carbonate source at the stream's weir than southern planar and south swale valley floor porewaters. Additionally, the chloride normalized strontium isotope ratio of nearby stream headwaters (Table 2.22), known to be dominated by atmospheric strontium inputs (Figure 2.28), was in close agreement to those determined in sugar maple and chestnut oak leaves sampled at valley floor positions of the northeastern quadrant (Table 2.12). Based on these observations, the same atmospheric and silicate weathering end-members used in calculations for ridge top and mid slope leaves and sap waters were applied to calculations for valley floor leaves in the northeastern quadrant.

It should be noted that strontium mixing calculations were not extended to infer sources of calcium in plants. This was largely due to uncertainty in the degree of fractionation between calcium and strontium during biological uptake and soil exchange processes. As noted by Drouet et al. (2005), application of Sr/Ca ratios in calcium mixing calculations requires an extensive knowledge of fractionation between calcium and strontium during biogeochemical processes where incorporation of discrimination factors are utilized to correct for changes in element ratios between soil components or plant tissues. Additionally, the Sr/Ca ratio of the weathering end-member (Sr/Ca = 0.04415) was found to be roughly an order of magnitude higher than the atmospheric end-member (Sr/Ca= 0.00430) which significantly biased results towards the atmospheric end-member in mixing equations for calcium (Equation 2 in Drouet et al., 2005). Due to these limitations, mixing calculations distinguishing atmospheric versus weathering derived sources of calcium were not performed for vegetation.

Streamwaters and Groundwaters

Significantly lower $^{87}\text{Sr}/^{86}\text{Sr}$ ratios in streamwaters (0.71362 to 0.71758, Table 2.22) and

groundwaters (0.71481 to 0.71746, Table 2.22) relative to ridge top and mid slope exchangeable soils and soil porewaters suggest that a source less radiogenic than shale is affecting strontium concentrations and strontium isotope compositions in streamwaters and groundwaters at the catchment. Relatively alkaline streamwaters and groundwaters with high calcium and magnesium concentrations (Table 2.22, Jin et al., 2011b) compared to those in precipitation, soils, and soil porewaters (Tables 2.1 and 2.3, Jin et al., 2011b) are consistent with the dissolution of carbonates. Carbonate (e.g. ankerite and calcite) has been identified in quantitative XRD patterns in abundances of 1.6 and 7.8 wt % for the deepest samples of the DC 1 ridge top drill core (DC 1-37 and DC 1-38, Jin et al., 2010) and in abundances between 0.4 and 17.3 wt % for all samples collected from the DC 3 valley floor drill core (DC 3-0-1 to DC 3-52-53, Brantley et al., 2013). In general, carbonate dissolution proceeds faster than silicate mineral weathering due to the greater reactivity and solubility of carbonate minerals relative to silicate minerals (MacDonald et al., 1991; White et al., 2005). Thus, even a small amount of carbonate underlying streamwaters and groundwaters at the catchment has the potential of shifting $^{87}\text{Sr}/^{86}\text{Sr}$ signatures to significantly lower values (Land, 2000; Shand et al., 2007, 2009). The average $^{87}\text{Sr}/^{86}\text{Sr}$ ratio for the carbonate fraction of DC 3 drill core samples ($^{87}\text{Sr}/^{86}\text{Sr} = 0.71132$, Table 2.23) was chosen as the carbonate mineral weathering end-member. As shown in the topographic map of the SSHCZO (Figure 1.2), streamwater and groundwater samples were located in closer proximity to DC 3 valley floor drill core samples than DC 1 ridge top drill core samples. Additionally, according to Jin et al. (2010) and Brantley et al. (2013), the carbonate weathering front at the valley floor is hypothesized to initiate at a shallower depth (~200 cm) than at the ridge top (~2200 cm). Thus, it is within reason to propose that carbonates derived from the DC 3 valley floor drill core rather than the DC 1 ridge top drill core are more likely influencing

streamwater and groundwater (depth range: 90 to 850 cm) strontium concentrations and strontium isotope compositions at the catchment.

The average $^{87}\text{Sr}/^{86}\text{Sr}$ ratio for the silicate fraction of DC 1 and DC 3 drill core samples (e.g. shale end-member, $^{87}\text{Sr}/^{86}\text{Sr} = 0.74558$, Table 2.24) was selected as the silicate mineral weathering end-member. As shown in Table 2.24, ranges of $^{87}\text{Sr}/^{86}\text{Sr}$ ratios in residual material were relatively uniform between DC 1 ridge top (0.74143 to 0.74919) and DC 3 valley floor (0.74297 to 0.74834) drill core sites. Thus, a composite average $^{87}\text{Sr}/^{86}\text{Sr}$ ratio using data compiled from both sites for determination of the silicate weathering end-member seems reasonable. The shale rather than “weathered shale” was chosen as the silicate mineral weathering end-member because streamwaters and groundwaters are more likely interacting with parent shale than “weathered shale”. Using average soil chemistry, soil density, and soil thickness, Jin et al. (2010) demonstrated that total chemical weathering processes are slow at valley floor sites where streamwaters and groundwaters are located with accumulation (e.g. Al, Si) and outfluxes (e.g. K, Fe, Mg) of certain elements even observed. Additionally, Ma et al. (2010) noted low weathering advance rates in valley floor soils. Furthermore, C.E.C.s of valley floor soils were comparable to parent materials suggesting that illite and chlorite dissolution processes are insignificant at valley floor sites of the catchment (Jin et al., 2010). As clay minerals are hypothesized to be influencing strontium concentrations and strontium isotope compositions of the “weathered shale” end-member through exchange reactions with feldspars, the shale’s $^{87}\text{Sr}/^{86}\text{Sr}$ ratio was considered a more suitable choice as the silicate mineral weathering end-member in mixing calculations than the “weathered shale’s” value.

Proportions of strontium derived from carbonate and silicate mineral weathering end-members in streamwaters and groundwaters were determined using two-component mixing on

chloride normalized strontium isotope ratios ($(^{87}\text{Sr}/^{86}\text{Sr})^*$). To this end, the mass fraction of strontium derived from the atmosphere ($X(\text{Sr})_{\text{Atmosphere}}$) was corrected for enabling calculation of relative proportions of strontium derived from carbonate and silicate mineral weathering sources through two-component mixing. Calculation of $(^{87}\text{Sr}/^{86}\text{Sr})^*$ was accomplished by first normalizing strontium elemental concentrations ($[\text{Sr}]^*$) using strontium and chloride concentrations measured in precipitation (ppn) and in streamwater (SW) or groundwater (GW) through Equation 2:

$$[\text{Sr}]_{\text{SW or GW}}^* = [\text{Sr}]_{\text{SW or GW}} - \frac{[\text{Sr}]_{\text{ppn}}}{[\text{Cl}]_{\text{ppn}}} \times [\text{Cl}]_{\text{SW or GW}} \quad (\text{Equation 2})$$

The atmospheric strontium contribution ($X(\text{Sr})_{\text{Atmosphere}}$) was then calculated by subtracting the ratio of chloride normalized strontium to measured strontium ($[\text{Sr}]^*/[\text{Sr}]$) in streamwaters and groundwaters from one. In order to calculate $(^{87}\text{Sr}/^{86}\text{Sr})^*$, the atmospheric strontium contribution ($X(\text{Sr})_{\text{Atmosphere}}$) was first multiplied by the average $^{87}\text{Sr}/^{86}\text{Sr}$ ratio for bulk precipitation and then subtracted from the $^{87}\text{Sr}/^{86}\text{Sr}$ ratio measured for a given streamwater (SW) or groundwater (GW) sample. This value was then divided by the ratio of chloride normalized strontium to measured strontium in a designated streamwater or groundwater sample as shown below in Equation 3:

$$\left(\frac{^{87}\text{Sr}}{^{86}\text{Sr}}\right)_{\text{SW or GW}}^* = \frac{\left(\frac{^{87}\text{Sr}}{^{86}\text{Sr}}\right)_{\text{SW or GW}} - \left(X(\text{Sr})_{\text{Atmosphere}} \left(\frac{^{87}\text{Sr}}{^{86}\text{Sr}}\right)_{\text{Atmosphere}}\right)}{\frac{[\text{Sr}]_{\text{SW or GW}}^*}{[\text{Sr}]_{\text{SW or GW}}}} \quad (\text{Equation 3})$$

Chloride normalized strontium isotope ratios ($(^{87}\text{Sr}/^{86}\text{Sr})^*$) were then incorporated into mixing calculations where proportions of strontium derived from carbonate and silicate weathering end-members in streamwaters and groundwaters were calculated through two-component mixing (Capo et al., 1998). As shown below in Equation 4, $X(\text{Sr})_{\text{Carbonate Weathering}}$ reflects the mass fraction of strontium derived from carbonate weathering:

$$X(Sr)_{Carbonate\ Weathering} = \frac{\left(\frac{^{87}Sr}{^{86}Sr}\right)^*_{Streamwater\ or\ Groundwater} - \left(\frac{^{87}Sr}{^{86}Sr}\right)_{Silicate\ Weathering}}{\left(\frac{^{87}Sr}{^{86}Sr}\right)_{Carbonate\ Weathering} - \left(\frac{^{87}Sr}{^{86}Sr}\right)_{Silicate\ Weathering}} \quad (\text{Equation 4})$$

Valley Floor Exchangeable Soils and Soil Porewaters

Significantly lower $^{87}\text{Sr}/^{86}\text{Sr}$ ratios in southern planar valley floor exchangeable soils and soil porewaters (0.71749 to 0.71954, Tables 2.1 and 2.3) and in south swale valley floor soil porewaters (0.71889 to 0.72005, Table 2.1) compared to those observed in exchangeable soils and soil porewaters sampled from ridge top and mid slope locations (Tables 2.1 and 2.3) also suggest that a source less radiogenic than shale is affecting strontium concentrations and strontium isotope compositions in southern quadrant valley floor exchangeable soils and soil porewaters. Jin et al. (2011b) reported recharge by groundwaters to valley floor soils of the catchment during wet periods. Additionally, Lin et al. (2006) identified redoximorphic features in valley floor soils (e.g. fragipan-like layer at 30 to 50 cm depth) indicative of seasonal soil saturation and the formation of shallow water tables. As groundwater is hypothesized to be affected by a carbonate source, proportions of strontium derived from carbonate and silicate mineral weathering end-members in valley floor exchangeable soils and soil porewaters were calculated through Equation 5 where $X(Sr)_{Silicate\ Weathering}$ reflects the mass fraction of strontium derived from silicate weathering and $\left(\frac{^{87}\text{Sr}}{^{86}\text{Sr}}\right)_{Mixture}$ represents the measured $^{87}\text{Sr}/^{86}\text{Sr}$ ratio for a given valley floor exchangeable soil or soil porewater:

$$X(Sr)_{Silicate\ Weathering} = \frac{\left(\frac{^{87}Sr}{^{86}Sr}\right)_{Mixture} - X(Sr)_{Atm} \left(\frac{^{87}Sr}{^{86}Sr}\right)_{Atmosphere} - ((1-X(Sr)_{Atm}) \left(\frac{^{87}Sr}{^{86}Sr}\right)_{Carbonate\ Weathering}}{\left(\frac{^{87}Sr}{^{86}Sr}\right)_{Silicate\ Weathering} - \left(\frac{^{87}Sr}{^{86}Sr}\right)_{Carbonate\ Weathering}} \quad (\text{Equation 5})$$

Atmospheric proportions of strontium in valley floor soils and soil porewaters were estimated using average proportions determined in mixing calculations for ridge top and mid

slope soils and soil porewaters sampled at similar depths. Atmospheric proportions of strontium calculated through Equation 1 for south swale ridge top and mid slope soil porewaters sampled at shallow (0.30 versus 0.28) and deep (0.21 versus 0.20) depths were shown to be rather similar. However, atmospheric proportions of strontium calculated through Equation 1 for southern planar ridge top and mid slope exchangeable soils and soil porewaters showed slightly greater variation at shallow (0.34 versus 0.44 and 0.26 versus 0.39 for exchangeable soils and soil porewaters, respectively) and deep (0.33 versus 0.28 and 0.25 versus 0.31 for exchangeable soils and soil porewaters, respectively) depths. As a consequence, results obtained from mixing calculations (Equation 5) should be approached with caution as they may inaccurately estimate proportions of strontium derived from weathering sources to valley floor exchangeable soils and soil porewaters. To better assess atmospheric and weathering derived sources of strontium in valley floor exchangeable soils and soil porewaters, chloride concentrations should be measured for these reservoir components in the future. In this way, mixing calculations can be performed on chloride normalized strontium isotope ratios (Equations 2 through 4) where mass fractions of strontium derived from atmospheric components are corrected for enabling better estimation of relative proportions of strontium derived from weathering sources through two-component mixing. The carbonate ($^{87}\text{Sr}/^{86}\text{Sr} = 0.71132$, Table 2.23) and silicate (e.g. shale end-member, $^{87}\text{Sr}/^{86}\text{Sr} = 0.74558$, Table 2.24) weathering end-members used to calculate proportions of strontium in streamwaters and groundwaters were applied to mixing calculations for valley floor exchangeable soils and soil porewaters based on the logic established previously.

3.2 Plant Fractionation Factors

Fractionation factors ($K_{\text{Sr}/\text{Ca}}$) were calculated for sugar maple, chestnut oak, and red oak species in southwestern and southeastern quadrants by dividing the ratio of concentrations of

strontium and calcium in leaves to the corresponding ratio in the soil porewater solution as shown below in Equation 6 (White et al., 2012):

$$K_{Sr/Ca} = \frac{[\frac{Sr}{Ca}]_{Leaf}}{[\frac{Sr}{Ca}]_{Soil\ Porewater}} \text{ (Equation 6)}$$

In the equation, fractionation factors greater than one indicate preferential uptake of calcium relative to strontium by vegetation, while fractionation factors less than one reflect discrimination against strontium (White et al., 2012). In the case of preferential discrimination against strontium, the upper and lower bounds are defined as no calcium and strontium discrimination ($K_{Sr/Ca}=1$) and the complete exclusion of strontium ($K_{Sr/Ca}=0$) by vegetation, respectively. Considering soil porewater is the most readily available reservoir of plant nutrients (Wytenbach et al., 1995), soil porewater Sr/Ca ratios were used as opposed to exchangeable soil Sr/Ca ratios in the calculation. However, as will be discussed in detail later, disequilibrium was observed between soil porewaters and the exchangeable cation pool reflecting the inefficiency of exchange between these reservoir components (Figures 2.5 and 2.9). This was attributed to preferential flow pathways in macropores which have been confirmed in soil moisture monitoring and ground penetrating radar studies at the catchment (Lin et al., 2006; Lin and Zhou, 2008; Graham and Lin, 2011; Takagi and Lin; 2012; Zhang et al., 2014). As a consequence, there is the possibility of lysimeters sampling soil porewaters from macropores rather than the soil exchange complex. Due to these limitations, fractionation factors calculated for tree species through Equation 6 should be approached with caution. Additionally, leaf Sr/Ca ratios were chosen to represent vegetation as xylem sap waters were shown to have similar Sr/Ca ratios as soil porewaters (Tables 2.1 and 2.16). Fractionation factors were not calculated for leaves and sap waters in northwestern and northeastern quadrants as soil porewaters were not collected in these quadrants of the catchment.

3.3 Streamwater Flux and Carbonate Propagation Front Calculations

Using elemental and stream discharge data compiled from 2008 to 2010 (Brantley and Duffy, 2008, 2009, 2010 and Duffy, 2008, 2009, 2010), strontium fluxes ($\text{mol ha}^{-1} \text{y}^{-1}$) were determined by dividing the product of the geometric mean of strontium concentration and stream discharge at a given position (stream headwater, mid stream, weir) by the total watershed area of the catchment. Due to the variable nature of daily stream discharge and elemental concentration measurements, geometric means were used in place of arithmetic means to better represent the central tendency of average values. Application of Beale's ratio and log-linear regression for determination of average values can be undertaken; however, Fulweiler and Nixon (2005) demonstrated that results from these methods are no different than those obtained using the geometric mean. In order to delineate atmospheric versus weathering sources of strontium in streamwaters, fluxes were multiplied by proportions of strontium determined through mixing calculations (Equation 4). Calcium fluxes ($\text{mol ha}^{-1} \text{y}^{-1}$) were determined using average molar Ca/Sr ratios and previously calculated strontium flux values. In order to determine the atmospheric calcium flux, the average molar Ca/Sr ratio of bulk precipitation (Ca/Sr=233) was multiplied by the atmospheric strontium flux at a given streamwater position (stream headwater, mid stream, weir). For weathering derived calcium fluxes, the atmospheric strontium flux was first subtracted from the total strontium flux. This value was then multiplied by the average molar Ca/Sr ratio of the carbonate end-member (Ca/Sr=882). Distinction between carbonate and silicate weathering derived calcium was accomplished by multiplying the total weathering calcium flux by mass fractions of calcium determined through mixing calculations. Specifically, proportions of calcium derived from carbonate and silicate mineral weathering end-members in streamwaters were determined using two-component mixing (Equation 7 shown below) on

chloride normalized strontium isotope ratios ($(^{87}\text{Sr}/^{86}\text{Sr})^*$) (Equation 3) where $X(\text{Ca})_{\text{Carbonate}}$ reflects the mass fraction of calcium from the carbonate source:

$$X(\text{Ca})_{\text{Carbonate}} =$$

$$\frac{\left(\left(\frac{^{87}\text{Sr}}{^{86}\text{Sr}}\right)^*_{\text{SW or GW}} - \left(\frac{^{87}\text{Sr}}{^{86}\text{Sr}}\right)_{\text{Silicate Weathering}}\right) \left(\frac{\text{Sr}}{\text{Ca}}\right)_{\text{Silicate Weathering}}}{\left(\left(\frac{^{87}\text{Sr}}{^{86}\text{Sr}}\right)^*_{\text{SW or GW}} - \left(\frac{^{87}\text{Sr}}{^{86}\text{Sr}}\right)_{\text{Silicate Weathering}}\right) \left(\frac{\text{Sr}}{\text{Ca}}\right)_{\text{Silicate Weathering}} + \left(\left(\frac{^{87}\text{Sr}}{^{86}\text{Sr}}\right)_{\text{Carbonate}} - \left(\frac{^{87}\text{Sr}}{^{86}\text{Sr}}\right)^*_{\text{SW or GW}}\right) \left(\frac{\text{Sr}}{\text{Ca}}\right)_{\text{Carbonate}}}$$

(Equation 7)

To this end, the mass fraction of calcium derived from the atmosphere ($X(\text{Ca})_{\text{Atmosphere}}$) was corrected for enabling determination of relative proportions of calcium acquired from carbonate and silicate mineral weathering sources through two-component mixing. The same end-members used in two-component mixing to calculate proportions of strontium derived from carbonate and silicate mineral weathering sources to streamwaters and groundwaters were used in calculations for calcium due to strontium's utility as an tracer for calcium in catchment studies (Miller et al., 1993; Bailey et al., 1996; Blum et al., 2002; Kennedy et al., 2002; Bullen and Bailey, 2005; Pett-Ridge et al., 2009; Belanger et al., 2012). Specifically, average $^{87}\text{Sr}/^{86}\text{Sr}$ and Sr/Ca ratios for the carbonate fraction of DC 3 valley floor drill core samples (0.71132 and 0.00113, respectively) and the silicate fraction of DC 1 ridge top and DC 3 valley floor drill core samples (e.g. shale end-member, 0.74558 and 0.02015, respectively) were incorporated into mixing calculations.

To calculate the rate of carbonate propagation for the carbonate source at the CZMW 2 borehole near the stream's weir (DC 3), the calcium flux for carbonate at the stream's weir was first divided by the proportion of calcium in calcite (CaCO_3). This value was then divided by the product of the average density of CaCO_3 (2.71 g/cm³, Mandarino and Anderson, 1989) and the proportion of carbonates in DC 3 valley floor drill core samples as estimated by quantitative XRD patterns at Shale Hills (Average = 0.03125; Brantley et al., 2013). Calcite, as opposed to

ankerite, was chosen to represent the carbonate source at the DC 3 valley floor site due to mineralogical observations in studies at Shale Hills. According to previous studies, $\delta^{13}\text{C}$ for valley floor carbonates (-1.1‰) better resemble values for marine carbonates (~0‰) than those for ankerites sampled from the northern ridge location (-5.9 ‰) (Jin et al., 2014). Additionally, low $\text{Sr}^{2+}/(\text{Ca}^{2+} + \text{Mg}^{2+})$ ratios in groundwaters at valley floor locations reflect the tendency of Sr^{2+} to remain in solution rather than substitute calcium in secondary mineral phases such as pedogenic calcite (Gabitov et al., 2014). Furthermore, Brantley et al. (2013) observed precipitation of secondary calcites at depths below the carbonate weathering front (~4 m depth) at the valley floor with dissolution of these carbonates likely above this depth due to their fast dissolving nature in the local equilibrium regime of the catchment. As shown in Table 2.24, carbonate fractions of DC1-37 and DC1-38 samples at the ridge displayed significantly higher $^{87}\text{Sr}/^{86}\text{Sr}$ ratios (0.71935 and 0.71910, respectively) than those observed for DC 3 drill core samples at the valley floor (Average $^{87}\text{Sr}/^{86}\text{Sr} = 0.71132$). Such distinctive strontium isotope ratios reflect differences in the composition of carbonates at the ridge and the valley. To this end, ankerites are hypothesized to be largely contributing to the $^{87}\text{Sr}/^{86}\text{Sr}$ ratio at the DC 1 ridge top site with influences to the strontium isotope signature by secondary calcites assumed to be more significant at the DC 3 valley floor site. Consequently, physical and chemical properties of calcite were used in calculations to estimate the rate of carbonate propagation for the carbonate source at the CZMW 2 borehole near the stream's weir.

4. Results and discussion

4.1 Exchangeable Soils and Soil Porewaters

Soil porewater $^{87}\text{Sr}/^{86}\text{Sr}$ ratios at southern planar ridge top, mid slope, and valley floor sites ranged from 0.72473 to 0.72494, 0.72217 to 0.72384, and 0.71749 to 0.71865 (Table 2.1,

Figure 2.1), respectively, with average values of 0.72484 ± 0.00011 , 0.72340 ± 0.00031 , and 0.71817 ± 0.00018 , respectively (Table 2.2, Figure 2.2). At south swale ridge top, mid slope, and valley floor sites, soil porewater $^{87}\text{Sr}/^{86}\text{Sr}$ ratios ranged from 0.72400 to 0.72648, 0.72411 to 0.72599, and 0.71889 to 0.72005 (Table 2.1, Figure 2.1), respectively, with average values of 0.72509 ± 0.00073 , 0.72546 ± 0.00016 , and 0.71952 ± 0.00017 (Table 2.2, Figure 2.2), respectively. Soil exchangeable $^{87}\text{Sr}/^{86}\text{Sr}$ ratios at southern planar ridge top, mid slope, and valley floor sites ranged from 0.72276 to 0.72385, 0.72118 to 0.72493, and 0.71780 to 0.71954 (Table 2.3, Figure 2.1), respectively, with weighted average values of 0.72329 ± 0.00032 , 0.72290 ± 0.00070 , and 0.71892 ± 0.00016 , respectively (Table 2.4, Figure 2.2). With the exception of carbonate affected exchangeable soils and soil porewaters sampled at valley floor locations, $^{87}\text{Sr}/^{86}\text{Sr}$ ratios of exchangeable soil horizons and soil porewaters were found to be in close agreement to those observed in leaves and sap waters (Tables 2.9, 2.10, 2.16 and 2.17, Figure 2.2). This suggests that biological nutrient cycling processes at the catchment are rapidly homogenizing strontium inputs added from weathering and atmospheric sources, particularly for exchangeable soils and soil porewaters sampled at shallow depths. However, $^{87}\text{Sr}/^{86}\text{Sr}$ ratios in leaves and sapwaters were found to correlate less closely to those in exchangeable soil mineral horizons and deep soil porewaters (Tables 2.1 to 2.5, Tables 2.9, 2.10, 2.16, and 2.17). This seems to indicate that influences of litter restitutions on strontium isotope compositions for these reservoir components become less important with increased sampling depth.

As mentioned in the Data Analysis Methods section, two-component mixing calculations were performed for southern planar and south swale ridge top and mid slope exchangeable soils and soil porewaters through Equation 1 using strontium isotope ratios for bulk precipitation ($^{87}\text{Sr}/^{86}\text{Sr} = 0.71054$) and “weathered shale” ($^{87}\text{Sr}/^{86}\text{Sr} = 0.72967$) as atmospheric and silicate

weathering end-members, respectively. Additionally, mixing calculations were performed for southern planar and south swale valley floor exchangeable soils and soil porewaters through Equation 5 using strontium isotope ratios for shale ($^{87}\text{Sr}/^{86}\text{Sr} = 0.74558$) and the carbonate fraction of DC 3 valley floor drill core samples ($^{87}\text{Sr}/^{86}\text{Sr} = 0.71132$) as silicate and carbonate weathering end-members, respectively. As noted previously, this was accomplished using atmospheric proportions determined in mixing calculations for ridge top and mid slope exchangeable soils and soil porewaters sampled from similar depths. Use of the carbonate end-member in mixing calculations for valley floor exchangeable soils and soil porewaters is supported by field observations (Lin, 2006; Jin et al., 2011b) which suggest recharge of carbonate affected groundwaters to valley floor soils and soil porewaters at the catchment. Additionally, significantly lower strontium isotope ratios observed in exchangeable soils and soil porewaters at valley floor relative to ridge top and mid slope sites (Table 2.1 and Figure 2.1), outside the range expected from analytical uncertainty, indicate that a source less radiogenic than shale (e.g. carbonate) is affecting chemistry in valley floor exchangeable soils and soil porewaters in southern quadrants of the catchment. Detailed rationale behind selection of end-members and parameters used in mixing calculations can be found in the Data Analysis Methods section.

As shown in Figure 2.3, ridge top and mid slope organic soil horizons and shallow soil porewaters were observed to have the highest atmospheric proportions of strontium based on mixing calculations. Specifically, percentages of atmospheric strontium in ridge top and mid slope organic horizons of southern planar exchangeable soils were found to be 34% and 44% compared to $33 \pm 2.8\%$ and $28 \pm 2.1\%$ in mineral horizons, respectively. Furthermore, results from mixing calculations indicated that 26 and 39% of strontium in ridge top and mid slope

shallow southern planar soil porewaters were derived from the atmosphere, respectively, while only 25 and $31 \pm 0.4\%$ of atmospheric strontium were found for soil porewaters sampled at deeper depths in corresponding locations. Additionally, atmospheric strontium percentages in shallow south swale ridge top and mid slope soil porewaters were found to be 30 and $28 \pm 0.7\%$, respectively, compared to $21 \pm 4.4\%$ and $21 \pm 0.3\%$ for soil porewaters collected at deeper depths in corresponding locations.

These results are unsurprising given the close proximity of organic horizons and shallow soil porewaters to the surface. Here, weathering products are either transported downslope through lateral subsurface flow pathways at soil horizons and/or at the soil-bedrock interface or translocated downward from upper to lower soil horizons through vertical macropore flow at high-permeability zones or as a result of hydrophobic organic surface layers (Lin, 2006; Lin and Zhou, 2008; Graham and Lin, 2011; Jin et al., 2011a). As noted by Jin et al. (2011a), precipitation inputs infiltrate into regolith and saprock through a mixture of connected and unconnected pores wherein a series of chemical (clay dissolution), biological (disaggregation by tree roots or animal burrows), and physical (periglacial and temperature induced fracturing) processes enable production of new pores and enhance development of pre-existing pores. Indeed, longer water residence times during summer months, as indicated by consistently low standard deviations in the summer porewater $\delta^{18}\text{O}$ profile of the catchment (Thomas, 2013), suggest greater influences from chemical weathering along deeper flow paths (Hogan and Blum, 2002). Additionally, Jin et al. (2011a) and Brantley et al. (2013) have noted significant fluid flow in upper fractured shale underlying regolith as corroborated by observations of clay depletion present there as well as of a highly connected pore network in weathered regolith. Hence, the possibility of upward transport of weathering products to mineral horizons and deep

soil porewaters by advection along bedrock/saprock interfaces and fractures or by diffusion in the matrix between major fractures (Jin et al., 2011a). Consequently, larger proportions of silicate weathering derived strontium in mineral horizons and deep soil porewaters are hypothesized to be the result of combined weathering processes in regolith and underlying saprock. However, influences of plants on strontium isotope compositions and proportions of weathering derived strontium in organic horizons and shallow porewaters should not be overlooked. According to Takagi and Lin (2012), evapotranspiration by plants has been implicated as the primary cause of diminished near-surface soil moisture at the SSHCZO during the summer. Hence, less water available to initiate weathering processes in shallow soil horizons and porewaters. Additionally, high peat contents observed in quantitative XRD patterns for organic soil horizons (between 7.7 and 9.8 wt%, Jin et al., 2010) compared to mineral horizons (between 0.0 and 3.6 wt%, Jin et al., 2010) suggest that strontium contributions from less radiogenic litterfall (Table 2.9) are also greater in organic soil horizons and shallow soil porewaters. As a consequence, lower $^{87}\text{Sr}/^{86}\text{Sr}$ ratios and proportions of silicate weathering derived strontium may be the result of plant influences on shallow exchangeable soil horizons and soil porewaters.

At the southern planar transect, ridge top exchangeable soils and soil porewaters were found to have more radiogenic isotope compositions (Tables 2.1 and 2.3, Figures 2.1 and 2.2) and derive less strontium from atmospheric sources than those sampled at mid slope locations (Figure 2.3). Observed discrepancy in strontium isotope composition at ridge top and mid slope locations suggests divergent hydrologic flow pathways as a result of differences in hillslope geometry at these locations. According to Jin et al. (2010), due to the flat and planar geometry at ridge top and mid slope locations of the southern planar transect (Figure 1.2), respectively,

subsurface fluid flow is largely one dimensional and vertical at the ridge top yet two dimensional and downslope at the mid slope. Additionally the presence of conifers with deep tap roots at the ridge top (Figure 1.3, Naithani et al., 2013) ensures considerable vertical fracturing. In this way, precipitation inputs to top soils at the ridge will flow downward in soils or in underlying fractured shale and be immobilized there instead of being lost through downslope flow or evapotranspiration processes. In fact, field observations have confirmed fluid flow at the soil-rock interface at ridge top locations of the southern planar transect (Lin, 2006; Lin and Zhou, 2008). In addition to vertical flow, water at the mid slope location flows rapidly downslope along a series of macropores through lateral subsurface flow pathways which transfer weathering products from mid slope to valley floor locations. Thus, confinement of precipitation inputs within the soil profile or in underlying fractured shale enhances weathering processes at ridge top locations of the southern planar transect. Conversely, weathering products are largely transported downslope through lateral subsurface flow pathways from mid slope to valley floor locations. This may be responsible for the higher observed $^{87}\text{Sr}/^{86}\text{Sr}$ ratios and proportions of strontium derived from silicate weathering sources in exchangeable soils and soil porewaters sampled at southern planar ridge top relative to mid slope locations.

On the contrary, south swale ridge top soil porewaters were found to have less radiogenic isotope compositions (Tables 2.1 and 2.3, Figures 2.1 and 2.2) and derive more strontium from atmospheric sources than those sampled at mid slope locations (Figure 2.3). Steeper slopes in soils and underlying shales (Lin et al., 2006), coupled with lower tree species density at the swale's ridge (Figure 1.3, Naithani et al., 2013), facilitate downslope movement of water through subsurface lateral flow processes to transfer more radiogenic weathering products from ridge top to mid slope locations along swale edges or other areas where large surface or subsurface

gradients exist (Lin, 2006; Lin et al., 2006; Lin and Zhou, 2008). In fact, the topographic map of the SSHCZO (Figure 1.2) shows a sharp drop in elevation near the south swale mid slope position with accumulation from upslope positions supported by field observations of thick soils at this location (Figure 1.4, Lin et al., 2006). As preferential flow processes are typically instigated by perched water tables (Dunne, 1978; Weiler and McDonnell, 2004), wetter soils at swale relative to planar locations, possibly due to less vegetation cover (and hence, less evapotranspiration) in surface horizons (Figure 1.3, Takagi and Lin, 2012; Naithani et al., 2013), indicate greater hydrologic connectivity and incidence of lateral preferential flow processes at swale locations. Indeed, this has been confirmed by in situ observations as well as in quantitative soil moisture and hydrologic data for the catchment (Lin, 2006; Lin et al., 2006; Lin and Zhou, 2008, Takagi and Lin, 2012). Additionally, the presence of a positive cerium (Ce) anomaly, indicative of a generally oxic environment, suggests rapid water penetration along preferential flow paths to prevent water saturation in thick and wet soils at the swale location (Figure 1.2, Jin and Brantley, 2011). Indeed, Jin et al. (2010) and Ma et al. (2010) demonstrated that total chemical weathering rates were higher, while residence times were shorter in regolith derived from ridge top compared to mid slope locations of the catchment's southern quadrant. Thus, higher strontium isotope ratios and proportions of weathering derived strontium in soil porewaters sampled at mid slope relative to ridge top positions of the south swale transect are likely due to a dominance of lateral preferential flow processes involved in the transfer of weathering products downslope.

Additionally, less variability in proportions of strontium derived from atmospheric sources was observed between organic and mineral horizons of exchangeable soils and between shallow and deep soil porewaters at the ridge top relative to mid slope location. Soil thickness at

the ridge top (depth range: 0 to 30 cm) is shallower than at the mid slope (depth range: 0 to 60 cm and 0 to 160 cm for southern planar and south swale, respectively) (Figure 1.2).

Consequently, similarities in strontium isotope compositions between organic and mineral soil horizons and shallow and deep soil porewaters at the ridge top location can be explained by poorly defined classification schemes (e.g. organic versus mineral and shallow versus deep) wherein strontium contributions from atmospheric and weathering sources are spatially invariant as a result of the shallow soil profile present at ridge top locations.

As shown in Figure 2.4, proportions of strontium derived from carbonate mineral weathering increased with depth for valley floor exchangeable soils and soil porewaters. At the southern planar location, carbonate derived proportions of strontium in exchangeable soils increased from 0.41 ± 0.003 in organic horizons to 0.51 ± 0.003 in mineral horizons, while proportions in soil porewaters increased from 0.43 ± 0.001 at shallow depths to 0.49 ± 0.005 at deep depths. Furthermore, proportions of strontium derived from carbonate weathering in south swale soil porewaters increased from 0.42 ± 0.001 at shallow depths to 0.48 ± 0.011 at deep depths. Considering that the carbonate reaction front at the valley floor is hypothesized to initiate at a depth of ~ 200 cm (Brantley et al., 2013), exposure of valley floor exchangeable soils or soil porewaters to carbonates (Table 2.23) or carbonate affected groundwaters (Table 2.22) with increased depth is likely. This may partially explain the higher proportions of strontium derived from carbonate weathering in mineral horizons and in soil porewaters sampled at deep depths. On the contrary, proportions of strontium derived from silicate mineral weathering sources in southern planar valley floor exchangeable soils (range: 0.20 to 0.25) and soil porewaters (range: 0.19 to 0.22) and in south swale soil porewaters (range: 0.23 to 0.26) were found to be relatively uniform with depth, consistent with the slow kinetics of clay dissolution at the catchment (Jin et

al., 2010). Predictably, strontium contributions to exchangeable soils and soil porewaters from carbonate dissolution processes were found to be greater than those from silicate mineral weathering due to the greater reactivity and solubility of carbonate minerals relative to silicate minerals (MacDonald et al., 1991; White et. al, 2005). As observed for ridge top and mid slope exchangeable soils and soil porewaters, organic horizons and shallow soil porewaters derived greater proportions of strontium from the atmosphere than mineral horizons and deep soil porewaters. As mentioned previously, weathering products from surface horizons and porewaters are either transported downslope through lateral subsurface flow or translocated downward from upper to lower horizons through vertical macropore flow. Atmospheric proportions were directly estimated based on proportions determined from mixing calculations for ridge top and mid slope exchangeable soils and soil porewaters. To better assess atmospheric and weathering derived sources of strontium in valley floor exchangeable soils and soil porewaters, chloride concentrations should be measured for these reservoir components in the future. In this manner, mixing calculations can be performed on chloride normalized strontium isotope ratios (Equations 2 through 4) where mass fractions of strontium from atmospheric sources are corrected for enabling better estimation of relative proportions of strontium derived from weathering sources through two-component mixing.

At all transect positions of the southern quadrant, $^{87}\text{Sr}/^{86}\text{Sr}$ ratios (Tables 2.1 and 2.2, Figures 2.1 and 2.2) and proportions of strontium derived from silicate weathering sources (Figure 2.3 and 2.3) were higher for soil porewaters collected from swale relative to planar locations. Swale locations are known to be wetter and store greater soil moisture throughout the year compared to planar locations (Lin, 2006; Lin et al., 2006; Lin and Zhou, 2008). Additionally, tree species density is lower at swale relative to planar locations of the southern

quadrant due to the presence of wetter soils which inhibit growth and vitality of dominant deciduous species such as oaks (Figure 1.3, Naithani et al., 2013). Hence, less evapotranspiration and the increased opportunity for water percolation into the soil profile or in underlying shale to initiate subsurface weathering processes at swale locations. In the case of southern quadrant valley floor porewaters, planar sites were located closer to the carbonate source near the stream's weir than swale sites (Figure 1.2). Accordingly, less radiogenic strontium isotope compositions and lower proportions of strontium derived from silicate weathering sources for southern planar valley floor porewaters seem reasonable.

Furthermore, on average, southern planar ridge top and mid slope porewaters were found to be more radiogenic, while southern planar valley floor porewaters were found to be less radiogenic than exchangeable soils sampled at similar depths (Tables 2.1 and 2.3, Figures 2.1 and 2.2). Indeed, mixing calculations (Figures 2.3 and 2.4) indicate higher proportions of strontium derived from dominant weathering processes at ridge top and mid slope locations (e.g. more radiogenic silicate weathering) and at valley floor locations (e.g. less radiogenic carbonate weathering) for southern planar soil porewaters compared to corresponding soil exchangeable horizons sampled from similar depths. Inefficiency of strontium exchange between soil porewaters and the exchange pool (Figure 2.5) is likely resulting in observed variation in $^{87}\text{Sr}/^{86}\text{Sr}$ ratio and relative proportions of strontium derived from atmospheric versus weathering sources for these reservoir components. Such discrepancy may be related to rapid transit times of porewaters through the soil profile (Lin et al., 2006; Jin et al., 2011b; Jin and Brantley, 2011), the unavailability of exchangeable strontium as the result of preferential flowpaths along macropores at the catchment (Lin, 2006; Lin et al., 2006; Lin and Zhou, 2008; Jin et al., 2011b; Takagi and Lin, 2012; Thomas, 2013; Zhang et al., 2014), heterogeneity in the nature of the soils

(e.g. variation in K_d , Jin et al., 2010), or formation of acetate complexes during ammonium acetate extractions (Shand et al., 2009). Observations of isotopic disequilibrium conflict with the longstanding view that cation exchange between exchange sites and soil solutions is a near-instantaneous process (Davis and Kent, 1990; Johnson and DePaolo, 1997). However, it should be noted that numerous studies conducted in a wide range of ecosystems (Clow et al., 1997; Stewart et al., 1998; Poszwa et al., 2000; Drouet et al., 2005; Pett-Ridge et al., 2009) have similarly observed disequilibrium between the exchange pool and soil solution.

Table 2.1 Strontium and calcium elemental concentrations and Ca/Sr and $^{87}\text{Sr}/^{86}\text{Sr}$ ratios for soil porewaters sampled from southern planar (SP) and south swale (SS) ridge top (RT), mid slope (MS), and valley floor (VF) locations

Sample Date	Sample ID	Depth (cm)	Sr (μM)	Ca (μM)	Ca/Sr (molar)	$^{87}\text{Sr}/^{86}\text{Sr}$
5/17/2013	SPVF	20	0.16	60	377	0.71865
5/17/2013	SPVF	30	0.25	91	358	0.71852
5/17/2013	SPVF	40	0.20	71	349	0.71827
5/17/2013	SPVF	60	0.24	79	321	0.71749
5/17/2013	SPMS	40	0.14	52	371	0.72382
5/17/2013	SPMS	50	0.16	63	381	0.72358
5/17/2013	SSMS	40	0.18	41	229	0.72457
5/17/2013	SSMS	100	0.23	63	274	0.72589
5/24/2013	SSVF	20	0.16	92	563	0.71997
5/24/2013	SSMS	140	0.23	61	263	0.72580
5/24/2013	SSMS	160	0.25	75	297	0.72572
5/24/2013	SSRT	30	0.12	30	244	0.72480
5/30/2013	SSMS	120	0.24	70	289	0.72580
5/30/2013	SPRT	30	0.19	60	322	0.72494
5/30/2013	SSRT	20	0.07	16	219	0.72648
6/05/2013	SSMS	100	0.22	60	268	0.72582
6/05/2013	SSMS	160	0.24	65	270	0.72591
6/12/2013	SSVF	10	0.12	63	534	0.71900
6/12/2013	SSVF	30	0.14	36	252	0.71934
6/12/2013	SSVF	40	0.24	65	266	0.71972
6/12/2013	SSMS	40	0.17	32	198	0.72411
6/12/2013	SSMS	60	0.20	48	240	0.72531
6/12/2013	SSMS	80	0.21	52	249	0.72531
6/12/2013	SSMS	120	0.22	61	273	0.72599
6/12/2013	SSMS	140	0.23	65	266	0.72572

6/28/2013	SPVF	30	0.14	44	307	0.71855
6/28/2013	SPVF	50	0.12	26	227	0.71818
6/28/2013	SPVF	60	0.20	58	287	0.71753
6/28/2013	SSVF	80	0.07	13	173	0.72005
6/28/2013	SPMS	10	0.05	11	238	0.72217
6/28/2013	SPMS	50	0.15	48	321	0.72361
6/28/2013	SSRT	10	0.06	10	174	0.72400
7/12/2013	SSVF	10	0.10	43	403	0.71889
7/12/2013	SSVF	40	0.22	45	206	0.71967
7/12/2013	SPMS	40	0.15	48	312	0.72384
7/12/2013	SSMS	20	0.09	23	266	0.72422
7/12/2013	SSMS	140	0.24	65	238	0.72573
7/12/2013	SSMS	160	0.23	65	234	0.72594
7/18/2013	SPRT	20	0.13	36	267	0.72473

*Ca/Sr ratios and Sr and Ca elemental concentrations for additional soil porewater samples where Sr isotope ratios were not measured are displayed in the appendix.

Table 2.2 Average Ca/Sr and $^{87}\text{Sr}/^{86}\text{Sr}$ ratios for soil porewaters sampled from southern planar and south swale ridge top, mid slope, and valley floor locations

Location	Average Ca/Sr (molar)	Average $^{87}\text{Sr}/^{86}\text{Sr}$
Southern Planar Ridge Top	300 ± 8	0.72484 ± 0.00011
Southern Planar Mid Slope	325 ± 12	0.72340 ± 0.00031
Southern Planar Valley Floor	329 ± 7	0.71817 ± 0.00018
South Swale Ridge Top	184 ± 13	0.72509 ± 0.00073
South Swale Mid Slope	246 ± 4	0.72546 ± 0.00016
South Swale Valley Floor	273 ± 15	0.71952 ± 0.00017

Table 2.3 Ca/Sr and $^{87}\text{Sr}/^{86}\text{Sr}$ ratios for exchangeable soils sampled from southern planar (SP) ridge top (RT), mid slope (MS), and valley floor (VF) locations

Sample Date	Sample ID	Average Depth (cm)	Ca/Sr (molar)	$^{87}\text{Sr}/^{86}\text{Sr}$
10/06/2011	SPRT Organic	0	224	0.72322
10/06/2011	SPRT 11-16	13.5	242	0.72276
10/06/2011	SPRT 16-21	18.5	174	0.72385
10/06/2011	SPMS 0-13	6.5	152	0.72118
10/06/2011	SPMS 13-21	17.0	100	0.72317
10/06/2011	SPMS 21-27	24.0	134	0.72443
10/06/2011	SPMS 27-32	29.5	134	0.72472
10/06/2011	SPMS 32-33	32.5	134	0.72493
10/06/2011	SPVF 0-6	3.0	214	0.71780
10/06/2011	SPVF 6-14	10.0	176	0.71834

10/06/2011	SPVF 14-22	18.0	150	0.71877
10/06/2011	SPVF 22-28	25.0	154	0.71890
10/06/2011	SPVF 28-36	32.0	152	0.71899
10/06/2011	SPVF 36-41	39.0	140	0.71939
10/06/2011	SPVF 41-46	44.0	144	0.71954
10/06/2011	SPVF 46-53	49.5	150	0.71944
10/06/2011	SPVF 53-59	56.0	156	0.71933
10/06/2011	SPVF 59-62	61.0	132	0.71921
10/06/2011	SPVF 62-66	64.0	106	0.71892

Table 2.4 Weighted average Ca/Sr and $^{87}\text{Sr}/^{86}\text{Sr}$ ratios for exchangeable soils sampled from southern planar ridge top, mid slope, and valley floor locations

Location	Average Ca/Sr (molar)	Average $^{87}\text{Sr}/^{86}\text{Sr}$
Southern Planar Ridge Top	216 ± 20	0.72329 ± 0.00032
Southern Planar Mid Slope	132 ± 8	0.72290 ± 0.00070
Southern Planar Valley Floor	155 ± 8	0.71892 ± 0.00016

Table 2.5 Weighted average Ca/Sr and $^{87}\text{Sr}/^{86}\text{Sr}$ ratios for organic and mineral soil exchangeable horizons sampled from southern planar ridge top, mid slope, and valley floor locations

Location	Horizon Type	Average Ca/Sr (molar)	Average $^{87}\text{Sr}/^{86}\text{Sr}$
Southern Planar Ridge Top	Organic	224	0.72322
Southern Planar Ridge Top	Mineral	208 ± 34	0.72331 ± 0.00055
Southern Planar Mid Slope	Organic	152	0.72118
Southern Planar Mid Slope	Mineral	120 ± 9	0.72402 ± 0.00039
Southern Planar Valley Floor	Organic	214	0.71780
Southern Planar Valley Floor	Mineral	150 ± 6	0.71904 ± 0.00012

*Error bars are excluded from horizons where only one Ca/Sr or $^{87}\text{Sr}/^{86}\text{Sr}$ ratio was measured at a designated location.

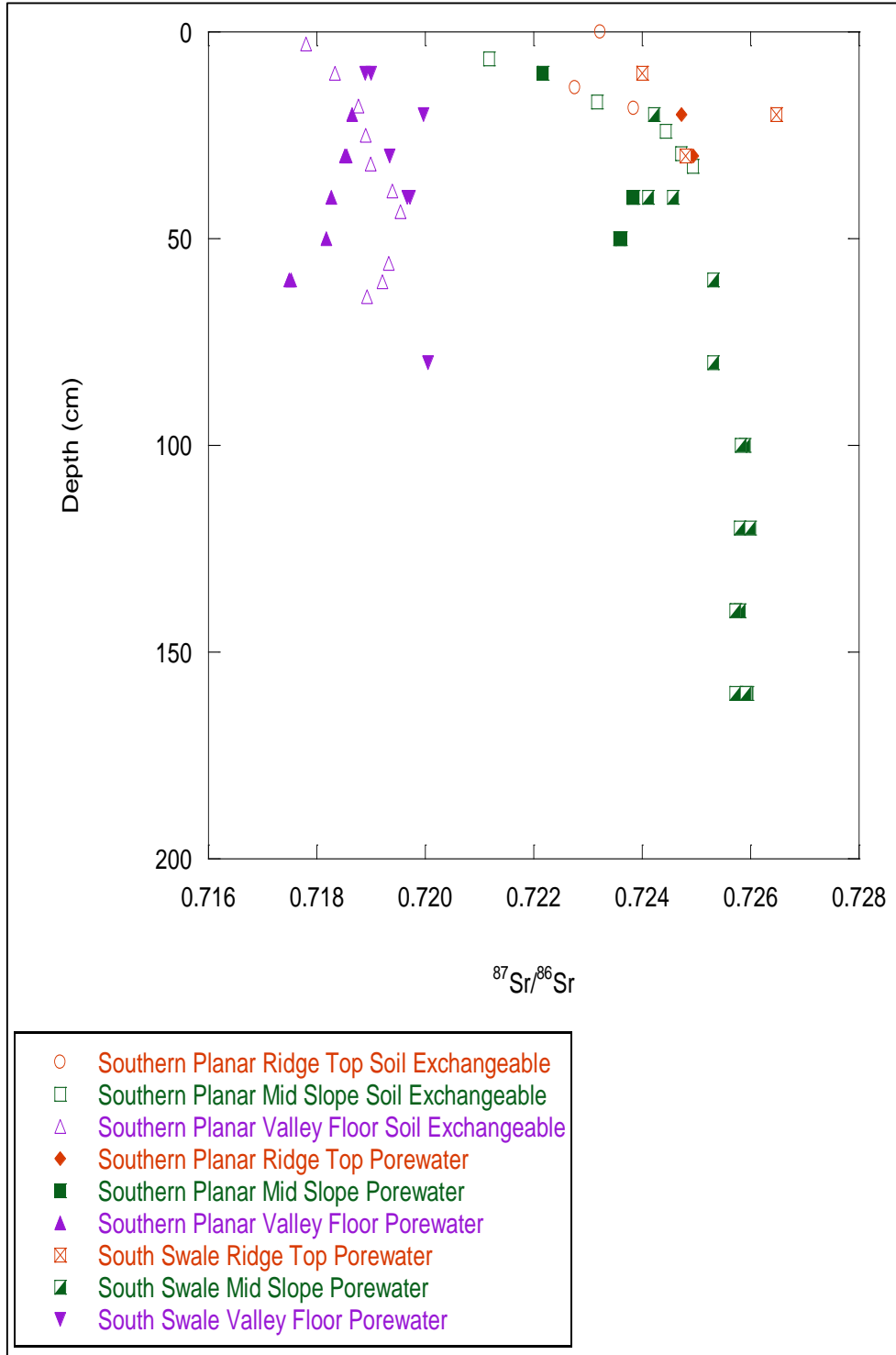


Figure 2.1 Depth versus $^{87}\text{Sr}/^{86}\text{Sr}$ ratio for southern planar ridge top, mid slope, and valley floor exchangeable soils and soil porewaters and for south swale ridge top, mid slope, and valley floor soil porewaters.

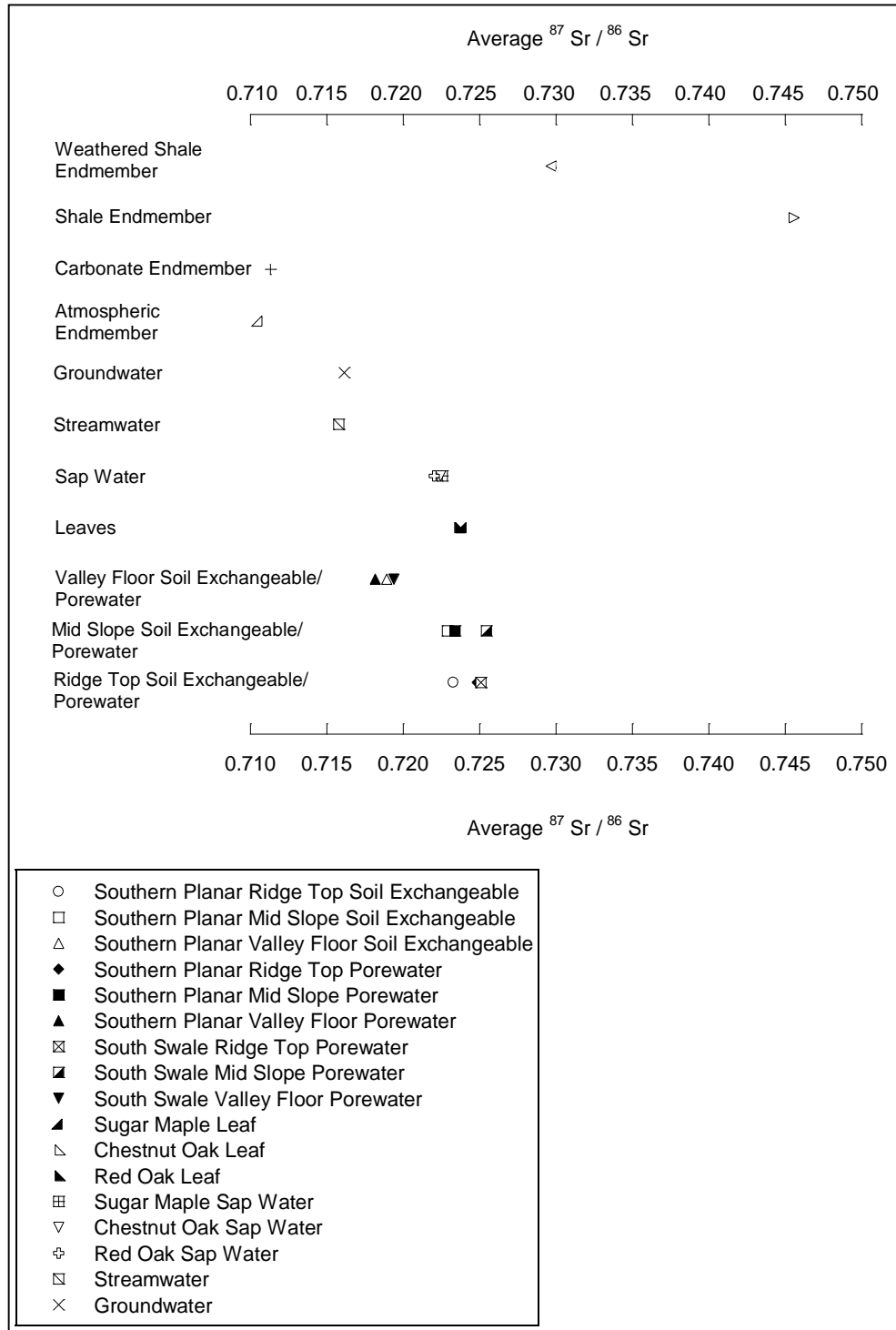


Figure 2.2 Average $^{87}\text{Sr} / ^{86}\text{Sr}$ ratios for southern planar ridge top, mid slope, and valley floor exchangeable soils and soil porewaters, south swale ridge top, mid slope, and valley floor soil porewaters, sugar maple, chestnut oak, and red oak leaves and sap water, and streamwaters and groundwaters. Average $^{87}\text{Sr} / ^{86}\text{Sr}$ ratios for the atmospheric end-member and for carbonate, shale, and weathered shale weathering end-members are also shown on the figure.

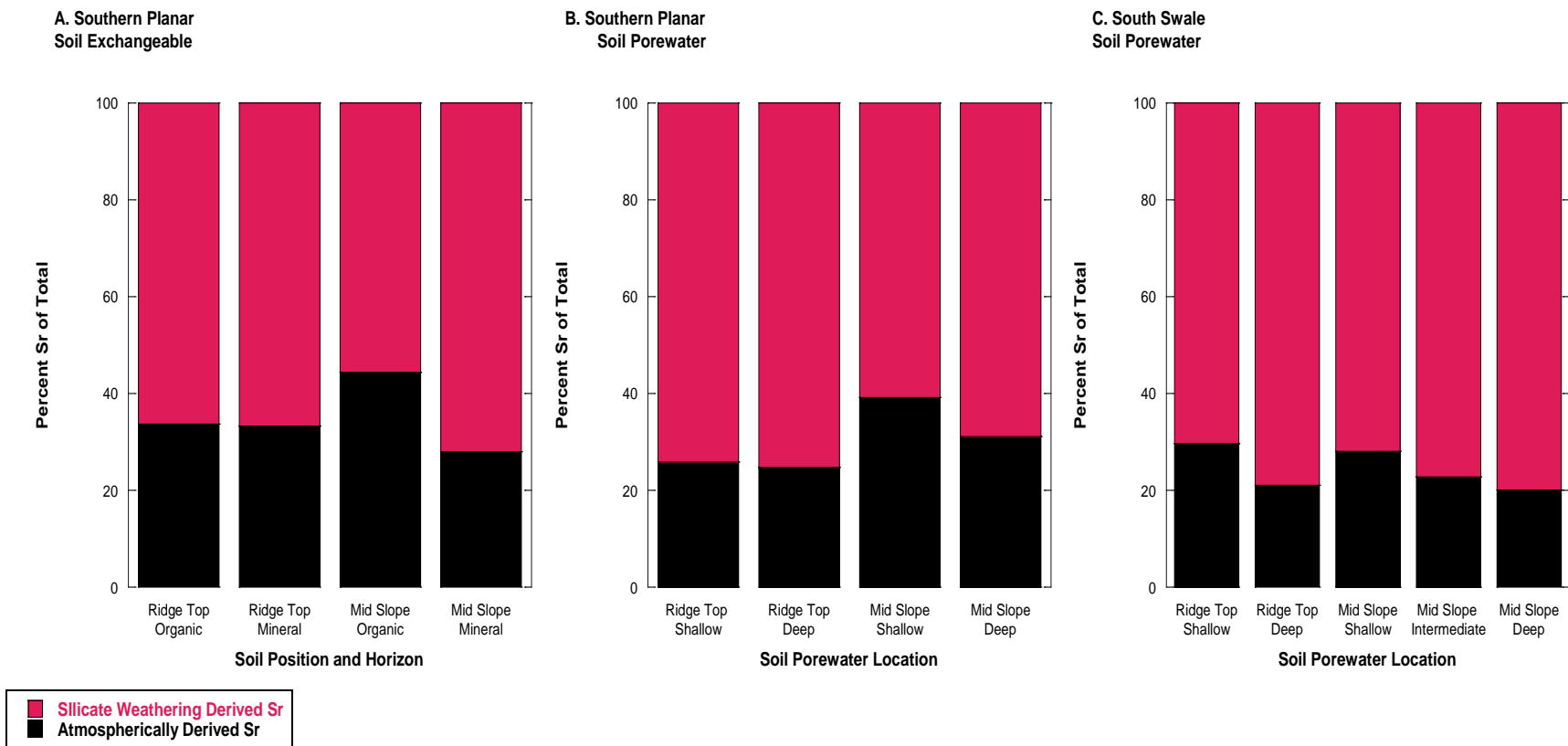


Figure 2.3 Percentage of strontium derived from silicate mineral weathering (pink) and atmospheric (black) sources for southern planar exchangeable soils (A), southern planar soil porewaters (B), and south swale soil porewaters (C) sampled at ridge top and mid slope positions in southwestern (southern planar) and southeastern (south swale) quadrants of the catchment.

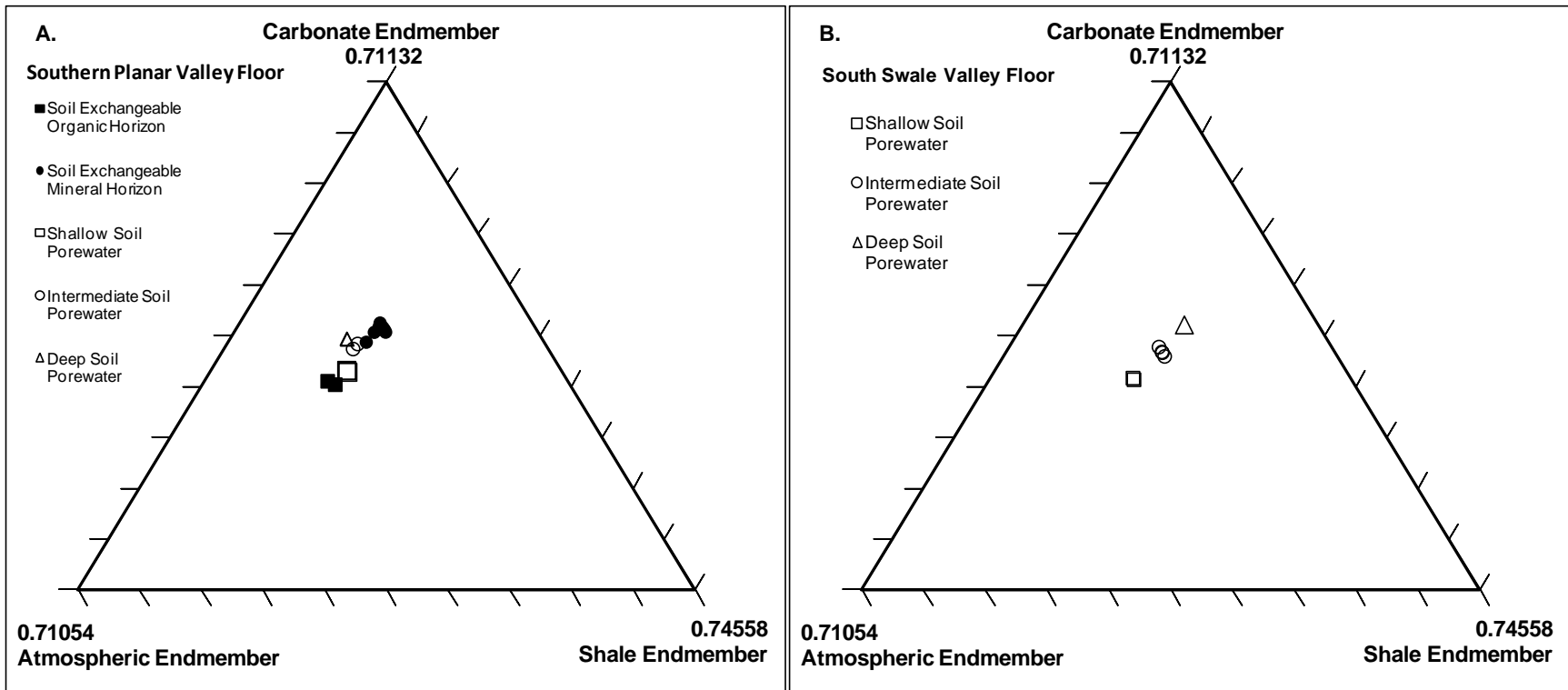


Figure 2.4 Ternary plots depicting relative proportions of strontium derived from atmospheric, carbonate weathering, and silicate weathering sources in southern planar exchangeable soils and soil porewaters (A) and south swale soil porewaters (B) sampled at valley floor positions in southwestern (southern planar) and southeastern (south swale) quadrants of the catchment.

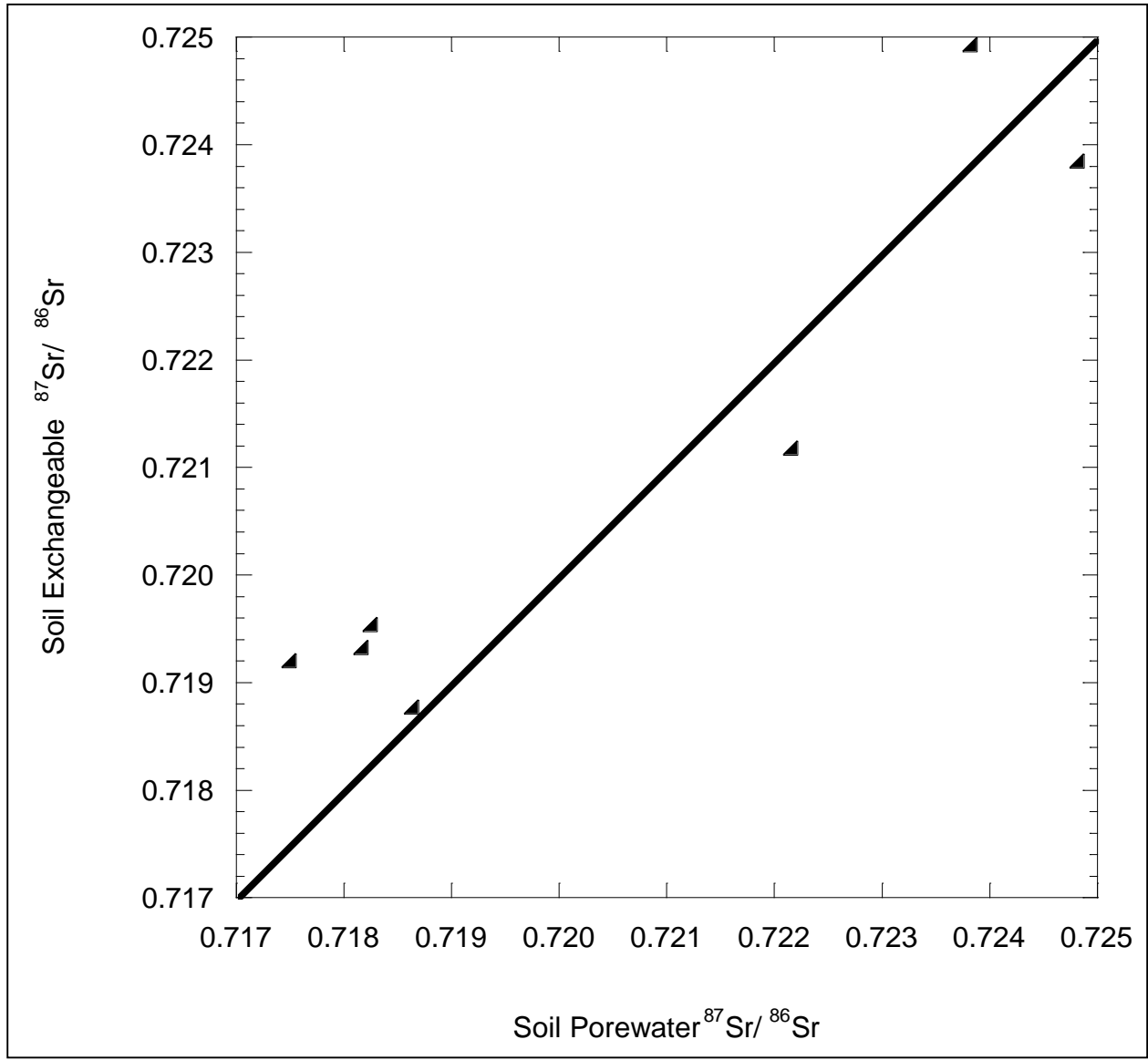


Figure 2.5 Soil exchangeable $^{87}\text{Sr}/^{86}\text{Sr}$ ratio versus soil porewater $^{87}\text{Sr}/^{86}\text{Sr}$ ratio for samples collected at similar positions and depths of the southern planar transect. The diagonal line represents isotopic equilibrium between the exchange pool and soil porewaters.

Soil porewater Ca/Sr ratios at southern planar ridge top, mid slope, and valley floor sites ranged from 261 to 344, 221 to 383, and 227 to 400 (Table 2.1, Figures 2.6 and 2.7), respectively, with average values of 300 ± 8 , 325 ± 12 , and 329 ± 7 , respectively (Table 2.2, Figure 2.8). At south swale ridge top, mid slope, and valley floor sites, soil porewater Ca/Sr ratios ranged from 113 to 244, 181 to 324, and 162 to 456 (Table 2.1, Figures 2.6 and 2.7), respectively, with average values of 184 ± 13 , 246 ± 4 , and 273 ± 15 (Table 2.2, Figure 2.8), respectively. Soil exchangeable Ca/Sr ratios at southern planar ridge top, mid slope, and valley floor sites ranged from 174 to 224, 100 to 152, and 106 to 214 (Table 2.3, Figures 2.6 and 2.7), respectively, with average values of 216 ± 20 , 132 ± 8 , and 155 ± 8 , respectively (Table 2.4, Figure 2.8).

As was observed for $^{87}\text{Sr}/^{86}\text{Sr}$ ratios, Ca/Sr ratio varied according to sampling location and depth (Tables 2.1 to 2.6, Figures 2.6 to 2.8). Specifically, modest increases in average porewater Ca/Sr ratio were observed in the progression from ridge top to mid slope to valley floor locations at both southern planar and south swale sites, while Ca/Sr ratios for southern planar exchangeable soils decreased from ridge top to mid slope locations and then increased from mid slope to valley floor locations. Graham et al. (1990) and Jin et al. (2010) noted that porewaters in contact with minerals at the southern planar ridge top location are expected to be dilute and in chemical disequilibrium due to high chemical weathering rates and short porewater residence times present there as a result of the rapid movement of precipitation inputs first through the soil profile and then into underlying fractured shale. Hence, the lower Ca/Sr ratios for ridge top relative to mid slope porewaters at the southern planar location. Moreover, Jin and Brantley (2011) hypothesized rapid penetration of water through the south swale soil profile along preferential flow paths as demonstrated by the presence of a positive Ce anomaly

indicative of oxic conditions in wet and thick soils at this location (Figure 1.2). As a consequence, rapid preferential movement of water (and hence, solutes) downslope via lateral subsurface flow processes may be resulting in increases in Ca/Sr ratio in the progression from ridge top to mid slope to valley floor positions at the swale location. In the case of southern planar exchangeable soils, soils were thinner at ridge top relative to mid slope locations (Figure 1.2). Hence, average Ca/Sr ratios at ridge top locations will be weighted more heavily toward calcium enriched organic horizons (where enrichment is hypothesized to occur either through preferential retention of calcium relative to strontium on ion exchange sites or through calcium inputs from organic restitutions or a combination thereof). Variation in Ca/Sr ratio on a site to site basis was more pronounced at the swale location. As discussed earlier, due to steep topography and sparser vegetation cover (Figure 1.3), lateral subsurface flow dominates hydrological processes at swale locations. Higher Ca/Sr ratios also reflect increased cation exchange capacities in soils in the progression from ridge top to mid slope to valley floor locations of the catchment (Jin et al., 2010). Additionally, groundwater recharge has been found to contribute solutes to porewaters at valley floor locations (Jin et al., 2011b). Groundwaters at Shale Hills are known to contain higher levels of calcium and strontium than soil porewaters (Table 2.1, Table 2.22). The fact that both concentrations are elevated in groundwaters relative to soil porewaters may be responsible for observations of slightly higher porewater Ca/Sr ratios for valley floor compared to ridge top and mid slope locations.

Overall, southern planar porewaters had higher Ca/Sr ratios than those sampled from south swale locations. Steeper topography (Figure 1.2) enhances lateral subsurface flow activities (Lin, 2006; Lin and Zhou, 2008; Graham and Lin, 2011; Jin et al., 2011b; Jin and Brantley, 2011) at swale relative to planar locations to shorten residence times for solutes present

in porewaters at the swale location. Additionally, Naithani et al. (2013) found that tree species density is higher at southern planar relative to south swale locations due to resistance by dominant oak species for growth on wetter soils present at the swale. Furthermore, sugar maple species were found to be more prevalent at planar relative to swale sites of the southern quadrant (Naithani et al., 2013). As will be discussed in detail later, plants preferentially discriminate against strontium relative to calcium but can increase porewater Ca/Sr ratios by releasing calcium through litter decomposition. In fact, Dijkstra and Smits (2002) observed calcium release by sugar maple species to the exchangeable pool through litter decomposition to be especially significant at a temperate forested catchment in Connecticut. Thus, a combination of longer residence times and greater calcium inputs by plants through organic restitutions may be resulting in higher observed Ca/Sr ratios in soil porewaters derived from planar relative to swale locations.

As shown in Table 2.6 and Figure 2.6, southern planar and south swale porewaters and southern planar exchangeable soils showed variation in Ca/Sr ratio with sampling depth. The Ca/Sr ratio was found to increase with depth for southern planar ridge top and mid slope porewaters. For southern planar valley floor porewaters, Ca/Sr ratio decreased down to a depth of 50 cm where increases in Ca/Sr ratio were observed between 50 and 60 cm depths. Ca/Sr ratios for south swale porewaters and southern planar exchangeable soils exhibited more complex patterns across depth gradients (Table 2.6, Figure 2.6). Specifically, Ca/Sr ratios for south swale ridge top porewaters decreased from 10 to 20 cm and then increased from 20 to 30 cm. For south swale mid slope porewaters, Ca/Sr ratios initially decreased down to a depth of 40 cm where increases in Ca/Sr ratio were observed between 40 and 80 cm depths. The south swale mid slope porewater Ca/Sr ratio ultimately stabilized at a value near 260 for depths

corresponding to 100, 120, 140, and 160 cm. For south swale valley floor porewaters, Ca/Sr ratios decreased down to a depth of 40 cm. Thereafter, the Ca/Sr ratio increased from 40 cm to the 60 cm depth. The Ca/Sr ratio settled at a value of 168 for depths between 70 and 80 cm before increasing again from 80 cm to the 90 cm depth. For southern planar ridge top exchangeable soils, the Ca/Sr ratio increased until a depth of 16 cm had been reached beyond which decreases in Ca/Sr ratio were observed. Ca/Sr ratios for southern planar mid slope exchangeable soils decreased down to a depth of 21 cm, ultimately stabilizing at a value of 134 for depths between 21 and 33 cm. For southern planar valley floor exchangeable soils, an alternating decreasing/increasing pattern was observed for depth intervals corresponding to 0 to 22 cm, 22 to 28 cm, 28 to 41 cm, 41 to 59 cm, and 59 to 66 cm.

Patterns in Ca/Sr ratio are consistent with observed preferential flow pathways, particularly at mid slope and valley floor sites of the catchment. As noted by Jin et al. (2011b), mineral weathering largely occurs within soils in low flow zones between A-B horizons of the soil profile due to longer mineral-water contact times present there. From the A-B horizons, solutes released from low flow zones diffuse or laterally flow into high flow zones at A-B and B-C horizon interfaces where weathering is not as intensive and residence times are shorter (Jin et al., 2011b). Thereafter, porewaters advect quickly downslope in perched saturated layers where they can recharge to groundwater (Jin et al., 2011b). Longer water residence times in low flow zones promote greater porewater exposure to clay dissolution processes and, consequently, higher observed solute concentrations for porewaters in these zones (Jin et al., 2011b). Solute concentrations present in high flow zones are attributed to release from ion exchange sites (Jin et al., 2011b) where exchange sites account for 20% of total calcium in ridge top and mid slope soils and 50% of total calcium in valley floor soils (Jin et al., 2010). As mentioned previously,

Lin et al. (2006) observed the accumulation of groundwater at valley floor sites of the catchment. If perched water tables form, fast fluid flushing of soil porewaters with dilute precipitation inputs along both vertical and lateral preferential flow paths may be resulting in the erratic “zig-zag” patterns in Ca/Sr ratio observed for valley floor exchangeable soils and soil porewaters as was observed for magnesium (Jin et al., 2011b).

As shown in Figure 2.9, Ca/Sr ratios of southern planar exchangeable soils and soil porewaters were found to be in disequilibrium, with soil porewater Ca/Sr ratios observed to be roughly twice those measured for exchangeable soils sampled at similar depths. Veresoglou et al. (1996), Capo et al (1998), Poszwa et al. (2000), and Dasch et al (2006) have attributed higher Ca/Sr ratios in porewaters relative to exchangeable soils to the preferential retention of strontium over calcium on exchange sites and hence, less availability of strontium relative to calcium in soil porewaters. Preferential flowpaths along roots or soil aggregates (Lin, 2006; Lin et al., 2006; Lin and Zhou, 2008; Graham and Lin, 2011; Jin et al., 2011b) could also be resulting in the observed disequilibrium between soil porewaters and the exchange pool. The difference between Ca/Sr ratio in the soil solution and on the exchange complex increased with soil depth (Tables 2.1 and 2.3) which lends support to lysimeters sampling soil porewaters from macropores rather than from the soil exchange complex.

Organic horizons for all southern planar locations had higher Ca/Sr ratios than mineral horizons (Table 2.5). As mentioned earlier, quantitative XRD patterns (Jin et al., 2010) indicate greater peat contents in organic relative to mineral horizons at all locations. The preferential retention of calcium over strontium by ion exchange processes has been demonstrated in peat through adsorption isotherms (Baes and Bloom, 1988). In contrast, identical retention of both ions is observed in mineral horizons (Lefevre et al., 1996). Furthermore, additions of calcium

through litter decomposition to organic horizons may be contributing to their higher Ca/Sr ratios.

Table 2.6 Average Ca/Sr ratios for soil porewaters sampled at various depths from southern planar (SP) and south swale (SS) ridge top (RT), mid slope (MS), and valley floor (VF) locations

Location	Depth (cm)	Sr (μM)	Ca (μM)	Average Ca/Sr (molar)
SPRT	10	0.10	27	261
SPRT	20	0.13 ± 0.01	40 ± 4	293 ± 9
SPRT	30	0.14 ± 0.02	46 ± 7	325 ± 12
SPMS	10	0.05 ± 0.00	13 ± 1	241 ± 8
SPMS	40	0.14 ± 0.01	47 ± 2	342 ± 10
SPMS	50	0.15 ± 0.01	53 ± 3	353 ± 11
SPVF	20	0.15 ± 0.01	51 ± 5	341 ± 17
SPVF	30	0.22 ± 0.02	76 ± 10	340 ± 11
SPVF	40	0.18 ± 0.01	59 ± 5	334 ± 8
SPVF	50	0.12	26	227
SPVF	60	0.23 ± 0.01	74 ± 5	312 ± 9
SSRT	10	0.08 ± 0.01	17 ± 2	195 ± 9
SSRT	20	0.07 ± 0.01	10 ± 2	131 ± 13
SSRT	30	0.11 ± 0.01	26 ± 4	231 ± 13
SSMS	10	0.07	23	324
SSMS	20	0.08 ± 0.01	19 ± 2	232 ± 14
SSMS	40	0.16 ± 0.01	36 ± 3	211 ± 7
SSMS	60	0.17 ± 0.01	40 ± 4	218 ± 11
SSMS	80	0.20 ± 0.01	47 ± 4	238 ± 9
SSMS	100	0.21 ± 0.01	56 ± 2	260 ± 5
SSMS	120	0.22 ± 0.01	58 ± 3	260 ± 6
SSMS	140	0.22 ± 0.01	56 ± 4	257 ± 5
SSMS	160	0.22 ± 0.01	58 ± 4	258 ± 8
SSVF	10	0.08 ± 0.01	38 ± 7	425 ± 14
SSVF	20	0.14 ± 0.01	52 ± 9	325 ± 15
SSVF	30	0.13 ± 0.01	34 ± 3	248 ± 10
SSVF	40	0.22 ± 0.01	50 ± 5	230 ± 12
SSVF	50	0.16 ± 0.01	51 ± 10	244 ± 5
SSVF	60	0.12 ± 0.00	30 ± 2	255 ± 14
SSVF	70	0.10	16	168
SSVF	80	0.08 ± 0.00	13 ± 1	168 ± 3
SSVF	90	0.13	30	237

* Error bars are excluded from depths where only one Ca/Sr ratio was measured for a porewater sample at a designated location.

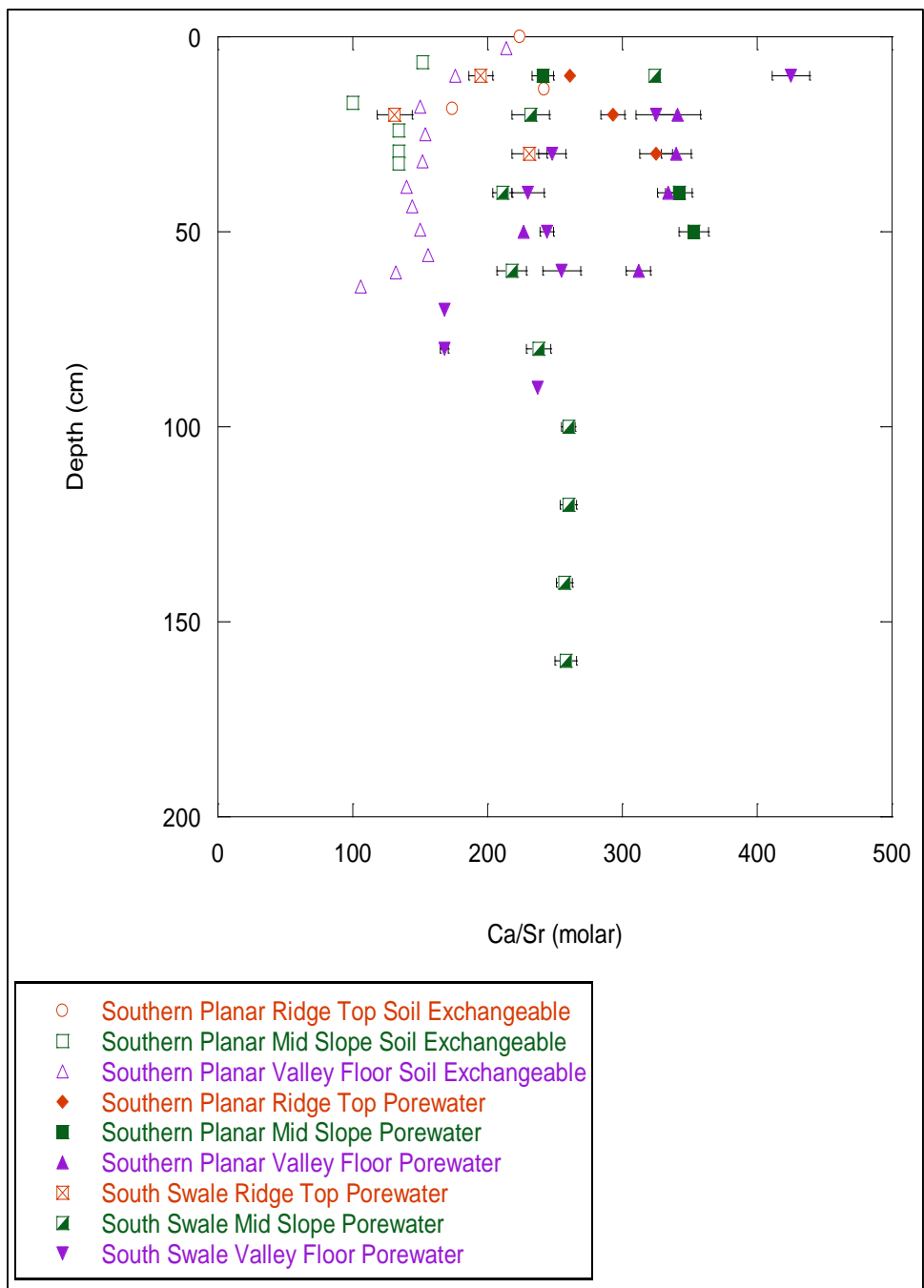


Figure 2.6 Depth versus Ca/Sr ratio for southern planar ridge top, mid slope, and valley floor exchangeable soils and soil porewaters and for south swale ridge top, mid slope, and valley floor soil porewaters with error bars shown for average values. Note that some points on the figure are overlapping.

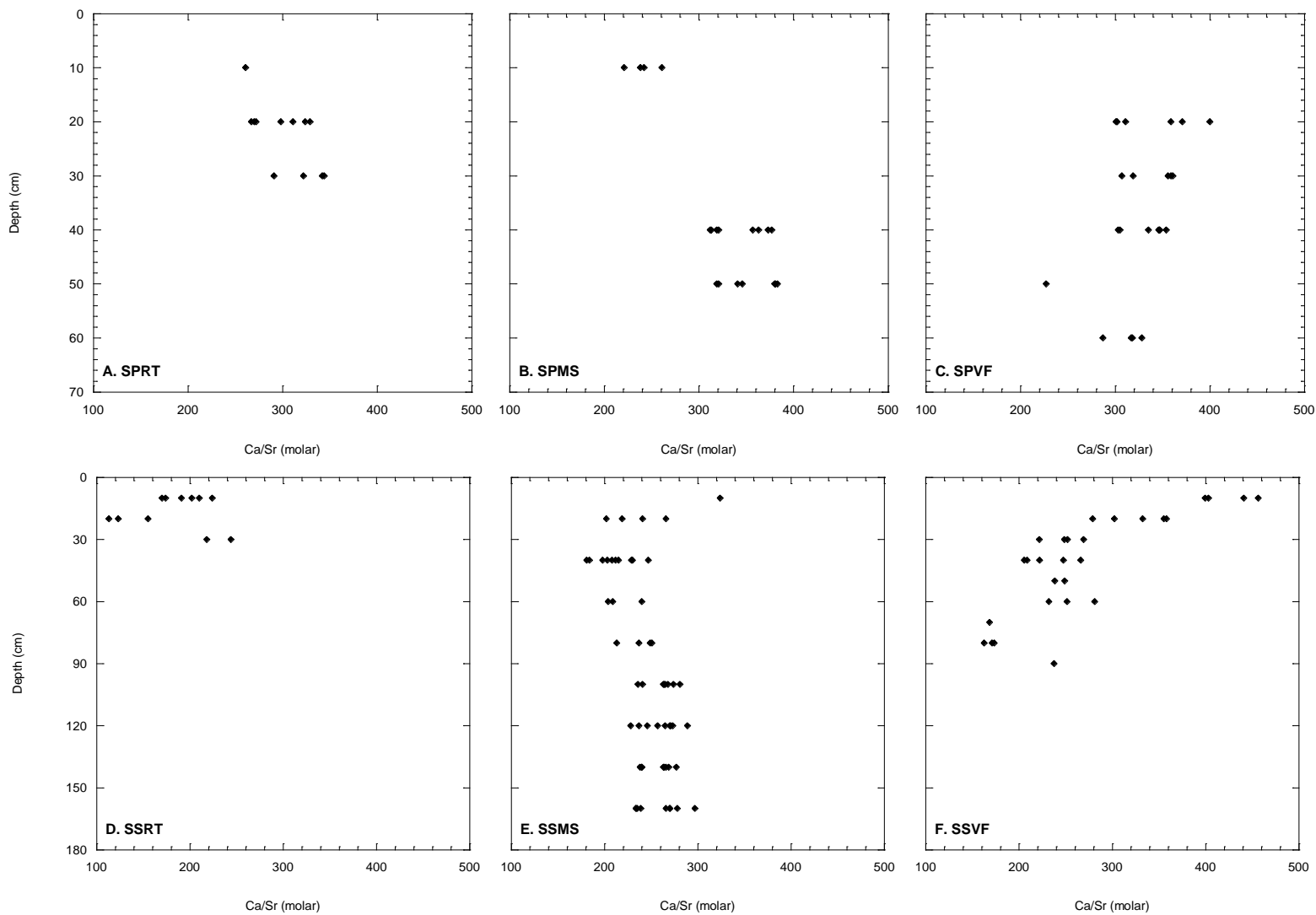


Figure 2.7 Ca/Sr ratios for soil porewaters as a function of depth at southern planar ridge top (SPRT) (A), mid slope (SPMS) (B), and valley floor (SPVF) (C) sites and at south swale ridge top (SSRT) (D), mid slope (SSMS) (E), and valley floor (SSVF) (F) sites.

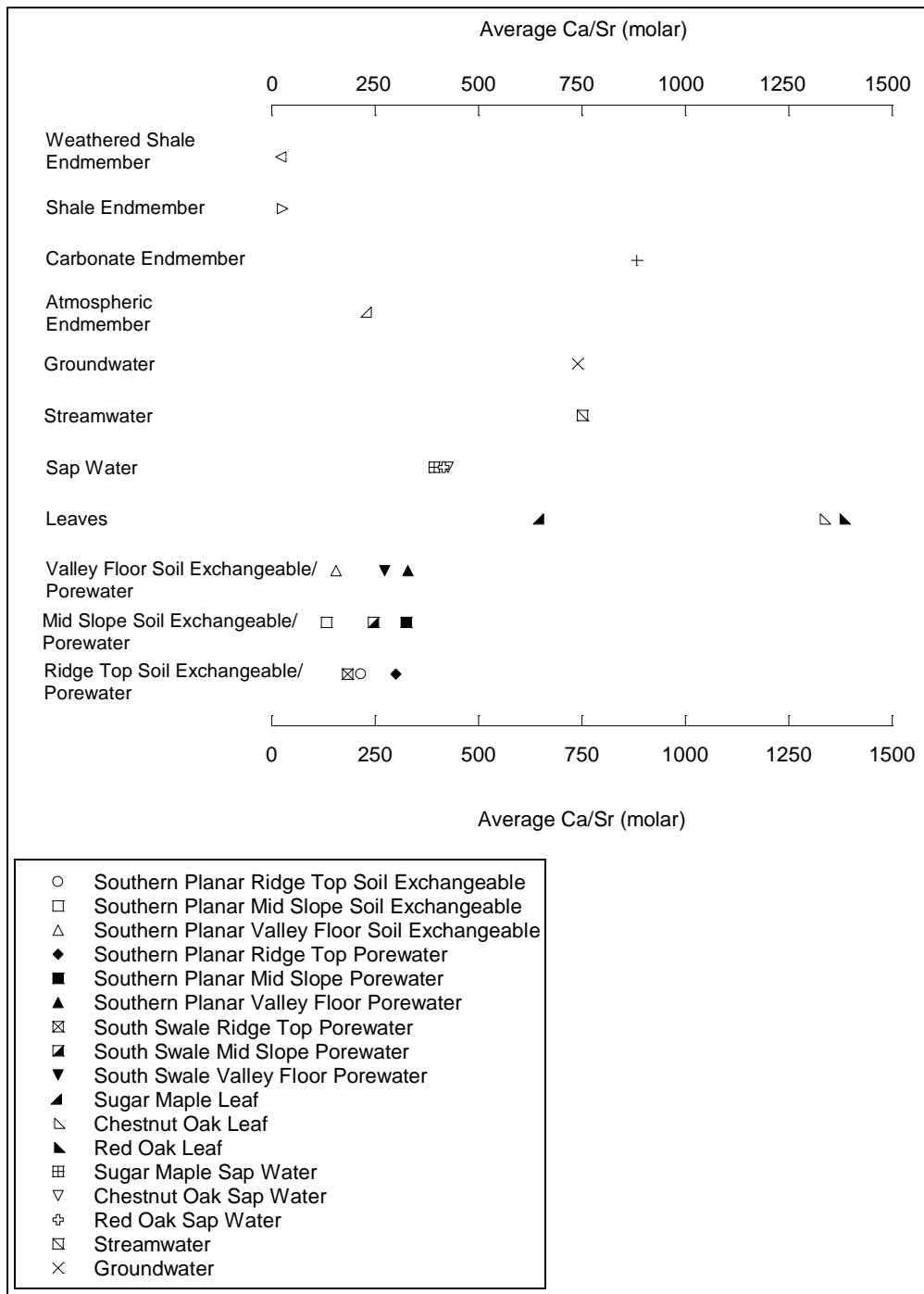


Figure 2.8 Average Ca/Sr ratios for southern planar ridge top, mid slope, and valley floor exchangeable soils and soil porewaters, south swale ridge top, mid slope, and valley floor soil porewaters, sugar maple, chestnut oak, and red oak leaves and sap waters, and streamwaters, groundwaters, and precipitation. Average Ca/Sr ratios for the atmospheric end-member and for carbonate, shale, and weathered shale weathering end-members are also shown on the figure.

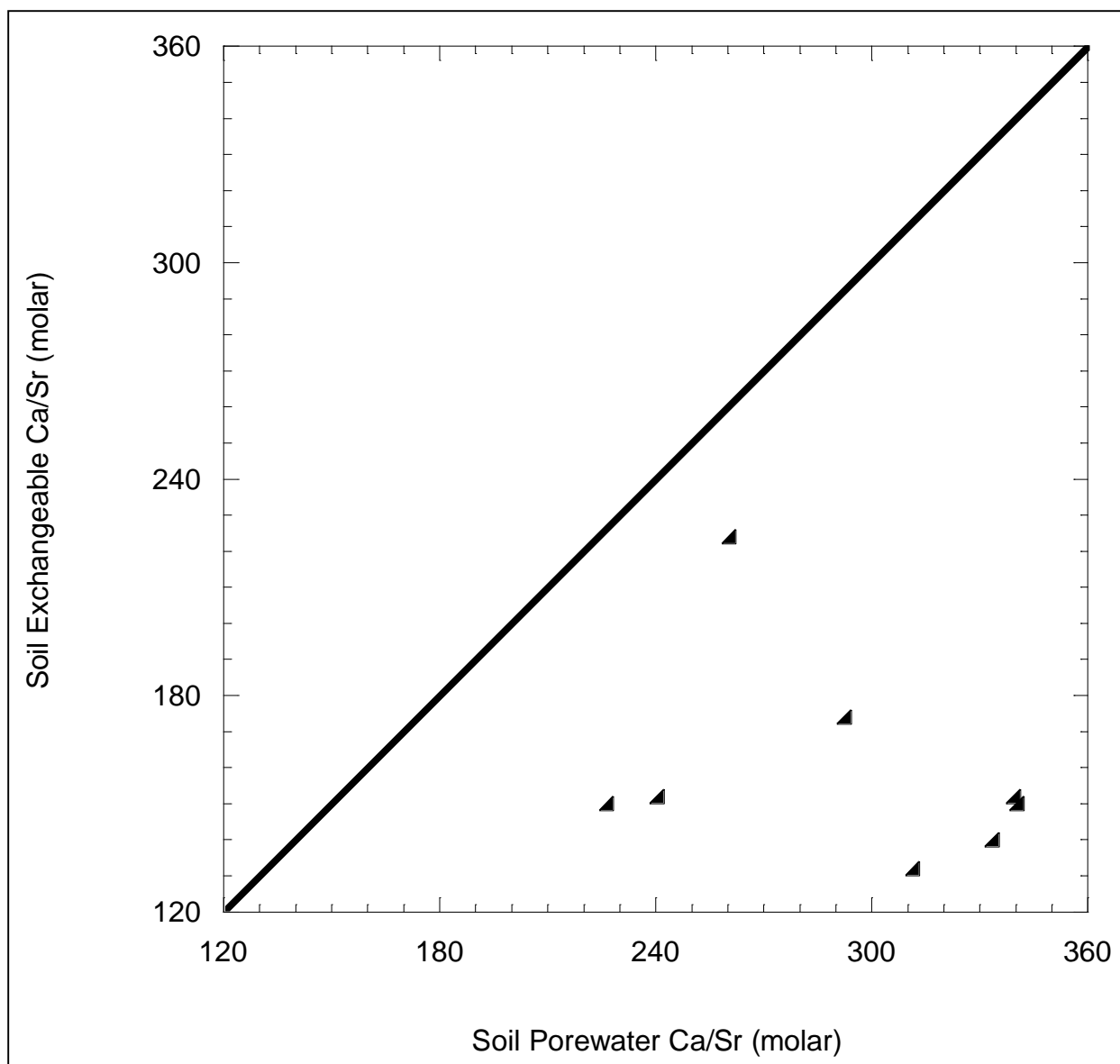


Figure 2.9 Soil exchangeable Ca/Sr ratio versus soil porewater Ca/Sr ratio for samples collected at similar positions and depths of the southern planar transect. The diagonal line represents equilibrium between the exchange pool and soil porewaters.

Over the course of the growing season, $^{87}\text{Sr}/^{86}\text{Sr}$ ratios did not change appreciably for soil porewaters (Table 2.7). As shown in Figure 2.10, plotting individual porewater $^{87}\text{Sr}/^{86}\text{Sr}$ ratios sampled from identical sites and depths during one month of the growing season against corresponding $^{87}\text{Sr}/^{86}\text{Sr}$ ratios measured during a separate month yields a correlation with an R^2 value of 0.99. Southern planar ridge top and south swale valley floor porewaters exhibited the largest monthly variation in $^{87}\text{Sr}/^{86}\text{Sr}$ ratio. The $^{87}\text{Sr}/^{86}\text{Sr}$ ratio of a southern planar ridge top porewater sampled in May was 0.00021 larger than its corresponding ratio measured in July, while the average $^{87}\text{Sr}/^{86}\text{Sr}$ ratio of south swale valley floor porewaters sampled in June was 0.00008 larger than the corresponding average ratio observed in July. Southern planar mid slope porewater $^{87}\text{Sr}/^{86}\text{Sr}$ ratios sampled in May were 0.00003 and 0.00002 smaller than those measured in June and July, respectively. Furthermore, the average $^{87}\text{Sr}/^{86}\text{Sr}$ ratio for southern planar valley floor porewaters in May was 0.00004 smaller than the corresponding average ratio observed in June, while south swale mid slope porewater $^{87}\text{Sr}/^{86}\text{Sr}$ ratios sampled in May were, on average, 0.00006 and 0.00002 smaller than corresponding ratios measured in June and July, respectively. It should be noted that a small sample set was used to test temporal variations in $^{87}\text{Sr}/^{86}\text{Sr}$ ratios for porewaters. A larger data set is necessary to fully assess whether porewater $^{87}\text{Sr}/^{86}\text{Sr}$ ratios significantly change over the course of the growing season across sites.

As shown in Table 2.8 and Figures 2.11 and 2.12, changes in Ca/Sr ratio for porewaters were also modest over the course of the growing season. Overall, average Ca/Sr ratios decreased from May to July for ridge top and mid slope porewaters sampled at both southern planar and south swale locations. Additionally, the average Ca/Sr ratio for southern planar valley floor porewaters decreased from May to June and then increased slightly from June to July, while the average Ca/Sr ratio for south swale valley floor porewaters increased over the course of the

growing season. Leaching of strontium from plant to porewater reservoirs is likely resulting in observed decreases in porewater Ca/Sr over the course of the growing season. Fractionation factors ($K_{Sr/Ca}$) less than one calculated for maple (range: 0.42 to 0.48) and oak (range: 0.19 to 0.24) species lend support to the hypothesis of preferential discrimination against strontium relative to calcium in plants at the catchment. Furthermore, on a monthly basis, plants from all species were shown to accumulate calcium in leaf tissue at a greater rate than strontium based on observations of more positive slopes in linear trends for calcium and strontium (Figure 2.21). Indeed, such partitioning between calcium and strontium has been observed in numerous plant species sampled across a wide range of ecosystems (Poszwa et al., 2000; Watmough and Dillon, 2003; Bullen and Bailey, 2005; Drouet and Herbauts, 2008; Pett-Ridge et al., 2009).

Additionally, higher levels of evapotranspiration over the course of the growing season, as evidenced by more positive $\delta^{18}O$ and δ^2H values observed in shallow soil waters from July to September (Gregor, unpublished data), imply enhanced plant uptake of calcium over strontium to deplete porewaters in calcium relative to strontium. Specifically, shallow soil water $\delta^{18}O$ values increased from July to August to September from -8.67 to -6.81 to -4.77 ‰ (Gregor, unpublished data) and from -8.37 to -5.66 to -4.29 ‰ (Gregor, unpublished data) in southwestern and southeastern quadrants of the catchment, respectively. Additionally, shallow soil water δ^2H values in southwestern and southeastern quadrants increased from -58.55 to -52.40 to -42.09 ‰ (Gregor, unpublished data) and from -62.14 to -43.87 to -38.82 ‰ (Gregor, unpublished data), respectively, from July to August to September. For valley floor locations, direct additions of calcium through groundwater recharge (Lin et al., 2006; Jin et al., 2011b) may be counteracting calcium losses through plant uptake to result in the observed monthly increases in Ca/Sr ratio.

Table 2.7 Seasonal $^{87}\text{Sr}/^{86}\text{Sr}$ ratios for selected southern planar (SP) and south swale (SS) mid slope (MS) and valley floor (VF) soil porewaters

Sample ID	Depth (cm)	May $^{87}\text{Sr}/^{86}\text{Sr}$	June $^{87}\text{Sr}/^{86}\text{Sr}$	July $^{87}\text{Sr}/^{86}\text{Sr}$
SPMS	40	0.72382	nm	0.72384
SPMS	50	0.72358	0.72361	nm
SPVF	30	0.71852	0.71855	nm
SPVF	60	0.71749	0.71753	nm
SSMS	100	0.72589	0.72582	nm
SSMS	120	0.72580	0.72599	nm
SSMS	140	0.72580	0.72572	0.72573
SSMS	160	0.72572	0.72591	0.72594
SSVF	10	nm	0.71900	0.71889
SSVF	40	nm	0.71972	0.71967

*The 'nm' term refers to months when strontium isotope ratios were not measured for a designated porewater sample

Table 2.8 Seasonal Ca/Sr ratios for soil porewaters sampled from southern planar and south swale ridge top, mid slope, and valley floor locations

Location	Average May Ca/Sr (molar)	Average June Ca/Sr (molar)	Average July Ca/Sr (molar)
Southern Planar Ridge Top	323 ± 13	302 ± 12	280 ± 14
Southern Planar Mid Slope	360 ± 17	310 ± 16	294 ± 24
Southern Planar Valley Floor	351 ± 7	294 ± 15	317 ± 8
South Swale Ridge Top	219 ± 13	174 ± 17	167 ± 30
South Swale Mid Slope	258 ± 6	247 ± 6	231 ± 6
South Swale Valley Floor	260 ± 30	265 ± 24	291 ± 27

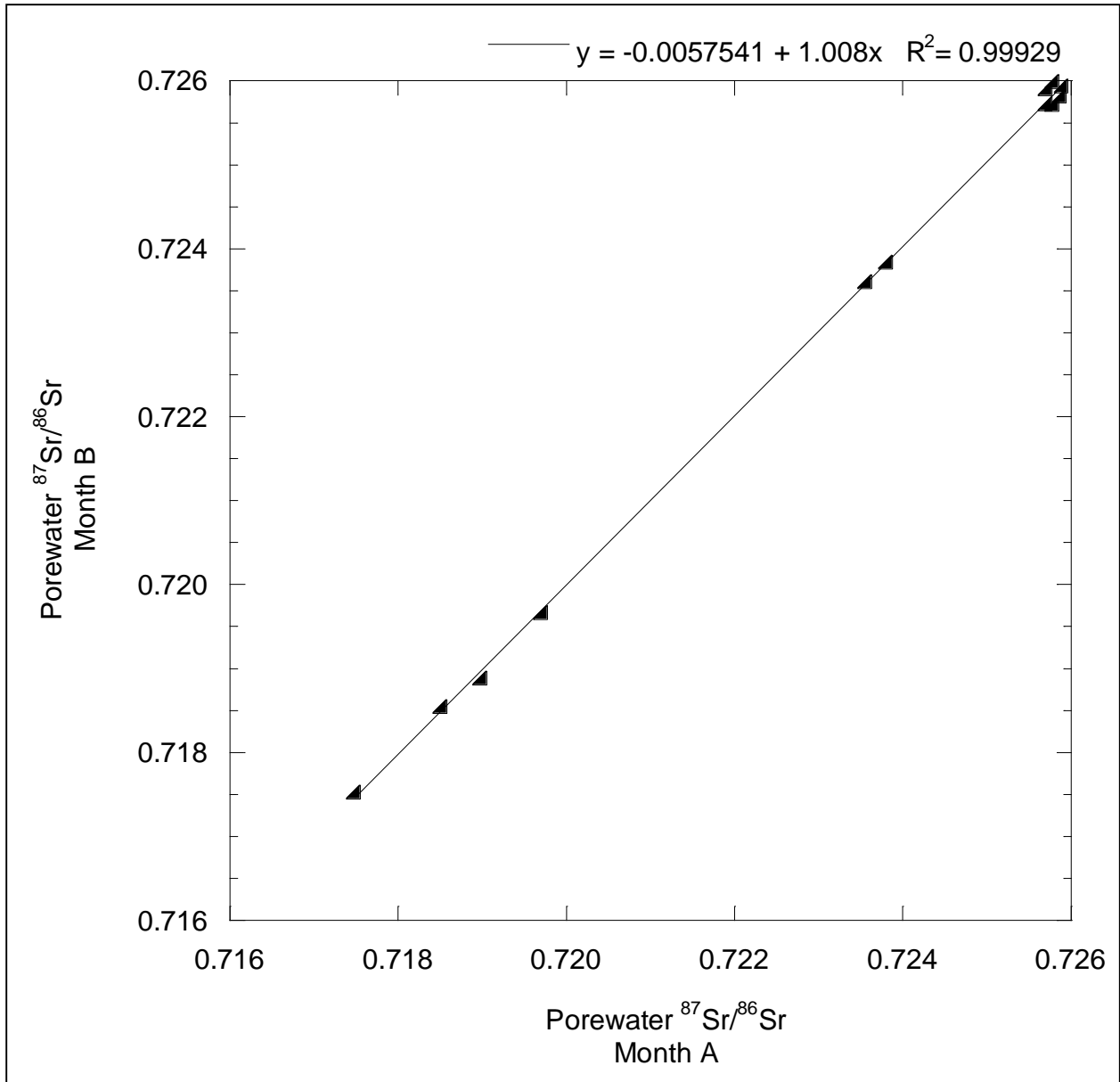


Figure 2.10 Soil porewater ⁸⁷Sr/⁸⁶Sr ratio of month B versus soil porewater ⁸⁷Sr/⁸⁶Sr ratio of month A for individual porewaters sampled at identical sites and depths. A correlation yielding an R² value of 0.99 is shown.

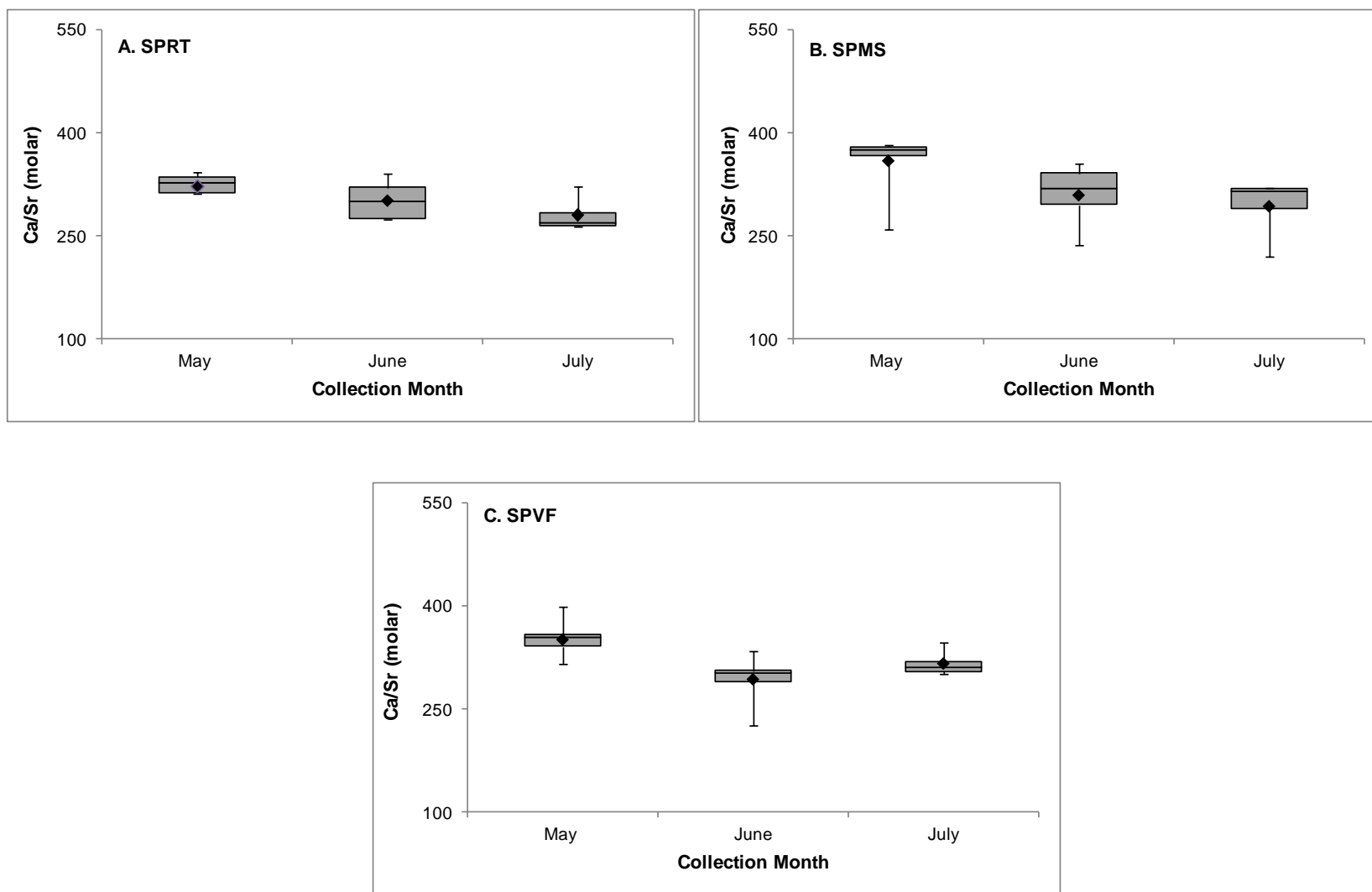


Figure 2.11 Box plots of Ca/Sr ratio for southern planar ridge top (SPRT, A), mid slope (SPMS, B), and valley floor (SPVF, C) soil porewaters over the course of the growing season with mean values shown as closed diamonds.

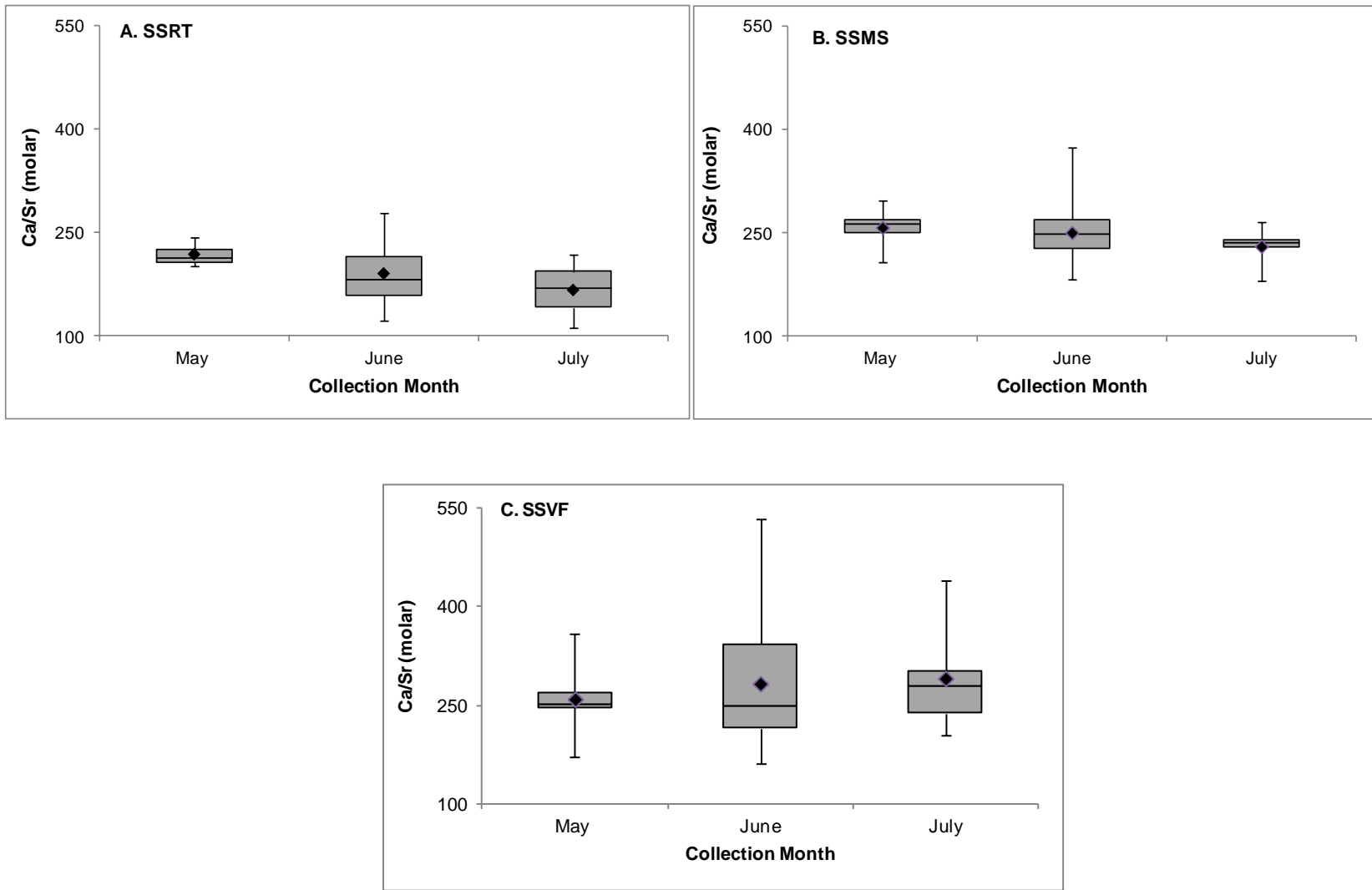


Figure 2.12 Box plots of Ca/Sr ratio for south swale ridge top (SSRT, A), mid slope (SSMS, B), and valley floor (SSVF, C) soil porewaters over the course of the growing season with mean values shown as closed diamonds.

4.2 Leaves

Sugar maple, chestnut oak, and red oak leaf $^{87}\text{Sr}/^{86}\text{Sr}$ ratios ranged from 0.72218 to 0.72585, 0.72101 to 0.72484, and 0.72275 to 0.72472 (Table 2.9), respectively, with average values of 0.72388 ± 0.00019 , 0.72359 ± 0.00024 , and 0.72364 ± 0.00058 , respectively (Table 2.10, Figure 2.2). Minimal variation in leaf $^{87}\text{Sr}/^{86}\text{Sr}$ ratio existed between tree species with sugar maple leaves found to be slightly more radiogenic than oak leaves. Within oak species, slight variations in average $^{87}\text{Sr}/^{86}\text{Sr}$ ratio were observed with red oak leaves found to be more radiogenic than chestnut oak leaves. These observations are illustrated through mixing calculations (Figures 2.14 and 2.15) which indicate relatively similar proportions of strontium derived from atmospheric and weathering sources for maple and oak leaves and sap waters sampled from similar quadrants and transect positions. As noted previously, $^{87}\text{Sr}/^{86}\text{Sr}$ ratios in leaves were found to be in close agreement to those measured in soil exchangeable horizons and soil porewaters (Table 2.1, Figure 2.2), suggestive of the rapid homogenization of strontium added from weathering and atmospheric inputs by biological nutrient cycling processes.

Two-component strontium mixing calculations were performed for leaves and sap waters through Equation 1 using strontium isotope ratios for bulk precipitation ($^{87}\text{Sr}/^{86}\text{Sr} = 0.71054$) and “weathered shale” ($^{87}\text{Sr}/^{86}\text{Sr} = 0.72967$) as atmospheric and silicate weathering end-members, respectively. As mentioned previously, Gaines (unpublished data) and Gregor (unpublished data) have found that $\delta^{18}\text{O}$ values in leaves and sap waters correspond more closely to those in shallow underlying soils than groundwaters with typical plant rooting depths estimated to be less than 50 cm. These observations suggest that trees in this study are largely acquiring water (and hence, solutes) from shallow soil exchange pool and soil porewater sources. Consequently, leaves and sap waters were modeled using the same end-members as those used in mixing calculations for

ridge top and mid slope exchangeable soils and soil porewaters. As mentioned in the Data Analysis Methods section, $^{87}\text{Sr}/^{86}\text{Sr}$ ratios for sugar maple and chestnut oak leaves collected at valley floor positions closely resembled those sampled at ridge top and mid slope positions of the northeastern quadrant (Table 2.9). Strontium isotope ratios were not measured for north swale valley floor exchangeable soils or soil porewaters where northeastern leaves were collected. However, strontium isotope ratios of sugar maple and oak leaves sampled at valley floor positions of this quadrant seem to suggest that the carbonate source affecting chemistry in southern quadrant valley floor exchangeable soils and soil porewaters and in groundwaters and streamwaters is not influencing chemistry in north swale valley floor exchangeable soils or soil porewaters. Consequently, two component mixing calculations were also applied to valley floor leaves in the northeastern quadrant using the same atmospheric and silicate weathering end-members as those used in calculations for ridge top and mid slope leaves and sap waters. Detailed rationale behind selection of end-members and parameters used in mixing calculations can be found in the Data Analysis Methods section. No significant difference in $^{87}\text{Sr}/^{86}\text{Sr}$ ratio was observed for sap waters and leaves collected from identical trees at the same time as evidenced by an R^2 value of 0.93 generated from the plot of leaf $^{87}\text{Sr}/^{86}\text{Sr}$ versus sap water $^{87}\text{Sr}/^{86}\text{Sr}$ (Figure 2.13). As such, combined results from mixing calculations performed for leaves and sap waters collected at mid slope positions from all quadrant locations in 2013 are depicted in Figure 2.14.

As shown in Table 2.11 and Figure 2.14, leaves and sap waters sampled from mid slope positions in western quadrants had lower $^{87}\text{Sr}/^{86}\text{Sr}$ ratios and derived greater proportions of strontium from atmospheric sources than those collected in eastern quadrants for all tree species analyzed. Specifically, mixing calculations indicated that percentages of atmospherically derived

strontium in northwestern sugar maple, chestnut oak, and red oak leaves and sap waters were $39 \pm 0.4\%$, 40% , and $47 \pm 0.7\%$, respectively, compared to $31 \pm 0.8\%$, $30 \pm 1.3\%$, and $32 \pm 2.6\%$, respectively, for leaves and sap waters collected from corresponding species in the northeastern quadrant. Additionally, southwestern sugar maple, chestnut oak, and red oak leaves and sap waters derived $40 \pm 2.0\%$, $43 \pm 1.3\%$; and $47 \pm 1.0\%$ of strontium from atmospheric sources, respectively, compared to $33 \pm 2.5\%$, $38 \pm 5.1\%$, and $33 \pm 3.8\%$, respectively, for leaves and sap waters collected from corresponding species in the southeastern quadrant. Proportions of atmospherically derived strontium in southeastern and southwestern leaves and sap waters sampled at mid slope positions (Figure 2.14) fall within the range of values reported for organic soil horizons and shallow soil porewaters sampled from similar quadrants and transect positions (Figure 2.3). Accordingly, lower $^{87}\text{Sr}/^{86}\text{Sr}$ ratios and higher atmospheric proportions of strontium were also observed for shallow southern planar mid slope (southwestern) soil porewaters compared to those sampled at the south swale (southeastern) mid slope location (Table 2.1, Figures 2.1 and 2.3). As mentioned previously, field observations of wetter and thicker soils with less vegetation cover at swale relative to planar locations (Figures 1.2 and 1.3) suggest greater hydrologic activity to initiate subsurface weathering reactions at swale locations. This will presumably increase $^{87}\text{Sr}/^{86}\text{Sr}$ ratios and proportions of strontium derived from silicate weathering sources in leaves collected from eastern (swale) relative to western (planar) locations.

However, strontium isotope ratios (Table 2.11) and atmospheric percentages of strontium in leaves and sap waters (Figure 2.14) from all species were shown to be rather similar between northeastern and southeastern quadrants (31 vs. 33% , 30 vs. 38% , and 32 vs. 33% for sugar maple, chestnut oak, and red oak species) and between northwestern and southwestern quadrants (39 vs. 40% , 40 vs. 43% , and 47 vs. 47%). Interestingly, erosion rates, topography, solar

radiation levels, and vegetation cover vary considerably between northern and southern quadrants of the catchment. Specifically, a combination of physical (e.g. higher frequency cycles of freeze/thaw and drying/wetting, snow cover over shorter time periods due to increased sunlight exposure from the east-west orientation of the catchment, Ma et al., 2011), hydrological (e.g. connected macropore system facilitating lateral subsurface flow processes downslope, Lin, 2006), and biological (e.g. less evapotranspiration as a result of less vegetation cover enabling infiltration of precipitation to surface soils and the subsequent downslope transport of water through lateral subsurface flow processes, Naithani et al., 2013) accelerate surface erosion rates in the northern quadrant. As a consequence, shorter durations of chemical weathering have been identified in surface regolith particles sampled from northern quadrants of the catchment (Ma et al., 2010). These observations would suggest less radiogenic $^{87}\text{Sr}/^{86}\text{Sr}$ ratios and lower proportions of strontium derived from silicate weathering in exchangeable soils and soil porewaters from which leaves are acquiring strontium in northern quadrants. Reasons for discrepancy between observed and predicted outcomes are unclear and require future research.

In the northeastern quadrant, percentages of atmospherically derived strontium decreased (Figure 2.15) while strontium isotope ratios increased (Table 2.12) in the progression from ridge top to mid slope to valley floor positions for maple (from 33 to 30 to 25%, respectively) and oak (from 34 to 32 to 28%, respectively) species. No strontium isotope data was compiled for porewaters in the north swale transect preventing a rigorous interpretation of these observed patterns. However, hypotheses can be developed based on observations from this study as well as other studies at the catchment (Lin, 2006; Naithani et al., 2013; Gaines, unpublished data). Deeper, more hydrologically active soils with well-connected macropores in the northeastern quadrant (Lin, 2006) facilitate subsurface lateral flow pathways which transfer weathering

products from ridge top to mid slope to valley floor locations. Additionally, less vegetation cover at the ridge (Figure 1.3, Naithani et al., 2013) coupled with slightly higher cumulative rainfall (Lin, 2006) enable infiltration to surface soils and the subsequent downslope transport of weathering products through lateral subsurface flow processes in the northeastern quadrant. Based on these observations, increases in $^{87}\text{Sr}/^{86}\text{Sr}$ ratio and proportions of weathering derived strontium in leaves in the progression from ridge top to mid slope to valley floor locations of the northeastern quadrant seem reasonable. Furthermore, higher elevation ridge top locations have greater exposure to inputs from atmospheric sources than shielded canopies at the valley floor (Parker, 1983) where highly soluble particles are transferred through throughfall and stemflow to the forest floor and ultimately to tree roots. Additionally, Gaines (unpublished data) has noted that trees sampled from valley floor locations have deeper effective rooting depths (up to 100 cm) than those sampled from ridge top and mid slope locations, on average. It has been shown that proportions of strontium derived from silicate mineral weathering sources increases with depth for exchangeable soils and soil porewaters in the southern quadrant of the catchment (Figures 2.3 and 2.4). If these observations are extended to exchangeable soils and soil porewaters in the northeastern quadrant, then greater weathering derived sources of strontium (Figure 2.15) and higher $^{87}\text{Sr}/^{86}\text{Sr}$ ratios (Table 2.12) in valley floor relative to ridge top leaves may be due to deeper effective rooting depths which enable trees to acquire strontium from deeper, more radiogenic exchangeable soil and soil porewater reservoirs at valley floor locations.

Table 2.9 Strontium and calcium elemental concentrations and Ca/Sr and $^{87}\text{Sr}/^{86}\text{Sr}$ ratios for chestnut oak (QUPR), red oak (QURU), and sugar maple (ACSA) leaves sampled at ridge top (RT), mid slope (MS), and valley floor (VF) sites in northeastern (NE), northwestern (NW), southeastern (SE), and southwestern (SW) quadrants of the catchment

Sample Date	Sample ID	Species Code	Site	Sr (mg/g dry leaf)	Ca (mg/g dry leaf)	Ca/Sr (molar)	$^{87}\text{Sr}/^{86}\text{Sr}$
6/9/2011	AS 356	ACSA	MS	0.06	11.25	740	0.72383
6/9/2011	AS 437	ACSA	RT	0.05	6.15	649	0.72348
6/14/2011	QP 358	QUPR	MS	0.02	10.29	670	0.72376
6/16/2011	AS 352	ACSA	MS	0.06	11.85	215	0.72296
6/21/2011	AS 2062	ACSA	VF	0.07	7.52	249	0.72585
6/21/2011	AS Near AS 2063	ACSA	MS	0.06	5.00	184	0.72514
6/24/2011	QR 325	QURU	VF	0.02	5.59	648	0.72275
6/24/2011	AS Near QP 347	ACSA	MS	0.03	7.79	277	0.72436
6/27/2011	AS Near QP 330	ACSA	VF	0.05	7.77	319	0.72422
6/27/2011	QP 330	QUPR	VF	0.02	5.07	585	0.72440
7/6/2011	AS 2059	ACSA	RT	0.07	8.74	258	0.72303
7/6/2011	AS 2061	ACSA	MS	0.04	6.79	428	0.72393
7/6/2011	QP 2060	QUPR	MS	0.04	11.59	684	0.72287
7/6/2011	QP 393	QUPR	RT	0.01	7.66	1231	0.72396
7/6/2011	QP 396	QUPR	RT	0.01	9.61	1451	0.72384
7/7/2011	AS 2063	ACSA	MS	0.04	10.71	650	0.72425
7/7/2011	QP 347	QUPR	MS	0.02	15.95	1358	0.72420
7/12/2011	AS 2062	ACSA	VF	0.05	6.44	338	0.72583
7/12/2011	AS 2064	ACSA	VF	0.04	7.67	372	0.72429
7/12/2011	AS 2067	ACSA	VF	0.05	5.42	229	0.72370
7/12/2011	QP 330	QUPR	VF	0.01	9.93	1747	0.72416
7/12/2011	QP 332	QUPR	VF	0.01	2.67	585	0.72452
7/12/2011	QP 340	QUPR	VF	0.03	7.76	588	0.72484
7/14/2011	AS 387	ACSA	MS	0.08	8.59	275	0.72408
7/14/2011	QP 390	QUPR	MS	0.02	10.13	1252	0.72359
7/19/2011	QP 1219	QUPR	VF	0.00	3.24	1095	0.72420
7/19/2011	QP 230	QUPR	RT	0.03	8.73	1063	0.72223
8/30/2011	AS 2061	ACSA	MS	0.10	6.01	130	0.72392
8/30/2011	AS 352	ACSA	MS	0.06	16.78	337	0.72308
8/30/2011	AS 356	ACSA	MS	0.05	19.17	550	0.72377
8/30/2011	QP 230	QUPR	RT	0.08	7.21	474	0.72254
8/30/2011	QP 351	QUPR	MS	0.02	9.61	1151	0.72326
9/13/2011	AS 2064	ACSA	VF	0.05	7.63	307	0.72464

9/13/2011	AS 2065	ACSA	VF	0.06	8.97	337	0.72525
9/13/2011	AS 2066	ACSA	RT	0.07	13.14	414	0.72383
9/13/2011	QP 330	QUPR	VF	0.02	7.46	1083	0.72406
7/17/2013	NE NO TAG	ACSA	MS	0.03	9.34	617	0.72360
8/12/2013	NW 137	ACSA	MS	0.03	9.83	756	0.72218
8/12/2013	SW 1164	ASCA	MS	0.05	14.19	623	0.72258
8/13/2013	SE DOWNHILL	ACSA	MS	0.03	6.88	536	0.72341
9/27/2013	NE DOWNHILL	ACSA	MS	0.08	20.88	606	0.72340
9/27/2013	NW UPHILL	ACSA	MS	0.06	17.58	681	0.72224
9/27/2013	NE 622	QUPR	MS	0.02	11.46	1091	0.72476
9/27/2013	SE 1329	QUPR	MS	0.02	13.74	1425	0.72235
9/27/2013	SW 1080	QUPR	MS	0.02	10.27	1301	0.72101
9/27/2013	SE 1271	QURU	MS	0.03	14.23	1182	0.72345
9/27/2013	SE 1331	QURU	MS	0.02	8.23	1036	0.72472

*Ca/Sr ratios and Sr and Ca elemental concentrations for additional leaf samples where Sr isotope ratios were not measured are displayed in the appendix.

Table 2.10 Average Ca/Sr and $^{87}\text{Sr}/^{86}\text{Sr}$ ratios for sugar maple, chestnut oak, and red oak leaves

Tree Species	Average Ca/Sr	Average $^{87}\text{Sr}/^{86}\text{Sr}$
Sugar Maple	649 ± 16	0.72388 ± 0.00019
Chestnut Oak	1335 ± 35	0.72359 ± 0.00024
Red Oak	1382 ± 47	0.72364 ± 0.00058

*The average Ca/Sr ratios listed correspond to leaves sampled from June to September of 2013.

Table 2.11 Average $^{87}\text{Sr}/^{86}\text{Sr}$ ratios for sugar maple, chestnut oak, and red oak leaves sampled at mid slope positions in northeastern (NE), northwestern (NW), southeastern (SE), and southwestern (SW) quadrants of the catchment

Location	Average Sugar Maple $^{87}\text{Sr}/^{86}\text{Sr}$	Average Chestnut Oak $^{87}\text{Sr}/^{86}\text{Sr}$	Average Red Oak $^{87}\text{Sr}/^{86}\text{Sr}$
NE	0.72411 ± 0.00017	0.72382 ± 0.00019	0.72275
NW	0.72221 ± 0.00003	nm	nm
SE	0.72341	0.72235	0.72409 ± 0.00019
SW	0.72258	0.72101	nm

*The 'nm' term refers to quadrant locations where strontium isotope ratios were not measured for leaves collected from a designated tree species.

*Error bars are excluded from locations where only one $^{87}\text{Sr}/^{86}\text{Sr}$ ratio was measured for a designated leaf species.

Table 2.12 Average $^{87}\text{Sr}/^{86}\text{Sr}$ ratios and Ca/Sr ratios for sugar maple and chestnut oak leaves collected at ridge top, mid slope, and valley floor positions of the northeastern quadrant from June to September of 2011

Parameter	Ridge Top	Mid Slope	Valley Floor
<i>Sugar Maple</i>			
Average $^{87}\text{Sr}/^{86}\text{Sr}$	0.72345 ± 0.00023	0.72393 ± 0.00016	0.72483 ± 0.00032
Average Ca/Sr (molar)	505 ± 103	365 ± 51	300 ± 18
<i>Chestnut Oak</i>			
Average $^{87}\text{Sr}/^{86}\text{Sr}$	0.72314 ± 0.00044	0.72354 ± 0.00023	0.72436 ± 0.00025
Average Ca/Sr (molar)	844 ± 107	752 ± 115	1061 ± 125

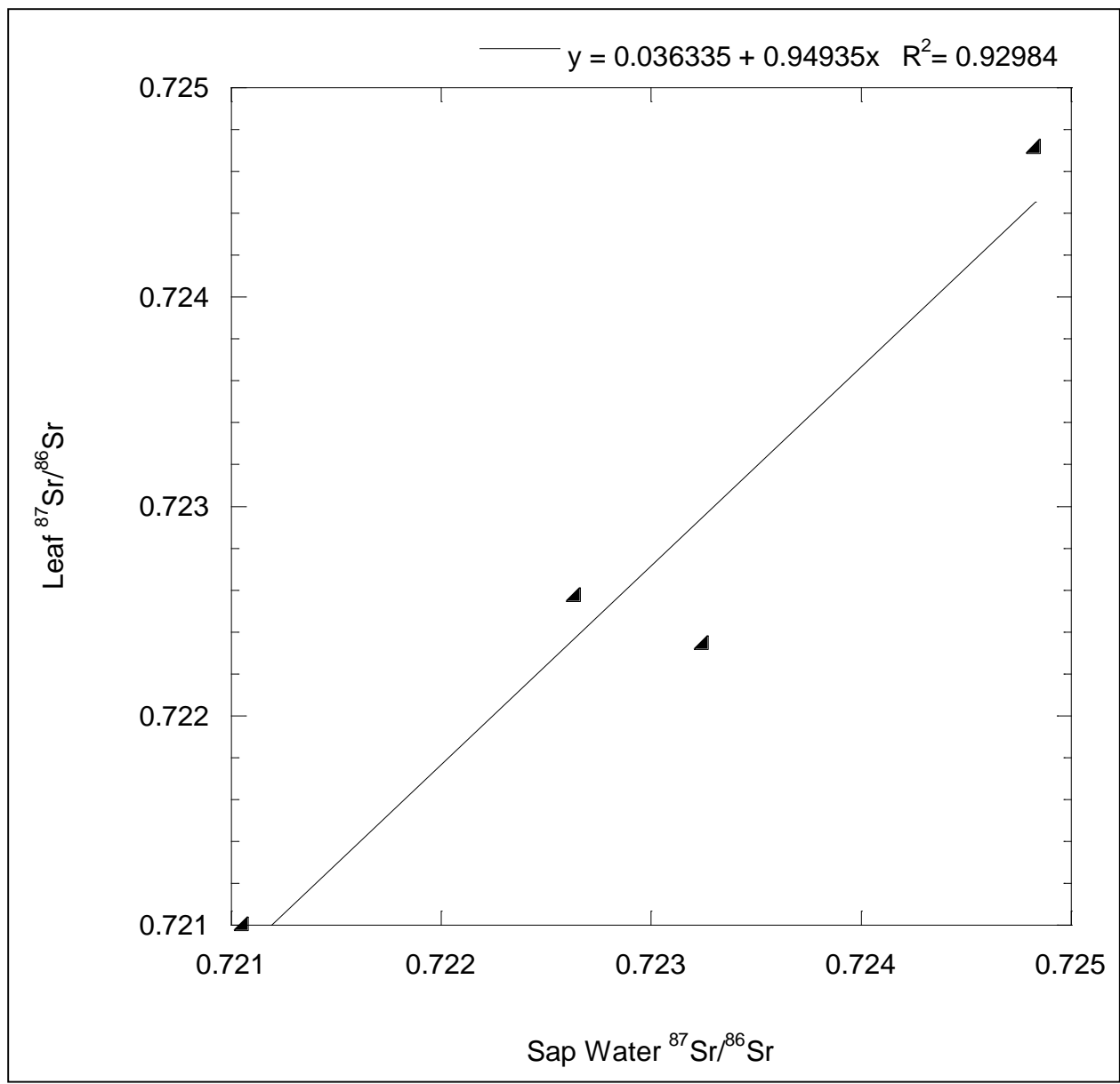
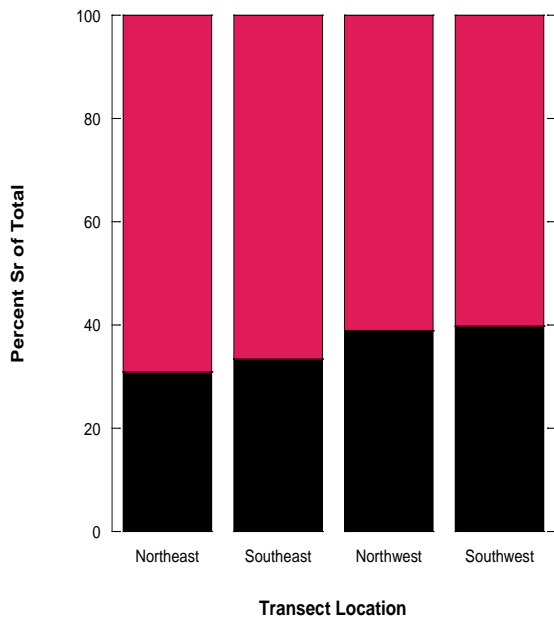
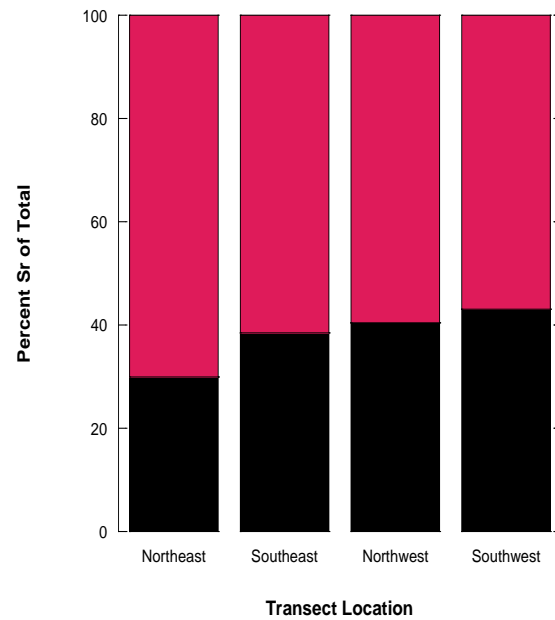


Figure 2.13 Leaf ⁸⁷Sr/⁸⁶Sr ratio versus sap water ⁸⁷Sr/⁸⁶Sr ratio for samples collected at the same time from identical trees. A correlation yielding an R² value of 0.93 is shown.

A. Sugar Maple



B. Chestnut Oak



C. Red Oak

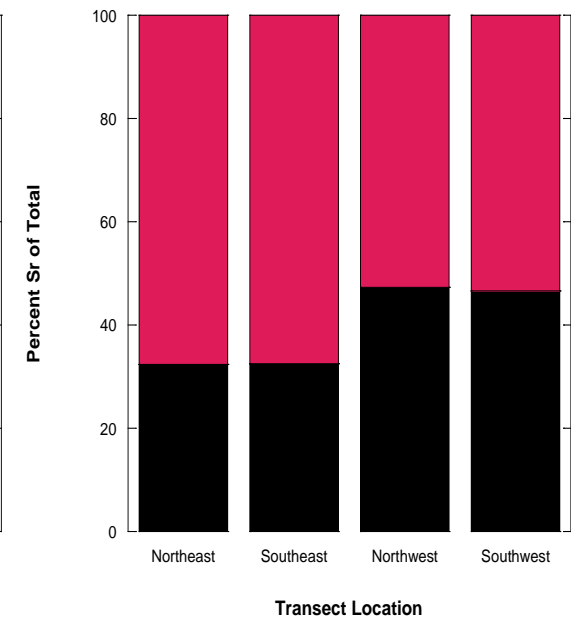
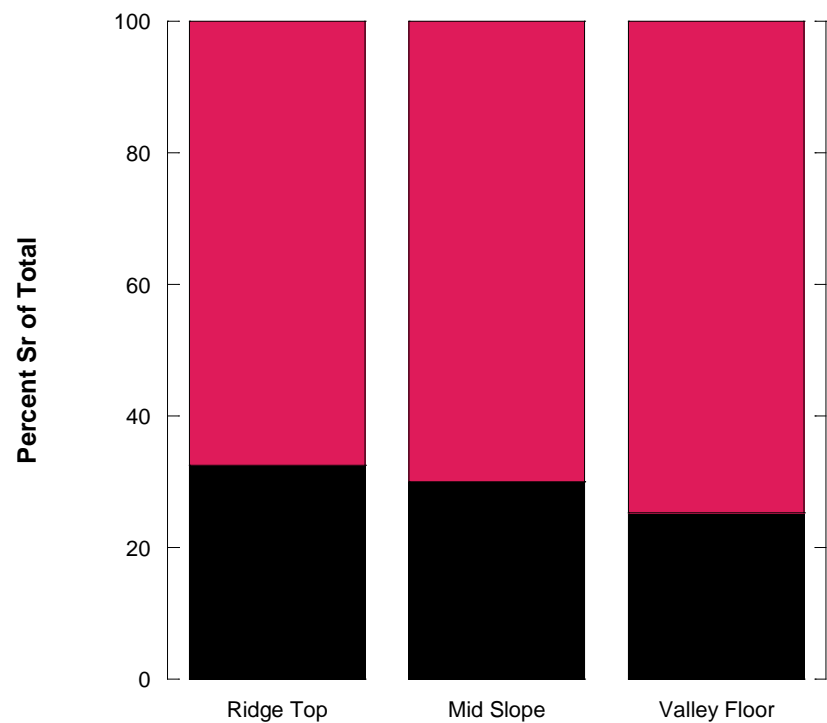
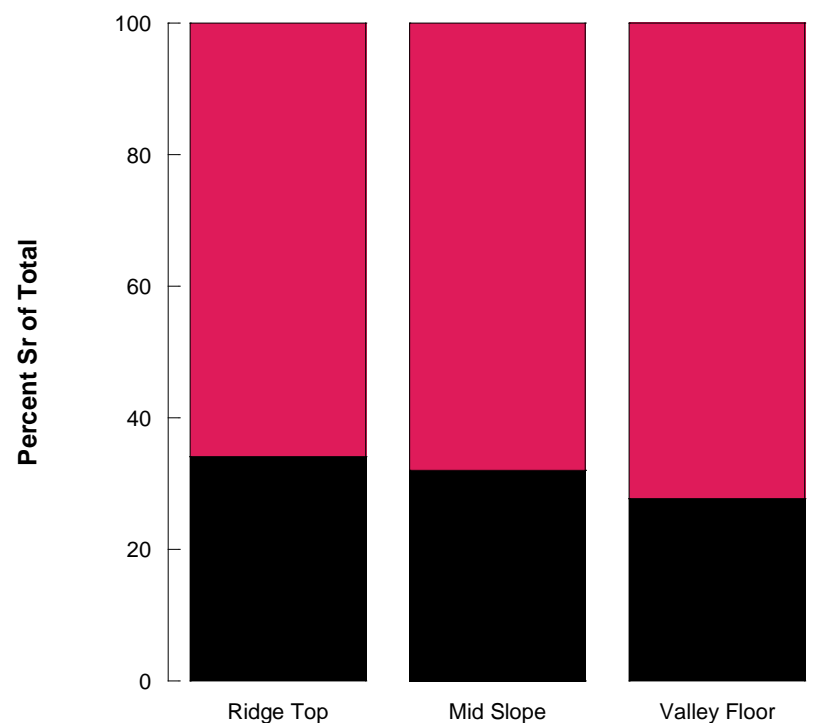


Figure 2.14 Percentage of strontium derived from silicate weathering (pink) and atmospheric (black) sources for sugar maple (A), chestnut oak (B), and red oak (C) leaves and sap waters sampled at mid slope positions in northeastern, southeastern, northwestern, and southwestern quadrants of the catchment in 2013.

A. Sugar Maple



B. Chestnut Oak



Northeastern Transect Position

Northeastern Transect Position



Figure 2.15 Percentage of strontium derived from silicate weathering (pink) and atmospheric (black) sources for sugar maple (A) and chestnut oak (B) leaves sampled at ridge top, mid slope, and valley floor positions of the northeastern quadrant in 2011.

Sugar maple, chestnut oak, and red oak average Ca/Sr ratios for leaves sampled at mid slope positions in northeastern, northwestern, southeastern, and southwestern quadrants from June to September of 2013 ranged from 534 to 796, 1080 to 1762, and 1036 to 1799 (Table 2.9), respectively, with average values of 649 ± 16 , 1335 ± 35 , and 1382 ± 47 , respectively (Table 2.10, Figure 2.8). Ca/Sr ratios for sugar maple leaves sampled at ridge top, mid slope, and valley floor positions in the northeastern quadrant from June to September of 2011 ranged from 258 to 700, 130 to 740, and 229 to 372 (Appendix), respectively, with average values of 505 ± 103 , 365 ± 51 , and 300 ± 18 (Table 2.12), respectively. For chestnut oak leaves sampled at ridge top, mid slope, and valley floor positions of the northeastern quadrant from June to September of 2011, Ca/Sr ratios ranged from 328 to 1451, 218 to 1358, and 585 to 1747 (Appendix), respectively, with average values of 844 ± 107 , 752 ± 115 , and 1061 ± 125 , respectively (Table 2.12). Composite average Ca/Sr ratios for sugar maple and chestnut oak leaves collected from all positions in 2011 were 367 ± 33 and 888 ± 68 , respectively. A Ca/Sr ratio of 648 was observed for an individual red oak leaf sampled at a mid slope position of the northeastern quadrant in 2011. Observed calcium and strontium concentrations used for determination of molar Ca/Sr ratios are consistent with those reported by Herndon (2012) for maple and oak leaves at the catchment. As shown in Figure 2.8, average leaf Ca/Sr ratios were significantly higher than those determined for exchangeable soils, soil porewaters, sap waters, streamwaters, groundwaters, and bedrock. Higher Ca/Sr ratios in leaves are likely due to the preferential discrimination against strontium relative to calcium by plants which has been observed in numerous studies conducted in a wide range of ecosystems (Bailey et al., 1996; Poszwa et al., 2000; Bullen and Bailey, 2005; Dasch et al, 2006; Blum et al., 2008, 2012; Pett-Ridge et al., 2009; Funk and Amantangelo, 2013; Watmough, 2014).

Average leaf Ca/Sr ratios suggest that biological fractionation occurs between calcium and strontium to varying degrees among tree species at the catchment. As shown in Tables 2.9, 2.10, 2.12, and 2.13 and Figure 2.8, leaves derived from maples displayed significantly lower Ca/Sr ratios than those derived from oaks. Within oak species, red oak leaves had higher Ca/Sr ratios than chestnut oak leaves, on average (Tables 2.9, 2.10, and 2.13, Figure 2.8). Given strontium's utility as a tracer for calcium in catchment studies (Miller et al., 1993; Bailey et al., 1996; Kennedy et al., 2002; Bullen and Bailey, 2005; Blum et al., 2008; Pett-Ridge et al., 2009), similarities in strontium isotope ratio among foliage derived from maple and oak species (Table 2.1, Figure 2.8) seem to imply that discrepancy in foliar Ca/Sr ratio among species reflects variable degrees of uptake rather than different sources from which plants are acquiring solutes. Indeed, variation in partitioning between calcium and strontium among tree species growing in the same soil agrees with findings in other studies (Runia, 1987; Veresoglou et al., 1996; West et al., 2001; Drouet and Herbauts, 2008; Blum et al., 2012). Fractionation factors were calculated through Equation 6 using Sr/Ca ratios for leaves and soil porewaters collected in southern quadrants of the catchment. Fractionation factors ($K_{Sr/Ca}$) less than one calculated for all species suggest preferential discrimination against strontium relative to calcium in plants at the catchment. Specifically, sugar maple leaves in southwestern and southeastern quadrants were shown to have higher fractionation factors (0.48 and 0.43, respectively) and discriminate to a lesser degree against strontium than chestnut oak (0.24 and 0.19, respectively) and red oak (0.22 and 0.19, respectively) leaves. Greater preferential discrimination against strontium in oak relative to maple leaves is likely related to physiological differences between the two species and is consistent with findings from other studies conducted in the northeastern United States (Blum et al., 2008, 2012; Lucash et al., 2012).

Strontium concentrations in oak leaves were rather uniform ([Sr] range: 0.01 to 0.03 mg/g) with variation in leaf Ca/Sr ratio largely reflective of differences in calcium concentration across sites ([Ca] range: 9.16 to 17.44 mg/g). Similarly, differences in sugar maple leaf Ca/Sr ratio on a site by site basis can be largely attributed to variation in calcium concentration ([Ca] range: 7.64 to 14.59 mg/g) rather than strontium concentration ([Sr] range: 0.03 to 0.05 mg/g). Average calcium and strontium concentrations for sugar maple leaves from all quadrants (11.86 and 0.04 mg/g, respectively) exceeded those observed in chestnut oak (11.12 and 0.02 mg/g, respectively) and red oak (10.32 and 0.02 mg/g, respectively) leaves. This conforms to observations of higher calcium requirements in sugar maple species as has been documented in other studies conducted in temperate deciduous ecosystems (Boggs et al., 2005; Dijkstra and Smits, 2002; Page et al., 2008; Park and Yanai, 2009). On the other hand, calcium and strontium concentrations in oak sap waters (869 ± 5 and 2.17 ± 0.10 μM , respectively) were found to be 1.5 and 1.4 greater than corresponding concentrations in sugar maple sap waters (578 and 1.59 μM , respectively). Concurrently, daily sap fluxes were observed to be higher in sugar maple relative to oak species (Meinzer et al., 2013) which suggest higher levels of transpiration for maple species at the catchment (Granier et al., 1996; Oren et al., 1999; Ewers and Oren, 2000; Pataki and Oren, 2003). A close positive relationship exists between transpiration rate and calcium distribution in leaves (Mix and Marschner, 1976; White, 2001; Funk and Amatangelo, 2013) where translocation rates are more receptive to tree transpiration rates than calcium uptake levels (Marschner and Schafarczyk, 1967). Hence, higher calcium and strontium concentrations in maple relative to oak leaves seem reasonable as convection processes involved in the transport of calcium (and by inference, strontium) through the xylem toward rapidly transpiring leaf tissues are facilitated by higher transpiration rates in maple species (Clarkson, 1984; McLaughlin and

Wimmer, 1999; Marschner, 2012). Observed variation in calcium concentration may also be due to differences in cation exchange capacity among species where strontium is known to be preferentially retained to a greater degree than calcium on cell walls of xylem vessels and surrounding tissues (Jacoby, 1967; Clarkson, 1984; Wolterbeek, 1984; Veresoglou et al., 1996; Bailey et al., 1996; McLaughlin and Wimmer, 1999; Dasch et al., 2006; Drouet and Herbauts, 2008; Funk and Amatangelo, 2013). Further complicating the situation are observations of differences among species in relative concentrations of cellulose, hemicellulose, and lignin constituents in cell walls which affect the adsorption of specific ions onto cell walls (McLaughlin and Wimmer, 1999). Additionally, calcium oxalate accumulation in leaf tissue is known to vary according to tree species (McNair, 1932; Gulpin et al., 1995; Sattelmacher, 2001; Franceschi and Nakata, 2005; Funk and Amatangelo, 2013).

A wide range of leaf Ca/Sr ratios were observed for each tree species based on sampling location (Table 2.13, Figure 2.16). For both oak species, leaves sampled at mid slope positions in northwestern locations had the highest Ca/Sr ratios followed by leaves sampled at these positions in southwestern, southeastern, and northeastern locations. Furthermore, sugar maple leaves at mid slope positions in northwestern locations had the greatest Ca/Sr ratios followed by leaves sampled at these positions in southwestern, northeastern, and southeastern locations. Higher leaf Ca/Sr ratios in western relative to eastern quadrants conform to patterns observed for soil porewaters where planar (southwestern) locations were shown to have greater Ca/Sr ratios than swale (southeastern) locations (Tables 2.1 and 2.2, Figure 2.8). As mentioned previously, steeper topography at swale relative to planar locations (Figure 1.2) accelerate subsurface flow processes to reduce residence times for solutes present in porewaters at swale locations. As a positive relationship exists between accumulation of calcium and strontium in leaf tissue and

concentrations of these cations in source porewaters (White, 2001; Marschner, 2012), observed similarities in spatial patterns between soil porewaters and mid slope leaves seem reasonable.

In the northeastern quadrant, average Ca/Sr ratio was shown to decrease in the progression from ridge top to mid slope to valley floor locations for sugar maple leaves, while average Ca/Sr ratio for chestnut oak leaves initially decreased from ridge top to mid slope locations and then increased from mid slope to valley floor locations (Table 2.12, Figure 2.17). Soil porewaters were not collected in the north swale location where northeastern leaves are located. However, these patterns are consistent with observations by Belanger and Holmden (2010) and Belanger et al. (2012) for deciduous canopies in Canada. The authors attributed these patterns to greater canopy exposure to atmospheric inputs at high elevation ridge top locations compared to shielded canopy valley floor locations. To this end, solutes captured from dry deposition at the ridge top are transferred to a greater degree than at valley floor locations as throughfall and stemflow to the forest floor and ultimately to tree roots. Considering atmospheric Ca/Sr ratios were found to well exceed values determined for shale (Figure 2.8), downslope decreases in leaf Ca/Sr ratio seem reasonable. Additionally, several studies have documented the preferential sequestration of strontium in plant roots (Handley and Overstreet, 1963; Poszwa et al., 2000; Dasch et al., 2006; Drouet and Herbauts, 2008). However, Handley and Overstreet (1963) noted that anaerobic soil conditions facilitate strontium entry into leaf mesophyll tissues. As indicated by Lin et al. (2006) and Jin et al. (2011b), soil moisture generally increases downslope as soil profiles thicken (Figure 1.2). Hence, the increased possibility of water saturation and anaerobic conditions in soils downslope which could enable uptake of strontium by leaves and decrease Ca/Sr ratios at valley floor locations. Additionally, higher average chestnut oak leaf Ca/Sr ratios at valley floor relative to mid slope locations may be due to uptake

of carbonate affected shallow groundwaters (Table 2.22) by taproots where trees are known to acquire water sources from depths of up to 100 cm at valley floor locations (Gaines, unpublished data). However, this effect would not be apparent for sugar maple species due to their shallower root systems which only permit solute acquisition from deep sources through hydraulic lift during unusually dry conditions (Dawson, 1993).

On average, Ca/Sr ratios for sugar maple and chestnut oak leaves sampled at mid slope positions in the northeastern quadrant in 2011 were found to be lower than those sampled from the same quadrant in 2013 (Tables 2.12 and 2.13, Figure 2.18). Specifically, mid slope sugar maple and chestnut oak leaf Ca/Sr ratios in the northeastern quadrant were found to be 1.6 times smaller in 2011 compared to 2013. Additionally, the red oak leaf Ca/Sr ratio sampled at a mid slope position of the northeastern quadrant was found to be 1.7 times smaller in 2011 than in 2013. As will be explored in Chapter 3, higher average silicon concentrations were observed for identical leaves sampled in the northeastern quadrant in 2011 compared to 2013. Ma and Takahashi (1993) and Brackhage et al. (2013) found that leaves accumulating greater concentrations of silicon had correspondingly lower calcium concentrations, on average. This was attributed to lower energy demands involving uptake and polymerization of silica relative to calcium on plant membranes and cell wall matrices (Ma and Takahashi, 1993; Brackhage et al., 2013). It should be noted that, although from the same species, leaves sampled in the northeastern quadrant in 2011 were obtained from different individual trees than those sampled in 2013. As such, variation in Ca/Sr ratio may simply reflect sampling inconsistencies between 2011 and 2013.

Table 2.13 Average Ca/Sr ratios for sugar maple, chestnut oak, and red oak leaves sampled at mid slope positions in northeastern (NE), northwestern (NW), southeastern (SE), and southwestern (SW) quadrants of the catchment in 2013

Location	Average Sugar Maple Ca/Sr	Average Chestnut Oak Ca/Sr	Average Red Oak Ca/Sr
NE	595 ± 10	1181 ± 41	1128 ± 19
NW	730 ± 17	1588 ± 71	1645 ± 38
SE	582 ± 23	1290 ± 50	1294 ± 92
SW	671 ± 22	1373 ± 42	1449 ± 56

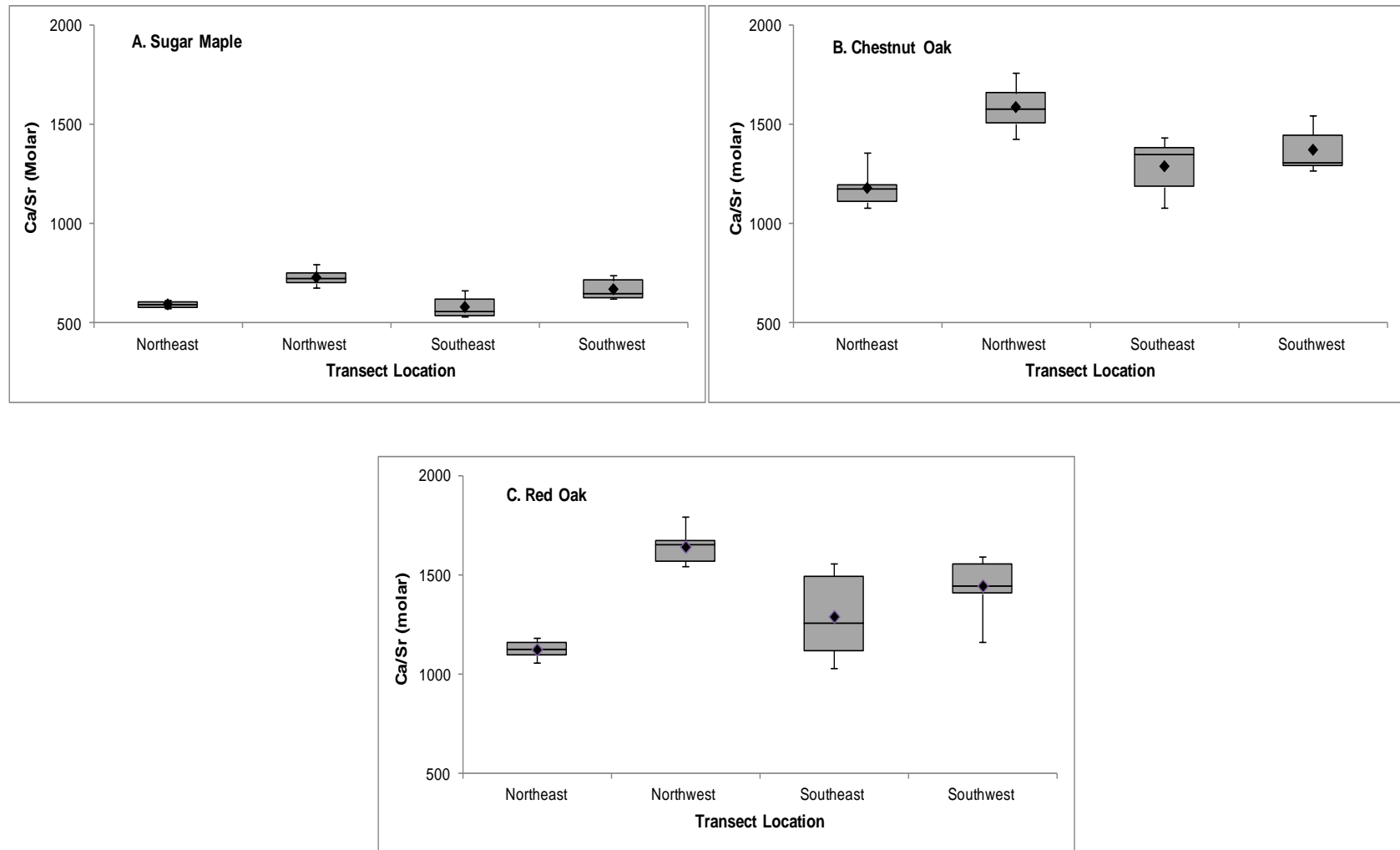


Figure 2.16 Box plots of Ca/Sr ratio based on sampling location for sugar maple (A), chestnut oak (B), and red oak (C) leaves collected in northeastern, northwestern, southeastern, and southwestern quadrants at mid slope positions of the catchment in 2013 with mean values shown as closed diamonds.

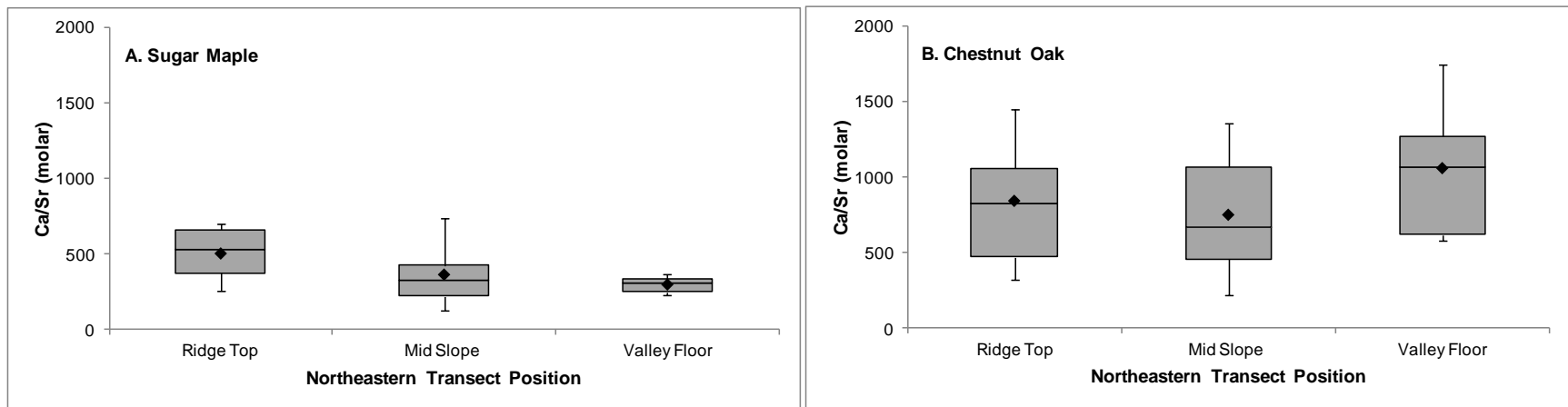


Figure 2.17 Box plots of Ca/Sr ratio based on sampling position for sugar maple (A) and chestnut oak (B) leaves sampled at ridge top, mid slope, and valley positions of the northeastern quadrant of the catchment in 2011 with mean values shown as closed diamonds.

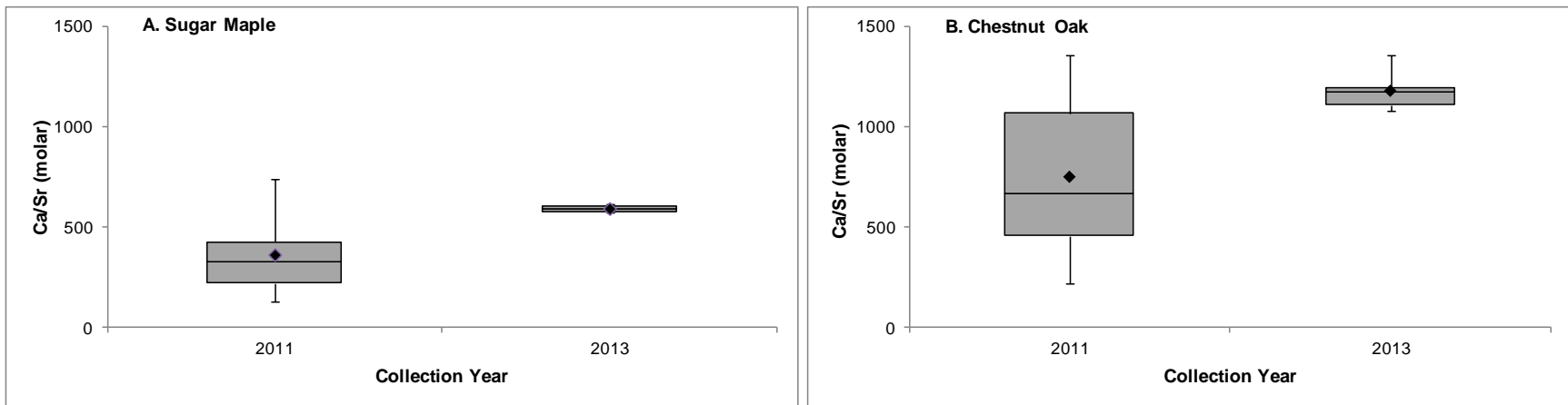


Figure 2.18 Box plots of Ca/Sr ratio based on sampling year for sugar maple (A) and chestnut oak (B) leaves sampled at mid slope positions of the northeastern quadrant in 2011 and 2013 with mean values shown as closed diamonds.

Overall, minimal temporal variation in leaf $^{87}\text{Sr}/^{86}\text{Sr}$ ratio was observed over the course of the growing season. As shown in Figure 2.19, plotting individual leaf $^{87}\text{Sr}/^{86}\text{Sr}$ ratios sampled from identical trees during one month of the growing season against corresponding $^{87}\text{Sr}/^{86}\text{Sr}$ ratios measured from a separate month yields a correlation with an R^2 value of 0.97. However, the extent of temporal variation in leaf $^{87}\text{Sr}/^{86}\text{Sr}$ ratio ranged from 0.00001 to 0.00035 indicating differences between trees sampled (Table 2.14). Replicate leaves derived from trees corresponding to sample IDs AS 2061, AS 2062, and AS 356 demonstrated minimal variation in $^{87}\text{Sr}/^{86}\text{Sr}$ ratio with monthly differences ranging from 0.00001 to 0.00006. Conversely, trees corresponding to sample IDs AS 2064, AS 352, and QP 330 showed more pronounced temporal variations in $^{87}\text{Sr}/^{86}\text{Sr}$ ratio, with monthly differences ranging from 0.00010 to 0.00035.

As indicated in Table 2.15 and Figure 2.20, modest temporal variations in Ca/Sr ratio were observed for leaves sampled at mid slope positions in northeastern, southeastern, northwestern, and southwestern quadrants of the catchment from June to September of 2013. The most dramatic monthly changes in Ca/Sr ratio were exhibited by sugar maple leaves from August to September, chestnut oak leaves from July to August and from August to September, and red oak leaves from June to July (Table 2.15, Figure 2.20). Overall, Ca/Sr ratios for sugar maple and chestnut oak leaves decreased from June to July to August and then increased from August to September. For red oak leaves, average Ca/Sr ratio increased from June to July to August and then decreased from August to September. For leaves sampled at ridge top, mid slope, and valley floor sites in the northeastern quadrant of the catchment in 2011, seasonal averages for each species could not be determined as leaves from identical trees were not consistently sampled on a month by month basis as they were in 2013. Although not directly apparent from monthly Ca/Sr ratios (Figure 2.20), calcium concentrations were observed to accumulate in leaf tissue over the

course of the growing season for all tree species (Figure 2.21) which is consistent with literature findings (Schlesinger, 1997). As shown in Figure 2.21, concurrent accumulation of strontium in leaf tissue over the course of the growing season obscured the direct observation of this pattern in monthly Ca/Sr ratios. As mentioned earlier, shallow soil $\delta^{18}\text{O}$ and $\delta^2\text{H}$ values were observed to become more positive from July to September indicating greater levels of evapotranspiration (Hsieh et al., 1998). High levels of tree transpiration facilitate convection processes which transport calcium (and by inference, strontium) through the xylem towards rapidly transpiring leaf tissues (Clarkson, 1984; Mix and Marschner, 1976; McLaughlin and Wimmer, 1999; White and Broadley, 2003; Marschner, 2012; Funk and Amatangelo, 2013). As a consequence, concomitant increases in calcium and strontium concentration with enhanced levels of evapotranspiration over the course of the growing season seem reasonable.

Table 2.14 Seasonal $^{87}\text{Sr}/^{86}\text{Sr}$ ratios for selected sugar maple (ACSA) and chestnut oak (QUPR) leaves

Sample ID	Species Code	June $^{87}\text{Sr}/^{86}\text{Sr}$	July $^{87}\text{Sr}/^{86}\text{Sr}$	August $^{87}\text{Sr}/^{86}\text{Sr}$	September $^{87}\text{Sr}/^{86}\text{Sr}$
AS 2061	ACSA	nm	0.72393	0.72392	nm
AS 2062	ACSA	0.72585	0.72583	nm	nm
AS 2064	ACSA	nm	0.72429	nm	0.72464
AS 352	ACSA	0.72296	nm	0.72308	nm
AS 356	ACSA	0.72383	nm	0.72377	nm
QP 230	QUPR	nm	0.72223	0.72254	nm
QP 330	QUPR	0.72440	0.72416	nm	0.72406

*The 'nm' term refers to months when strontium isotope ratios were not measured for a designated leaf sample

Table 2.15 Seasonal Ca/Sr ratios for sugar maple, chestnut oak, and red oak leaves collected at mid slope positions in northeastern, northwestern, southeastern, and southwestern quadrants of the catchment in 2013

Tree Species	Average June Ca/Sr (molar)	Average July Ca/Sr (molar)	Average August Ca/Sr (molar)	Average September Ca/Sr (molar)
Sugar Maple	655 ± 35	646 ± 32	633 ± 35	673 ± 25
Chestnut Oak	1420 ± 122	1386 ± 77	1264 ± 64	1324 ± 43
Red Oak	1260 ± 144	1395 ± 84	1401 ± 78	1380 ± 110

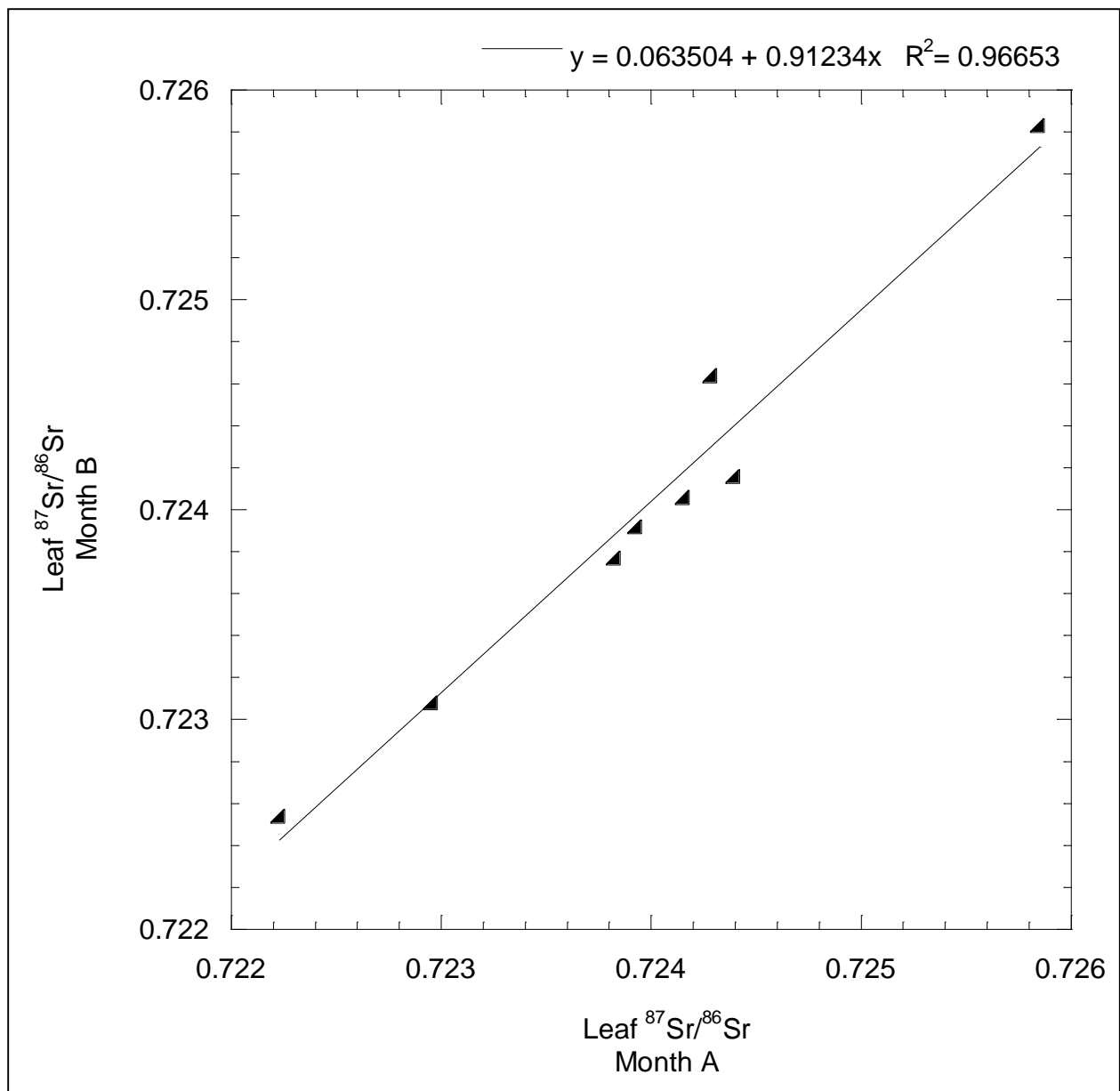


Figure 2.19 Leaf ⁸⁷Sr/⁸⁶Sr ratio of month B versus leaf ⁸⁷Sr/⁸⁶Sr ratio of month A for individual leaves sampled from identical trees. A correlation yielding an R^2 value of 0.97 is shown.

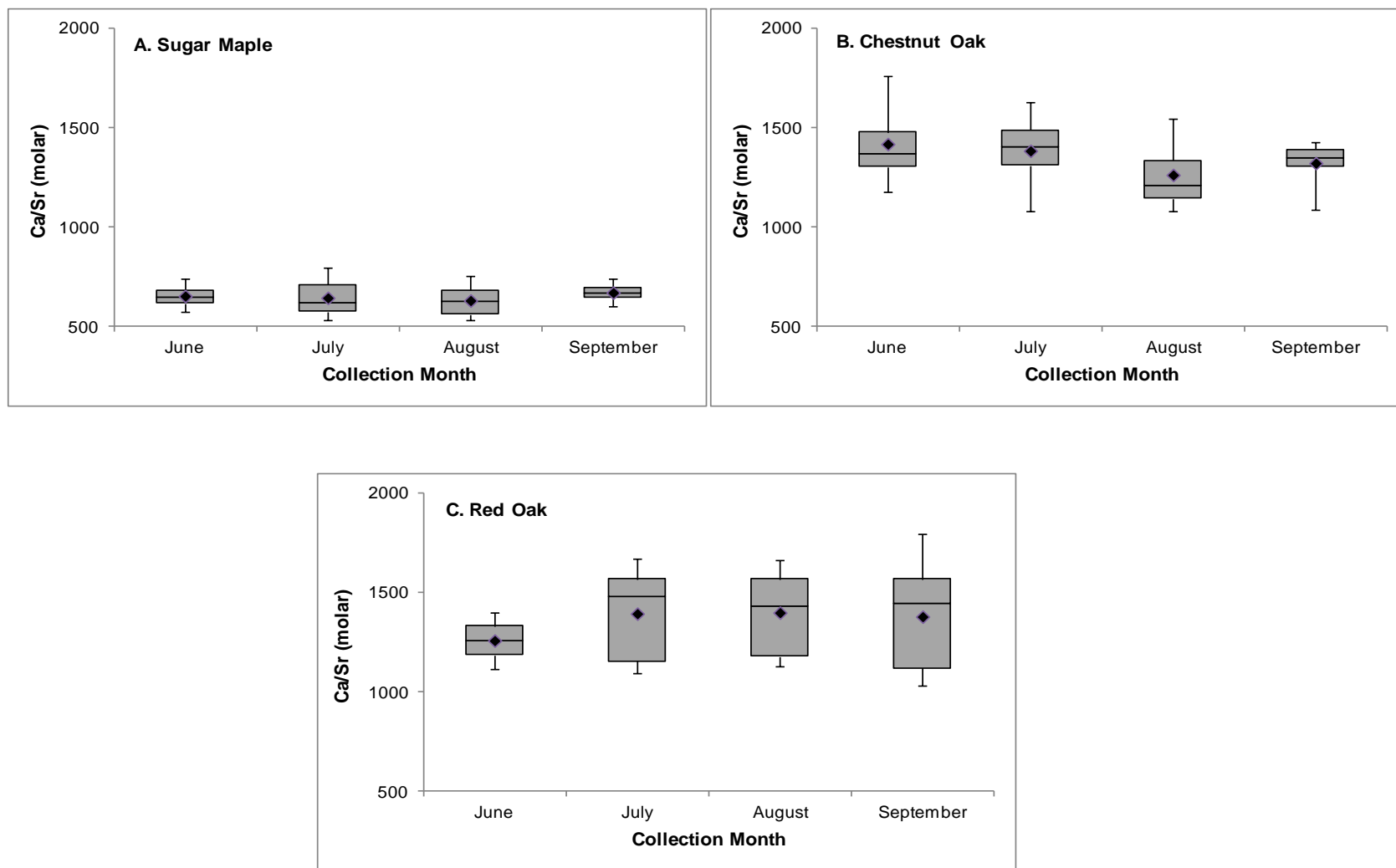


Figure 2.20 Box plots of Ca/Sr ratio for sugar maple (A), chestnut oak (B), and red oak (C) leaves collected over the course of the growing season in 2013 with mean values shown as closed diamonds.

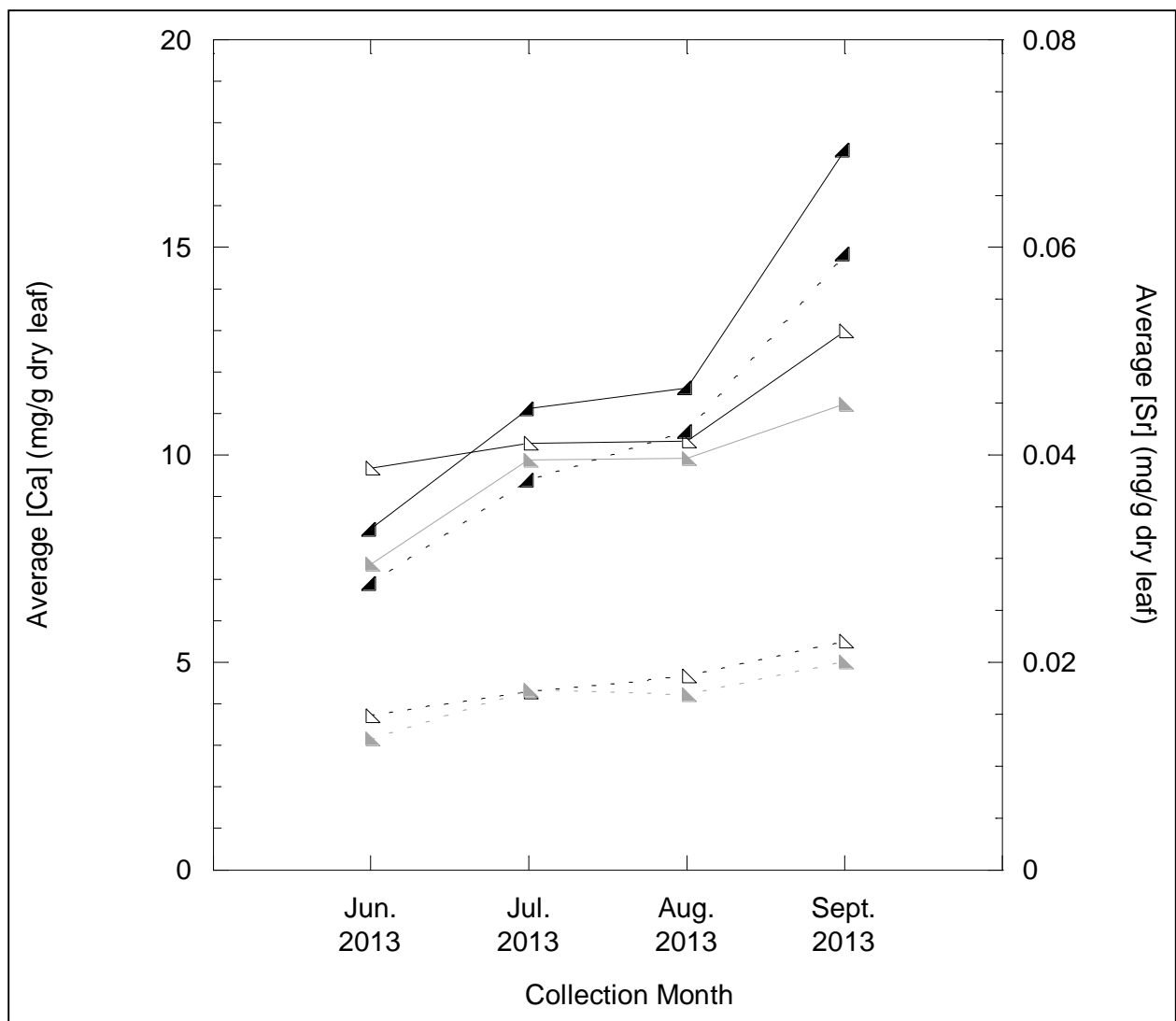


Figure 2.21 Monthly average calcium and strontium concentrations for sugar maple (closed black triangles), chestnut oak (open triangles), and red oak (closed gray triangles) leaves. Solid lines connect average leaf calcium concentrations, while dashed lines connect average leaf strontium concentrations.

4.3 Sap Waters

Sugar maple, chestnut oak, and red oak sap water $^{87}\text{Sr}/^{86}\text{Sr}$ ratios ranged from 0.72102 to 0.72451, 0.72078 to 0.72521, and 0.72033 to 0.72508 (Table 2.16), respectively, with average values of 0.72257 ± 0.00027 , 0.72246 ± 0.00043 , and 0.72205 ± 0.00045 , respectively (Table 2.17, Figure 2.2). Sugar maple, chestnut oak, and red oak sap water $^{87}\text{Sr}/^{86}\text{Sr}$ ratios were, on average, slightly less radiogenic than corresponding leaves sampled from the same tree species. However, it should be noted that differences in $^{87}\text{Sr}/^{86}\text{Sr}$ ratio for sap waters and leaves collected from identical trees at the same time were insignificant (Figure 2.13). Additionally, sap waters collected from sugar maple trees at the northwestern quadrant, from chestnut oak trees at northeastern and southwestern quadrants, and from red oak trees at the northeastern quadrant were slightly more radiogenic than leaves sampled at corresponding locations. Similarities between leaf and sap water $^{87}\text{Sr}/^{86}\text{Sr}$ ratio are not surprising considering the nature of the xylem as a conduit through which root and above ground leaf components are connected via the transpiration stream (Hanger, 1979) with strontium isotopes known to exhibit negligible fractionation during transport (Bailey et al., 1996; Capo et al., 1998; Bullen and Bailey, 2005; Dasch et al., 2006).

Average $^{87}\text{Sr}/^{86}\text{Sr}$ ratios for sugar maple, chestnut oak, and red oak sap waters collected at mid slope positions in the southwestern quadrant (Table 2.16) corresponded reasonably well to ratios determined for mid slope exchangeable soil organic horizons and shallow soil porewaters (Table 2.2). Average $^{87}\text{Sr}/^{86}\text{Sr}$ ratios for sugar maple, chestnut oak, and red oak sap waters (Table 2.16) sampled at mid slope positions in the southeastern quadrant were found to be lower than those measured for mid slope porewaters at shallow depths of the soil horizon (Table 2.6). $^{87}\text{Sr}/^{86}\text{Sr}$ ratios for exchangeable soils and porewaters were not measured in northeastern or

northwestern quadrants of the catchment so no comparisons can be made between $^{87}\text{Sr}/^{86}\text{Sr}$ ratios for exchangeable soils/porewaters and sap waters in these locations at the current time.

Table 2.16 Strontium and calcium elemental concentrations and Ca/Sr and $^{87}\text{Sr}/^{86}\text{Sr}$ ratios for sap waters collected from chestnut oak (QUPR), red oak (QURU), and sugar maple (ACSA) trees sampled at mid slope positions in northeastern (NE), northwestern (NW), southeastern (SE), and southwestern (SW) quadrants of the catchment

Sample Date	Sample ID	Species Code	Sr (μM)	Ca (μM)	Ca/Sr (molar)	$^{87}\text{Sr}/^{86}\text{Sr}$
7/16/2013	NE 620	ACSA	1.42	380	267	0.72300
7/16/2013	NW 137	ACSA	1.59	325	205	0.72221
7/16/2013	NW 102	QURU	1.11	589	530	0.72033
7/16/2013	NW 110	QURU	1.54	1555	1010	0.72076
7/16/2013	NW 121	QUPR	0.92	479	521	0.72193
7/16/2013	NW UPHILL	ACSA	1.61	428	266	0.72252
7/16/2013	NE NOTAG	ACSA	1.25	363	291	0.72325
7/16/2013	SW 1080	QUPR	2.03	618	305	0.72078
7/16/2013	SW 1170	QUPR	1.32	480	363	0.72154
7/16/2013	SW 1077	QURU	2.63	714	271	0.72115
7/16/2013	SW 1074	QURU	1.76	468	266	0.72035
7/16/2013	SE UPHILL	ACSA	1.90	409	215	0.72451
7/16/2013	SE 1331	QURU	1.98	458	231	0.72508
7/16/2013	SE 1271	QURU	1.51	945	625	0.72169
7/17/2013	NE 637	QUPR	1.21	612	504	0.72352
7/17/2013	NE 613	QURU	1.76	447	254	0.72222
7/17/2013	NE 636	QURU	2.43	603	248	0.72475
7/17/2013	NE 622	QUPR	1.35	310	229	0.72431
7/17/2013	SW 1073	ACSA	2.19	507	231	0.72102
7/17/2013	SE 1266	QUPR	2.41	1560	648	0.72131
7/17/2013	SE DOWNHILL	ACSA	1.21	354	321	0.72298
8/12/2013	NE 622	QUPR	1.63	639	392	0.72521
8/12/2013	NE 613	QURU	3.82	838	219	0.72314
8/12/2013	SW 1170	QUPR	1.65	355	215	0.72232
8/12/2013	SW 1077	QURU	2.62	643	246	0.72123
8/13/2013	NW 110	QURU	2.54	2166	854	0.72076
8/13/2013	NW UPHILL	ACSA	1.59	452	287	0.72201
8/13/2013	SW 1080	QUPR	1.73	667	386	0.72190
8/13/2013	SW 1164	ACSA	2.16	833	386	0.72264
8/13/2013	SW 1074	QURU	2.19	1425	651	0.72060
9/22/2013	SE DOWNHILL	ACSA	0.26	116	448	0.72219
9/27/2013	SW 1080	QUPR	5.63	2039	362	0.72106
9/27/2013	NE 636	QURU	4.54	1006	221	0.72452
9/27/2013	SE 1271	QURU	1.68	513	305	0.72090

9/27/2013	SE 1331	QURU	3.31	1209	365	0.72483
9/27/2013	SE 1329	QUPR	3.94	1009	256	0.72325
9/28/2013	SW 1164	ACSA	0.31	190	609	0.72197
9/28/2013	SW 1074	QURU	2.37	612	259	0.72043

*Ca/Sr ratios and Sr and Ca elemental concentrations for additional sap water samples where Sr isotope ratios were not measured are displayed in the appendix.

Table 2.17 Average Ca/Sr and $^{87}\text{Sr}/^{86}\text{Sr}$ ratios for sugar maple, chestnut oak, and red oak sap waters

Tree Species	Average Ca/Sr (molar)	Average $^{87}\text{Sr}/^{86}\text{Sr}$
Sugar Maple	393 ± 38	0.72257 ± 0.00027
Chestnut Oak	426 ± 39	0.72246 ± 0.00043
Red Oak	416 ± 53	0.72205 ± 0.00045

Minimal variation in sap water $^{87}\text{Sr}/^{86}\text{Sr}$ ratio was found between tree species (Table 2.17, Figure 2.2), with sap water $^{87}\text{Sr}/^{86}\text{Sr}$ ratios following a pattern similar to what was observed for leaf $^{87}\text{Sr}/^{86}\text{Sr}$ ratios. Specifically, sap water derived from sugar maple trees was shown to be slightly more radiogenic than sap water derived from oak trees, on average. Within oak species, sap water derived from chestnut oak trees had higher average $^{87}\text{Sr}/^{86}\text{Sr}$ ratios than red oak trees. It should be noted, however, that average $^{87}\text{Sr}/^{86}\text{Sr}$ ratios for oak sapwaters were greater than the average $^{87}\text{Sr}/^{86}\text{Sr}$ ratio for sugar maple sapwaters in the northeastern quadrant and that the average $^{87}\text{Sr}/^{86}\text{Sr}$ ratio for sap waters derived from red oaks was higher than that obtained for chestnut oaks in the southeastern quadrant (Table 2.18).

Furthermore, variation in sap water $^{87}\text{Sr}/^{86}\text{Sr}$ ratio was observed within each tree species as demonstrated by the wide range of $^{87}\text{Sr}/^{86}\text{Sr}$ ratios measured (Table 2.16). Variation in sap water $^{87}\text{Sr}/^{86}\text{Sr}$ ratio for each tree species may be attributed to sampling location across the catchment (Table 2.18). For sugar maple trees, sap waters sampled at southeastern locations had the highest average $^{87}\text{Sr}/^{86}\text{Sr}$ ratios followed by sap waters collected at northeastern,

northwestern, and southwestern locations. Decreases in $^{87}\text{Sr}/^{86}\text{Sr}$ ratio for chestnut oak sap waters were observed across the catchment from northeastern to southeastern to northwestern to southwestern locations. For red oak trees, sap waters sampled at northeastern locations were found to be the most radiogenic followed by sap waters collected at southeastern, southwestern, and northwestern locations. Higher strontium isotope ratios for sap waters at southeastern relative to southwestern quadrants are consistent with higher porewater $^{87}\text{Sr}/^{86}\text{Sr}$ ratios in southeastern quadrants of the catchment (Tables 2.1 and 2.2, Figures 2.1 and 2.2). As mentioned previously, field observations of wetter and thicker soils at swale relative to planar locations (Figure 1.4) suggest greater hydrologic activity and enhanced weathering at swale locations. This will presumably increase $^{87}\text{Sr}/^{86}\text{Sr}$ ratios and proportions of strontium derived from silicate weathering sources in sap waters collected from eastern (swale) relative to western (planar) locations. With the exception of chestnut oak species sampled from eastern quadrants, minimal disparity in sap water $^{87}\text{Sr}/^{86}\text{Sr}$ ratio existed between northeastern and southeastern and between northwestern and southwestern quadrants (Table 2.18). As mentioned previously, this is surprising considering the steep topography (e.g. higher incidence of topographic depressions (swales)), faster erosion rates (e.g. less duration of chemical weathering for surface regolith particles), greater hydrologic activity (e.g. well connected macropore system to facilitate downslope flow to the stream), and less vegetation cover (e.g. less evapotranspiration enabling infiltration into surface soils and the subsequent transport of weathering products downslope through lateral subsurface flow processes) (Lin, 2006; Jin et al., 2011a; Ma et al., 2010, 2011; Naithani et al., 2013) in northern quadrants of the catchment which would suggest lower sap water $^{87}\text{Sr}/^{86}\text{Sr}$ ratios in northern relative to southern quadrants of the catchment.

Table 2.18 Average $^{87}\text{Sr}/^{86}\text{Sr}$ ratios for sugar maple, chestnut oak, and red oak sap waters sampled at northeastern (NE), northwestern (NW), southeastern (SE), and southwestern (SW) quadrants of the catchment

Location	Average Sugar Maple $^{87}\text{Sr}/^{86}\text{Sr}$	Average Chestnut Oak $^{87}\text{Sr}/^{86}\text{Sr}$	Average Red Oak $^{87}\text{Sr}/^{86}\text{Sr}$
NE	0.72312 ± 0.00012	0.72434 ± 0.00049	0.72366 ± 0.00060
NW	0.72224 ± 0.00015	0.72193	0.72062 ± 0.00014
SE	0.72322 ± 0.00068	0.72228 ± 0.00097	0.72312 ± 0.00107
SW	0.72188 ± 0.00047	0.72152 ± 0.00028	0.72075 ± 0.00018

* Error bars are excluded from tree species where only one $^{87}\text{Sr}/^{86}\text{Sr}$ ratio was measured at a designated location

Sugar maple, chestnut oak, and red oak sap water Ca/Sr ratios ranged from 189 to 702, 215 to 747, and 219 to 1010 (Table 2.16), respectively, with average values of 393 ± 38 , 426 ± 39 , and 416 ± 53 , respectively (Table 2.17, Figures 2.8 and 2.22). As shown in Figures 2.8 and 2.22, sugar maple, chestnut oak, and red oak sap waters had significantly lower average Ca/Sr ratios than those observed in paired leaf samples. Specifically, average Ca/Sr ratios for sugar maple, chestnut oak, and red oak sap waters were 1.7, 3.1, and 3.3 times smaller than those obtained for leaves from corresponding trees, respectively. Instead, sap water Ca/Sr ratios were comparable to porewater Ca/Sr ratios sampled at similar locations (Figures 2.8 and 2.22). For example, average Ca/Sr ratios for sugar maple, chestnut oak, and red oak sap waters collected at mid slope locations of the southwestern quadrant (Table 2.19) corresponded reasonably well to the average Ca/Sr ratio for mid slope porewaters of 325 (Table 2.2), while average Ca/Sr ratios for sugar maple, chestnut oak, and red oak sap waters collected at mid slope locations of the southeastern quadrant (Table 2.19) were generally similar to the average Ca/Sr value for south swale mid slope shallow porewaters of 324 (Table 2.6). However, calcium and strontium concentrations were larger than those found in soil porewaters which has been interpreted by researchers as a consequence of the more negative electrical potential in the stellar apoplast

relative to the source solution (Shone, 1968; Marschner, 2012). Interestingly, tree transpiration processes were shown to concentrate calcium and strontium in sap waters to similar degrees. Indeed, average strontium and calcium concentrations in southwestern sugar maple sap waters (1.46 and 521 μM , respectively) were observed to be 13 and 14 times larger than those in corresponding southern planar mid slope soil porewaters where average strontium and calcium concentrations were found to be 0.11 and 38 μM , respectively. Furthermore, strontium and calcium concentrations for southwestern oak sap waters (2.30 ± 0.06 and 793 ± 12 μM , respectively) were reported to be 20 and 21 times larger, respectively, than those for southern planar mid slope soil porewaters, on average. In the southeastern quadrant, average strontium and calcium concentrations for sugar maple sap waters (1.90 and 429 μM , respectively) were observed to be 11 and 10 times larger than those for corresponding south swale mid slope soil porewaters where average strontium and calcium concentrations were found to be 0.17 and 44 μM , respectively. However, slightly greater variation existed when comparing average strontium and calcium concentrations in southeastern oak sap waters to those in south swale mid slope porewaters. Average strontium and calcium concentrations for chestnut oak (1.92 and 681 μM , respectively) and red oak (2.87 and 1271 μM , respectively) sap waters were observed to be 11 and 17 times larger and 16 and 29 times larger, respectively, than average concentrations determined for south swale mid slope soil porewaters. Ca/Sr ratios for soil porewaters were not measured in northeastern or northwestern quadrants of the catchment so comparisons cannot be made between porewater and sap water Ca/Sr ratios in these quadrants of the catchment at the present time. Observations of similar Ca/Sr ratios in sap waters compared to source porewaters and accumulation of calcium and strontium by plant species growing in the same substrate suggest limited competition between these divalent cations during transport (Wytenbach et al.,

1995; Veresoglou et al., 1996; Dasch et al., 2006; Drouet and Herbauts, 2008). Considering that the apoplastic pathway is relatively non-selective between divalent cations (White, 2001; White et al., 2002; White and Broadley, 2003), transport of calcium through the root to the xylem is hypothesized to occur largely along apoplastic rather than highly selective symplastic pathways as has been suggested by other researchers (Clarkson, 1984; McLaughlin and Wimmer, 1999; White, 2001; White et al., 2002). However, this interpretation conflicts with the longstanding view that calcium transport to the xylem occurs predominately through symplastic pathways in endodermal cells (Marschner, 2012). Relative contributions of calcium to the xylem through apoplastic and symplastic pathways for individual plant species remain unresolved and require future research.

Table 2.19 Average Ca/Sr ratios for sugar maple, chestnut oak, and red oak sap waters sampled at northeastern (NE), northwestern (NW), southeastern (SE), and southwestern (SW) quadrants of the catchment

Location	Average Sugar Maple Ca/Sr (molar)	Average Chestnut Oak Ca/Sr (molar)	Average Red Oak Ca/Sr (molar)
NE	421 ± 83	432 ± 68	247 ± 13
NW	417 ± 82	550 ± 106	646 ± 136
SE	293 ± 59	482 ± 115	390 ± 68
SW	426 ± 79	320 ± 26	362 ± 96

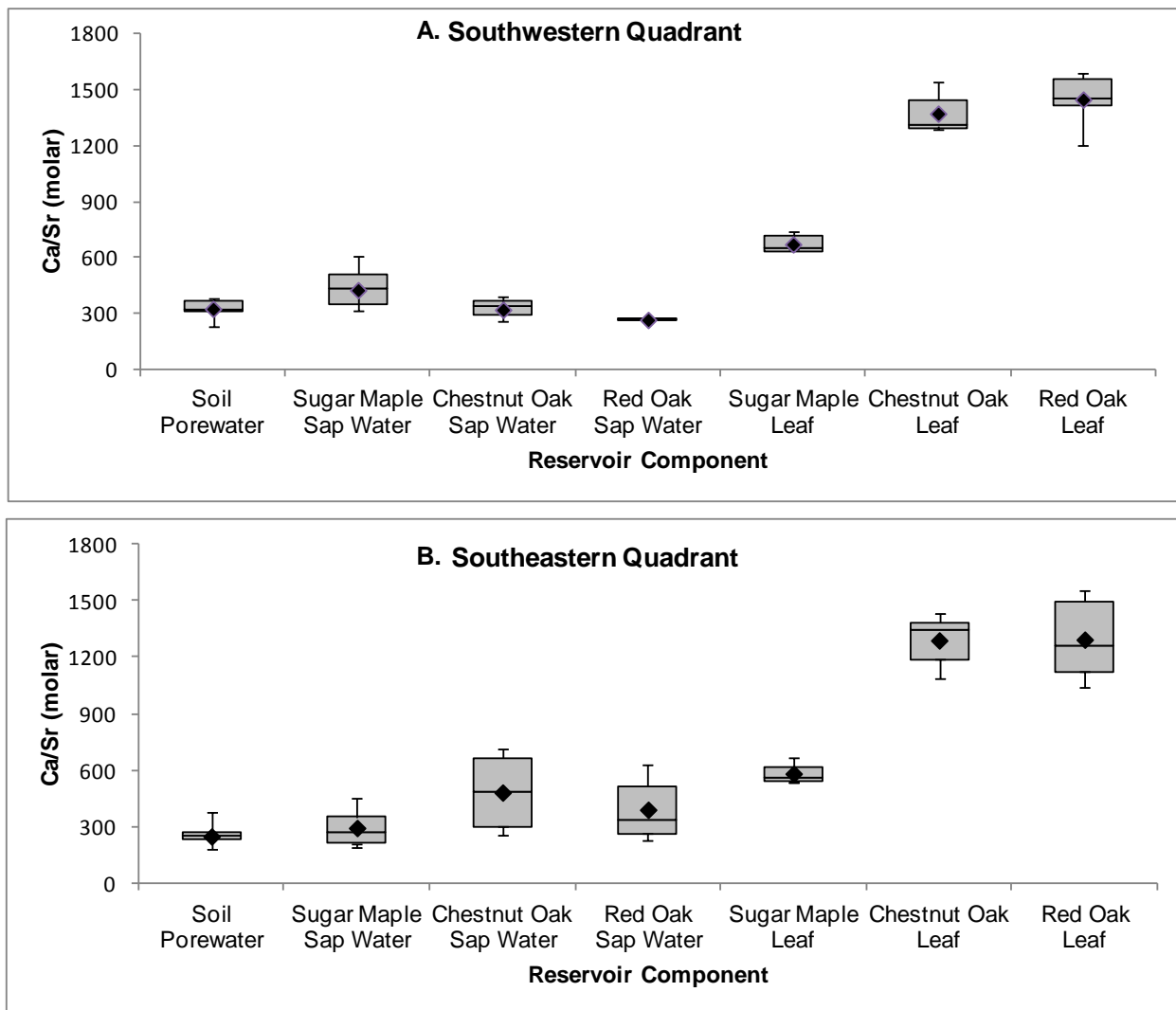


Figure 2.22 Box plots of Ca/Sr ratio for soil porewaters and sugar maple, chestnut oak, and red oak sapwaters and leaves collected from mid slope positions of the southwestern (A) and southeastern (B) quadrants with mean values shown as closed diamonds.

Nevertheless, fractionation between calcium and strontium must take place further along the transpiration stream as evidenced by the higher Ca/Sr ratios observed in leaf tissues (Figures 2.8 and 2.22). As indicated earlier, convection in the xylem transports calcium (and by inference, strontium) ions towards rapidly transpiring organs such as leaves (Clarkson, 1984; Marschner, 2012). During transport, increased translocation of calcium relative to strontium, with strontium retained by cation exchange sites to a greater degree than calcium on cell walls of xylem vessels and surrounding tissues, has been suggested during apoplastic transport through the xylem to above ground leaf components (Jacoby, 1967; Clarkson, 1984; Wolterbeek, 1984; Veresoglou et al., 1996; Bailey et al., 1996; Dasch et al., 2006; Drouet and Herbauts, 2008; Funk and Amatangelo, 2013). Furthermore, other studies have argued that discrimination between calcium and strontium is the result of preferential calcium binding in calcium oxalate complexes which are released by bark or other plant tissues and accumulate in leaf mesophyll cells (McNair, 1932; Gulpin et al., 1995; Sattelmacher, 2001; Franceschi and Nakata, 2005; Funk and Amatangelo, 2013).

Negligible variation in sap water Ca/Sr ratio was observed among tree species. Average Ca/Sr ratios of sap water collected from oaks were slightly higher than the average Ca/Sr ratio observed for maples (Table 2.17, Figures 2.8 and 2.22). Within oak species, sap waters derived from chestnut oak species were found to have a higher average Ca/Sr ratio than those collected from red oak trees (Table 2.17, Figures 2.8 and 2.22). Relatively uniform Ca/Sr ratios in sap waters sampled from different species at the catchment imply similar calcium and strontium uptake mechanisms in plants at the catchment. However, slight discrepancy in sapwater Ca/Sr ratios may be due to differences in transpiration rates among species at the catchment. According to Jacoby and Moran (2002), low solute concentrations are expected in xylem sap water when

transpiration levels are high with the reverse holding true under lower levels of tree transpiration. To this end, greater daily sap fluxes in sugar maple relative to oak species (Meinzer et al., 2013) suggest higher levels of transpiration for these species at the catchment. Hence, the lower observed calcium and strontium concentrations and Ca/Sr ratios in sap waters derived from maple relative to oak species (Tables 2.16 and 2.17, Figure 2.8). Additionally, it has been suggested that variation in sap water Ca/Sr ratio among species may be due to differences in cation exchange capacities (CEC) of roots (Keller and Deuel, 1957; White and Broadley, 2003). Root CEC has the potential of affecting shoot calcium and strontium concentrations by influencing cation transport through the apoplast (Asher and Ozanne, 1961; Wacquant, 1977). Interestingly, the Fagales order (e.g. oaks) is reported to have higher root C.E.C.s than the Sapindales order (e.g. maples) (White and Broadley, 2003). Furthermore, chelation of calcium ions in xylem sap by organic acids (e.g. malate and citrate), known to be present in variable quantities among tree species (Franceschi and Nakata, 2005; Marschner, 2012), may be resulting in the observed discrepancy.

A wide range of sap water Ca/Sr ratios were observed within each tree species (Table 2.16), likely reflecting differences in sampling location among sap waters collected across the catchment (Table 2.19, Figure 2.23). For sugar maple trees, sap water average Ca/Sr ratios at northeastern, northwestern, and southwestern quadrants were remarkably similar (avg. Ca/Sr range: 417 to 426) with sap waters collected from the southeastern quadrant having a lower average Ca/Sr ratio of 293. For red oak trees, sap water average Ca/Sr ratios at southwestern and southeastern quadrants were relatively similar (avg. Ca/Sr=362 and 390, respectively) with sap waters derived from northeastern (avg. Ca/Sr=247) and northwestern (avg. Ca/Sr=646) quadrants displaying lower and higher overall Ca/Sr ratios, respectively, than these quadrants. The greatest

variability in Ca/Sr ratio was found for chestnut oak sap waters with the northwestern (avg. Ca/Sr=550) quadrant having the highest Ca/Sr ratios followed by the southeastern (avg. Ca/Sr=482), northeastern (avg. Ca/Sr=432), and southwestern (avg. Ca/Sr=320) quadrants. Based on sampling location across the catchment, Ca/Sr ratios of sap waters were found to exhibit more spatial homogeneity than leaves sampled at similar locations. Lower average sap water Ca/Sr ratios for southeastern (swale) sites relative to southwestern (planar) sites correspond to observations of lower Ca/Sr ratios in porewaters of the southeastern quadrant (Table 2.2, Figure 2.22). As discussed earlier, steeper topography at swale relative to planar locations (Figure 1.2) accelerate subsurface flow processes to reduce residence times for solutes in porewaters at swale locations. Interestingly, patterns in Ca/Sr ratio for oak sap waters collected in the southern quadrant conflict with those observed for soil porewaters (Tables 2.2 and 2.19). To this end, variable levels of transpiration may be responsible for observed deviation from spatial patterns predicted based on porewater chemistry as transpiration is known to reduce Ca/Sr ratios in sap waters by facilitating calcium transport from the xylem to leaf tissues via convection processes (Clarkson, 1984).

However, sap water samples were shown to display greater temporal variation in $^{87}\text{Sr}/^{86}\text{Sr}$ ratio compared to corresponding leaves sampled at similar locations (Table 2.20). Plotting individual sap water $^{87}\text{Sr}/^{86}\text{Sr}$ ratios sampled from identical trees during one month of the growing season against corresponding $^{87}\text{Sr}/^{86}\text{Sr}$ ratios measured from a separate month yields a correlation with an R^2 value of 0.82 (Figure 2.24), a value lower than what was observed for leaves (Figure 2.19, $R^2=0.97$). A subset of sap water samples collected during separate months of the growing season indicated rather significant monthly differences in $^{87}\text{Sr}/^{86}\text{Sr}$ ratio with the exception of sap waters derived from trees corresponding to sample IDs NW 110 and SW 1077

(Table 2.20). For sugar maple sap waters, average $^{87}\text{Sr}/^{86}\text{Sr}$ ratios decreased by 0.00051 and 0.00067 from July to August and from August to September, respectively. On average, chestnut oak sap water $^{87}\text{Sr}/^{86}\text{Sr}$ ratios increased by 0.00093 from July to August and decreased by 0.00089 from August to September, respectively. Average red oak sap water $^{87}\text{Sr}/^{86}\text{Sr}$ ratios increased by 0.00059 from July to August and decreased by 0.00017 from July to September, respectively. Observed monthly decreases may be the result of differences in sources from which roots are acquiring strontium. As mentioned previously, shallow soil $\delta^{18}\text{O}$ and $\delta^2\text{H}$ values were observed to become more positive from July to September indicating greater levels of evapotranspiration (Hsieh et al., 1998). During dry periods, groundwater would be expected to contribute more strontium to sap waters than would be the case during wet periods. This can be accomplished through tap roots in oak trees (Meinzer et al., 2013) and through hydraulic lift processes in maple trees (Dawson, 1993). As groundwaters (Table 2.22, Figure 2.2) at the catchment are known to be less radiogenic than porewaters (Table 2.1, Figure 2.2), monthly decreases in sap water $^{87}\text{Sr}/^{86}\text{Sr}$ ratio from July to September may be the result of different sources from which sap waters are extracting strontium. Indeed, studies (Meinzer et al., 2013; Gaines, unpublished data) have indicated that trees at the catchment tap deeper water sources as the summer season progresses. On the contrary, increases in sap water $^{87}\text{Sr}/^{86}\text{Sr}$ ratio over the course of the growing season may be due to a switch in solute acquisition by plants from “mobile” to “immobile” soil waters held in larger and smaller soil pores, respectively, over shorter and longer residence times, respectively (Brooks et al., 2010). This would lead to increased porewater interaction with more radiogenic silicate minerals and hence, higher sap water $^{87}\text{Sr}/^{86}\text{Sr}$ ratios during drier conditions later in the growing season at the catchment.

Significant changes in sapwater Ca/Sr ratio were also observed for sugar maple and red

oak species during the course of the growing season. As shown in Figure 2.25 and in Table 2.21, average Ca/Sr ratios for sapwaters collected from sugar maple trees were shown to increase by 78 and by 229 from July to August and from August to September, respectively. Average Ca/Sr ratios for sapwaters collected from red oak species increased by 112 from July to August before decreasing by 266 from August to September. Average Ca/Sr ratios for sap waters derived from chestnut oak trees remained fairly constant at a value near 430 over the course of the growing season increasing slightly from July to August before decreasing slightly from August to September. Monthly decreases in sap water Ca/Sr ratio may be attributed to increased evapotranspiration over the course of the growing season where convection in the xylem will passively transport calcium ions towards rapidly transpiring leaf tissues (Clarkson, 1984). On the contrary, maturation of leaves over the growing season results in a weak sink from which apoplastic binding sites can release calcium bound in the xylem walls to leaf tissues. Hence, the higher calcium levels and Ca/Sr ratios in xylem sap water later in the growing season (Clarkson, 1984). In studies at Shale Hills, Meinzer et al. (2013) demonstrated that transpiration rates in diffuse-porous maple species were responsive to fluctuations in soil moisture (e.g. isohydric), while ring porous oak species were relatively unaffected by soil moisture content (e.g. anisohydric) which is consistent with findings by other researchers (Abrams, 1990; Tardieu and Simonneau, 1998; Ewers et al., 2007; McDowell, 2011). As the calcium (and by inference, strontium) flux to the xylem through the apoplastic pathway is highly influenced by tree transpiration (Clarkson, 1984; McLaughlin and Wimmer, 1999; White and Broadley, 2003; Marschner, 2012), temporal variations in Ca/Sr should be expected to be larger for sugar maple species whose transpiration rates vary as a result of differences in soil moisture content over the course of the growing season. Reasons for such large temporal variations in Ca/Sr ratio for

anisohydric red oak species remain unclear and require future research.

Table 2.20 Seasonal $^{87}\text{Sr}/^{86}\text{Sr}$ ratios for selected sugar maple (ACSA), chestnut oak (QUPR), and red oak (QURU) sap waters sampled at northeastern (NE), northwestern (NW), southeastern (SE), and southwestern (SW) quadrants of the catchment

Sample ID	Species Code	July $^{87}\text{Sr}/^{86}\text{Sr}$	August $^{87}\text{Sr}/^{86}\text{Sr}$	September $^{87}\text{Sr}/^{86}\text{Sr}$
NE 622	QUPR	0.72431	0.72521	nm
NE 613	QURU	0.72222	0.72314	nm
NE 636	QURU	0.72475	nm	0.72452
NW UPHILL	ACSA	0.72252	0.72201	nm
NW 110	QURU	0.72076	0.72076	nm
SE DOWNHILL	ACSA	0.72298	nm	0.72219
SE 1271	QURU	0.72169	nm	0.72090
SE 1331	QURU	0.72508	nm	0.72483
SW 1164	ACSA	nm	0.72264	0.72197
SW 1080	QUPR	0.72078	0.72190	0.72106
SW 1170	QUPR	0.72154	0.72232	nm
SW 1074	QURU	0.72035	0.72060	0.72043
SW 1077	QURU	0.72115	0.72123	nm

*The 'nm' term refers to months when strontium isotope ratios were not measured for a designated sap water sample

Table 2.21 Seasonal Ca/Sr ratios for sugar maple, chestnut oak, and red oak sap waters

Tree Species	Average July Ca/Sr (molar)	Average August Ca/Sr (molar)	Average September Ca/Sr (molar)
Sugar Maple	260 ± 14	338 ± 76	567 ± 33
Chestnut Oak	428 ± 64	455 ± 91	398 ± 56
Red Oak	429 ± 98	541 ± 111	275 ± 18

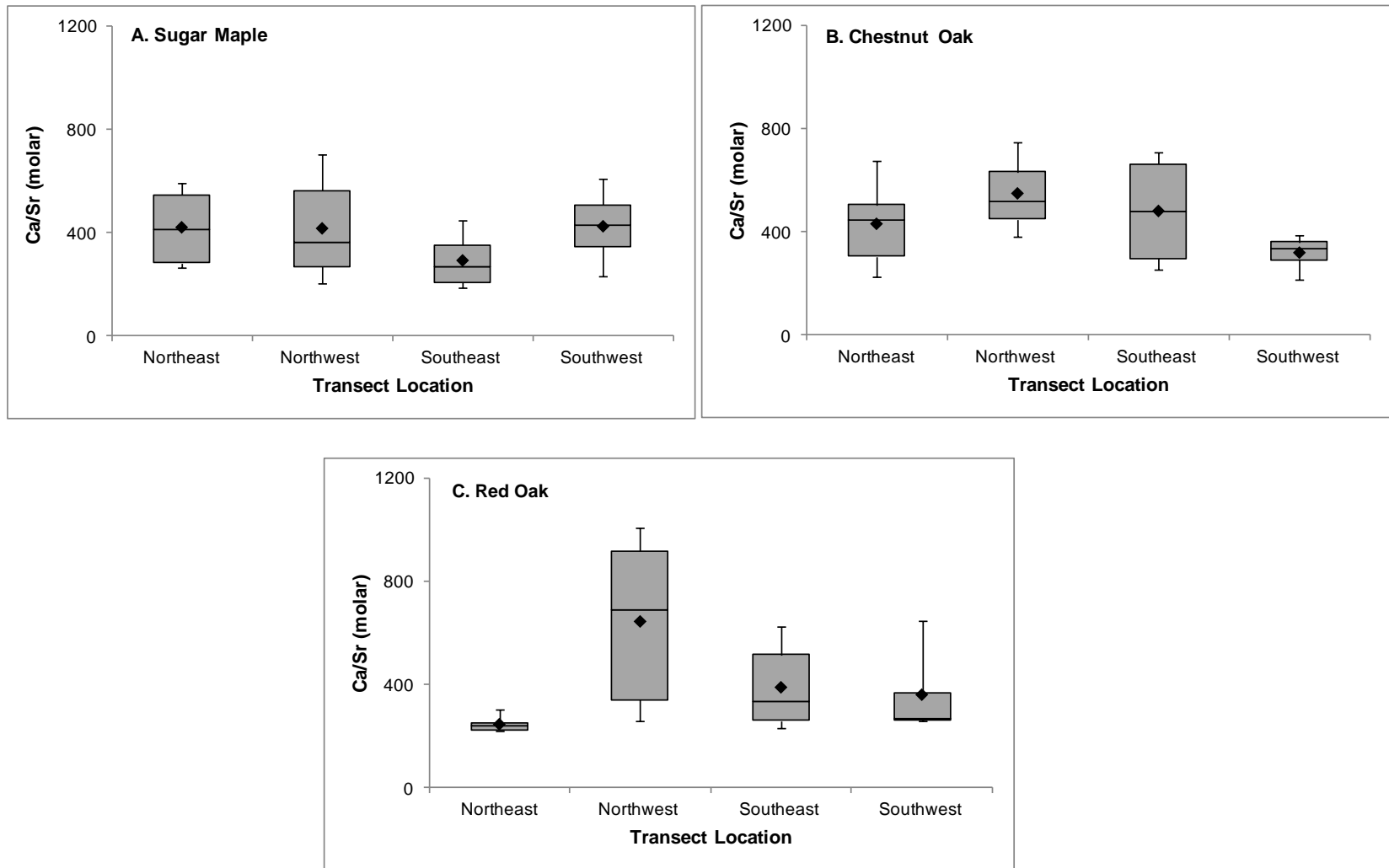


Figure 2.23 Box plots of Ca/Sr ratio based on sampling location for sugar maple (A), chestnut oak (B), and red oak (C) sap waters collected in northeastern, northwestern, southeastern, and southwestern quadrants of the catchment with mean values shown as closed diamonds.

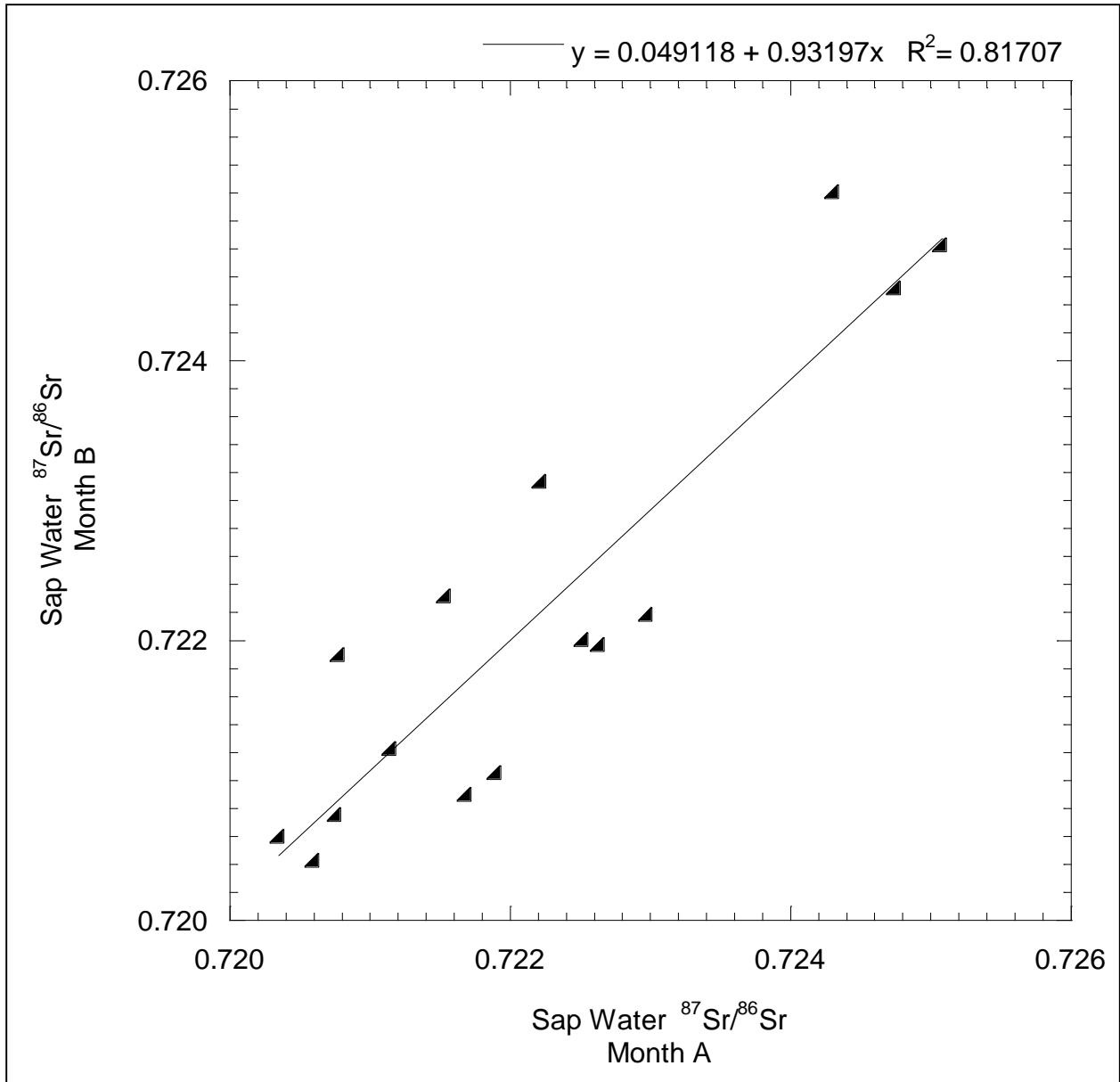


Figure 2.24 Sap water ⁸⁷Sr/⁸⁶Sr ratio of month B versus sap water ⁸⁷Sr/⁸⁶Sr ratio of month A for individual sap waters collected from identical trees. A correlation yielding an R² value of 0.82 is shown.

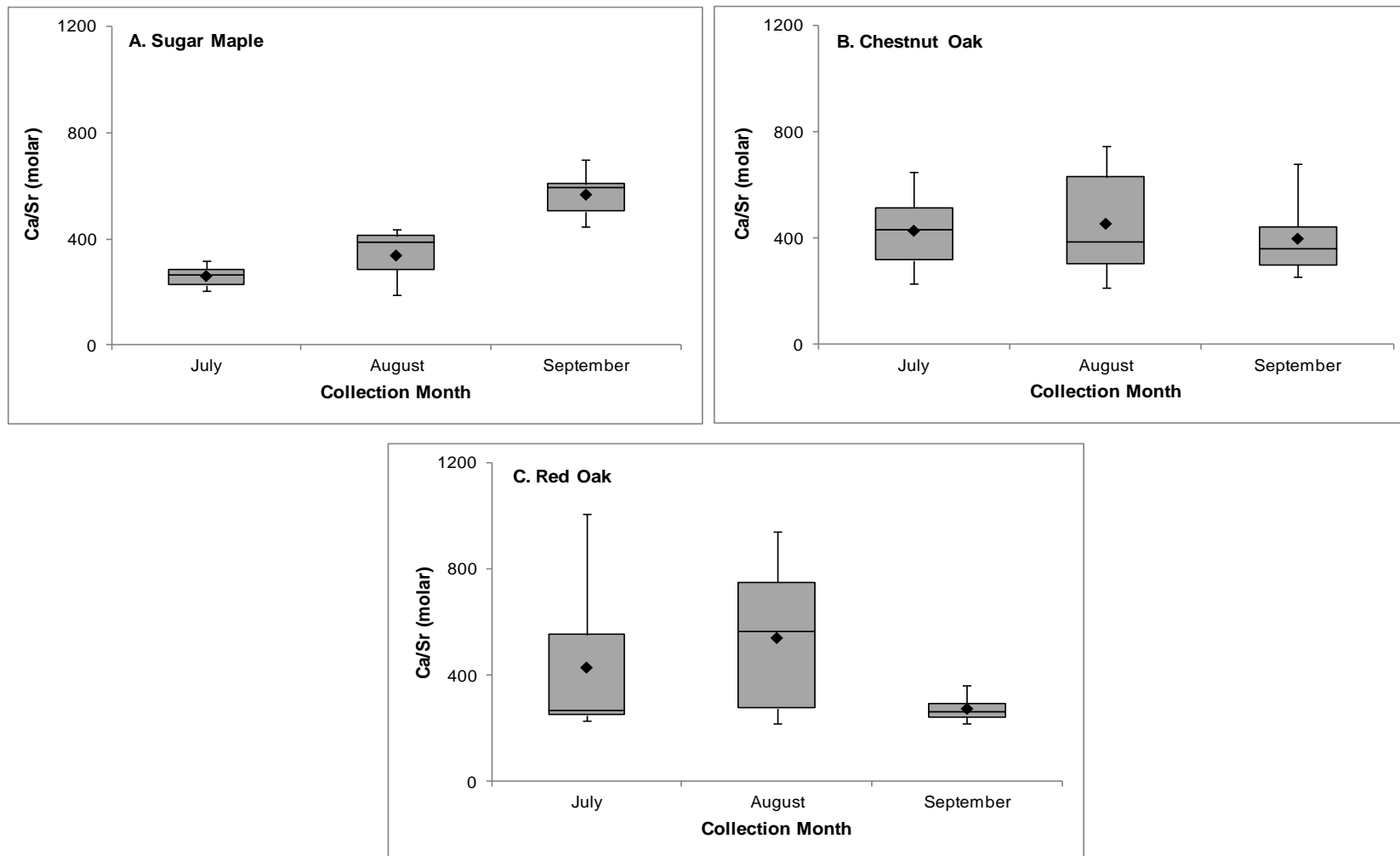


Figure 2.25 Box plots of Ca/Sr ratio for sugar maple (A), chestnut oak (B), and red oak (C) sap waters collected over the course of the growing season with mean values shown as closed diamonds.

4.4 Groundwaters and Streamwaters

Strontium isotope ratios of 0.71481 and 0.71746 were measured for groundwaters sampled at shallow (91 cm) and deep (849 cm) boreholes, respectively (Table 2.22, Figure 2.26). Strontium isotope ratios were also collected for groundwaters sampled from wells at depths of 230, 276, and 478 cm and found to be 0.71683, 0.71577, and 0.71585, respectively (Table 2.22, Figure 2.26). An average $^{87}\text{Sr}/^{86}\text{Sr}$ ratio of 0.71614 ± 0.00046 was obtained for all groundwaters (Figure 2.2). With the exception of the $^{87}\text{Sr}/^{86}\text{Sr}$ ratio for the groundwater sampled at the 276 cm depth, $^{87}\text{Sr}/^{86}\text{Sr}$ ratios were observed to increase with depth. Increases in strontium isotope composition with depth may be reflective of increased interaction of groundwater with more radiogenic parent shale (Average $^{87}\text{Sr}/^{86}\text{Sr} = 0.74558$) where subsurface groundwater is likely existing within fractured bedrock at the catchment (Jin et al., 2010, 2011a, 2011b; Brantley et al., 2013). Interestingly, no correlation was observed between a groundwater's $^{87}\text{Sr}/^{86}\text{Sr}$ ratio and its spatial proximity to the less radiogenic DC 3 valley floor carbonate source near the stream's weir (Table 2.22 and Figure 1.2). Additionally, strontium isotope ratios of 0.71362, 0.71610, and 0.71758 were obtained for streamwaters sampled from weir, mid stream, and stream headwater positions of a first-order catchment stream, respectively (Table 2.22, Figure 2.26). As shown in Figure 2.26, $^{87}\text{Sr}/^{86}\text{Sr}$ ratios were found to increase from weir to mid stream to stream headwater locations.

Significantly lower $^{87}\text{Sr}/^{86}\text{Sr}$ ratios in groundwaters and streamwaters (Table 2.22, Figure 2.2) relative to ridge top and mid slope exchangeable soils, soil porewaters, and vegetation (Tables 2.1, 2.3, 2.9, and 2.16, Figure 2.2) suggest that a source less radiogenic than shale (Table 2.24) is affecting strontium concentrations and strontium isotope compositions in streamwaters and groundwaters. Relatively alkaline streamwaters and groundwaters with high calcium and

magnesium concentrations (Table 2.22, Figure 2.27, Jin et al., 2011b) relative to precipitation, soils, and soil porewaters (Tables 2.1 and 2.3, Jin et al., 2011b) lend support to the hypothesis that lower strontium isotope compositions in groundwaters and streamwaters are resulting from the dissolution of carbonates at the catchment. As mentioned earlier, carbonates (e.g. ankerite and calcite) have been identified in quantitative XRDs for the deepest samples of the DC 1 ridge top drill core (DC 1-37 and DC 1-38, Jin et al., 2010) and for all samples analyzed from the DC 3 valley floor drill core (DC 3-0-1 to DC 3-52-53, Brantley et al., 2013). In general, carbonate dissolution proceeds more rapidly than silicate mineral weathering due to the greater reactivity and solubility of carbonate minerals relative to silicate minerals (MacDonald et al., 1991; White et al., 2005). Thus, even a small amount of carbonate underlying streamwaters and groundwaters at the catchment has the potential of shifting $^{87}\text{Sr}/^{86}\text{Sr}$ signatures to significantly lower values (Land, 2000; Shand et al., 2007; Shand et al., 2009). The carbonate weathering end-member was determined using the average $^{87}\text{Sr}/^{86}\text{Sr}$ ratio for the carbonate fraction of DC 3 drill core samples ($^{87}\text{Sr}/^{86}\text{Sr} = 0.71132$, Table 2.23) which are proximally located to groundwaters and streamwaters sampled at the catchment (Figure 1.2). For the silicate mineral weathering end-member, the composite average $^{87}\text{Sr}/^{86}\text{Sr}$ ratio from the silicate fraction of DC 1 and DC 3 drill core samples (e.g. shale end-member, $^{87}\text{Sr}/^{86}\text{Sr} = 0.74558$, Table 2.24) was selected based on observations of relatively uniform $^{87}\text{Sr}/^{86}\text{Sr}$ ratios in residuum material between DC 1 and DC 3 drill core sites (Table 2.24). The shale rather than “weathered shale” was chosen as the silicate mineral weathering end-member as streamwaters and groundwaters are more likely interacting with parent shale than “weathered shale” according to mineralogical observations (e.g. slower chemical weathering and weathering advance rates and C.E.C.s similar to parent materials) for nearby valley floor soils at the catchment (Jin et al., 2010). Proportions of strontium derived

from carbonate and silicate mineral weathering end-members in streamwaters and groundwaters were determined using two-component mixing on chloride normalized strontium isotope ratios ($(^{87}\text{Sr}/^{86}\text{Sr})^*$) (Equations 2 through 4). The mass fraction of strontium derived from the atmosphere ($X(\text{Sr})_{\text{Atmosphere}}$) was corrected for, enabling calculation of relative proportions of strontium from carbonate and silicate mineral weathering through two-component mixing (Equation 4). Detailed rationale behind end-member selection and parameters used in mixing calculations can be found in the Data Analysis Methods section.

Consistent with observations of low strontium isotope ratios, high calcium, strontium, and magnesium concentrations, and high pH values (Table 2.22, Figure 2.27, and Jin et al., 2011b), mixing calculations indicated significant proportions of strontium derived from carbonate weathering sources in groundwaters (Figure 2.28). Specifically, carbonate weathering derived proportions of strontium ranged from 0.76 to 0.87 and from 0.67 to 0.70 in borehole and well groundwaters, respectively. This contrasts with minor strontium contributions from silicate mineral weathering (range: 0.10 to 0.18 and 0.13 to 0.16 for borehole and well groundwaters, respectively) and atmospheric (range: 0.02 to 0.06 for borehole groundwaters and 0.16 for all well groundwaters) sources. As shown in Figure 2.28, proportions of strontium derived from carbonate weathering sources increased from stream headwater (0.30) to mid stream (0.50) to weir locations (0.77). These findings conform to observations of decreases in strontium isotope ratio, increases in calcium, strontium, and magnesium concentrations, and increases in pH value for streamwaters in the progression from stream headwater to mid stream to weir locations (Table 2.22, Figure 2.27, and Jin et al., 2011b). Additionally, in streamwaters, lower proportions of strontium derived from silicate weathering (0.19, 0.15, and 0.07 for stream headwater, mid stream, and weir locations, respectively) relative to atmospheric (0.50, 0.35, and 0.16 for stream

headwater, mid stream, and weir locations, respectively) sources were observed (Figure 2.28). These observations are consistent with the slow kinetics of clay dissolution at the catchment (Jin et al., 2010). Furthermore, high proportions of atmospherically derived strontium in stream headwaters (Figure 2.28) agree with field observations which indicate that stream flow at this location occurs exclusively during snowmelt and rainstorms in the early spring and fall, respectively (Jin et al., 2011b). On the contrary, streamwaters at the weir are known to flow a larger proportion of the year due to greater influxes of carbonate affected groundwaters to streamwaters at this location (Jin et al., 2011b). Accordingly, significantly larger proportions of strontium derived from carbonate weathering were observed in weir streamwaters relative to those sampled at mid stream and stream headwater locations (Figure 2.28). Mid stream locations presumably integrate biogeochemical processes at upstream (e.g. stream headwater) and downstream (e.g. weir) locations. Thus, proportions of strontium derived from carbonate weathering, silicate weathering, and atmospheric sources in streamwaters at the mid stream location roughly represented a 50:50 mixture of proportions determined for streamwaters sampled at stream headwater and weir locations (Figure 2.28). Interestingly, chloride normalized $^{87}\text{Sr}/^{86}\text{Sr}$ ratios in stream headwaters resembled those of nearby north swale valley floor leaves (Tables 2.9 and 2.22). As leaves at the catchment largely derive solutes from shallow soil exchangeable pool and porewater sources (Jin et al., 2011b), similarity in $^{87}\text{Sr}/^{86}\text{Sr}$ ratio between stream headwaters and leaves suggest a possible soil porewater source of strontium to stream headwaters.

Table 2.22 Strontium, calcium, and chloride elemental concentrations, pH values, and Ca/Sr, $^{87}\text{Sr}/^{86}\text{Sr}$, and $(^{87}\text{Sr}/^{86}\text{Sr})^*$ ratios for groundwaters and streamwaters sampled on October 8, 2013

Sample ID	Depth to water from top of casing (cm)	pH	Sr (μM)	Ca (μM)	Ca/Sr (molar)	Cl ^β (μM)	$^{87}\text{Sr}/^{86}\text{Sr}$	$(^{87}\text{Sr}/^{86}\text{Sr})^*$
CZMW 1	91	8.08	3.08	1070	347	23.7	0.71481	0.71492
CZMW 6	849	6.25	1.37	948	692	24.4	0.71746	0.71787
Well 8	230	6.62	0.34	195	568	17.7	0.71683	0.71805
Well 11	478	6.44	0.11	81	708	nm ^α	0.71585	0.71688
Well 13	276	6.68	0.46	631	1383	23.8	0.71577	0.71678
Weir	0	6.07	0.83	871	1044	43.2	0.71362	0.71422
Streamwater								
Mid Stream	0	nm ^α	0.37	227	601	41.7	0.71610	0.71914
Stream	0	5.80	0.25	155	610	40.2	0.71758	0.72475
Headwater								

^α The ‘nm’ term refers to a sample where a measurement was not taken.

^β Chloride elemental concentrations provided by Sullivan, 2013 (unpublished data).

*The chloride normalized $^{87}\text{Sr}/^{86}\text{Sr}$ ratio for a designated sample.

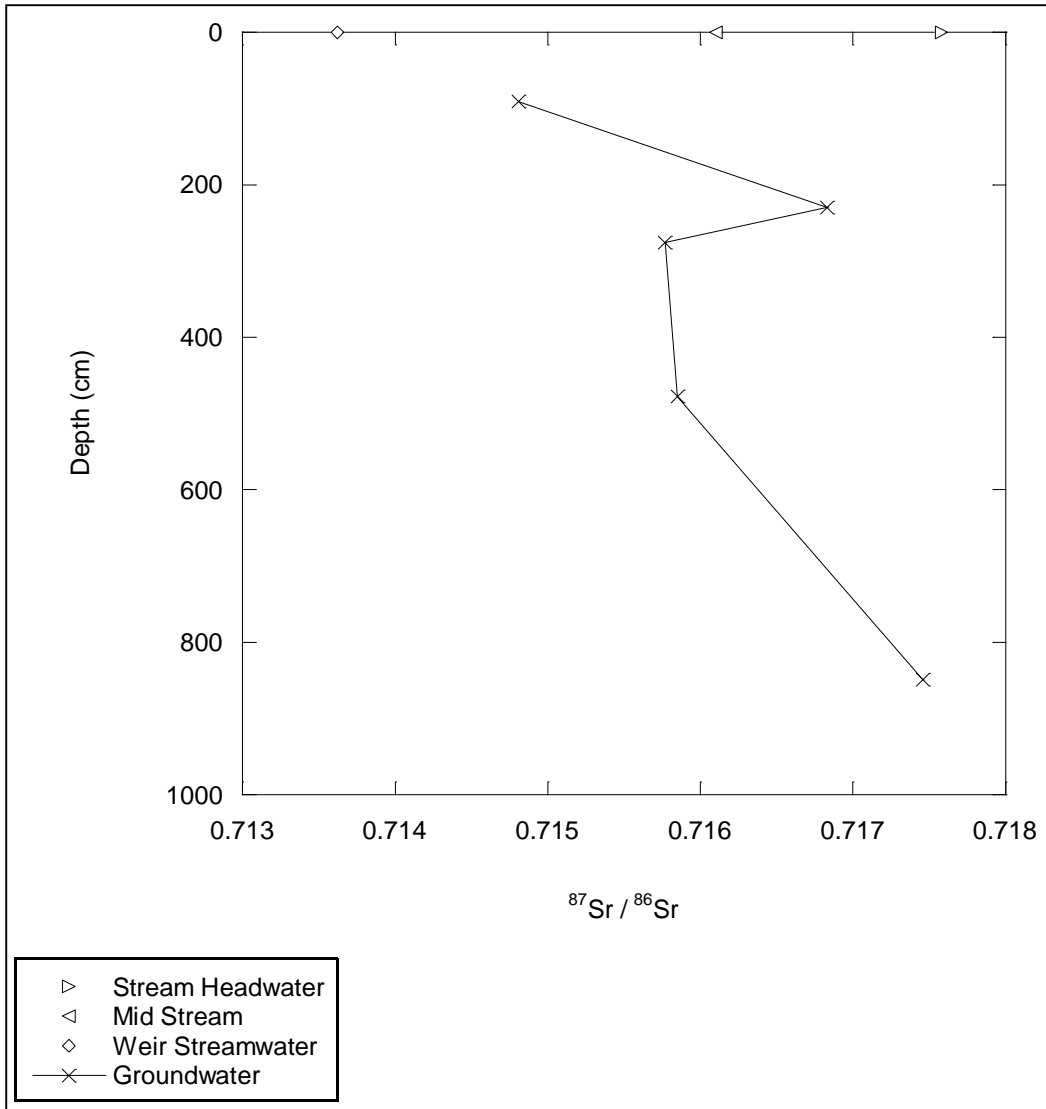


Figure 2.26 Depth versus $^{87}\text{Sr}/^{86}\text{Sr}$ ratio for groundwaters and streamwaters.

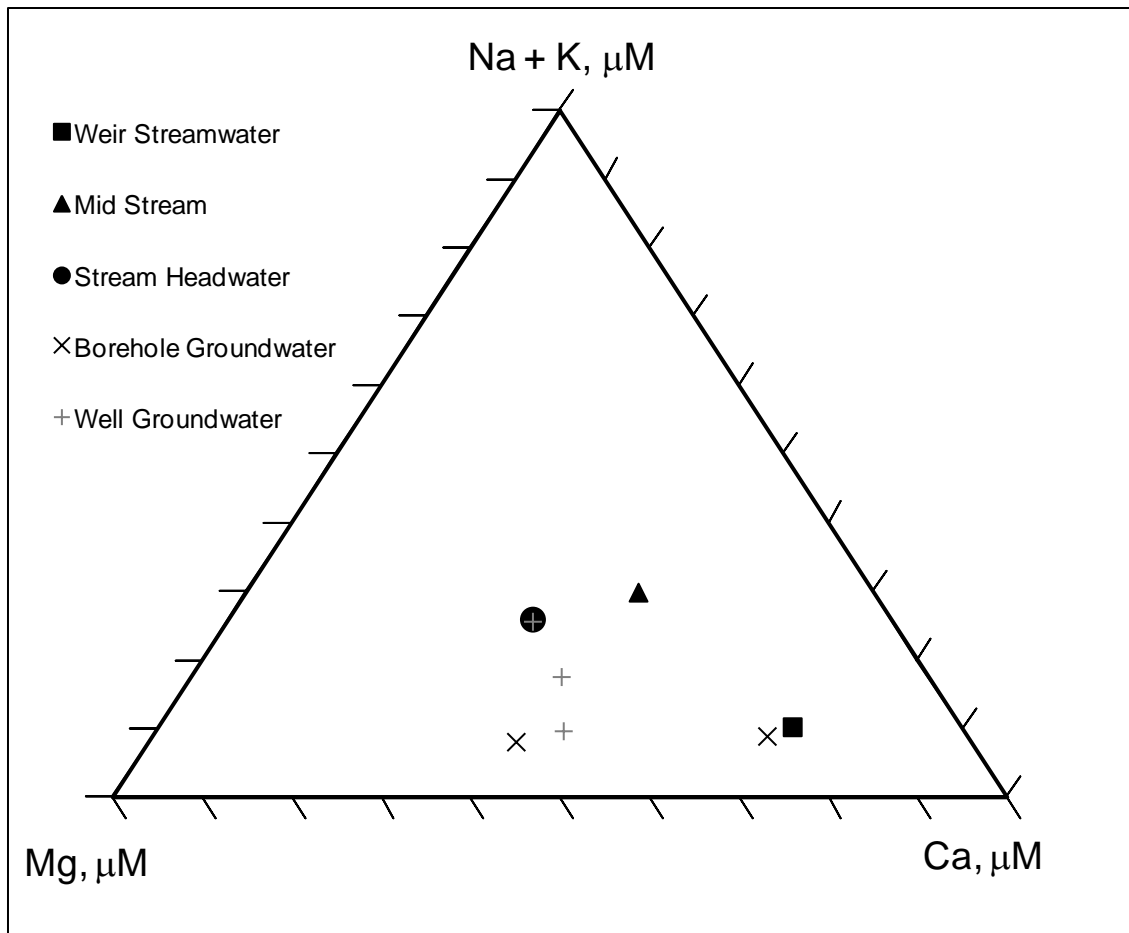


Figure 2.27 Ternary cation plot for groundwaters and streamwaters. Note that relative proportions of cations for stream headwater and Well 11 overlap on the figure.

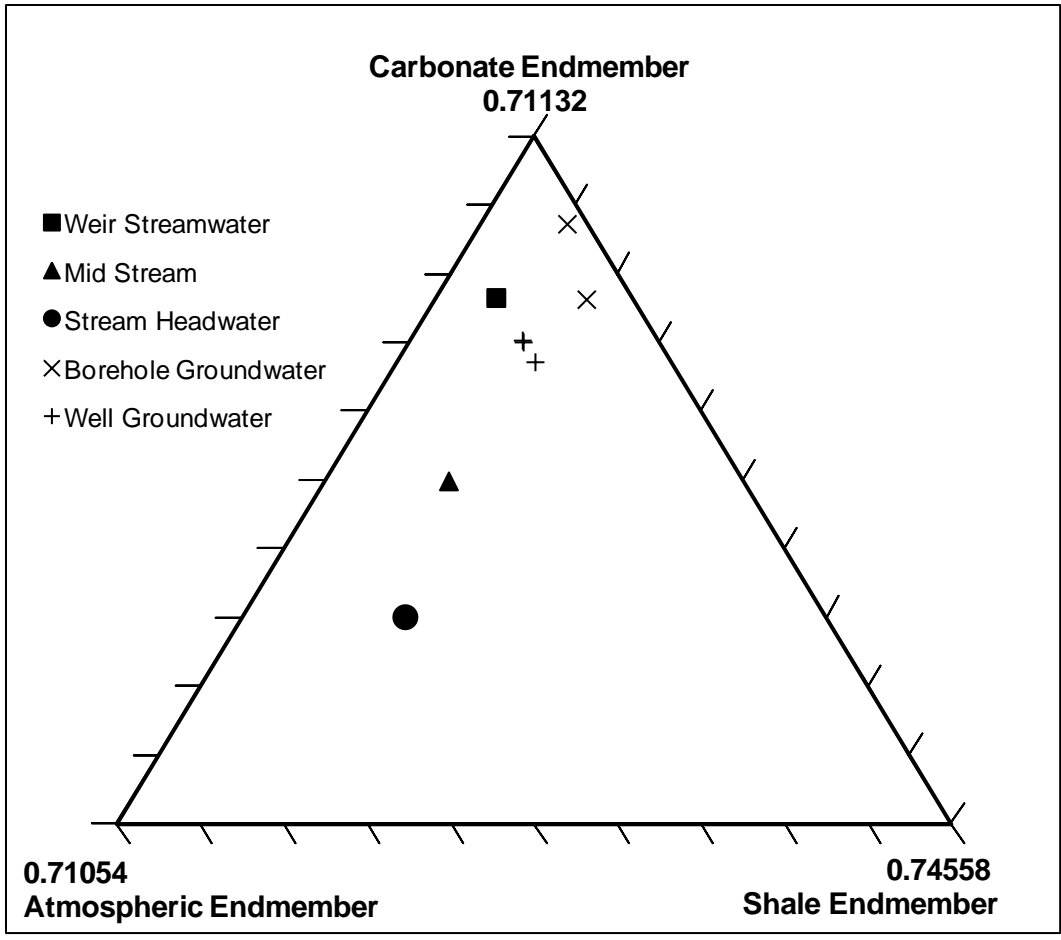


Figure 2.28 Ternary plot depicting relative proportions of strontium derived from atmospheric, carbonate weathering, and silicate weathering sources in groundwaters and streamwaters.

Ca/Sr ratios of 347 and 692 were measured for groundwaters sampled at shallow (91 cm) and deep (849 cm) boreholes, respectively (Table 2.22, Figure 2.29). Ca/Sr ratios of 568, 1383, and 708 were also observed for groundwaters sampled from wells at depths of 230, 276, and 478 cm, respectively (Table 2.22, Figure 2.29). An average Ca/Sr ratio of 740 ± 173 was obtained for groundwaters sampled from both sites (Figure 2.8), relatively similar to the average value determined for carbonates at the catchment (Figure 2.8). Ca/Sr ratios were found to increase with depth for borehole samples. No discernible dependence of Ca/Sr ratio on depth was observed for well samples. Differences in the composition of carbonates and in dissolved CO₂ concentrations in groundwaters may be responsible for the observed variation in groundwater Ca/Sr ratio with depth as was hypothesized for magnesium (Jin et al., 2011b; Brantley et al., 2013). Specifically, Jin et al. (2011b) and Brantley et al. (2013) suggested that variable degrees of CO₂ acquisition and degassing will affect the dissolution or precipitation of carbonates to increase and decrease, respectively, both calcium and strontium concentrations in groundwaters at the catchment. This complements observations of high carbonate depletion and calcium and strontium concentrations in groundwaters at locations where CO₂ charged fluids are flushed through fractured bedrock (Jin et al., 2011b; Brantley et al., 2013). As shown in Table 2.22, groundwater calcium and strontium concentrations sampled from boreholes were considerably larger than those sampled from wells. At boreholes, average groundwater calcium and strontium concentrations were found to be between 2 and 12 and between 5 and 20 times larger than those for groundwaters sampled from wells, respectively. As shown in the topographic map of the SSHCZO (Figure 1.2), groundwaters sampled from boreholes are proximally closer to the carbonate source near the stream's weir than well groundwaters. Overall, groundwater calcium concentrations far exceeded those found in soil porewaters. As mentioned previously, mixing calculations indicate that

groundwaters at the catchment are acquiring significant proportions of strontium from carbonate weathering sources (Figure 2.27). Given strontium's utility as an analog for calcium in watershed studies (Bailey et al., 1996; Clow et al., 1997; Kennedy et al., 2002; Drouet et al., 2005; Blum et al., 2006), elevated levels of calcium in groundwaters can similarly be attributed to increased interaction with carbonates by groundwaters at the catchment.

Ca/Sr ratios of 1044, 601, and 610 were obtained for weir, mid stream, and stream headwater locations, respectively (Table 2.22, Figure 2.29). An average Ca/Sr ratio of 752 ± 146 was obtained for streamwaters sampled from all locations (Figure 2.8), relatively consistent with the average value determined for groundwaters and carbonates at the catchment (Figure 2.8). As displayed in Figure 2.29, Ca/Sr ratios were observed to decrease from weir to mid stream locations and then to increase slightly from mid stream to stream headwater locations. Ca/Sr ratios obtained for mid stream and stream headwater positions were found to be rather similar. The weir position, however, had a much higher Ca/Sr ratio than mid stream and stream headwater locations differing by a factor of 1.7 compared to these locations. Furthermore, the Ca/Sr ratio at the weir location corresponded reasonably well to groundwaters sampled at the catchment. As mentioned previously, mixing calculations indicate that streamwaters at the weir are receiving significant strontium inputs from carbonate weathering sources, presumably due to greater influxes of carbonate affected groundwaters to weir streamwaters (Jin et al., 2011b). Given strontium's efficacy as a proxy for calcium in catchment studies (Bailey et al., 1996; Clow et al., 1997; Kennedy et al., 2002; Drouet et al., 2005), higher calcium concentrations and Ca/Sr ratios in streamwaters at weir relative to mid stream and stream headwater locations can be attributed to greater influxes of carbonate affected groundwaters to the weir location.

Strontium fluxes were calculated for streamwaters at weir, mid stream, and stream

headwater locations using geometric means of strontium concentration and stream discharge compiled from 2008 to 2010, the watershed area, and proportions of strontium estimated through mixing calculations (Equation 4), while calcium fluxes were calculated using average molar Ca/Sr ratios, previously calculated strontium flux values, and proportions of calcium estimated through mixing calculations (Equation 7). For streamwaters at weir, mid stream, and stream headwater locations, total strontium fluxes were estimated to be 3.22, 0.97, and 0.79 mol ha⁻¹ yr⁻¹, respectively. Specifically, atmospheric strontium flux estimates for weir, mid stream, and head streamwaters were found to be 0.53, 0.35, and 0.40 mol ha⁻¹ yr⁻¹, respectively. Additionally, strontium flux estimates to weir, mid stream, and head streamwaters from carbonate weathering sources were 2.68, 0.49, and 0.24 mol ha⁻¹ yr⁻¹, while those from silicate weathering sources were 0.01, 0.14, and 0.15 mol ha⁻¹ yr⁻¹, respectively. Total calcium fluxes of 2499, 635, and 436 mol ha⁻¹ yr⁻¹ were estimated for streamwaters at weir, mid stream, and stream headwater locations, respectively. Specifically, calcium fluxes from atmospheric sources in streamwaters at weir, mid stream, and stream headwater locations were estimated to be 122, 80, and 92 mol ha⁻¹ yr⁻¹, respectively. Furthermore, calcium flux estimates to weir, mid stream, and head streamwaters from carbonate weathering sources were 2365, 546, and 332 mol ha⁻¹ yr⁻¹, respectively, while those derived from silicate weathering sources were 12, 9, and 12 mol ha⁻¹ yr⁻¹, respectively. Although not directly apparent from Ca/Sr ratios, both calcium and strontium concentrations (Table 2.22) and fluxes in streamwaters were observed to increase from stream headwater to mid stream to weir locations. Jin et al. (2011b) observed a similar pattern for magnesium in streamwaters at Shale Hills where increases downstream were similarly attributed to more substantial contributions by carbonate affected groundwaters to weir streamwaters.

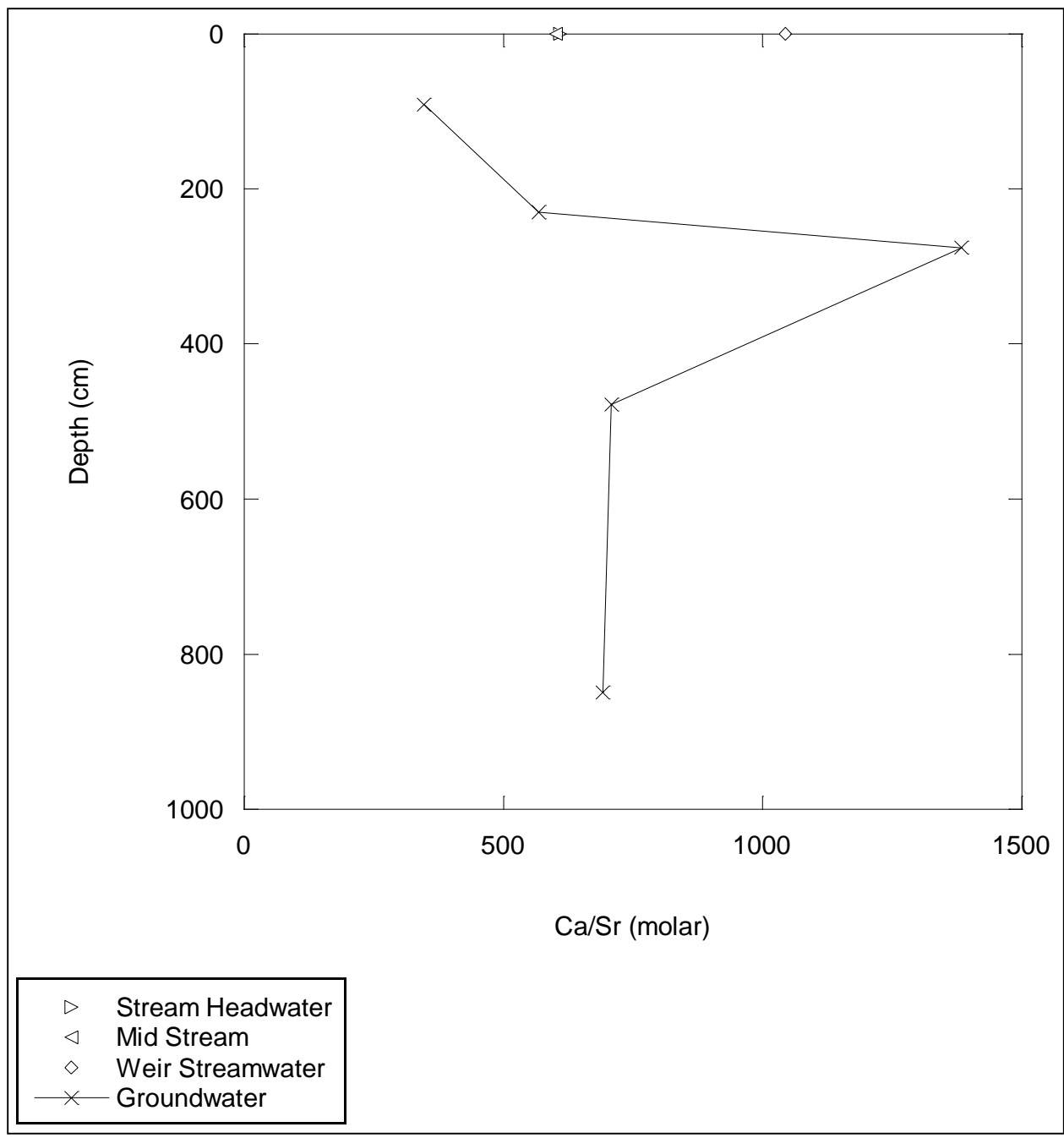


Figure 2.29 Depth versus Ca/Sr ratio for groundwaters and streamwaters. Note that Ca/Sr ratios for stream headwater and mid stream samples are overlapping on the figure.

4.5 Precipitation

Reported precipitation $^{87}\text{Sr}/^{86}\text{Sr}$ ratios for samples collected bimonthly from the months of April to September of 2005 at the Pennsylvania State University were obtained from Kim (2007). Kim (2007) measured an average $^{87}\text{Sr}/^{86}\text{Sr}$ ratio of 0.71054 for precipitation samples collected from April to September of 2005 (Figure 2.2). According to Kim (2007), $^{87}\text{Sr}/^{86}\text{Sr}$ ratios of 0.70855, 0.70934, and 0.71371 were obtained for precipitation samples collected from April to May, June to July, and August to September of 2005, respectively. The average $^{87}\text{Sr}/^{86}\text{Sr}$ ratio for precipitation reported by Kim (2007) is consistent with reported precipitation $^{87}\text{Sr}/^{86}\text{Sr}$ ratios in other locations of the northeastern United States (Dasch, 1969; Miller et al., 1993; Bailey et al., 1996; Dijkstra et al., 2003; Dasch et al., 2006) where the strontium isotope composition in precipitation has been shown to be relatively constant over time. The $^{87}\text{Sr}/^{86}\text{Sr}$ ratio in bulk precipitation is slightly higher than the $^{87}\text{Sr}/^{86}\text{Sr}$ ratio reported for ocean water with deviation likely reflecting minor contributions to precipitation from mineral dust and biological materials. As indicated by Kim (2007), $^{87}\text{Sr}/^{86}\text{Sr}$ ratios were relatively uniform over the summer but were found to increase quite considerably in the fall. A similar pattern was observed in France (Negrel and Roy, 1998) where the $^{87}\text{Sr}/^{86}\text{Sr}$ ratio for precipitation remained rather constant over the summer ($^{87}\text{Sr}/^{86}\text{Sr}$ range: 0.70920 to 0.70944) only to increase dramatically in the fall ($^{87}\text{Sr}/^{86}\text{Sr}$ range: 0.71226 to 0.71314).

Ca/Sr ratios for precipitation were derived from calcium and strontium concentrations reported for the Pennsylvania State Monitoring Station (PA 15) by the National Atmospheric Deposition Program (NADP) (2005) and by Kim (2007) in April to September of 2005. Using data from these sources, Ca/Sr ratios were found to range from 81 to 473. An average molar Ca/Sr value of 233 was determined for precipitation (Figure 2.8). This value falls within the

range of Ca/Sr ratios reported for precipitation in other locations of the northeastern United States (Miller et al., 1993; Bailey et al., 1996; Dasch et al., 2006). Based on data provided by the NADP and Kim (2007), the Ca/Sr ratio of precipitation was found to remain fairly constant from April to July increasing from 81 to 144 from April-May to June-July. Significant increases in Ca/Sr ratio were observed thereafter, where an average Ca/Sr ratio for August-September was found to be 473. Calcium concentrations ranged from 2.69 to 4.95 μM , with an average concentration of $3.78 \pm 0.65 \mu\text{M}$ (NADP, 2005). Calcium concentrations were observed to decrease moderately over the course of the growing season. Strontium concentrations ranged from 0.0057 to 0.046 μM , with an average concentration of $0.029 \pm 0.012 \mu\text{M}$ (Kim, 2007). Modest increases in strontium concentration were observed from the seasonal period from April-May to June-July where concentrations increased from 0.034 to 0.046 μM . Conversely, significant decreases in strontium concentration were found from the seasonal period from June-July to August-September where concentrations decreased by an 8 fold factor from 0.046 μM to 0.006 μM . A considerably lower strontium concentration relative to calcium concentration in August-September resulted in the higher Ca/Sr ratio observed for precipitation during this seasonal period. Bailey et al (1996) observed a similar pattern at the Cone Pond watershed in New Hampshire where strontium concentrations in precipitation dropped considerably from summer to fall months resulting in higher Ca/Sr ratios for precipitation collected in the fall compared to the summer.

4.6 Drill Core

Carbonate Fraction

For samples where calcite and ankerite were identified in quantitative XRD patterns (Jin et al., 2010; Brantley et al., 2013), strontium isotope ratios for carbonate fractions of DC 1 ridge

top and DC 3 valley floor drill core samples ranged from 0.71910 to 0.71935 and from 0.70812 to 0.71408 (Table 2.23, Figures 2.30 and 2.31), respectively, with average values of 0.71922 ± 0.00013 and 0.71132 ± 0.00084 , respectively. Isotopically distinct ratios for carbonate fractions of DC 1 ridge and DC 3 valley floor drill core samples (Table 2.23, Figure 2.30) support the presence of diverse carbonate compositions at the catchment possibly due to the heterogeneous lithology of the Rose Hill formation (Flueckinger, 1969) where carbonate layers at the ridge and valley are likely originating from different strata. Interestingly, the average $^{87}\text{Sr}/^{86}\text{Sr}$ ratio for the carbonate fraction of DC 1 ridge top drill core samples was significantly higher than the value determined for drill core samples collected from the DC 3 valley floor site. Similar $^{87}\text{Sr}/^{86}\text{Sr}$ ratios observed in carbonate affected DC 1 drill core samples (e.g. DC 1-37 and DC 1-38, Table 2.23, Figures 2.30 and 2.31) suggest that a single carbonate source is affecting strontium isotope compositions at this location. On the contrary, strontium isotope ratios for the carbonate fraction of DC 3 valley floor drill core samples reflect a mixture of calcite and ankerite (Brantley et al., 2013). As mentioned previously, ankerite has been identified at the DC 1 site based on high iron, manganese, and calcium elemental compositions, high loss on ignition content, and grey coloration in drill core samples collected from this site (Jin et al., 2010). Furthermore, average $\delta^{13}\text{C}$ compositions for carbonates collected at the DC 3 site (-1.1‰ , Jin et al., 2014) better resemble values for marine carbonates ($\sim 0\text{‰}$, Jin et al., 2014) than those obtained for carbonates sampled at the DC 1 site (-5.9‰ , Jin et al., 2014). Additionally, low $\text{Sr}^{2+}/(\text{Ca}^{2+} + \text{Mg}^{2+})$ ratios in groundwaters at valley floor locations reflect the tendency of Sr^{2+} to remain in solution rather than substitute calcium in secondary mineral phases such as pedogenic calcite (Gabitov et al., 2014). Moreover, Brantley et al. (2013) observed precipitation of secondary calcites at depths below the carbonate weathering front ($\sim 4\text{ m}$ depth) at the valley floor with dissolution of these

carbonates likely above this depth due to their fast dissolving nature in the local equilibrium regime of the catchment. To this end, ankerites are hypothesized to be largely contributing to the $^{87}\text{Sr}/^{86}\text{Sr}$ ratio at the DC 1 ridge top site with influences to the strontium isotope signature by secondary calcites assumed to be significant at the DC 3 valley floor site. If, in fact, strontium isotope compositions in drill core samples at the ridge top are truly reflective of ankerite and valley floor drill core samples are known to contain calcite (Brantley et al., 2013; Jin et al., 2014), then considerably lower $^{87}\text{Sr}/^{86}\text{Sr}$ ratios in drill core samples derived from DC 3 relative to DC 1 suggest that calcites are less radiogenic than ankerites at the catchment.

If calcites are, indeed, less radiogenic than ankerites at the catchment, then greater variability in strontium isotope composition with depth in the carbonate fraction of drill core samples at DC 3 relative to DC 1 (Figure 2.31) can be attributed to differences in relative proportions of strontium derived from calcite and ankerite where lower $^{87}\text{Sr}/^{86}\text{Sr}$ ratios are hypothesized to reflect greater proportions of strontium derived from calcite for a given drill core sample. As shown in Figure 2.30, increased proportions of calcite + ankerite, as determined in quantitative XRD patterns (Brantley et al., 2013), generally correlated with lower strontium isotope ratios for DC 3 valley floor drill core samples (Table 2.23, Figure 2.31). In fact, Brantley et al. (2013) recasted total carbon as wt% calcite for the DC 3 21-22 sample with the highest abundance of carbonate which yielded a value of 18.8 wt% calcite through RockJock calculations, in close accord with the XRD determined value of 17.7 wt% calcite + ankerite (Brantley et al., 2013). Consequently, the importance of less radiogenic calcite contributions to DC 3 drill core samples should not be overlooked. If less radiogenic calcites are contributing greater proportions of strontium to DC 3 valley floor drill core samples, then concomitant decreases in strontium isotope ratio with increased carbonate content seem reasonable

As shown in Figure 2.30, variation in $^{87}\text{Sr}/^{86}\text{Sr}$ ratio was observed based on sampling depth for carbonate fractions of DC 1 and DC 3 drill core samples. Spatial differences in $^{87}\text{Sr}/^{86}\text{Sr}$ ratio were largely reflective of the variability in proportions of carbonate present in drill core samples as estimated by quantitative XRD patterns (Figure 2.31). Specifically, a narrow range of strontium isotope ratios was observed for “carbonate free” DC 1 samples; hence, the minimal variation observed in $^{87}\text{Sr}/^{86}\text{Sr}$ ratio from 465 cm to the 2143 cm depth. At the 2294 cm depth, the presence of the Rb poor, carbonate bearing mineral ankerite (Table 2.23) significantly lowered the $^{87}\text{Sr}/^{86}\text{Sr}$ ratio for the DC 1-37 drill core sample. Minimal variation was observed in $^{87}\text{Sr}/^{86}\text{Sr}$ ratio between DC 1-37 and DC 1-38 drill core samples collected at 2294 and 2446 cm depths, respectively, despite differences in ankerite content (Table 2.23). With the exception of DC 3-5-6 (168 cm) and DC 3-42-43 (1296 cm), spatial variation in $^{87}\text{Sr}/^{86}\text{Sr}$ ratio can also be attributed to differences in relative proportions of carbonate present in DC 3 drill core samples as estimated by quantitative XRD patterns (Brantley et al., 2013). As mentioned earlier, less radiogenic calcites are hypothesized to be contributing greater proportions of strontium to DC 3 valley floor drill core samples than ankerite. Thus, concurrent decreases in strontium isotope ratio with increases in carbonate content were observed in most DC 3 samples. However, it should be noted that iron concentrations in carbonate fractions of DC 3-5-6 and DC 3-42-43 (549 and 1181 ppm, respectively) far exceeded the range observed for a majority of DC 3 samples (between 18 and 232 ppm). Thus, greater strontium contributions from more radiogenic ankerite in DC 3-5-6 and DC 3-42-43 relative to less radiogenic calcite may have resulted in deviation from the patterns described earlier between carbonate content and $^{87}\text{Sr}/^{86}\text{Sr}$ ratio.

Generally, $^{87}\text{Sr}/^{86}\text{Sr}$ isotope ratios in carbonates at the catchment (Table 2.23) exceeded the value expected for ocean water (Average $^{87}\text{Sr}/^{86}\text{Sr} = 0.7092$, Hess et al., 1986). As such,

carbonates at the catchment are inferred to be diagenetic with strontium isotope compositions influenced by meteoric pore fluids (Brantley et al., 2013). These fluids are hypothesized to have interacted with more radiogenic Rb bearing shales and clay silicates at the catchment. As mentioned previously, carbonate weathering fronts at Shale Hills are deep (~200 and 2200 cm at valley floor and ridge locations, respectively, Brantley et al., 2013). Neutron scattering studies at the catchment (Jin et al., 2011a) have indicated that bedrock chips collected at deep depths are relatively impermeable and low in porosity. Thus, advective transport of diagenetic components in meteoric pore fluids is hypothesized to occur along the bedrock/saprock interface and along fractures (Jin et al., 2011a). Additionally, diffusive transport processes are possible for pore fluids in the matrix between major fractures (Jin et al., 2011a).

Strontium isotope ratios of the carbonate fraction of “carbonate free” DC 1 samples (DC 1-21 to DC 1-36) ranged from 0.72833 to 0.73087 (Table 2.23, Figures 2.30 and 2.31), with an average value of 0.72967 ± 0.00056 (Figure 2.2). These ratios are likely reflective of weathering processes in the parent shale. As discussed in the Procedural Methods section, the carbonate fraction of drill core samples was extracted by means of a combined NaOAc/HOAc leach. This procedure releases carbonates as well as exchangeable cations into solution and, thus, “carbonate free” DC 1 samples should be reflective of weathering processes involving strontium containing mineral phases. As mentioned in the Data Analysis Methods section, calcium and strontium loss from parent material and bulk soils has been hypothesized to be resulting from feldspar (e.g. plagioclase) dissolution processes (Jin et al., 2010; Jin and Brantley, 2011; Ma et al., 2011a; Ma et al., 2011b). Despite low feldspar contents in bulk soils at the catchment (Jin et al., 2010), preferential weathering during soil forming processes of calcium and strontium enriched minerals with low $^{87}\text{Sr}/^{86}\text{Sr}$ ratios (e.g. plagioclase feldspar) has been shown to be significant in

determining a soil's strontium isotope composition (Aberg et al. 1989; Bain and Bacon, 1994; Bailey et al., 1996; Drouet et al., 2005). Procession of feldspar dissolution before clay mineral weathering is based on mineralogical observations at the catchment (Jin et al., 2010) which indicate that soil cores are depleted in sodium and calcium but not in potassium, magnesium, aluminum, and iron relative to drill cores. Additionally, significantly positive europium (Eu) anomalies in natural waters and exchangeable pools at Shale Hills (Ma et al., 2011a; Ma et al., 2011b) indicate preferential dissolution of plagioclase feldspar during chemical weathering. Thus lower $^{87}\text{Sr}/^{86}\text{Sr}$ ratio of the "carbonate free" DC 1 samples relative to shales (Table 2.24, Figure 2.2) is inferred to be from leaching of less radiogenic strontium from feldspar dissolution processes at interlayer and adsorption sites of clay minerals (e.g. illites and chlorites) which are known to dominate the mineralogy of shales at the catchment according to quantitative XRD patterns (Jin et al., 2010). In this way, the less radiogenic isotope signature of feldspar (Faure and Mensing, 2005) would be incorporated into "carbonate free" DC 1 samples through exchange reactions at interlayer and adsorption sites with more radiogenic clay minerals.

For the DC 1 ridge top drill core, Ca/Sr ratios in carbonate fractions of carbonate bearing samples (Average Ca/Sr = 2882 ± 17) were between 3 to 8 times higher than those observed in "carbonate free" samples (range: 376 to 951) (Table 2.23). As shown in Table 2.23 and Figure 2.32, Ca/Sr ratios in DC 1-21 through DC 1-33 were found to be relatively similar; however, DC 1-36 exhibited a significantly higher Ca/Sr ratio. Ca/Sr ratios for DC 1-37 and DC 1-38 were also shown to be remarkably similar (Table 2.23, Figure 2.31). At first glance, the close proximity of DC 1-36 to carbonate bearing drill core samples (DC 1-37 and DC 1-38) would suggest possible interaction of DC 1-36 with dissolved carbonates at deeper depths. However, this is unlikely considering the similarity in strontium isotope ratio observed between DC 1-36

($^{87}\text{Sr}/^{86}\text{Sr} = 0.73026$) and other “carbonate free” samples (Table 2.23). For the DC 3 valley floor site, Ca/Sr ratios in carbonate fractions of drill core samples were found to be rather similar with a range of 734 to 1110 and an average value of 882 ± 65 observed (Table 2.23). Although not directly apparent from Ca/Sr ratios, calcium concentrations corresponded reasonably well to proportions of carbonates estimated in DC 1 and DC 3 drill core samples through quantitative XRD patterns (Table 2.23). With the exception of DC 3-5-6 and DC 3-42-43 where respective calcium concentrations were lower and higher than predictions based on carbonate compositions, higher carbonate contents generally translated to higher calcium concentrations for drill core samples collected from both sites. As shown in Table 2.23 and Figure 2.32, Ca/Sr ratios for DC 1 ridge top drill core samples generally increased with depth (with the exception of DC 1-33). No discernible dependence on depth was observed for drill core samples collected from the DC 3 valley floor location (Table 2.23, Figure 2.32); hence, the alternating decreasing/increasing pattern in Ca/Sr ratio found for depth intervals corresponding to 137 to 168 cm, 168 to 686 cm, and 686 to 1296 cm. Differences in Ca/Sr ratio for DC 1 and DC 3 drill core samples with depth may be due to variations in carbonate composition or degrees of CO_2 acquisition and CO_2 degassing as these processes lead to the dissolution or precipitation of carbonates at the catchment, respectively (Jin et al., 2011a; Brantley et al., 2013). Accordingly, Jin et al. (2011a) noted the greatest carbonate depletion to occur where CO_2 charged fluids were flushed through fractured bedrock.

Silicate Fraction

Strontium isotope ratios of the silicate fraction of DC 1 ridge top and DC 3 valley floor drill core samples ranged from 0.74143 to 0.74919 and from 0.74297 to 0.74834 (Table 2.24, Figure 2.30), respectively, with average values of 0.74604 ± 0.00113 and 0.74512 ± 0.00090 ,

respectively. As ranges of strontium isotope ratios were shown to be rather similar between DC 1 and DC 3 drill core sites, a composite average $^{87}\text{Sr}/^{86}\text{Sr}$ ratio of 0.74558 ± 0.00070 was determined for the silicate fraction of drill core samples collected from both sites. Observed strontium isotope ratios in residual material (Table 2.24) fall within the range of values reported by Whitney and Hurley (1964) for shales in the area. The highly radiogenic strontium isotope signature for the silicate fraction of drill core samples is unsurprising given the high rubidium content typically present in shales (Capo et al., 1998).

As shown in Table 2.24 and Figure 2.30, variation in $^{87}\text{Sr}/^{86}\text{Sr}$ ratio was observed based on sampling depth for silicate fractions of DC 1 and DC 3 drill core samples. For the DC 1 ridge top drill core, initial decreases in $^{87}\text{Sr}/^{86}\text{Sr}$ ratio from 465 cm to the 1074 cm depth were followed by increases for the depth interval corresponding to 1074 and 2143 cm. Beyond the 2143 cm depth, $^{87}\text{Sr}/^{86}\text{Sr}$ ratios decreased down to a depth of 2446 cm. For the DC 3 valley floor, the strontium isotope ratio first decreased between 137 and 168 cm depths and then increased between 168 and 1296 cm depths. Heterogeneity in the composition of Rose Hill formation (Lynch, 1976) is likely resulting in observed spatial variability in strontium isotope ratio for drill core samples collected from both sites. Additionally, Jin et al. (2011a) noted differences in porosity with depth for DC 1 shale chips. As mentioned previously, increased porosity accelerates dissolution and disaggregation processes by enabling infiltrating precipitation inputs to penetrate into shale fractures or joints. In this study, weathered shale was found to be less radiogenic than unweathered shale (Figure 2.2). As such, observed discrepancy in $^{87}\text{Sr}/^{86}\text{Sr}$ ratio for silicate fractions of drill core samples (Table 2.24, Figure 2.30) may be the result of differences in porosity with depth where increased porosity leads to enhanced weathering and hence, lower strontium isotope ratios.

For the DC 1 ridge top site, Ca/Sr ratios for silicate fractions of “carbonate free” and carbonate bearing drill core samples ranged from 11 to 34 and from 89 to 101, respectively, with average values of 23 ± 6 and 95 ± 6 , respectively (Table 2.24 and Figure 2.32). Higher Ca/Sr ratios observed in carbonate bearing DC 1 samples are presumably due to contamination by carbonates unsuccessfully extracted through the combined NaOAc/HOAc leach. It should be noted that the average Ca/Sr ratio for “carbonate free” samples at the DC 1 ridge top drill core conforms to the value calculated using major (Jin et al., 2010) and trace element (Ma et al., 2011) data for the DC 1 drill core derived from previous studies at Shale Hills (Ca/Sr= 24). Excluding DC 3-21-22 and DC 3-42-43 drill core samples where contamination by carbonates is likely, Ca/Sr ratios for the silicate fraction of DC 3 valley floor drill core samples ranged from 22 to 38 with an average value of 31 ± 3 observed. Minimal discrepancy in average Ca/Sr ratio between DC 1 and DC 3 sites is consistent with relatively similar average strontium isotope ratios observed for drill core samples collected from both sites (Table 2.24). Interestingly, silicate fractions of drill core samples hypothesized to be affected by carbonate contamination according to Ca/Sr ratios did not necessarily display lower $^{87}\text{Sr}/^{86}\text{Sr}$ ratios (Table 2.24). Excluding samples affected by carbonate contamination (e.g. DC 1-37 and 38 and DC 3-21-22 and 42-43), depth dependent variability in Ca/Sr ratio was rather minimal between sites (Figure 2.32). However, it should be noted that greater variability existed between Ca/Sr ratio and depth for the DC 1 relative to DC 3 drill core where samples collected at shallower depths were shown to have lower Ca/Sr ratios than those sampled at deeper depths. Observed variation in Ca/Sr ratio may be the result of differences in porosity with depth. As discussed earlier, increased porosity accelerates dissolution and disaggregation processes by enabling infiltrating precipitation inputs to penetrate into shale fractures or joints. Neutron scattering studies at the catchment (Jin et al.,

2011a) have suggested that in low-porosity and low-permeability bedrock between fractures, fluid transport is controlled by slow diffusion processes where residence times for solutes in bedrock between fractures are long and small changes in porosity will significantly impact weathering processes.

Carbonate Propagation Front

As mentioned in the Data Analysis Methods section, the rate of carbonate propagation for the carbonate source at the CZMW 2 borehole near the stream's weir (DC 3) was calculated using the calcium flux for calcite at the stream's weir ($9.5 \times 10^{-4} \text{ g Ca cm}^{-2} \text{ yr}^{-1}$), the average density of calcite (1.1 g Ca cm^{-3}), and the average proportion of carbonates in DC 3 valley floor drill core samples as estimated by quantitative XRD patterns at Shale Hills (0.03125; Brantley et al., 2013). To this end, a preliminary estimate of the rate of carbonate propagation was found to be 280 m yr^{-1} which is 6 and 16 times larger than rates reported for regolith production at ridge top/mid slope (44 m/Myr , Ma et al., 2010) and valley floor (17 m/Myr , Ma et al., 2010) positions of the southern planar quadrant as calculated by U-series isotopes. Furthermore, the rate of carbonate propagation exceeds the catchment-wide erosion rate as inferred from cosmogenic ^{10}Be dating of sediments (15 m/Myr , Jin et al., 2010) by a factor of approximately 20.

Discrepancy between rates of regolith production and carbonate propagation conform to greater depths inferred for carbonate weathering at the catchment (Jin et al., 2010; Jin et al., 2011a; Brantley et al., 2013). In fact, elevated levels of calcium (Table 2.22) and magnesium (Jin et al., 2011b) are present in groundwaters relative to soil porewaters at Shale Hills consistent with a local equilibrium regime where erosion rates are slower than dissolution rates for carbonate minerals (Jin et al., 2010, 2011b; Brantley et al., 2013). Due to the high reactivity and solubility of carbonate minerals relative to silicate minerals (MacDonald et al., 1991; White et al., 2005),

carbonates are expected to dissolve under local equilibrium (Lebedeva et al., 2010). Hence, the ‘completely developed depletion profile’ for calcium referenced in Brantley et al. (2013) where carbonates are hypothesized to be completely dissolved in the upper portion of the profile at the DC 1 ridge top (above 2200 cm) and DC 3 valley floor (above 200 cm) drill core sites. On the contrary, incompletely developed depletion profiles, where erosion rates exceed dissolution rates, are expected for silicate minerals at the catchment with these slow dissolving and abundant minerals present at the land surface (Jin et al., 2010, 2011b; Brantley et al., 2013). However, it should be noted that the timescales for regolith production and carbonate propagation vary considerably. While soil chemistry documents extents of reactions over timescales of tens of thousands of years, carbonates reflect residence times for groundwaters which have been calculated to be less than one year at the catchment (Jin et al., 2011b).

Table 2.23 Strontium and calcium elemental concentrations, Ca/Sr and $^{87}\text{Sr}/^{86}\text{Sr}$ ratios, and carbonate compositions for the carbonate fraction of DC 1 and DC 3 drill core samples

Sample Date	Sample ID	Depth (cm)	Sr ($\mu\text{M/g}$)	Ca ($\mu\text{M/g}$)	Ca/Sr (molar)	$^{87}\text{Sr}/^{86}\text{Sr}$	Calcite and Ankerite (wt %) ^β
5/21/2014	DC 1-21	465	18	7.41×10^3	409	0.72922	0
5/21/2014	DC 1-29	1074	8	4.25×10^3	545	0.72833	0
5/21/2014	DC 1-33	1684	7	2.58×10^3	376	0.73087	0
5/21/2014	DC 1-36	2143	5	4.31×10^3	951	0.73026	0
5/21/2014	DC 1-37	2294	6	1.68×10^4	2865	0.71935	1.6 ^δ
5/21/2014	DC 1-38	2446	37	1.06×10^5	2899	0.71910	7.8 ^δ
5/21/2014	DC 3-4-5	137	18	1.51×10^4	849	0.71181	0.6
5/21/2014	DC 3-5-6	168	19	1.40×10^4	734	0.71222	4.0
5/21/2014	DC 3-8-9	259	30	2.27×10^4	760	0.71180	2.6
5/21/2014	DC 3-21-22	655	230	1.81×10^5	789	0.70812	17.3
5/21/2014	DC 3-22-23	686	71	7.86×10^4	1110	0.70987	3.6
5/21/2014	DC 3-42-43	1296	117	1.22×10^5	1049	0.71408	3.1

^β Quantitative mineralogy for DC 1 and DC 3 samples derived from Jin et al. (2010) and Brantley et al. (2013)

^δAnkerite carbonate composition as inferred from high Fe, Mn, and Ca elemental compositions, high LOI content, and the grey coloration of samples (Jin et al., 2010)

Table 2.24 Strontium and calcium elemental concentrations and Ca/Sr and $^{87}\text{Sr}/^{86}\text{Sr}$ ratios for the silicate fraction of DC 1 and DC 3 drill core samples

Sample Date	Sample ID	Depth (cm)	Sr ($\mu\text{M/g}$)	Ca ($\mu\text{M/g}$)	Ca/Sr (molar)	$^{87}\text{Sr}/^{86}\text{Sr}$
5/21/2014	DC 1-21	465	280	3.51×10^3	13	0.74537
5/21/2014	DC 1-29	1074	276	2.91×10^3	11	0.74497
5/21/2014	DC 1-33	1684	249	8.36×10^3	34	0.74806
5/21/2014	DC 1-36	2143	256	8.67×10^3	34	0.74919
5/21/2014	DC 1-37	2294	270	2.42×10^4	89	0.74720
5/21/2014	DC 1-38	2446	229	2.31×10^4	101	0.74143
5/21/2014	DC 3-4-5	137	305	1.15×10^4	38	0.74310
5/21/2014	DC 3-5-6	168	253	5.57×10^3	22	0.74297
5/21/2014	DC 3-8-9	259	310	9.49×10^3	31	0.74415
5/21/2014	DC 3-21-22	655	308	2.45×10^4	79	0.74501
5/21/2014	DC 3-22-23	686	332	1.09×10^4	33	0.74718
5/21/2014	DC 3-42-43	1296	311	3.47×10^4	112	0.74834

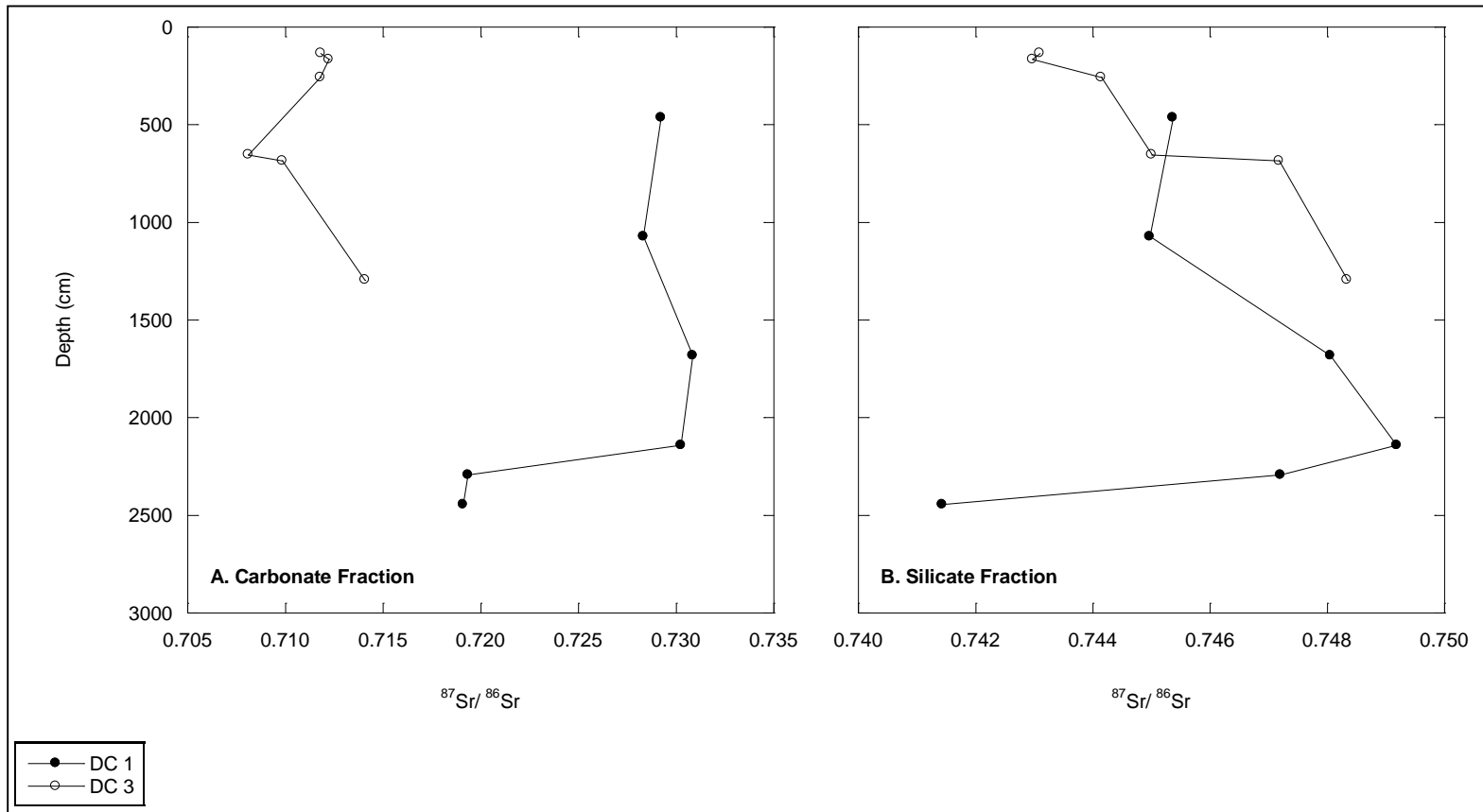


Figure 2.30 Depth versus $^{87}\text{Sr}/^{86}\text{Sr}$ ratio for carbonate (A) and silicate (B) fractions of DC 1 and DC 3 drill core samples

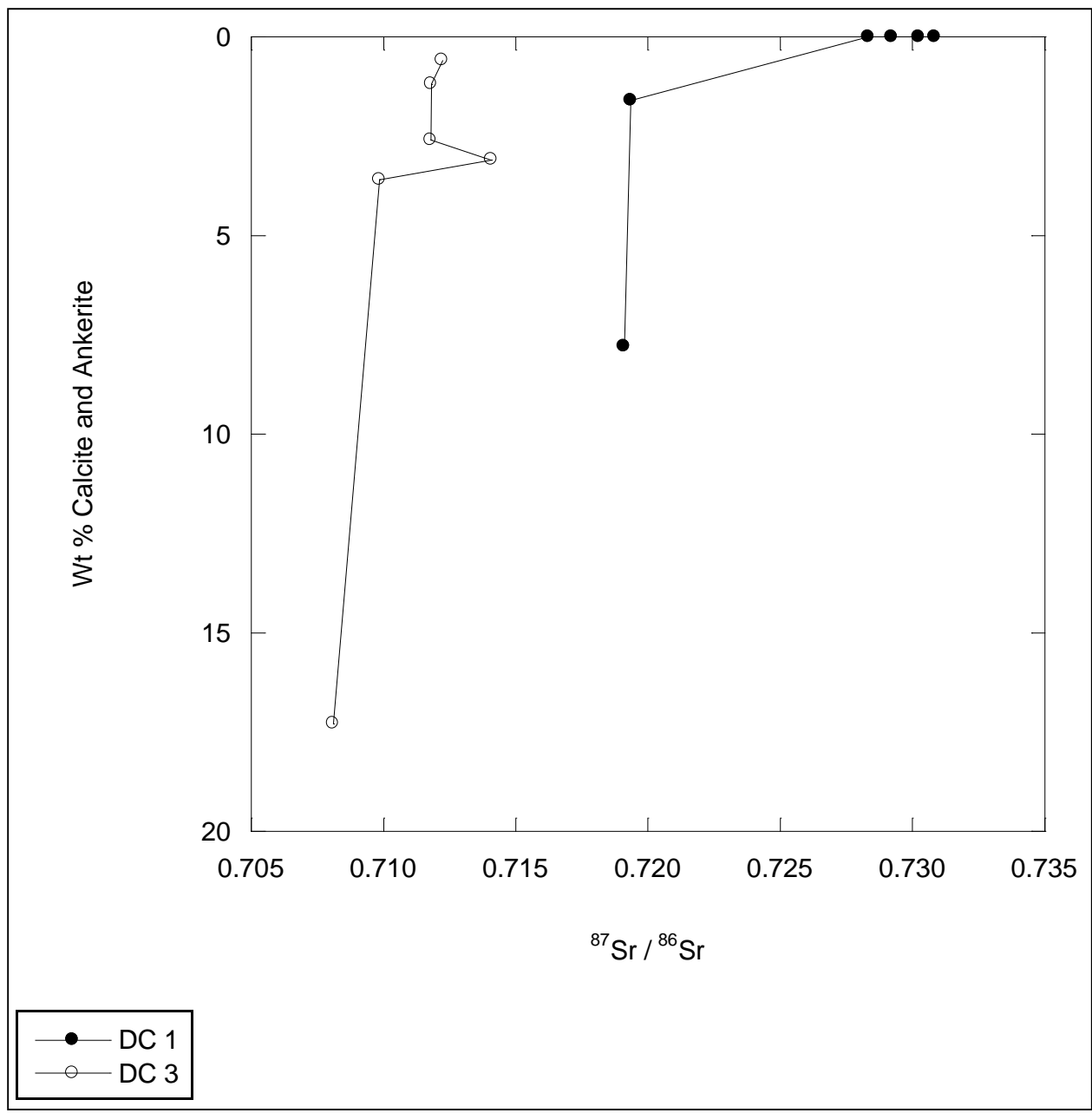


Figure 2.31 Weight percent calcite and ankerite versus $^{87}\text{Sr}/^{86}\text{Sr}$ ratio for DC 1 and DC 3 drill core samples. Weight percent calcite and ankerite data for DC 1 and DC 3 drill core samples were derived from information contained within Jin et al. (2010) and Brantley et al. (2013), respectively.

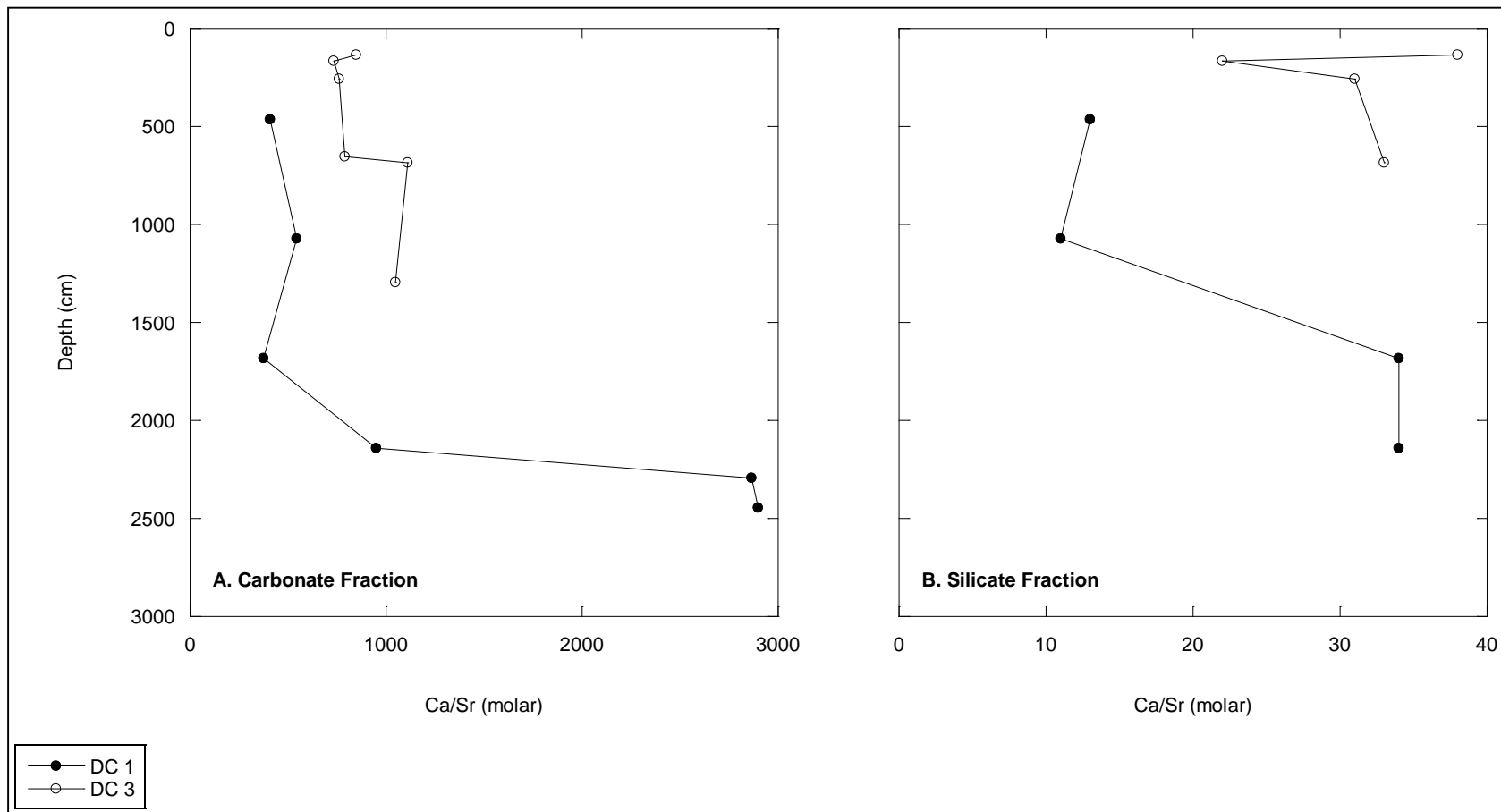


Figure 2.32 Depth versus Ca/Sr ratio for carbonate (A) and silicate (B) fractions of DC 1 and DC 3 drill core samples. Samples hypothesized to be affected by carbonate contamination (DC 1-37, DC 1-38, DC 3-22-23, and DC 3-42-43) are excluded from Figure 2.32B.

5. Conclusions

5.1 Exchangeable soils and soil porewaters

Strontium isotope compositions and proportions of strontium derived from silicate weathering sources in southern quadrant ridge top and mid slope exchangeable soils and soil porewaters were shown to be influenced by hydrological processes. Factors such as hillslope geometry, topography, vegetation cover, and soil macropore connectivity all affected lateral subsurface flow processes which are involved in the transfer of more radiogenic silicate weathering products from ridge top to valley floor locations. In the case of the southern planar transect, dominance of one dimensional vertical flow at the relatively flat ridge top confined precipitation inputs largely within the soil profile or in the underlying fractured shale. By contrast, two dimensional lateral flow at the planar mid slope location carried precipitation inputs, along with weathering products, downslope from mid slope to valley floor locations. Hence, the higher $^{87}\text{Sr}/^{86}\text{Sr}$ ratios and proportions of strontium derived from silicate weathering sources for southern planar ridge top exchangeable soils and soil porewaters compared to those sampled at mid slope locations. For the south swale transect, steep topography, combined with sparser vegetation cover at the swale's ridge, facilitated the downslope movement of water along a series of connected macropores through lateral subsurface flow pathways. Hence, the higher $^{87}\text{Sr}/^{86}\text{Sr}$ ratios and proportions of strontium derived from weathering sources in soil porewaters sampled from mid slope locations as the result of rapid downslope transport of more radiogenic silicate weathering products along swale edges or other areas where large surface and subsurface gradients existed. Presence of a less radiogenic carbonate source near valley floor locations significantly lowered strontium isotope compositions in valley floor exchangeable soils and soil porewaters compared to upslope locations. Due to the greater reactivity and solubility of

carbonate minerals relative to silicate minerals, weathering inputs to valley floor exchangeable soils and soil porewaters were dominated by carbonate dissolution processes. As a consequence, effects of lateral subsurface flow processes, which transport more radiogenic silicate weathering products from upslope positions, were obscured by inputs from a dominant, less radiogenic carbonate source to exchangeable soils and soil porewaters at the valley floor location.

For all locations, organic horizons and shallow soil porewaters were found to have less radiogenic isotope compositions and derive greater proportions of strontium from atmospheric sources. At the surface, weathering products are either transported downslope through lateral flow or translocated downward from shallow to deep horizons through vertical flow. Additionally, downward percolation of precipitation inputs into shale fractures increase proportions of strontium derived from silicate weathering processes in mineral horizons and deep porewaters overlying fractured shale as weathering products can be transported upward to these reservoir components through advection or diffusion. Furthermore, soil moisture levels have been confirmed to be lower in surface horizons due to higher levels of evapotranspiration present there as a result of enhanced plant activities. Hence, less water available for weathering processes to proceed at the surface. However, inputs from less radiogenic litterfall may also be responsible for lower strontium isotope compositions in organic horizons and shallow soil porewaters.

Swale locations were found to have more radiogenic isotope compositions and derive greater proportions of strontium from silicate weathering sources at all locations. Wetter soils combined with reduced vegetation cover at swale locations enable the increased incidence for percolation of infiltrating precipitation into the soil profile or in underlying shale to initiate subsurface weathering processes. In the case of southern quadrant valley floor porewaters, the

planar location was also located closer to the less radiogenic carbonate source near the stream's weir than the swale location.

For all locations, mixing calculations indicated higher proportions of strontium derived from dominant weathering processes at ridge top and mid slope locations (e.g. more radiogenic silicate weathering) and at valley floor locations (e.g. less radiogenic carbonate weathering) for southern planar soil porewaters compared to corresponding exchangeable soils sampled from similar depths. Observed variation in $^{87}\text{Sr}/^{86}\text{Sr}$ ratio and relative proportions of strontium derived from atmospheric versus weathering sources for these reservoir components seem to indicate the inefficiency in strontium exchange between soil porewaters and the exchange pool. Such disequilibrium may be related to rapid transit times of porewaters through the soil profile, the unavailability of exchangeable strontium as the result of preferential flowpaths along macropores at the catchment, heterogeneity in the nature of the soils, or formation of acetate complexes during ammonium acetate extractions.

For southern planar and south swale soil porewaters, Ca/Sr ratios increased in the progression from ridge top to mid slope to valley floor locations. Dilution of ridge top porewaters as a result of rapid infiltration of precipitation inputs first through the soil profile and then into underlying fractured shale, instead of being lost through evapotranspiration or downslope transport, may be resulting in faster reaction kinetics and lower Ca/Sr ratios at the southern planar ridge top location. On the contrary, preferential movement of water (and hence, solutes) downslope via lateral subsurface flow processes may be responsible for increases in porewater Ca/Sr ratio in the progression from ridge top to mid slope to valley floor locations at the south swale location. In the case of southern planar exchangeable soils, the average Ca/Sr ratio at the ridge top location was weighted toward the value obtained for the calcium enriched

organic horizon due to the presence of thinner soils at this location. Hence, the higher exchangeable soil average Ca/Sr ratio at the ridge top relative to mid slope location of the southern planar transect. Higher cation exchange capacities observed in valley floor soils relative to ridge top and mid slope soils may be responsible for higher Ca/Sr ratios at the valley floor location. Additionally, groundwater recharge has been found to contribute solutes to porewaters at valley floor locations. Groundwaters at Shale Hills are known to be enriched in calcium and strontium. Modest differences in Ca/Sr ratio across locations lend support to the hypothesis that variation in Ca/Sr ratio is reflective of groundwater contributions to valley floor locations as groundwaters are also known to contain higher strontium concentrations than porewaters.

In the southern quadrant, soil porewater Ca/Sr ratios collected from planar locations were found to be higher than those sampled from swale locations. At swale locations, steeper topography may be enhancing lateral subsurface flow activities and reducing residence times for solutes present in porewaters at this location. Additionally, tree species density is higher at planar relative to swale locations where calcium is added to planar porewaters through litter decomposition. Thus, a combination of longer residence times and greater calcium inputs by plants through organic restitutions may be resulting in higher Ca/Sr ratios in porewaters sampled from planar relative to swale locations.

Depth dependent patterns in Ca/Sr ratio are also consistent with observed preferential flow pathways. Specifically, low flow zones between A-B horizons of the soil profile have greater solute concentrations than high flow zones at A-B and B-C horizon interfaces because of enhanced weathering and longer mineral-water contact times present there. Accumulation of groundwater at valley floor locations of the catchment and the formation of perched water tables promote the rapid fluid flushing of soil porewaters with dilute precipitation inputs along both

vertical and lateral preferential flow paths. Hence, the erratic “zig-zag” patterns in Ca/Sr ratio observed for valley floor exchangeable soils and soil porewaters. Organic horizons for all southern planar locations had higher Ca/Sr ratios than mineral horizons, suggestive of the preferential retention of calcium over strontium by ion exchange processes in these horizons. Additions of calcium through litter decomposition may also be responsible for higher Ca/Sr ratios in organic horizons.

Temporal variations in porewater Ca/Sr and $^{87}\text{Sr}/^{86}\text{Sr}$ ratios were minimal for all locations sampled in the southern quadrant. Observed decreases in Ca/Sr ratio over the course of the growing season may be related to the leaching of strontium from plant to porewater reservoirs at the catchment. Indeed, fractionation factors for maple and oak leaves were calculated to be less than one lending support for the preferential discrimination against strontium relative to calcium in plants at the catchment. Furthermore, plants from all species were shown to accumulate calcium in leaf tissue at a greater rate than strontium based on observations of more positive slopes in linear trends for calcium and strontium. Higher levels of evapotranspiration over the course of the growing season imply enhanced plant uptake of calcium over strontium which would deplete porewaters in calcium relative to strontium and may also be responsible for observed monthly decreases in Ca/Sr ratio. At valley floor locations, direct additions of calcium through groundwater recharge may be counteracting calcium losses through plant uptake to result in the observed monthly increases in Ca/Sr ratio

5.2 Leaves and Sap Waters

Strontium isotope ratios in leaves and sap waters were found to be in close agreement to those measured in soil exchangeable horizons and soil porewaters which suggests rapid homogenization of strontium added from weathering and atmospheric inputs by biological

nutrient cycling processes. Minimal variation in leaf and sap water $^{87}\text{Sr}/^{86}\text{Sr}$ ratio and proportions of strontium derived from atmospheric and weathering sources were observed between tree species sampled from similar quadrants and transect positions implying a similar source (e.g. shallow exchangeable and porewater pools) from which trees are acquiring strontium (and by inference, calcium). On average, leaves and sap waters collected from maple trees were found to be slightly more radiogenic than those sampled from oak trees. Additionally, strontium isotope compositions in sap waters and leaves collected from identical trees at the same time were found to be nearly identical. Considering that strontium isotopes display negligible fractionation during transport, similarities between leaf and sap water $^{87}\text{Sr}/^{86}\text{Sr}$ ratio are not surprising.

For all tree species, leaves and sap waters sampled from mid slope positions in western quadrants had lower $^{87}\text{Sr}/^{86}\text{Sr}$ ratios and derived greater proportions of strontium from atmospheric sources than those collected in eastern quadrants, consistent with patterns observed for exchangeable soils and soil porewaters. As mentioned previously, field observations of wetter and thicker soils with less vegetation cover at swale relative to planar locations suggest greater hydrologic activity to initiate subsurface weathering processes at swale locations. This will presumably increase $^{87}\text{Sr}/^{86}\text{Sr}$ ratios and proportions of strontium derived from silicate weathering sources in eastern (swale) relative to western (planar) quadrant exchangeable soils and soil porewaters from which leaves and sap waters are extracting solutes. Strontium isotope ratios and atmospheric percentages of strontium in leaves and sap waters from all species were shown to be rather similar in northeastern and southeastern and in northwestern and southwestern quadrants. This is somewhat surprising considering that high surface erosion rates and short durations of chemical weathering in regolith particles of northern quadrants suggest lower $^{87}\text{Sr}/^{86}\text{Sr}$ ratios and proportions of strontium derived from silicate weathering in northern

quadrant exchangeable soils and soil porewaters from which leaves and sap waters are acquiring strontium.

For leaves from all tree species in the northeastern quadrant, strontium isotope ratios and proportions of strontium derived from silicate weathering sources increased in the progression from ridge top to mid slope to valley floor positions. Deeper, more hydrologically active soils with well connected macropores in the northeastern quadrant facilitate subsurface lateral flow pathways which transfer weathering products downslope. Additionally, less vegetation cover at the ridge, coupled with slightly higher cumulative rainfall, enable infiltration of precipitation inputs into surface soils and, thus, the subsequent downslope transport of weathering products through lateral subsurface flow processes. Furthermore, studies at the catchment have noted that trees sampled from valley floor locations have deeper effective rooting depths than those sampled from ridge top and mid slope locations, on average. If observations of higher proportions of strontium derived from silicate mineral weathering sources with increased depth in southern quadrant exchangeable soils and soil porewaters are extended to these reservoir components in the northeastern quadrant, then higher strontium isotope ratios and proportions of strontium derived from silicate weathering sources in leaves at the valley floor location may be due to the acquisition of solutes from deep exchangeable soil and soil porewater reservoirs. Lastly, other studies conducted in similar canopy settings have noted that higher elevation ridge top locations have greater exposure to less radiogenic inputs from atmospheric sources than shielded canopies at the valley floor.

Average leaf Ca/Sr ratios were significantly higher than those determined for exchangeable soils, soil porewaters, sap waters, streamwaters, groundwaters, and bedrock. Fractionation factors less than one calculated for all tree species indicate preferential

discrimination against strontium relative to calcium in plants at the catchment. Interestingly, maple leaves were found to have lower Ca/Sr ratios, higher fractionation factors, and discriminate to a lesser degree against strontium than oak leaves. This suggests that biological fractionation occurs to varying degrees among tree species at the catchment. Both leaf calcium and strontium concentrations in maples well exceeded those in oaks which may be due to physiological differences between species including variability in levels of tree transpiration, calcium requirements, cation exchange capacity on cell walls of xylem vessels and surrounding tissues, compositions of chemical constituents in cell walls, and levels of calcium oxalate accumulated in leaf tissue.

Interestingly, average Ca/Sr ratios in sap waters were significantly lower than those observed in paired leaf samples. Instead, sap water Ca/Sr ratios were comparable to porewater Ca/Sr ratios sampled at similar locations. Similarities in Ca/Sr ratio between porewaters and sap waters suggest non-selective, apoplastic transport through the xylem to leaves with fractionation occurring further along the transpiration stream as indicated by the significantly higher Ca/Sr ratios present in leaf tissues. Discrepancy in Ca/Sr ratio between sap waters and leaves is likely the result of increased translocation of calcium relative to strontium with strontium retained by cation exchange sites on cell walls to a greater degree than calcium during transport through the xylem to above ground leaf components. Another possible explanation is the preferential binding of calcium in oxalate complexes released by bark or other plant tissues. Additionally, negligible variation was observed in sapwater Ca/Sr ratio among tree species which contrasts with patterns found for leaves and implies similar calcium and strontium uptake mechanisms in plants at the catchment. Species differences in tree transpiration, root cation exchange capacity, and chelation of calcium by organic acids in sap waters are offered as possibilities for any observed

discrepancy.

For all tree species sampled from mid slope positions in 2013, leaves collected from western quadrants were found to have higher average Ca/Sr ratios than those from eastern quadrants, consistent with patterns observed for soil porewaters. As mentioned previously, a combination of longer residence times and greater calcium inputs by plants through organic restitutions may be resulting in higher Ca/Sr ratios in porewaters sampled from planar (western) relative to swale (eastern) locations. Additionally, in the northeastern quadrant, average Ca/Sr ratio was shown to decrease in the progression from ridge top to mid slope to valley floor locations for sugar maple leaves, while average Ca/Sr ratio for chestnut oak leaves initially decreased from ridge top to mid slope and then increased from mid slope to valley floor locations. Greater canopy exposure to atmospheric inputs at high elevation ridge top locations compared to shielded canopy valley floor locations may be responsible for these observed patterns as atmospheric Ca/Sr ratios are considerably higher than those in shales. Additionally, more anaerobic conditions, as soils become wetter and thicker downslope, facilitate strontium entry into leaf mesophyll tissues to decrease Ca/Sr ratios in the progression from ridge top to mid slope to valley floor locations. Higher average chestnut oak leaf Ca/Sr ratios at valley floor relative to mid slope locations may also be due to uptake by tap roots of carbonate affected shallow groundwaters at these locations. However, this effect would not be apparent for sugar maple species due to their shallower root systems where deep sources are only be extracted through hydraulic lift processes during unusually dry conditions. Based on sampling location across the catchment, Ca/Sr ratios of sap waters were found to exhibit more spatial homogeneity than paired leaves sampled at similar locations.

On average, calcium concentrations and Ca/Sr ratios were lower for sugar maple and

chestnut oak leaves sampled at mid slope positions in the northeastern quadrant in 2011 compared to 2013. Interestingly, higher average silicon concentrations were also observed for identical leaves sampled at mid slope positions in the northeastern quadrant in 2011 compared to 2013. Concomitant decreases in calcium concentration with increases in silicon concentration may be due to lower energy demands involving apoplastic uptake and polymerization of silicon relative to calcium on plant membranes and cell wall matrices.

Minimal temporal variation existed in leaf $^{87}\text{Sr}/^{86}\text{Sr}$ and Ca/Sr ratios over the course of the growing season. Calcium and strontium were shown to accumulate in leaf tissue for all tree species but concurrent accumulation of both chemical species led to the relatively uniform leaf Ca/Sr ratios observed over the course of the growing season. However, sap waters displayed greater temporal variation in Ca/Sr and $^{87}\text{Sr}/^{86}\text{Sr}$ ratios compared to corresponding leaves sampled at similar locations. Observed monthly decreases in sap water $^{87}\text{Sr}/^{86}\text{Sr}$ ratio and increases in Ca/Sr ratio may be the result of differences in source material from which roots are acquiring strontium. Indeed, studies at Shale Hills have demonstrated that trees tap deeper water sources as the summer season progresses. As groundwaters at the catchment are known to be less radiogenic and contain more calcium than porewaters, this may be shifting strontium isotope ratios to lower values and Ca/Sr ratios to higher values, respectively. Furthermore, studies at the catchment have demonstrated that transpiration rates in anisohydric ring-porous oak species are relatively unaffected by changes in soil moisture over the course of the growing season, while isohydric diffuse-porous sugar maple species are quite responsive to soil moisture conditions. As the calcium flux to the xylem through the apoplastic pathway is highly influenced by transpiration, monthly changes in Ca/Sr are reasonable for species whose transpiration rates vary over the course of the growing season. Additionally, maturation of leaves over the course of the

growing season inhibits the formation of a sink from which apoplastic binding locations can release calcium bound in the xylem walls to result in higher calcium levels present in xylem sap water in the late summer/early fall. On the contrary, increases in leaf and sap water $^{87}\text{Sr}/^{86}\text{Sr}$ and Ca/Sr ratios over the course of the growing season may be due to a switch in solute acquisition by plants from “mobile” to “immobile” soil waters held in larger and smaller soil pores, respectively, over shorter and longer residence times, respectively.

5.3 Groundwaters and Streamwaters

Consistent with observations of low strontium isotope ratios, high calcium, strontium, and magnesium concentrations, and high pH values, significant proportions of strontium were found to be derived from carbonate weathering sources in groundwaters. For streamwaters, proportions of strontium derived from carbonate weathering sources increased from stream headwater to mid stream to weir locations. Accordingly, concomitant decreases in strontium isotope ratio, increases in calcium and strontium concentrations, and increases in pH value were observed for streamwaters in the progression from stream headwater to mid stream to weir locations of the catchment. In streamwaters, lower proportions of strontium derived from silicate weathering relative to atmospheric sources are consistent with the slow kinetics of clay dissolution at the catchment. Additionally, high proportions of atmospherically derived strontium in stream headwaters agree to field observations which indicate stream flow exclusively during snowmelt and rainstorms in the early spring and fall, respectively, at this location. On the contrary, weir streamwaters flow a larger proportion of the year, where relatively high proportions of strontium derived from carbonate weathering suggest larger influxes of carbonate affected groundwaters to streamwaters at this location. Located at the midpoint of weir streamwaters and stream headwaters, strontium derived from carbonate weathering, silicate

weathering, and atmospheric sources in mid streamwaters represented roughly a 50:50 mixture of proportions determined for streamwaters at weir and stream headwater locations according to mixing calculations.

Predictably high Ca/Sr ratios were observed for carbonate affected groundwaters and streamwaters. Borehole groundwaters contained higher calcium and strontium concentrations than well groundwaters as they were proximally closer to the carbonate source near the stream's weir. Differences in the composition of carbonates and in dissolved CO₂ concentrations in groundwaters may be responsible for observed variation in groundwater Ca/Sr ratio with depth. Additionally, Ca/Sr ratios were observed to decrease from weir to mid stream locations and then to increase slightly from mid stream to stream headwater locations. Ca/Sr ratios obtained for mid stream and stream headwater positions were found to be rather similar; however, streamwaters at the weir position were observed to have much higher Ca/Sr ratios than those sampled at upstream positions. Although not directly apparent from Ca/Sr ratios, both calcium and strontium concentrations and fluxes in streamwaters were observed to increase from stream headwater to mid stream to weir locations. Given strontium's utility as an analog for calcium, higher calcium and strontium concentrations and fluxes in streamwaters downstream are consistent with observations of increased proportions of strontium derived from carbonate weathering in streamwaters in the progression from stream headwater to mid stream to weir locations.

5.4 Precipitation

Strontium isotope and Ca/Sr ratios in precipitation observed by Kim (2007) for the catchment are consistent with findings reported by Dasch (1969), Miller et al. (1993), Bailey et al. (1996), Dijkstra et al. (2003) and Dasch et al. (2006) for precipitation in the northeastern United States. According to Kim (2007), strontium isotope ratios remained fairly constant over

the summer only to increase dramatically in the early fall. Precipitation $^{87}\text{Sr}/^{86}\text{Sr}$ ratios reported by Kim (2007) were found to be in excess of the ratio obtained for seawater largely due to influences on precipitation from mineral dust and biological materials. Ca/Sr ratios were fairly uniform over the summer while a large increase in Ca/Sr ratio was observed from late summer to early fall.

5.5 Drill Core

The average $^{87}\text{Sr}/^{86}\text{Sr}$ ratio for the carbonate fraction of DC 1 ridge top drill core samples was significantly higher than the value determined for drill core samples collected from the DC 3 valley floor site, reflective of differences in the composition of carbonates between sites possibly due to the heterogeneous lithology of the Rose Hill formation where carbonate layers at the ridge and valley are likely originating from different strata. Specifically, mineralogical observations from previous studies at the catchment suggest that carbonates derived from the DC 1 drill core are ankerite, while those collected from the DC 3 drill core are a mixture of calcite and ankerite. If these observations are, in fact, correct, lower isotope ratios in drill core samples collected from DC 3 relative to DC 1 sites imply that calcites are less radiogenic than ankerites at the catchment where greater variability in strontium isotope composition with depth in the carbonate fraction of drill core samples at the DC 3 site is attributed to differences in relative proportions of strontium derived from calcite and ankerite. Interestingly, increased proportions of calcite and ankerite, as determined in quantitative XRD patterns, generally correlated with lower strontium isotope ratios for DC 3 valley floor drill core samples. This suggests greater contributions by less radiogenic calcites to DC 3 valley floor drill core samples.

Generally, $^{87}\text{Sr}/^{86}\text{Sr}$ isotope ratios in carbonates at the catchment exceeded the value expected for ocean water where carbonates at the catchment are inferred to be diagenetic with

strontium isotope compositions influenced by meteoric pore fluids. These fluids are hypothesized to have interacted with more radiogenic Rb bearing shales and clay silicates at the catchment. Two possible mechanisms involved in the transport of diagenetic components in meteoric pore fluids are advection along bedrock/saprock interfaces and fractures and diffusion in the matrix between major fractures. Lower $^{87}\text{Sr}/^{86}\text{Sr}$ ratios in “carbonate free” DC 1 samples (e.g. “weathered shale”) are hypothesized to be from leaching of less radiogenic strontium from plagioclase feldspar dissolution processes at interlayer and adsorption sites of clay minerals (e.g. illites and chlorites), known to dominate the mineralogy of shales at the catchment according to quantitative XRD patterns.

For the DC 1 ridge top drill core, Ca/Sr ratios in carbonate fractions of carbonate bearing samples were predictably higher than those observed in “carbonate free” samples. Although not directly apparent from Ca/Sr ratios, calcium concentrations corresponded reasonably well to proportions of carbonates estimated in DC 1 and DC 3 drill core samples through quantitative XRD patterns. Ca/Sr ratios for DC 1 ridge top drill core samples generally increased with depth, while no discernible dependence on depth was observed for drill core samples collected from the DC 3 valley floor site. Differences in Ca/Sr ratio for DC 1 and DC 3 drill core samples with depth may be due to variations in carbonate composition or degrees of CO_2 acquisition and CO_2 degassing as these processes lead to the dissolution and precipitation of carbonates at the catchment, respectively. The rate of carbonate propagation well exceeded those estimated for regolith production and erosion by other researchers and is consistent with the greater depth inferred for the carbonate weathering front at the catchment. However, different timescales used in calculations may be resulting in the observed discrepancy between carbonate propagation and regolith production and erosion rates.

Strontium isotope ratios for silicate fractions of drill core samples were shown to be rather similar between DC 1 and DC 3 sites and fall within the range of values reported for shales in the area. Highly radiogenic strontium isotope signatures for silicate fractions of drill core samples are consistent with high rubidium contents typically present in shales.

Heterogeneity in the composition of the Rose Hill shale may be responsible for observed spatial variability in $^{87}\text{Sr}/^{86}\text{Sr}$ ratio for drill core samples collected from both locations. Additionally, differences in porosity may be resulting in the observed discrepancy in strontium isotope ratio based on sampling depth. As such, increased porosity enables precipitation inputs to infiltrate into shale fractures or joints to accelerate dissolution and disaggregation processes in the shale. Considering that “weathered shale” was found to be less radiogenic than unweathered shale, increased porosity is hypothesized to be decreasing strontium isotope ratios in silicate fractions of drill core samples. Low Ca/Sr ratios were reported for both DC 1 and DC 3 silicate fractions of drill core samples uncontaminated by carbonates and are consistent with values calculated using major and trace element data derived from other studies at the catchment. As was observed in $^{87}\text{Sr}/^{86}\text{Sr}$ ratio, minimal variation in Ca/Sr ratio existed between silicate fractions of drill core samples collected from DC 1 and DC 3 sites where differences in Ca/Sr ratio are likely due to differences in porosity.

6. References

Aberg, G. Jacks, G., and Hamilton, P., 1989, Weathering rates and $^{87}\text{Sr}/^{86}\text{Sr}$ ratios: An isotopic approach: *Journal of Hydrology*, v. 109, p. 65-78.

Aberg, G., 1995, The use of natural strontium isotopes as tracers in environmental studies: *Water, Air and Soil Pollution*, v. 79, p. 209-322.

Andersson, P., Lofvendahl, R., and Aberg, G., 1990, Major element chemistry $\delta^2\text{H}$, $\delta^{18}\text{O}$, and $^{87}\text{Sr}/^{86}\text{Sr}$ in a snow profile across central Scandinavia: *Atmospheric Environment Part A*, v.24, p. 2601-2608.

Asher, C., and Ozanne, P., 1961, The cation exchange capacity of plant roots and its relationship to the uptake of insoluble nutrients: *Australian Journal of Agricultural Research*, v. 12, p. 755-766.

Aubert, D., Probst, A., Stille, P., and Viville, D., 2002, Evidence of hydrological control of Sr behavior in stream water (Strengbach catchment, Vosges mountains, France): *Applied Geochemistry*, v. 17, p. 285-300.

Baes, A., and Bloom, P., 1988, Exchange of alkaline earth cations in soil organic matter: *Soil Science*, v. 146, p. 6-14.

Bailey, S., Hornbeck, J., Driscoll, C., and Gaudette, H., 1996, Calcium inputs and transport in a base-poor forest system as interpreted by Sr isotopes: *Water Resources Research*, v. 32, p. 707-719.

Bain, D., and Bacon, J., 1994, Strontium isotopes as indicators of mineral weathering in catchments: *Catena*, v. 22, p. 201-214.

Bain, D., Midwood, A., and Miller, J., 1998, Strontium Isotope ratios in streams and the effect of flow rate in relation to weathering catchments: *Catena*, v. 32, p 143-151.

Belanger, N., and Holmden, C., 2010, Influence of landscape on the apportionment of Ca nutrition in a Boreal Shield forest of Saskatchewan (Canada) using $^{87}\text{Sr}/^{86}\text{Sr}$ as a tracer: *Canadian Journal of Soil Science*, v. 90, p. 267-288.

Belanger, N., Holmden, C., Courchesne, F., Cote, B., and Hendershot, W., 2012, Constraining soil mineral weathering $^{87}\text{Sr}/^{86}\text{Sr}$ for calcium apportionment studies of a deciduous forest

growing on soils developed from granitoid igneous rocks: *Geoderma*, v. 185-186, p. 84-96.

Blum, J., Klaue, A., Nezat, C., Driscoll, C., Johnson, C., Siccama, T., Eagar, C., Fahey, T., and Likens, G., 2002, Mycorrhizal weathering of apatite as an important calcium source in base-poor forest ecosystems: *Nature*, v. 417, p. 729-731.

Blum, J., Dasch, A., Hamburg, S., Yanai, R., and Arthur, M., 2008, Use of foliar Ca/Sr discrimination and $^{87}\text{Sr}/^{86}\text{Sr}$ ratios to determine soil Ca sources to sugar maple foliage in a northern hardwood forest: *Biogeochemistry*, v. 87, p. 287-296.

Blum, J., Hamburg, S., Yanai, R., and Arthur, M., 2012, Determination of foliar Ca/Sr discrimination factors for six tree species and implications for Ca sources in northern hardwood forests: *Plant Soil*, v. 356, p. 303-314.

Boggs, J., McNulty, S., Gavazzi, M., and Myers, J., 2005, Tree growth, foliar chemistry, and nitrogen cycling across a nitrogen deposition gradient in southern Appalachian deciduous forests: *Canadian Journal of Forest Research*, v. 35, p. 1901-1913.

Brackhage, C., Schaller, J., Baucker, E., and Dudel, E., 2013, Silicon availability affects the stoichiometry and content of calcium and micro nutrients in the leaves of common reed: *Silicon*, v. 5, p. 199-204.

Brantley, S., and Duffy, C., 2008, 2009, and 2010, CZO Dataset: Shale Hills – Stream Water Chemistry. Retrieved from <http://criticalzone.org/shale-hills/data/dataset/2582>.

Brantley, S., Holleran, M., Jin, L., and Bazilevskaya, E., 2013, Probing deep weathering in the Shale Hills Critical Zone Observatory, Pennsylvania (USA): the hypothesis of nested chemical reaction fronts in the subsurface: *Earth Surface Processes and Landforms*, v. 38, p. 1280-1298.

Brooks, J., Barnard, H., Coulombe, R., and McDonnell, J., 2009, Ecohydrologic separation of water between trees and streams in a Mediterranean climate: *Nature Geoscience*, v. 3, p. 100-104.

Bullen, T., and Bailey, S., 2005, Identifying calcium sources at an acid deposition-impacted spruce forest: A strontium isotope, alkaline earth element multi-tracer approach: *Biogeochemistry*, v. 75, p. 63-99.

Capo, R., Stewart, B., and Chadwick, O., 1998, Strontium isotopes as tracers of ecosystem processes: theory and methods: *Geoderma*, v. 82, p. 197-225.

Chadwick, O., Derry, L., Bern, C., and Vitousek, P., 2009, Changing sources of strontium to soils and ecosystems across the Hawaiian Islands: *Chemical Geology*, v. 267, p. 64-76.

Clarkson, D., 1984, Calcium transport between tissues and its distribution in the plant: *Plant, Cell and Environment*, v. 7, p. 449-456.

Clow, D., Mast, M., Bullen, T., and Turk, J., 1997, Strontium 87/strontium 86 as a tracer of mineral weathering reactions and calcium sources in an alpine/subalpine watershed, Loch Vale, Colorado: *Water Resources Research*, v. 33, p. 1335-1351.

Dasch, E., 1969, Strontium isotopes in weathering profiles, deep-sea sediments, and sedimentary rocks: *Geochimica et Cosmochimica Acta*, v. 33, p. 1521-1552.

Dasch, A., Blum, J., Eagar, C., Fahey, T., Driscoll, C., and Siccama, T., 2006, The relative uptake of Ca and Sr into tree foliage using a whole-watershed calcium addition: *Biogeochemistry*, v. 80, p. 21-41.

Davis, J., and Kent, D., 1990, Surface complexation modeling in aqueous geochemistry: *Reviews in Mineralogy*, v. 23, p. 177-260.

Dawson, T., 1993, Hydraulic lift and water use by plants: implications for water balance, performance, and plant-plant interactions: *Oecologia*, v. 95, p. 565-574.

Derry, L., Pett-Ridge, J., Kurtz, A., and Troester, J., 2006, Ge/Si and ⁸⁷Sr/⁸⁶Sr tracers of weathering reactions and hydrologic pathways in a tropical granitoid system: *Journal of Geochemical Exploration*, v. 88, p. 271-274.

Dijkstra, F., and Smits, M., 2002, Tree species effects on calcium cycling: the role of calcium uptake in deep soils: *Ecosystems*, v. 5, p. 385-398.

Dijkstra, F., Van Breeman, N., Jongmans, A., Davies, G., and Likens, G., 2003, Calcium weathering in forested soils and the effect of different tree species: *Biogeochemistry*, v. 62, p. 253-275.

Drouet, T., Herbauts, J., Gruber, W., and Demaiffe, D., 2005, Strontium isotope composition as a tracer of calcium sources in two forest ecosystems in Belgium: *Geoderma*, v. 126, p. 203-223.

Drouet, T., and Herbauts, J., 2008, Evaluation of the mobility and discrimination of Ca, Sr, and

Ba in forest ecosystems: consequence on the use of alkaline-earth element ratios as tracers of Ca: *Plant Soil*, v. 302, p. 105-124.

Duffy, C., 2008, 2009, and 2010, CZO Dataset: Shale Hills – Streamflow/Discharge. Retrieved from <http://criticalzone.org/shale-hills/data/dataset/3613/>.

Dunne, T., 1978, Field studies of hillslope flow processes, *in* Kirkby, M., ed.: *Hillslope Hydrology*: Chichester, UK, p. 227-293.

Elias, R., Hirao, Y., and Patterson, C., 1982, The circumvention of the natural biopurification of calcium along nutrient pathways by atmospheric inputs of industrial lead: *Geochimica et Cosmochimica Acta*, v. 46, p. 2561-2580.

Ewers, B., and Oren, 2000, Analyses of assumptions and errors in the calculation of conductance from sap flux measurements: *Tree Physiology*, v. 20, p. 579-589.

Faure, G., and Mensing, T., 2005, *Isotopes: principles and applications*, 3rd Ed: John Wiley and Sons, Inc., Chichester, UK.

Flueckinger, L., 1969, Report 176, *Geology of a portion of the Allensville Quadrangle, Centre and Huntingdon Counties, Pennsylvania*: Bureau of Topographic and Geologic Survey, Commonwealth of Pennsylvania State Planning Board: Harrisburg, PA.

Franceschi, V., and Nakata, P., 2005, Calcium oxalate in plants: formation and function: *Annual Review of Plant Biology*, v.56, 41-71

Fulweiler, R., and Nixon, S., 2005, Terrestrial vegetation and the seasonal cycle of dissolved silica in a southern New England coastal river: *Biogeochemistry*, v. 74, p. 115-130.

Funk, J., and Amatangelo, K., 2013, Physiological mechanisms drive differing foliar calcium content in ferns and angiosperms: *Oecologia*, v. 173, p. 23-32.

Gabitov, R., Sadekov, A., and Leinweber, A., 2014, Crystal growth rate effect on Mg/Ca and Sr/Ca partitioning between calcite and fluid: an in-situ approach: *Chemical Geology*, v. 367, p. 70-82.

Graustein, W., and Armstrong, R., 1983, The use of Strontium-87/Strontium-86 ratios to measure atmospheric transport into forested watersheds: *Nature*, v. 219, p. 289-292.

Graham, R., Daniels, R., and Buol, S., 1990, Soil-geomorphic relations on the Blue Ridge front: I. Regolith types and slope processes: Soil Science Society of America Journal, v. 54, p. 1362-1367.

Graham, C., and Lin, H., 2011, Controls and frequency of preferential flow occurrence: A 175-event analysis: Vadose Zone Journal, v. 10, p. 816-831.

Granier, A., Biron, P., Kostner, B., Gay, L., and Najjar, G., 1996, Comparisons of xylem sap flow and water vapour flux at the stand level and derivation of canopy conductance for Scots pine: Theoretical and Applied Climatology, v. 53, p. 115-122.

Gulpin, M., Turk, S., and Fink, S., 1995, Ca nutrition in conifers: Journal of Plant Nutrition and Soil Science, v. 158, p. 519-527.

Handley, R., and Overstreet, R., 1963, Uptake of strontium by roots of *Zea mays*: Plant Physiology, v. 38, p. 180-194.

Hanger, B., 1979, The movement of calcium in plants: Communications in Soil Science and Plant Analysis, v. 10, p. 171-193.

Herndon, E., 2012, Biogeochemistry of manganese contamination in a temperate forested watershed: Dissertation, The Pennsylvania State University, 290 p.

Hess, J., Bender, M., and Schilling, J., 1986, Evolution of the ratio of strontium-87 to strontium-86 in seawater from Cretaceous to present: Science, v. 231, p. 979-984.

Holmden, C., and Belanger, N., 2010, Ca isotope cycling in a forested ecosystem: Geochimica et Cosmochimica Acta, v. 74, p. 995-1015.

Hogan, J., Blum, J., Siegel, D., Glaser, P., 2000, $^{87}\text{Sr}/^{86}\text{Sr}$ as a tracer of groundwater discharge and precipitation recharge in the Glacial Lake Agassiz Peatlands, northern Minnesota: Water Resources Research, v. 36, p. 3701-3710.

Hogan, J., and Blum, J., 2002, Tracing hydrologic flowpaths in a small forested watershed using variations in $^{87}\text{Sr}/^{86}\text{Sr}$, $[\text{Ca}]/[\text{Sr}]$, $[\text{Ba}]/[\text{Sr}]$, and $\delta^{18}\text{O}$: Water Resources Research, v. 39, p. 1-12.

Hsieh, J., Chadwick, O., Kelly, E., and Savin, S., 1998, Oxygen isotopic composition of soil water: Quantifying evaporation and transpiration: Geoderma, v. 82, p.269-293.

Jacks, G., Aberg, G., and Hamilton, P., 1989, Calcium budgets for catchments as interpreted by strontium isotopes: *Nordic Hydrology*, v. 20, p. 85-96.

Jacobson, A., Blum, J., and Walter, L., 2002, Reconciling the elemental and Sr isotope composition of Himalayan weathering fluxes: insight from the carbonate geochemistry of stream waters: *Geochimica and Cosmochimica Acta*, v. 66, p. 3417-3429.

Jacoby, B., 1967, The effect of the roots on calcium ascent in bean stems: *Annals of Botany*, v. 31, p. 725-730.

Jacoby, B., and Moran, N., 2002, Mineral nutrient transport in plants, *in* Pessarakli, M., ed.: *Handbook of Plant and Crop Physiology*: New York, p. 337-362.

Jin L., Ravella, R., Ketchum, B., Bierman, P., Heaney, P., White, T., and Brantley, S., 2010, Mineral weathering and elemental transport during hillslope evolution at the Susquehanna/Shale Hills Critical Zone Observatory: *Geochimica et Cosmochimica Acta*, v. 74, p. 3669-3691.

Jin, L., Rother, G., Cole, D., Mildner, D., Duffy, C., and Brantley, S., 2011a, Characterization of deep weathering and nanoporosity development in shale – A neutron study: *American Mineralogist*, v. 96, p. 498-512.

Jin L., Andrews, D., Holmes, G., Lin, H., and Brantley, S., 2011b, Opening the “Black Box”: Water Chemistry Reveals Hydrological Controls on Weathering in the Susquehanna Shale Hills Critical Zone Observatory: *Vadose Zone Journal*, v. 10, p. 928-942.

Jin, L., Ogrinc, N., Yesavage, T., Hasenmueller, E., Ma, L., Sullivan, P., Kaye, J., Duffy, C., Brantley, S., 2014, The CO₂ consumption potential during gray shale weathering: Insights from the evolution of carbon isotopes in the Susquehanna Shale Hills critical zone observatory: *Geochimica et Cosmochimica Acta*, v. 142, p. 260-280.

Jin L., and Brantley S. , 2011, Soil chemistry and shale weathering on a hillslope influenced by convergent hydrologic flow regime at the Susquehanna/Shale Hills Critical Zone Observatory: *Applied Geochemistry*, v. 26, p. S51–S56.

Johnson, T., and DePaolo, D., 1997, Rapid exchange effects on isotope ratios in groundwater systems. 2. Flow investigation using Sr isotope ratios: *Water Resources Research*, v. 33, p. 197-209.

Keller, P., and Deuel, H., 1957, Kationenaustauschkapazität und Pektinengehalt von Pflanzenwurzeln: Zeitschrift für Pflanzenernährung und Bodenkunde, v. 79, p. 119-131.

Kim, H., 2007, Evaluating the effects of forest liming in Appalachian watersheds: chemistry and multi-isotope approaches: Dissertation, The Pennsylvania State University, 197 p.

Kennedy, M., Chadwick, O., Vitousek, P., Derry, L., and Henricks, D., 1998, Changing sources of base cations during ecosystem development, Hawaiian Islands: Geology, v. 26, p. 1015-1018.

Kennedy, M., Hedin, L., and Derry, L., 2002, Decoupling of unpolluted temperate forests from rock nutrient sources revealed by natural $^{87}\text{Sr}/^{86}\text{Sr}$ and ^{84}Sr tracer addition: PNAS, v. 15, p. 9639-9644.

Kuntz, B., Rubin, S., Berkowitz, B., and Singha, K., 2011, Quantifying solute transport at the Shale Hills Critical Zone Observatory: Vadose Zone Journal, v. 10, p. 843-857.

Land, M., Ingri, J., Andersson, P., and Ohlander, B., 2000, Ba/Sr, Ca/Sr and $^{87}\text{Sr}/^{86}\text{Sr}$ ratios in groundwater: implications for relative contributions to stream water discharge: Applied Geochemistry, v. 15, p. 311-325.

Lebedeva, M., Fletcher, R., and Brantley, S., 2010, A mathematical model for steady-state regolith production at constant erosion rate: Earth Surface Processes and Landforms, v. 35, p. 508-524.

Lefevre, F., Sardin, M., Vitorge, P., 1996, Migration of ^{45}Ca and ^{90}Sr in a clayey and calcareous sand: calculation of distribution coefficients by ion exchange theory and validation by column experiments: Journal of Contaminant Hydrology, v. 21, p. 175-188.

Leybourne, M., and Johannesson, K., 2008, Rare earth elements (REE) and yttrium in stream waters, stream sediments, and Fe-Mn oxyhydroxides: fractionation, speciation, and controls over REE + Y patterns in the surface environment: Geochimica et Cosmochimica Acta, v. 72, p. 5962-5983.

Lin, H., 2006, Temporal stability of soil moisture spatial pattern and subsurface preferential flow pathways in the Shale Hills catchment: Vadose Zone Journal, v. 5, p. 317-340.

Lin, H., Kogelmann, W., Walker, C., and Bruns, M., 2006, Soil moisture patterns in a forested catchment: A hydrogeological perspective: Geoderma, v. 131, p. 345-368.

- Lin H., and Zhou X., 2008, Evidence of subsurface preferential flow using soil hydrologic monitoring in the Shale Hills catchment: *European Journal of Soil Science*, v. 59, p. 34-49.
- Lucash, M., Yanai, R., Blum, J., and Park, B., 2012, Foliar nutrient concentrations related to soil sources across a range of sites in the northeastern United States: *Soil Science Society of America Journal*, v. 76, p. 674-683.
- Ma, J., and Takahashi, E., 1993, Interaction between calcium and silicon in water-cultured rice plants: *Plant and Soil*, v. 148, p. 107-113.
- Ma, L., Chabaux, F., Pelt, E., Blaes, E., Jin, L., and Brantley, S., 2010, Regolith production rates calculated with uranium-series isotopes at Susquehanna/Shale Hills Critical Zone Observatory: *Earth and Planetary Science Letters*, v. 297, p. 211-225.
- Ma, L., Jin, L., and Brantley, S., 2011a, Geochemical behaviors of different element groups during shale weathering at the Susquehanna/Shale Hills Critical Zone Observatory: *Applied Geochemistry*, v. 26, p. S89-S93.
- Ma, L., Jin, L., and Brantley, S., 2011b, How mineralogy and slope aspect affect REE release and fractionation during shale weathering in the Susquehanna/Shale Hills Critical Zone Observatory: *Chemical Geology*, v. 290, p. 31-49.
- MacDonald, N., Burton, A., Jurgensen, M., McLaughlin, J., and Mroz, G., 1991, Variation in forest soil properties along a Great Lakes pollution gradient: *Soil Science Society of America Journal*, v. 55, p. 1709-1715.
- Mandarino, J., and Anderson, V., 1989, *Monteregian Treasures: The Minerals of Mont Saint-Hilaire, Quebec*: Cambridge University Press, London.
- Marschner, H., and Schafarczyk, W., 1967, Vergleich der Nettoaufnahme von Natrium und Kalium bei Mais- und Zuckerrubenpflanzen: *Zeitschrift für Pflanzenernährung und Bodenkunde*, v. 118, p. 172-187.
- Marschner, P., 2012, *Mineral Nutrition of Higher Plants*, 3rd Edition: Academic Press, London.
- McLaughlin, S., and Wimmer, R., 1999, Calcium physiology and terrestrial ecosystem processes: *New Phytologist*, v. 142, p. 373-417.

McLennan, S., 1989, Rare earth elements in sedimentary rocks: influence of provenance and sedimentary processes: *Reviews in Mineralogy*, v. 21, p. 169-200.

McNair, J., 1932, The interrelation between substances in plants: essential oils and resins, cyanogens and oxalate: *American Journal of Botany*, v. 19, p. 255-272.

McNutt, R., 2000, *Environmental Tracers in Subsurface Hydrology*: Kluwer Academic Publishers, Norwell, MA.

Meinzer, F., Woodruff, D., Eissenstat, D., Lin, H., Adams, T., and McCulloh, K., 2013, Above- and belowground controls on water use by trees of different wood types in an eastern US deciduous forest: *Tree Physiology*, v. 33, p. 345-356.

Miller, E., Blum, J., and Friedland, A., 1993, Determination of soil exchangeable cation loss and weathering rates using Sr isotopes: *Nature*, v. 362, p. 438-441.

Mix, G., and Marschner, 1976, Einfluß exogener und endogener Faktoren auf den Calciumgehalt von Paprika- und Bohnenfruchten: *Zeitschrift für Pflanzenernährung und Bodenkunde*, v. 139, p. 551.

Naithani, K., Baldwin, D., Gaines, K., Lin, H., and Eissenstat, D., 2013, Spatial distribution of tree species governs the spatio-temporal interaction of leaf area index and soil moisture across a forested landscape: *PLoS ONE*, v. 8, p. 1-12.

National Atmospheric Deposition Program, 2005, Seasonal Precipitation-Weighted Mean Concentrations for PA-15. Retrieved from <http://nadp.sws.uiuc.edu>.

Negrel, P., and Roy, S., 1998, Chemistry of rainwater in the Massif Central (France): a strontium isotope and major element study: *Applied Geochemistry*, v. 13, p. 941-952.

Negrel, P., and Lachassagne, P., 2000, Geochemistry of the Maroni River (French Guiana) during the low water stage: implications for water-rock interaction and groundwater characteristics: *Journal of Hydrology*, v. 237, p. 212-233.

Negrel, P., Petelet-Giraud, E., and Widory, D., 2004, Strontium isotope geochemistry of alluvial groundwater: a tracer for groundwater resources characterization: *Hydrology and Earth System Sciences*, v. 8, p. 959-972.

- Oren, R., Phillips, N., Ewers, B., Pataki, D., and Megonigal, J., 1999, Sap-flux-scaled transpiration responses to light, vapor pressure deficit, and leaf area reduction in a flooded *Taxodium distichum* forest: *Tree Physiology*, v. 19, p. 337-347.
- Page, B., Bullen, T., and Mitchell, M., 2008, Influences of calcium availability and tree species on Ca isotope fractionation in soil and vegetation: *Biogeochemistry*, v. 88, p. 1-13.
- Park, B., and Yanai, R., 2009, Nutrient concentrations in roots, leaves and wood of seedling and mature sugar maple and American beech at two contrasting sites: *Forest Ecology and Management*, v. 258, p. 1153-1160.
- Parker, G., 1983, Throughfall and stemflow in the forest nutrient cycle: *Advances in Ecological Research*, v. 13, p. 57-133.
- Parr, J., Dolic, V., Lancaster, G., and Boyd, W., 2001, A microwave digestion method for the extraction of phytoliths from herbarium species: *Review of Palaeobotany and Palynology*, v. 116, p. 203-212.
- Pataki, D., and Oren, R., 2003, Species difference in stomatal control of water loss at the canopy scale in a mature bottomland deciduous forest: *Advances in Water Resources*, v. 26, p. 1267-1278.
- Pett-Ridge, J., Derry, L., and Barrows, J., 2009, Ca/Sr and $^{87}\text{Sr}/^{86}\text{Sr}$ ratios as tracers of Ca and Sr cycling in the Rio Icacos watershed, Luquillo Mountains, Puerto Rico: *Chemical Geology*, v. 267, p. 32-45.
- Poszwa, A., Dambrine, E., Pollier, B., and Atteia, O., 2000, A comparison between Ca and Sr cycling in forest ecosystems: *Plant and Soil*, v. 225, p. 299-310.
- Poszwa, A., Ferry, B., Dambrine, E., Pollier, B., Wickman, T., Loubet, M., and Bishop, K., 2004, Variations of bioavailable Sr concentration and $^{87}\text{Sr}/^{86}\text{Sr}$ ratio in boreal forest ecosystems: Role of biocycling, mineral weathering and depth of root uptake: *Biogeochemistry*, v. 67, p. 1-20.
- Runia, L., 1987, Strontium and calcium distribution in plants: effects on paleodietary studies: *Journal of Archeological Science*, v. 14, p. 599-608.
- Sattelmacher, B., 2011, The apoplast and its significance for plant mineral nutrition: *New Phytologist*, v. 149, p. 167-172.

Schlesinger, W., 1997, *Biogeochemistry: An Analysis of Global Change*, 2nd edition: Academic Press, San Diego.

Shand, P., Darbyshire, D., Gooddy, D., and Haria, A., 2007, $^{87}\text{Sr}/^{86}\text{Sr}$ as an indicator of flowpaths and weathering rates in the Plynlimon experimental catchments, Wales, U.K.: *Chemical Geology*, v. 236, p. 247-265.

Shand, P., Darbyshire, D., Love, A., and Edmunds, W., 2009, Sr isotopes in natural waters: Applications to source characterization and water-rock interaction in contrasting landscapes: *Applied Geochemistry*, v. 24, p. 574-586.

Shone, M., 1968, Electrochemical relations in the transfer of ions to the xylem sap of maize roots: *Journal of Experimental Botany*, v. 19, p. 468-485.

Stewart, B., Capo, R., and Chadwick, O., 1998, Quantitative strontium isotope models for weathering, pedogenesis, and biogeochemical cycling: *Geoderma*, v. 82, p. 173-195.

Takagi, K., and Lin, H., 2012, Changing controls of soil moisture spatial organization in the Shale Hills Catchment: *Geoderma*, v. 173-174, p. 289-302.

Thomas, E., 2013, Spatial and temporal patterns of water stable isotope compositions at the Susquehanna-Shale Hills Critical Zone Observatory: Master's Thesis, The Pennsylvania State University, 104 p.

Veresoglou, D., Barbayiannis, N., Matsi, T., Anagnostopoulos, C., and Zalidis, G., 1996, Shoot Sr concentrations in relation to shoot Ca concentrations and to soil properties: *Plant and Soil*, v. 178, p. 95-100.

Vitousek, P., Kennedy, M., Derry, L., and Chadwick, O., 1999, Weathering versus atmospheric sources of strontium in ecosystems on young volcanic soils: *Oecologia*, v. 121, p. 255-259.

Watmough, A., and Dillon, P., 2003, Calcium losses from a forested catchment in South-Central Ontario, Canada: *Environmental Science and Technology*, v. 37, p. 3085-3089.

Watmough, A., 2014, Calcium, strontium, and barium biogeochemistry in a forested catchment and insight into elemental discrimination: *Biogeochemistry*, v. 118, p. 357-369.

Wacquant, J., 1977, Physicochemical selectivity for cations and CEC of grass roots: *Plant and*

Soil, v. 47, p. 257-261.

Weiler, M., and McDonnell, J., 2004, Virtual experiments: a new approach for improving process conceptualization in hillslope hydrology: *Journal of Hydrology*, v. 285, p. 3-18.

West, H., Davies, S., Morgan, J., and Herbert, R., 2001, The relationship between Sr and Ca accumulation in the major constituents of a terrestrial community resident on a celestic (SrSO₄) soil in S.W. England: *European Journal of Soil Biology*, v. 37, p. 333-336.

White, P., 2001, The pathways of calcium movement to the xylem: *Journal of Experimental Botany*, v. 52, p. 891-899.

White, P., Whitting, S., Baker, A., and Broadley, M., 2002, Does zinc move apoplastically to the xylem in roots of *Thlaspi caerulescens*?: *New Phytologist*, v. 153, p. 199-211.

White, P., and Broadley, M., 2003, Calcium in plants: *Annals of Botany*, v. 92, p. 487-511.

White, A., Schulz, M., Lowenstern, J., Vivit, D., and Bullen, T., 2005, The ubiquitous nature of accessory calcite in granitoid rocks: Implications for weathering, solute evolution, and petrogenesis: *Geochimica et Cosmochimica*, v. 69, p. 1455-1471.

White, A., Schulz, M., Vivit, D., Bullen, T., Fitzpatrick, J., 2012, The impact of biotic/abiotic interfaces in mineral nutrient cycling: A study of soils of the Santa Cruz chronosequence, California: *Geochimica et Cosmochimica Acta*, v. 77, p. 62-85.

Whitney, P., and Hurley, P., 1964, The problem of inherited radiogenic strontium in sedimentary age determinations: *Geochimica et Cosmochimica Acta*, v. 28, p. 425-436.

Wolterbeek, H., van Luijpen, J., and de Bruin, M., 1984, Non-steady state xylem transport of fifteen elements into the tomato leaf as measured by gamma-ray spectroscopy: a model: *Physiologia Plantarum*, v. 61, p. 599-606.

Wubbels, J., 2010, Tree species distribution in relation to stem hydraulic traits and soil moisture in a mixed hardwood forest in central Pennsylvania: Master's Thesis, The Pennsylvania State University, 39 p.

Wytenbach, A., Furrer, V., and Tobler, L., 1995, The concentration ratios plant to soil for stable elements Cs, Rb, and K: *Science of the Total Environment*, v. 173, p. 361-367.

Zhang, J, Lin, H., and Doolittle, J., 2014, Soil layering and preferential flow impacts on seasonal changes of GPR signals in two contrasting soils: *Geoderma*, v. 213, p. 560-569.

CHAPTER THREE

GE/SI RATIOS AS TRACERS OF SILICON SOURCES AT THE SUSQUEHANNA SHALE HILLS CRITICAL ZONE OBSERVATORY

1. Introduction

Ge/Si ratios are commonly used to trace silicate weathering processes (Murnane and Stallard, 1990; Kurtz et al., 2002; Derry et al., 2006; Scribner et al., 2006; Lugolobi et al., 2010) and silicon pathways in the soil-plant system (Derry et al., 2005; Garvin, 2006; Blecker et al., 2007; Delvigne et al., 2009; Cornelis et al., 2010). Often considered a “pseudo-isotope” of silicon, germanium displays several chemical similarities to silicon including its nature as a group IV element, a similar ionic radius (Ge: 3.9 Å versus Si: 2.6 Å, Shannon, 1976), a similar tetrahedral bond length (Ge-O: 1.75 Å versus Si-O: 1.64 Å, Martin et al., 1996), and an identical outer electron configuration (Kurtz and Derry, 2004). These chemical properties enable germanium to substitute for silicon in tetrahedral sites of silicate minerals (Goldshmidt, 1958; Bernstein, 1985). As a consequence, silicate mineral weathering of crustal rocks represents an important source of dissolved germanium and silicon in terrestrial systems (Murnane and Stallard, 1990).

In biogeochemical systems, Ge/Si ratios reflect fractionation during weathering and plant uptake processes with germanium enriched in secondary minerals and depleted in biogenic materials. Specifically, during mineral weathering, germanium is retained to a greater degree than silicon in secondary phases (e.g. secondary soil aluminosilicates) which are known to contain weakly polymerized silicate tetrahedra (Murnane and Stallard, 1990). Consequently, Ge/Si ratios are oftentimes higher in soils than in parent bedrock (Murnane and Stallard, 1990; Kurtz et al., 2002; Anders et al., 2003; Scribner et al., 2006; Opfergelt et al., 2010). In the case of

plant uptake, germanium is discriminated against relative to silicon resulting in lower Ge/Si ratios in leaf phytoliths compared to soil minerals and porewaters (Blecker, 2005; Derry et al., 2005; Garvin, 2006; Blecker et al., 2007; Delvigne et al., 2009). Researchers have interpreted this observed partitioning as a possible plant defense mechanism against germanium toxicity (Puerner et al., 1990; Delvigne et al., 2009). On the other hand, silicon affords innumerable benefits to plants including pathogen resistance, increased photosynthetic capacity, and greater tolerance to heavy metal toxicity (Raven, 1983; Ma and Takahashi, 1990; Epstein, 1994, 1999; Cocker et al., 1998).

Silicon is a “pseudo-essential” nutrient whose presence in plant tissues promotes growth and vitality (Epstein, 1994). As mentioned earlier, silicon bestows several important benefits to plants. As a structural component in cell walls, silicon has been shown to facilitate light interception and photosynthesis as demonstrated by observations of more upright posture in plants abundantly supplied with silicon (Raven, 1983). Additionally, deposition of silicon in plant tissues generates a tough outer layer to provide protection against herbivory and infection (Epstein, 1999; Fauteux et al., 2005). Furthermore, silicon’s presence in plant tissue is responsible for the sequestration of aluminum, a known plant toxin, in aluminosilicate and hydroxyaluminosilicate complexes (Cocker et al., 1998; Doucet et al., 2001). Silicon has also been implicated in immobilizing iron and manganese by transforming them to less toxic forms in plant roots (Ma and Takahashi, 1990).

Plant roots acquire silicon from the soil solution as monosilicic acid (H_4SiO_4). Monosilicic acid is then transferred to stem and leaf components of the plant through the transpiration stream where it precipitates as amorphous opal phytoliths (Opal A: $\text{SiO}_2 \cdot n\text{H}_2\text{O}$) (Jones and Handreck, 1965; Epstein, 1999; Carnelli et al., 2001; Casey et al., 2003). Silicon

precipitation generally occurs at terminal sites of the transpiration stream where leaf tissues are located (Marschner, 1995). Consequently, higher silicon concentrations are oftentimes observed in leaves compared to other plant organs (Derry et al., 2005; Garvin, 2006; Blecker et al., 2007; Delvigne et al., 2009). Once deposited, phytoliths cannot be remobilized for retranslocation to other plant tissues (Raven, 1983). At the end of the growing season, phytoliths are recycled to soil reservoirs as single silicified cells and cell fragments through the decomposition of organic matter and plant death (Alexandre et al., 1997; Carnelli et al., 2001). Thereafter, they either dissolve or are preserved and buried in soil reservoirs from which silicon can be taken up again by plants in the future (Alexandre et al., 1997; Carnelli et al., 2001).

Silicon deposition is affected by the transpiration rate (Jones and Handreck, 1965) and quantity of silicic acid in transpired water (Raven, 1983; Raven, 2003). Furthermore, silicon uptake is either governed by passive diffusion processes across the lipid component of root cell membranes or by active processes involving aquaporin transporter genes (Mitani and Ma, 2005; Ma and Yamaji, 2006; Ma et al., 2007; Yamaji et al., 2008; Sparks et al., 2010), with the exact uptake mechanism an ongoing topic of research. Accumulators (e.g. primitive plants such as horsetails and rice paddies) undergo active uptake where silicon is extracted at a higher rate than water (Si content: 4.5 to 15%), while non-accumulators (e.g. dryland grasses such as rye and oats) exhibit passive uptake where water and silicon are taken up at nearly equivalent rates (Si content: 0.5-1.5%) (Ma and Takahashi, 2002). Excluders (e.g. dicotyledonous species) undergo rejective uptake where silicon is taken up at a slower rate than water (Si content: <0.5%) (Ma and Takahashi, 2002). Silicon phytoliths are ubiquitous in nature and have been observed in a wide range of ecosystems including rainforests (Alexandre et al., 1997; Meunier et al., 1999; Derry et al., 2005; Delvigne et al., 2009; Opfergelt et al., 2010), grasslands (Runge et al., 1999;

Carnelli et al., 2001; Blecker et al., 2007; Seyfferth et al., 2013), temperate deciduous and evergreen forests (Bartoli, 1983; Farmer et al., 2004; Garvin, 2006; Cornelis et al., 2011), and wetland areas (Norris and Hackney, 1999; Struyf et al., 2007).

In addition to influencing nutrient dynamics, plants impact feedback and water dynamics in terrestrial systems. Plants accelerate chemical weathering rates by releasing organic acids, expanding soil surface areas, and increasing soil water residence times (Drever, 1994; Kelly et al., 1998; Lucas, 2001). Furthermore, plants serve as important conduits through which soil water and groundwater can re-enter the hydrologic cycle (Lucas, 2001). Deep groundwaters and soil porewaters are transferred by plant roots to shallow soil porewater reservoirs through tap roots (e.g. oaks) or hydraulic lift processes (e.g. maples) where water and corresponding nutrients are taken up by plants when transpiration requirements surpass water uptake by roots alone (Dawson, 1993). As noted by Dawson (1996), mixed age stands, like those present at Shale Hills (Figure 1.3), generally influence hydrologic balances to a greater extent than old stands as water can be extracted from both porewater and groundwater reservoirs.

In this chapter, Ge/Si ratios and germanium and silicon elemental concentrations are used to identify silicon sources in soil porewaters, leaves, sap waters, groundwaters, and streamwaters at the Susquehanna Shale Hills Critical Zone Observatory (SSHCZO). Spatio-temporal patterns in silicon concentration and Ge/Si ratio are assessed and inferences are developed on sources of silicon to various reservoirs using silicon concentrations and Ge/Si ratios supplemented by observations on mineral weathering (Jin et al., 2010; Jin et al., 2011a, 2011b; Jin and Brantley, 2011), proposed preferential flow pathways, (Lin, 2006; Lin et al., 2006; Lin and Zhou, 2008; Graham and Lin, 2011; Takagi and Lin; 2012; Zhang et al., 2014) and silicon transport mechanisms in plants (Jones and Handreck, 1965; Raven, 1983; Raven, 2003; Mitani and Ma,

2005; Ma and Yamaji, 2006; Ma et al., 2007; Yamaji et al., 2008; Sparks et al., 2010) at the catchment.

2. Procedural and Data Analysis Methods

2.1 Waters

Silicon (Si) and germanium (Ge) concentrations were analyzed for filtered and acidified soil porewaters from southern planar and south swale ridge top, mid slope, and valley floor locations sampled in May to July of 2013 (Figure 1.2). Additionally, Si and Ge concentrations were measured for filtered and acidified streamwaters from weir, mid stream, and stream headwater locations and for groundwaters sampled in October of 2013 (Figure 1.2). Information pertaining to the depths of soil porewaters and groundwaters sampled at the catchment can be found in the Procedural Methods section of Chapter 2. Furthermore, Si and Ge concentrations were analyzed for filtered and acidified sap waters collected from sugar maple, chestnut oak, and red oak trees at mid slope positions in northeastern, southeastern, northwestern, and southwestern quadrants of the catchment in July to September of 2013 (Figure 1.2). Procedural details for the xylem sap water extraction can be found in the Procedural Methods section of Chapter 2. Si concentrations were analyzed on a SPECTROBLUE inductively coupled plasma optical emission spectrometer (ICP-OES) with typical analytical uncertainties of 5% or less. For Ge analysis, a ^{70}Ge spike was added to each sample to obtain a $^{70}\text{Ge}/^{74}\text{Ge}$ ratio of 3 or 4 depending on the germanium concentration estimated to be present based on the silicon concentration of the sample. All samples were allowed to equilibrate with the ^{70}Ge spike at room temperature for at least one night prior to analysis. In order to achieve a reasonable Ge signal to noise ratio on the mass spectrometer, soil porewater, streamwater, and groundwater samples were evaporated from 12 to 4 mL in an oven set to 90°C with samples weighed before and after

to determine the exact amount of water evaporated. Ge concentrations were measured on a Finnegan Element II inductively coupled mass spectrometer (ICP-MS), with typical relative standard deviations (RSDs) found to be between 3 and 5%.

The continuous flow isotope-dilution hydride generation ICP-MS technique was used to measure Ge concentrations (Mortlock and Froelich, 1996; Kurtz, 2000). Samples, interspaced with Ge standards, check standards, and 2% nitric acid (HNO₃) blanks, were placed into autosampler vials. From the vials, samples were pumped, individually, through a continuous flow apparatus. A 1 M Tris-HCl solution and 2% sodium borohydride solution (NaBH₄) were pumped simultaneously through separate tubes. At the nexus of the three tubes, a reaction involving the sample and the Tris-HCl solution buffered the sample to a pH of 6. Simultaneously, a reaction involving the sample and sodium borohydride reduced the germanic acid to germanium hydride (GeH₄). The GeH₄ was stripped from solution through an inert argon (Ar) gas stream and passed through a Teflon filter membrane, at which point another Ar gas stream transferred it into the ICP torch, producing a Ge signal from which a ⁷⁰Ge/⁷⁴Ge ratio was measured. A mass bias correction factor was applied to the ⁷⁰Ge/⁷⁴Ge ratio measured for each sample using ⁷⁰Ge/⁷⁴Ge ratios measured for standards and blanks within a run. Ge sample concentrations were calculated using the sample ⁷⁰Ge/⁷⁴Ge ratio, the mass bias correction factor, and the masses of both sample and spike in the mixture. Specifically, moles of Ge was calculated using Equation 8 below (Mortlock and Froelich, 1996; Kurtz, 2000):

$$\text{Moles Ge} = (74_s)/(74_n) * (T) * [R_c - R_s] / [R_n/R_c] \text{ (Equation 8)}$$

where 74_s is the abundance of ⁷⁴Ge in the spike (0.61%), 74_n is the natural abundance of ⁷⁴Ge (36.54%), T is the moles of spike added, R_c is the mass bias corrected ⁷⁰Ge/⁷⁴Ge ratio for the sample, R_s is the ⁷⁰Ge/⁷⁴Ge ratio in the spike (161.4), and R_n is the ⁷⁰Ge/⁷⁴Ge natural abundance

ratio (0.0562).

2.2 Leaves

Si and Ge concentrations were measured for upper canopy leaves collected from sugar maple, chestnut oak, and red oak trees at ridge top, mid slope, and valley floor positions in the northeastern quadrant of the catchment in June to September of 2011 (Figure 1.2) and for upper canopy leaves collected from sugar maple, chestnut oak, and red oak trees at mid slope positions in northeastern, southeastern, northwestern, and southwestern quadrants of the catchment in June to September of 2013 (Figure 1.2). As described in the Procedural Methods section of Chapter 2, air-dried leaves were powdered and then digested using a 9:1 mixture of HNO₃ (3N) to H₂O₂ (30%) inside a teflon reaction vessel exposed to high temperature and pressure. For germanium analyses, a ⁷⁰Ge spike was added to each sample to obtain a ⁷⁰Ge/⁷⁴Ge ratio of 3 or 4 depending on the germanium concentration estimated to be present based on the silicon concentration of the sample. As was performed for water samples, leaf Si concentrations were measured on the ICP-OES where typical analytical uncertainties were 5% or less, while leaf Ge concentrations were measured using continuous flow isotope-dilution hydride generation ICP-MS where typical RSDs ranged from 3 to 5%.

2.3 Drill Core

A lithium metaborate fusion procedure was applied to DC 3 drill core samples collected at the CZMW 2 borehole near the stream's weir (Figure 1.2) with Cody Shale (SCO-1) used as a reference standard for germanium analyses. Specifically, a 4:1 mixture of lithium metaborate flux (LiBO₂) and sample was added to a graphite crucible which was heated in a muffle furnace set to 1050^oC for 15 minutes. Fused beads were added to 50 mL of HNO₃ (10%) and then equilibrated on a shaker table to enhance dissolution of the fused bead. Filtered solutions (5 mL)

were diluted using 35 mL of HNO₃ (10%). For germanium analyses, a ⁷⁰Ge spike was added to diluted samples to obtain a ⁷⁰Ge/⁷⁴Ge ratio of 3 or 4 depending on the germanium concentration estimated to be present based on the silicon concentration of the sample. Germanium concentrations were measured using continuous flow isotope-dilution hydride generation ICP-MS where typical RSDs ranged from 3 to 5%.

2.4 Plant Fractionation Factors

Fractionation factors ($K_{Ge/Si}$) were calculated for sugar maple, chestnut oak, and red oak species in southwestern and southeastern quadrants by dividing the ratio of concentrations of germanium and silicon in leaves to the corresponding ratio in the soil porewater solution as shown in Equation 9 below (White et al., 2012):

$$K_{Ge/Si} = \frac{[\frac{Ge}{Si}]_{Leaf}}{[\frac{Ge}{Si}]_{Soil\ Porewater}} \quad (\text{Equation 9})$$

Fractionation factors less than one reflect discrimination against germanium (White et al., 2012). In the case of discrimination against germanium, the upper and lower bounds are defined as no silicon and germanium discrimination ($K_{Ge/Si}=1$) and the complete exclusion of germanium ($K_{Ge/Si}=0$) by vegetation, respectively.

3. Results and Discussion

3.1 Soil porewaters

Soil porewater silicon concentrations at southern planar ridge top, mid slope, and valley floor locations ranged from 71 to 147, 106 to 294, and 81 to 236 μM (Table 3.1, Figures 3.1 and 3.2), respectively, with average values of 116 ± 6 , 162 ± 11 , and 130 ± 9 μM (Table 3.2, Figure 3.3), respectively. At south swale ridge top, mid slope, and valley floor locations, soil porewater silicon concentrations ranged from 64 to 149, 72 to 148, and 96 to 239 μM (Table 3.1, Figures

3.1 and 3.2), respectively, with average values of 110 ± 8 , 108 ± 2 , and 155 ± 6 μM (Table 3.2, Figure 3.3), respectively. As indicated by Jin et al. (2010), silicon is directly released into the soil solution as silicic acid (H_4SiO_4) via the dissolution of illite and chlorite minerals at the catchment. Through this process, aluminum also forms secondary kaolinites with silicon (Jin et al., 2010) where kaolinite is inferred to be in a secondary phase as it is present in soils in abundances up to 2.8 wt % yet absent in bedrock (Jin et al., 2010). Additionally, observed Si/Al molar ratios near 1 for soils sampled from all locations of the southern planar transect (Jin et al., 2010) lend support to the presence of Si-poor clays from the kaolinite group (Cornelis et al., 2010). Furthermore, elemental profiles for soils in the southern quadrant of the catchment indicate that clay mineral weathering is controlled by slow dissolution kinetics in a weathering-limited system (Jin et al., 2010) amenable to the neoformation of clay minerals (Kump et al., 2000; Cornelis et al., 2010).

According to Tables 3.1 to 3.3 and Figures 3.1 to 3.3, variation in porewater silicon concentration was observed to be dependent on sampling location and depth. For southern planar porewaters, the highest average silicon concentration was found at the mid slope position followed by the valley floor and ridge top positions. Decreases in average porewater silicon concentration were observed from south swale ridge top to mid slope positions, while increases were found from mid slope to valley floor positions. Overall, the southern planar location had higher silicon concentrations at ridge top and mid slope positions than porewaters sampled at these positions in the south swale location. Conversely, valley floor porewaters sampled at the south swale location had higher silicon concentrations than those sampled at valley floor positions in the southern planar location, on average. These spatial patterns deviate slightly from those observed for calcium and strontium (Chapter 2) as silicon loss from soils occurs as both

solutes and fine particles, while calcium and strontium losses occur solely as solutes (Jin et al., 2010). Hence, the sequestration of silicon in secondary kaolinites or Si-Al amorphous materials is possible in addition to silicon release as solutes via illite and chlorite dissolution processes (Jin et al., 2010). At both locations, average silicon concentrations were lower in porewaters sampled from ridge top relative to valley floor positions (Table 3.2, Figure 3.3). A similar pattern was observed at the Rio Icacos watershed in Puerto Rico where upland porewaters were found to have lower silicon concentrations than lowland porewaters, on average (Kurtz et al., 2011).

Mineralogical and hydrological studies at Shale Hills (Graham et al., 1990; Lin, 2006; Lin and Zhou, 2008; Jin et al., 2010; Graham and Lin, 2011; Jin and Brantley, 2011) may shed light on observed spatial patterns in silicon concentration. Graham et al. (1990) and Jin et al. (2010) noted that porewaters in contact with minerals at the southern planar ridge top location are expected to be dilute and in chemical disequilibrium due to high chemical weathering rates and short porewater residence times present there as a result of the rapid movement of precipitation inputs first through the soil profile and then into underlying fractured shale. Moreover, Jin and Brantley (2011) hypothesized rapid penetration of water through the south swale soil profile along preferential flow paths as demonstrated by the presence of a positive cerium (Ce) anomaly indicative of oxic conditions in wet and thick soils at this location. Thus, rapid downslope transport processes may be responsible for reducing residence times and hence, silicon concentrations in porewaters at ridge top relative to valley floor locations. To this end, Jin et al. (2010) determined that between 30 and 50% of total element loss in soils of the southern quadrant location is due to chemical dissolution from ridge top and mid slope locations, with silicon and aluminum together accounting for 70% of total element loss at these locations. On the contrary, negative net silicon chemical weathering rates (Jin et al., 2010) suggest net

accumulation as opposed to net dissolution for silicon in soils at valley floor locations. Hillslopes at the catchment are known to serve as recharge areas where a complex network of subsurface macropores preferentially routes solutes downslope to valley floor locations through lateral flow pathways (Lin and Zhou, 2008). Consequently, valley floor porewaters are predominately receiving silicon inputs in the form of solutes from both ridge top and mid slope locations through downslope transport processes. Indeed, Lin et al. (2006) noted the presence of a Si-rich fragipan layer in soils exclusively at valley floor locations of the catchment. Interestingly, silicon concentrations in mid slope soil porewaters were significantly higher than those sampled at ridge top positions of the southern planar location, yet silicon concentrations were observed to be rather similar in porewaters sampled from these positions at the south swale location (Table 3.2, Figure 3.3). The convergent nature of the south swale location, where colluvial sediments collect and accumulate to form thick soils at the mid slope position (Figure, 1.4, Jin and Brantley, 2011), is likely responsible for deviation from patterns predicted based on hydrology as silicon is hypothesized to be present as particles rather than solutes at this location.

Biogeochemical processes such as adsorption and plant uptake may also be responsible for enriching or depleting silicon concentrations in soil porewaters at the catchment. Specifically, Jin et al. (2010) observed the accumulation of iron and aluminum particles at valley floor locations of the catchment. Preferential adsorption of germanium relative to silicon onto iron and aluminum hydroxides is known to enrich porewater solutions in silicon (Pokrovsky et al., 2006; Pokrovsky et al., 2014). Hence, the higher silicon concentrations and, as will be discussed later, lower Ge/Si ratios observed in porewaters sampled from valley floor relative to ridge top locations. Furthermore, ridge top soils are significantly thinner than those sampled from mid slope and valley floor positions at both locations (Figure 1.4, Lin et al., 2006). In fact, average

effective rooting depth for plants (~20 cm; Jin et al., 2011b) is shallow and corresponds closely to the average depth to bedrock for ridge top soils in southern quadrants of the catchment (~30 cm, Lin et al., 2006). As a consequence, average silicon concentrations in porewaters at ridge top locations will be more heavily weighted toward shallow soil horizons and porewaters which are strongly influenced by plant activities at the surface. As will be discussed in detail later, fractionation factors less than one calculated for sugar maple, chestnut oak, and red oak species indicate discrimination against germanium relative to silicon by plants at the catchment. Indeed, such partitioning between silicon and germanium has been observed in numerous plant species sampled across a wide range of ecosystems (Blecker, 2005; Derry et al., 2005; Garvin, 2006; Blecker et al., 2007; Delvigne et al., 2009). Hence, lower average silicon concentrations in porewaters derived from ridge top relative to valley floor locations may be the result of greater influences by plant activities on ridge top porewaters as plants at the catchment are known to preferentially extract silicon over germanium from porewater reservoirs (Tables 3.7, 3.8, 3.9, 3.11, 3.19, and 3.20 and Figures 3.6 and 3.24)

With the exception of soil porewaters sampled at valley floor positions, southern planar soil porewaters had higher average silicon concentrations than those sampled from south swale locations (Table 3.2, Figure 3.3). Steeper topography (Figure 1.2) enhances lateral subsurface flow activities (Lin, 2006; Lin and Zhou, 2008; Graham and Lin, 2011; Jin et al., 2011b; Jin and Brantley, 2011) at swale relative to planar locations to shorten residence times for solutes present in porewaters at the swale location. In valley floor soils, negative net chemical weathering rates for silicon suggest net accumulation as opposed to net dissolution for silicon (Jin et al., 2010). Hence, silicon is added to porewaters at the valley floor location primarily through lateral subsurface flow from ridge top and mid slope locations. Thus, it is hypothesized that the higher

average silicon concentrations in valley floor soil porewaters collected from swale relative to planar locations is a consequence of the convergent nature of the swale which acts to facilitate downward transport of silicon as solutes or particles from upslope positions.

As mentioned previously, southern planar and south swale porewaters varied in silicon concentration based on sampling depth (Table 3.3, Figures 3.1 and 3.2). Average silicon concentration for southern planar ridge top porewaters decreased with depth. For south swale ridge top porewaters, average silicon concentration increased between 10 and 20 cm depths before decreasing between 20 and 30 cm depths. Additionally, silicon concentration was shown to increase between 10 and 40 cm depths and then decrease between 40 and 50 cm depths for mid slope porewaters sampled from the southern planar location, on average. For south swale mid slope porewaters, average silicon concentration decreased down to the 40 cm depth, where increases were observed between depths of 40 and 100 cm. Slight decreases in silicon concentration were observed downward from the 100 cm depth.

Decreases in silicon concentration with depth are consistent with lower silicon concentrations observed in soil elemental profiles of the southern quadrant as a function of depth (Jin et al., 2010; Jin and Brantley, 2011). Upper horizons are highly affected by precipitation inputs where organic acids are released upon the decomposition of litterfall. Litterfall decomposition lowers pH and increases DOC in porewaters (Andrews et al., 2011) providing optimal conditions for the dissolution of silicate minerals in upper horizons (Barman et al., 1992; Drever, 1994; Lucas, 2001; Farmer et al., 2004). Additionally, silicon cycling by plants can either increase dissolved silicon concentrations in shallow porewaters through dissolution of biogenic silicon in litterfall or decrease dissolved silicon concentration in shallow porewaters through active root uptake or the storage of biogenic silicon in upper horizons to be later

translocated downwards to deeper horizons (Kelly et al., 1998; Lucas, 2001; Carnelli et al., 2001; Gerard et al., 2008). In the case of the former, observations of greater kaolinite abundances in upper horizons of the soil profile (Jin et al., 2010) may indicate greater interaction of dissolved biogenic silicon in porewaters with aluminum and iron oxides present in soils at the catchment (Lucas et al., 1993; Lucas, 2001; Opfergelt et al., 2010). Silicon concentration varied erratically with depth for southern planar and south swale porewaters sampled at valley floor locations. For southern planar valley floor porewaters, average silicon concentration displayed an alternating increasing/decreasing pattern between 10 cm depth intervals ranging from 20 to 60 cm. Furthermore, average silicon concentration for south swale valley floor porewaters initially exhibited an alternating decreasing/increasing pattern between depth intervals of 10 and 20 cm and 20 and 40 cm, respectively. Average silicon concentration then stabilized at a value of 177 μM between the 40 and 50 cm depth interval. Downward from the 50 cm depth, decreases were observed until the 70 cm depth where increases were found between 70 and 90 cm depths.

Depth dependent patterns in silicon concentration are also consistent with preferential flow pathways at the catchment. As noted by Jin et al. (2011b), mineral weathering largely occurs within soils in low flow zones between A-B horizons of the soil profile due to longer mineral-water contact times present there. From the A-B horizons, solutes released from low flow zones diffuse or laterally flow into high flow zones at A-B and B-C horizon interfaces where weathering is not as intensive and residence times are shorter (Jin et al., 2011b). Thereafter, porewaters advect quickly downslope in perched saturated layers where they can recharge to groundwater (Jin et al., 2011b). Longer water residence times in low flow zones promote greater porewater exposure to clay dissolution processes and, consequently, higher observed solute concentrations for porewaters in these zones (Jin et al., 2011b). As mentioned in

Chapter 2, Lin et al. (2006) noted the accumulation of groundwater at valley floor locations of the catchment. If perched water tables form, rapid fluid flushing of soil porewaters with dilute precipitation inputs along both vertical and lateral preferential flow paths may be responsible for the erratic “zig-zag” patterns in silicon concentration observed for valley floor soil porewaters as was shown for Ca/Sr ratio (Table 2.6 and Figure 2.6) and magnesium concentration (Jin et al., 2011b). As depicted in Figure 3.1 and Table 3.3, silicon concentrations in shallow porewaters from all locations were found to be highly variable. Jin et al., (2011b) noted significant temporal fluctuations in near-surface soil moisture, likely due to variable rates of evapotranspiration by plants at the catchment (Takagi and Lin, 2012). Since a strong positive relationship exists between transpiration rate and silicon uptake in plants (Jones and Handreck, 1965), increased levels of evapotranspiration should lead to concomitant increases in plant transpiration and silicon uptake by plants from shallow porewater solutions and vice versa under decreased levels of evapotranspiration.

Table 3.1 Silicon and germanium concentrations and Ge/Si ratios for soil porewaters sampled from southern planar (SP) and south swale (SS) ridge top (RT), mid slope (MS), and valley floor (VF) locations

Sample Date	Sample ID	Depth (cm)	Si ($\mu\text{M/kg}$)	Ge (pM/kg)	Ge/Si ($\mu\text{M/M}$)
5/17/2013	SPMS	40	170	181	1.1
5/17/2013	SPMS	50	125	187	1.5
5/17/2013	SPVF	20	111	240	2.2
5/17/2013	SPVF	30	210	176	0.8
5/17/2013	SPVF	40	105	145	1.4
5/17/2013	SPVF	60	113	112	1.0
5/17/2013	SSMS	40	83	144	1.7
5/24/2013	SPRT	20	113	320	2.8
5/24/2013	SSMS	100	121	102	0.8
5/24/2013	SSMS	120	102	89	0.9
5/24/2013	SSMS	140	111	83	0.7
5/24/2013	SSMS	160	106	101	0.9

5/24/2013	SSRT	10	107	130	1.2
5/24/2013	SSVF	20	123	235	1.9
5/30/2013	SPRT	30	89	261	2.9
5/30/2013	SSMS	140	111	92	0.8
5/30/2013	SSMS	160	105	106	1.0
5/30/2013	SSRT	20	146	340	2.3
6/5/2013	SSVF	10	230	167	0.7
6/5/2013	SSVF	20	123	188	1.5
6/5/2013	SSMS	100	117	86	0.7
6/5/2013	SSMS	100	117	116	1.0
6/5/2013	SSMS	120	113	110	1.0
6/5/2013	SSMS	160	108	89	0.8
6/11/2013	SSMS	40	109	191	1.8
6/11/2013	SSMS	120	110	105	1.0
6/11/2013	SSMS	140	111	91	0.8
6/12/2013	SSMS	10	127	289	2.0
6/12/2013	SSRT	10	134	256	1.9
6/12/2013	SSMS	20	111	171	1.5
6/12/2013	SPMS	10	147	282	1.9
6/12/2013	SPRT	20	112	395	3.5
6/12/2013	SSRT	20	150	253	1.7
6/12/2013	SSRT	30	83	179	2.1
6/12/2013	SSVF	30	138	282	2.0
6/12/2013	SSVF	40	165	176	1.1
6/12/2013	SPMS	50	125	191	1.5
6/12/2013	SSMS	60	112	139	1.2
6/12/2013	SSMS	80	114	138	1.2
6/12/2013	SSMS	160	108	88	0.8
6/21/2013	SSRT	10	126	261	2.1
6/21/2013	SPRT	20	113	373	3.3
6/21/2013	SSVF	30	101	197	2.0
6/21/2013	SPMS	40	195	254	1.3
6/21/2013	SSVF	50	153	128	0.8
6/21/2013	SPMS	50	107	200	1.9
6/21/2013	SSVF	80	154	79	0.5
6/21/2013	SSMS	160	101	89	0.9
6/28/2013	SSRT	10	80	270	3.4
6/28/2013	SSRT	20	64	180	2.8
6/28/2013	SSMS	20	111	211	1.9
6/28/2013	SPVF	20	81	177	2.2

6/28/2013	SPVF	30	102	148	1.4
6/28/2013	SPRT	30	147	241	1.6
6/28/2013	SSMS	40	72	130	1.8
6/28/2013	SSVF	40	109	142	1.3
6/28/2013	SPMS	40	183	163	0.9
6/28/2013	SPVF	40	94	125	1.3
6/28/2013	SSVF	50	114	142	1.2
6/28/2013	SPMS	50	117	211	1.8
6/28/2013	SPVF	50	122	229	1.9
6/28/2013	SSMS	60	89	130	1.5
6/28/2013	SSVF	60	107	152	1.4
6/28/2013	SSVF	60	107	109	1.0
6/28/2013	SPVF	60	93	131	1.4
6/28/2013	SSVF	70	97	139	1.4
6/28/2013	SSMS	80	94	146	1.6
6/28/2013	SSVF	80	128	113	0.9
6/28/2013	SSMS	100	80	84	1.0
6/28/2013	SSMS	120	93	89	1.0
6/28/2013	SSMS	140	124	94	0.8
6/28/2013	SSMS	160	94	93	1.0
7/12/2013	SPMS	10	179	153	0.9
7/12/2013	SPRT	20	104	419	4.0
7/12/2013	SPVF	20	117	253	2.2
7/12/2013	SPVF	20	117	277	2.4
7/12/2013	SPVF	40	128	188	1.5
7/12/2013	SPVF	50	181	196	1.1
7/12/2013	SSMS	40	105	207	2.0
7/12/2013	SSMS	60	114	208	1.8
7/12/2013	SSMS	60	114	163	1.4
7/12/2013	SSMS	100	127	109	0.9
7/12/2013	SSMS	120	115	118	1.0
7/12/2013	SSMS	140	114	113	1.0
7/12/2013	SSMS	160	101	97	1.0
7/12/2013	SSRT	10	117	327	2.8
7/12/2013	SSRT	20	135	331	2.5
7/12/2013	SSRT	30	80	196	2.5
7/12/2013	SSVF	10	196	141	0.7
7/12/2013	SSVF	10	128	351	2.8
7/12/2013	SSVF	20	119	246	2.1
7/12/2013	SSVF	30	153	299	2.0

7/12/2013	SSVF	40	191	180	0.9
7/12/2013	SSVF	50	181	196	1.1
7/18/2013	SPMS	10	106	348	3.3
7/18/2013	SPMS	50	131	288	2.2
7/18/2013	SPVF	20	131	304	2.3
7/18/2013	SSMS	100	134	114	0.9
7/18/2013	SSMS	120	121	124	1.0
7/18/2013	SSMS	140	124	121	1.0
7/18/2013	SSMS	160	109	105	1.0
7/18/2013	SSVF	20	119	248	2.1
7/18/2013	SPRT	20	145	471	3.2

*Silicon elemental concentrations for additional soil porewater samples where Ge/Si ratios were not measured are displayed in the appendix.

Table 3.2 Average silicon concentrations and Ge/Si ratios for soil porewaters sampled from southern planar and south swale ridge top, mid slope, and valley floor locations

Location	Average [Si] ($\mu\text{M}/\text{kg}$)	Average Ge/Si ($\mu\text{M}/\text{M}$)
Southern Planar Ridge Top	116 ± 6	3.3 ± 0.18
Southern Planar Mid Slope	162 ± 11	1.7 ± 0.21
Southern Planar Valley Floor	130 ± 9	1.6 ± 0.14
South Swale Ridge Top	110 ± 8	2.3 ± 0.18
South Swale Mid Slope	108 ± 2	1.2 ± 0.07
South Swale Valley Floor	155 ± 6	1.4 ± 0.13

Table 3.3 Average silicon and germanium concentrations and Ge/Si ratios for soil porewaters sampled at various depths from southern planar (SP) and south swale (SS) ridge top (RT), mid slope (MS), and valley floor (VF) locations.

Location	Depth (cm)	Average [Si] (μM)	Average [Ge] (pM)	Average Ge/Si ($\mu\text{M}/\text{M}$)
SPRT	10	131	nm	nm
SPRT	20	118 \pm 5	396 \pm 25	3.4 \pm 0.20
SPRT	30	108 \pm 17	251 \pm 10	2.9
SPMS	10	168 \pm 9	261 \pm 57	2.0 \pm 0.70
SPMS	40	203 \pm 16	199 \pm 28	1.1 \pm 0.12
SPMS	50	122 \pm 3	215 \pm 19	1.8 \pm 0.13
SPVF	20	110 \pm 7	250 \pm 21	2.2 \pm 0.04
SPVF	30	216 \pm 7	162 \pm 14	1.1 \pm 0.30
SPVF	40	116 \pm 7	153 \pm 19	1.4 \pm 0.04
SPVF	50	118 \pm 4	213 \pm 17	1.5 \pm 0.39
SPVF	60	107 \pm 4	122 \pm 10	1.2 \pm 0.21
SSRT	10	104 \pm 9	249 \pm 32	2.3 \pm 0.38
SSRT	20	143 \pm 5	276 \pm 37	2.3 \pm 0.23
SSRT	30	81 \pm 2	188 \pm 9	2.3 \pm 0.17
SSMS	10	127	289	2.3
SSMS	20	112 \pm 2	191 \pm 20	1.7 \pm 0.18
SSMS	40	96 \pm 4	168 \pm 18	1.8 \pm 0.06
SSMS	60	105 \pm 8	160 \pm 17	1.5 \pm 0.12
SSMS	80	110 \pm 6	142 \pm 4	1.4 \pm 0.17
SSMS	100	115 \pm 3	102 \pm 6	0.9 \pm 0.05
SSMS	120	110 \pm 3	106 \pm 6	1.0 \pm 0.02
SSMS	140	109 \pm 4	99 \pm 6	0.9 \pm 0.04
SSMS	160	105 \pm 2	96 \pm 3	0.9 \pm 0.03
SSVF	10	172 \pm 18	220 \pm 66	1.4 \pm 0.68
SSVF	20	121 \pm 5	229 \pm 14	1.9 \pm 0.13
SSVF	30	152 \pm 6	259 \pm 32	2.0 \pm 0.03
SSVF	40	177 \pm 5	166 \pm 12	1.1 \pm 0.12
SSVF	50	177 \pm 13	155 \pm 21	1.1 \pm 0.12
SSVF	60	148 \pm 2	131 \pm 22	1.2 \pm 0.20
SSVF	70	96	139	1.4
SSVF	80	148 \pm 11	96 \pm 17	0.7 \pm 0.19
SSVF	90	239	nm	nm

*The 'nm' term refers to depths where Ge/Si ratios were not measured for a designated porewater sample.

*Error bars are excluded from depths where only one porewater was measured for silicon concentration or Ge/Si ratio at a designated location.

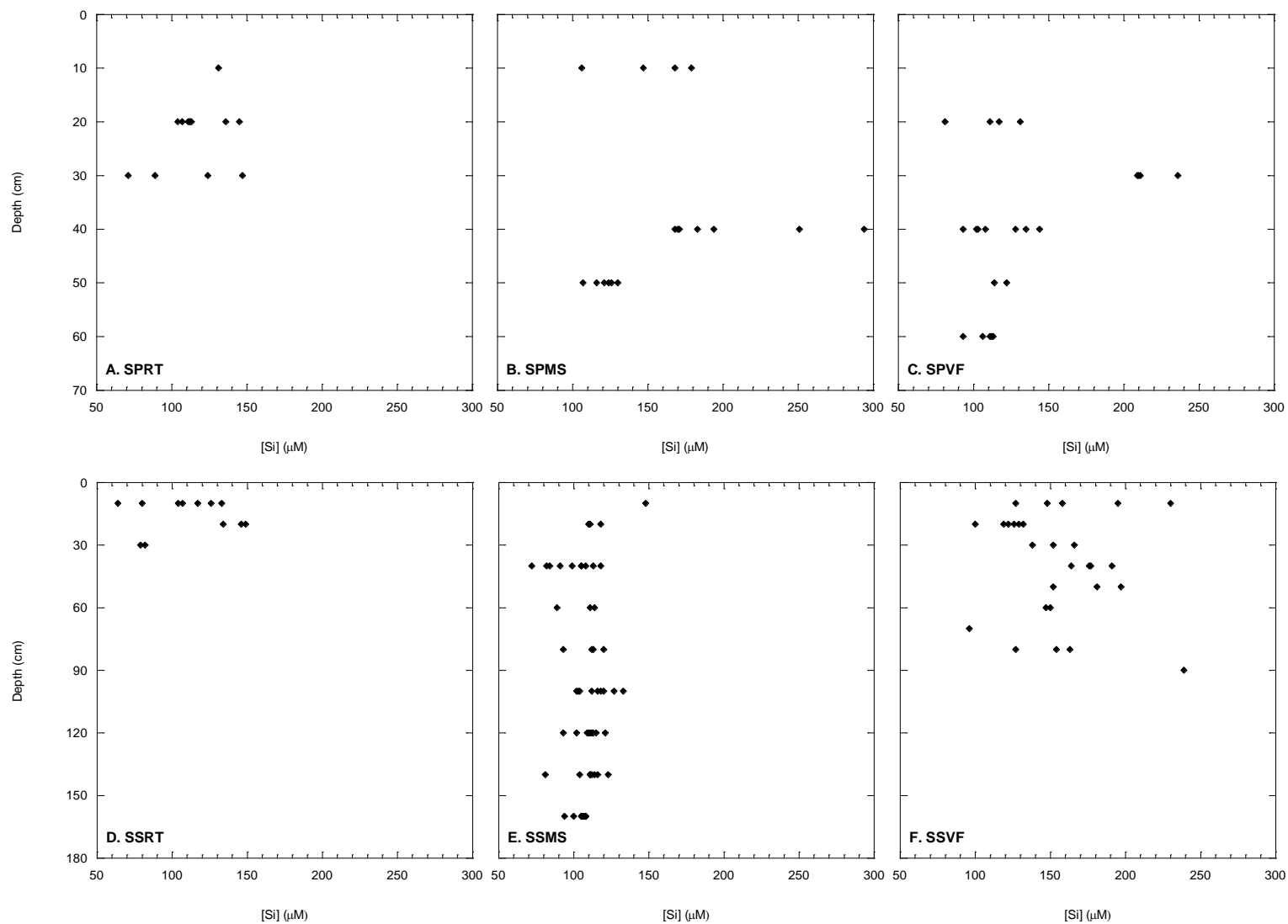


Figure 3.1 Silicon concentrations for soil porewaters as a function of depth at southern planar ridge top (SPRT) (A), mid slope (SPMS) (B), and valley floor (SPVF) (C) locations and at south swale ridge top (SSRT) (D), mid slope (SSMS) (E), and valley floor (SSVF) (F) locations.

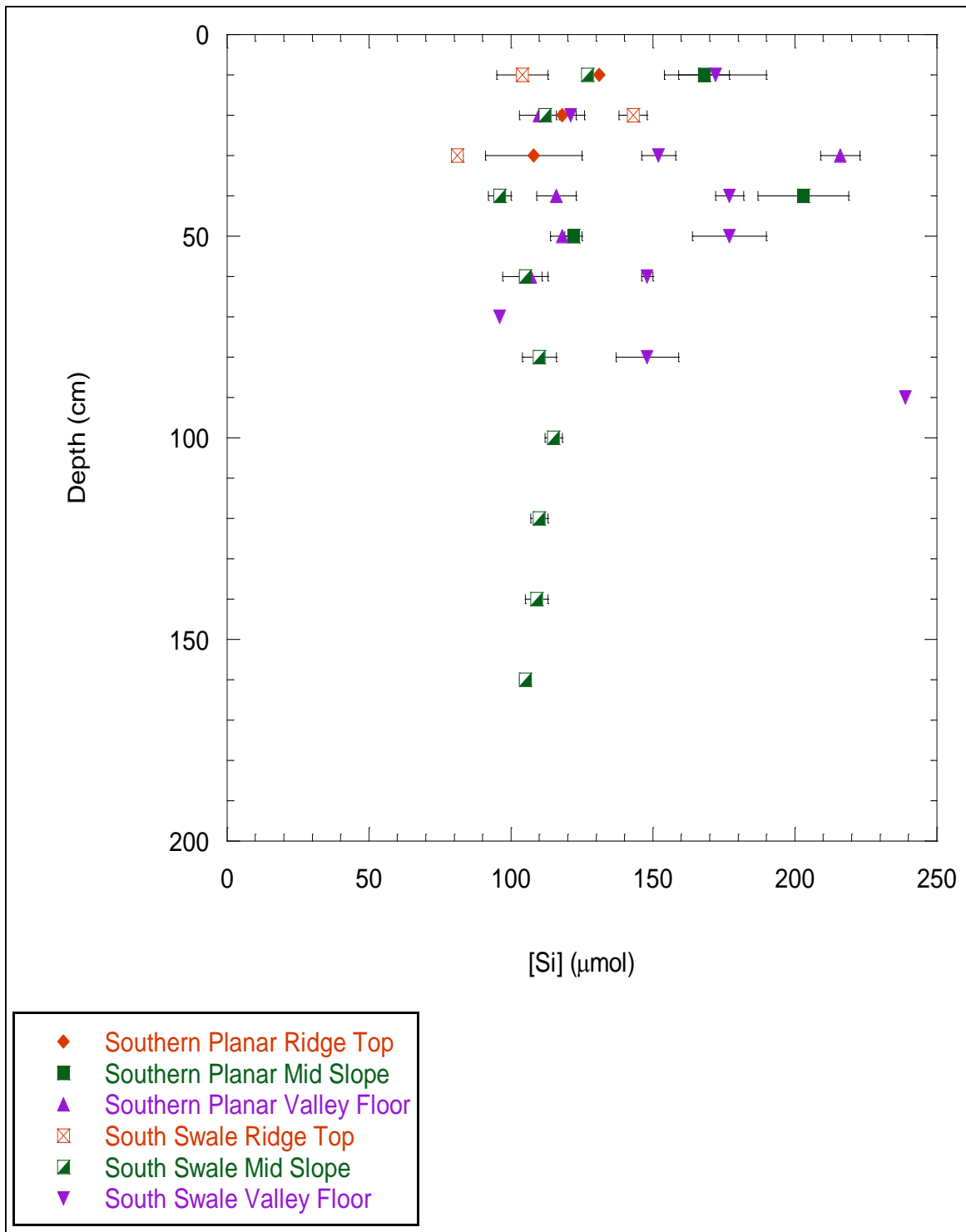


Figure 3.2 Depth versus silicon concentration for southern planar and south swale ridge top, mid slope, and valley floor soil porewaters with error bars shown for average values. Note that some points displayed on the figure are overlapping.

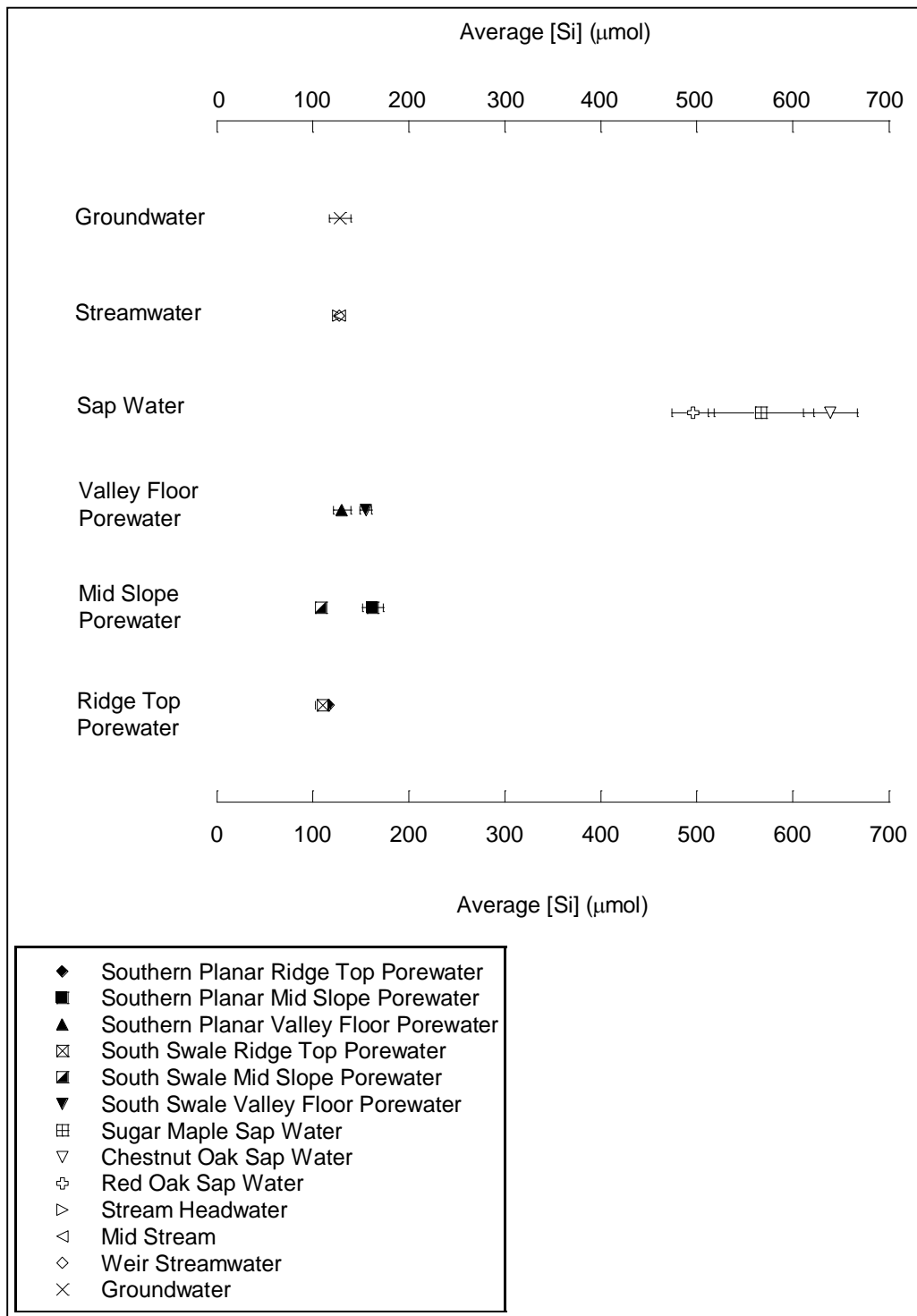


Figure 3.3 Average silicon concentrations for southern planar and south swale ridge top, mid slope, and valley floor soil porewaters, sugar maple, chestnut oak, and red oak sap waters, and streamwaters and groundwaters with error bars shown. Note the overlapping silicon concentrations for southern planar and south swale ridge top porewaters and for streamwaters at headwater, mid stream, and weir locations.

Soil porewater Ge/Si ratios at southern planar ridge top, mid slope, and valley floor locations ranged from 2.8 to 4.0, 0.9 to 3.3, and 0.8 to 2.4 $\mu\text{M}/\text{M}$ (Table 3.1, Figures 3.4 and 3.5), respectively, with average values of 3.3 ± 0.18 , 1.7 ± 0.21 , and 1.6 ± 0.14 $\mu\text{M}/\text{M}$ (Table 3.2, Figure 3.6), respectively. At south swale ridge top, mid slope, and valley floor locations, soil porewater Ge/Si ratios ranged from 1.2 to 3.4, 0.7 to 2.3, and 0.5 to 2.8 $\mu\text{M}/\text{M}$ (Table 3.1, Figures 3.4 and 3.5), respectively, with average values of 2.3 ± 0.18 , 1.2 ± 0.07 , and 1.4 ± 0.13 $\mu\text{M}/\text{M}$ (Table 3.2, Figure 3.6), respectively. Due to the fine grain nature of shales at the catchment, silicon and germanium concentrations were not measured for mineral separates preventing adequate interpretation of porewater Ge/Si ratios based on the data alone. However, hypotheses on source materials are formulated in the following paragraph using observations on mineralogy and plant uptake processes at the catchment.

For both southern planar and south swale locations, porewaters sampled from ridge top locations displayed the highest average Ge/Si ratios (Table 3.2, Figure 3.6). While average silicon concentrations were only slightly lower in porewaters at ridge top locations compared to the other locations (Table 3.2, Figure 3.6), average germanium concentrations were 1.7 and 1.9 times higher than those in porewaters at southern planar mid slope and valley floor locations, respectively, and 2.0 and 1.3 times higher than those in porewaters at south swale mid slope and valley floor locations, respectively. At southern planar and south swale locations, ridge top soils are thinner than those sampled at mid slope and valley floor positions (Figure 1.4). In fact, average rooting depth (~ 20 cm; Jin et al., 2011b) is rather similar to average depth to bedrock for ridge top soils in southern quadrants of the catchment (~ 30 cm, Lin et al., 2006). As mentioned previously, fractionation factors less than one calculated for sugar maple, chestnut oak, and red oak species lend support to the hypothesis of preferential discrimination against germanium

relative to silicon in plants at the catchment. Thus, leaching of germanium from plant to soil porewater reservoirs will be greater in thinner soils at ridge top locations where influences on porewaters by plant activities are more significant. Hence, the higher observed germanium concentrations and Ge/Si ratios in porewaters sampled at ridge top relative to mid slope and valley floor locations (Table 3.2, Figure 3.6). On the other hand, Ge/Si ratios in porewaters sampled from thicker soils with more substantial mineral horizons at mid slope and valley floor locations (Figure 1.4) should resemble primary weathering of silicate minerals. According to Murnane and Stallard (1990), Froelich et al. (1992), Kurtz et al. (2002), and Scribner et al. (2006), primary weathering of silicate minerals generally produces lower Ge/Si ratios in solution relative to ratios determined for unweathered bedrock (Tables 3.2 and 3.25, Figure 3.6) due to the preferential sequestration of germanium in secondary clay minerals. Furthermore, as mentioned in Chapter 2, solute source contributions are largely influenced by groundwater recharge at valley floor locations. In fact, average silicon concentrations for southern planar valley floor porewaters (Avg. [Si] = 130 μM) and groundwaters (Avg. [Si] = 128 μM) were remarkably similar. Additionally, average silicon concentrations for deep valley floor porewaters (Avg. [Si] = 114 μM) and nearby CZMW 1 groundwaters (Avg. [Si] = 112 μM) were found to be nearly identical. As the average Ge/Si ratio in groundwater was observed to be quite low (Avg. Ge/Si = 0.73 $\mu\text{M}/\text{M}$), groundwater recharge may also be responsible for the low Ge/Si ratios found in valley floor porewaters. It should be noted that, although germanium enriched disordered kaolinite was observed to be in its highest abundance in ridge top soils sampled from the shallowest horizons (2.8 wt %, Jin et al., 2010), no significant correlation was found between Ge/Si and Al/Si ratios in porewaters as would be expected if solutes were released into porewater solutions from dissolution of secondary aluminosilicates such as kaolinite (Kurtz et al., 2002).

Furthermore, in temperate regions such as the SSHCZO, kaolinite is inferred to be in its stable secondary phase (Jin et al., 2008; Cornelis et al., 2010). Thus, addition of germanium to soil porewaters by dissolution of secondary kaolinites is unlikely at the catchment.

As was observed for silicon concentration, ridge top, mid slope, and valley floor planar porewaters displayed higher Ge/Si ratios than those sampled from swale locations (Tables 3.1 and 3.2, Figure 3.6). As shown in Tables 3.1 and 3.2 and Figure 3.2, silicon concentrations were relatively similar yet germanium concentrations were 1.4 times greater in planar relative to swale porewaters. In the case of mid slope porewaters, silicon and germanium concentrations were 1.5 and 1.8 times greater in planar compared to swale locations, respectively. At planar and swale locations, germanium concentrations were relatively uniform in valley floor porewaters, while silicon concentrations were 1.2 times greater in swale relative to planar valley floor porewaters. Based on these observations, differences in Ge/Si ratio between planar and swale soil porewaters were greatest at ridge top locations followed by mid slope and valley floor locations. As mentioned earlier, steeper topography (Figure 1.3) enhances lateral subsurface flow activities (Lin, 2006; Lin and Zhou, 2008; Graham and Lin, 2011; Jin et al., 2011b; Jin and Brantley, 2011) at swale relative to planar locations to reduce residence times for solutes present in porewaters at the swale location.

Furthermore, Ge/Si ratios were shown to vary according to sampling depth for all locations with the exception of the south swale ridge top location where average Ge/Si ratios remained constant at a value of 2.3 $\mu\text{M}/\text{M}$ for all depths sampled (Table 3.3, Figures 3.4 and 3.5). Overall decreases in Ge/Si ratios were observed with depth for porewaters sampled from the southern planar ridge top location. For southern planar and south swale mid slope porewaters, an alternating decreasing/increasing pattern was observed in average Ge/Si ratio from depth

intervals corresponding to 10 to 40 and 40 to 50 cm and to 10 to 20, 20 to 40, 40 to 100, 100 to 120, and 120 to 140 cm, respectively. The average south swale mid slope porewater Ge/Si ratio ultimately stabilized at a value of 0.9 $\mu\text{M}/\text{M}$ in the depth interval between 140 and 160 cm. Initial decreases in average Ge/Si ratio were observed for southern planar valley floor porewaters from 20 cm to the 30 cm depth. Beyond the 30 cm depth, the average Ge/Si ratio increased between 30 and 50 cm depths and then decreased between 50 and 60 cm depths. For south swale valley floor porewaters, an alternating increasing/decreasing pattern in Ge/Si ratio was observed for depth intervals corresponding to 10 to 30, 30 to 50, 50 to 70, and 70 to 80 cm.

At all southern planar sites and the south swale mid slope site, porewaters sampled at the shallowest depth had the highest average Ge/Si ratios (Table 3.3, Figures 3.4 and 3.5). Formation of complexes between germanium and dissolved organic matter (DOM) may be responsible for high Ge/Si ratios in shallow porewaters (Pokrovski and Schott, 1998; Pokrovsky et al., 2006). In most natural waters, such complexes are not observed to form between silicon and dissolved organic matter in significant quantities (Pokrovski and Schott, 1998). Specifically, Pokrovski and Schott (1998) found Ge-DOM to account for 95% of total aqueous germanium while Si-humic acid complexation was < 0.1% of aqueous silicon in natural waters. Hence, germanium porewater concentrations will presumably increase, while silicon porewater concentrations will remain unchanged in the presence of organic matter resulting in the higher Ge/Si ratios in shallow porewaters. Additionally, high silicon requirements by plants, especially early in the growing season when young plants are growing and developing, will deplete shallow porewater reservoirs of silicon released from phytolith dissolution during the fallow season (Alexandre et al., 1997; Seyfferth et al., 2013). As plants are known to highly discriminate against germanium relative to silicon during uptake (Tables 3.7, 3.8, 3.9, 3.11, 3.19, and 3.20 and Figure 3.6, Derry

et al., 2005; Garvin, 2006; Blecker et al., 2007; Delvigne et al., 2009; Cornelis et al., 2010), silicon concentrations in porewaters should decrease while germanium concentrations should increase to result in higher Ge/Si ratios in shallow porewaters. Indeed, calculated fractionation factors significantly less than one for sugar maple (Avg. $K_{\text{Ge/Si}} = 0.01$), chestnut oak (Avg. $K_{\text{Ge/Si}} = 0.01$), and red oak (Avg. $K_{\text{Ge/Si}} = 0.27$) species seem to indicate strong discrimination against germanium relative to silicon in plants at the catchment.

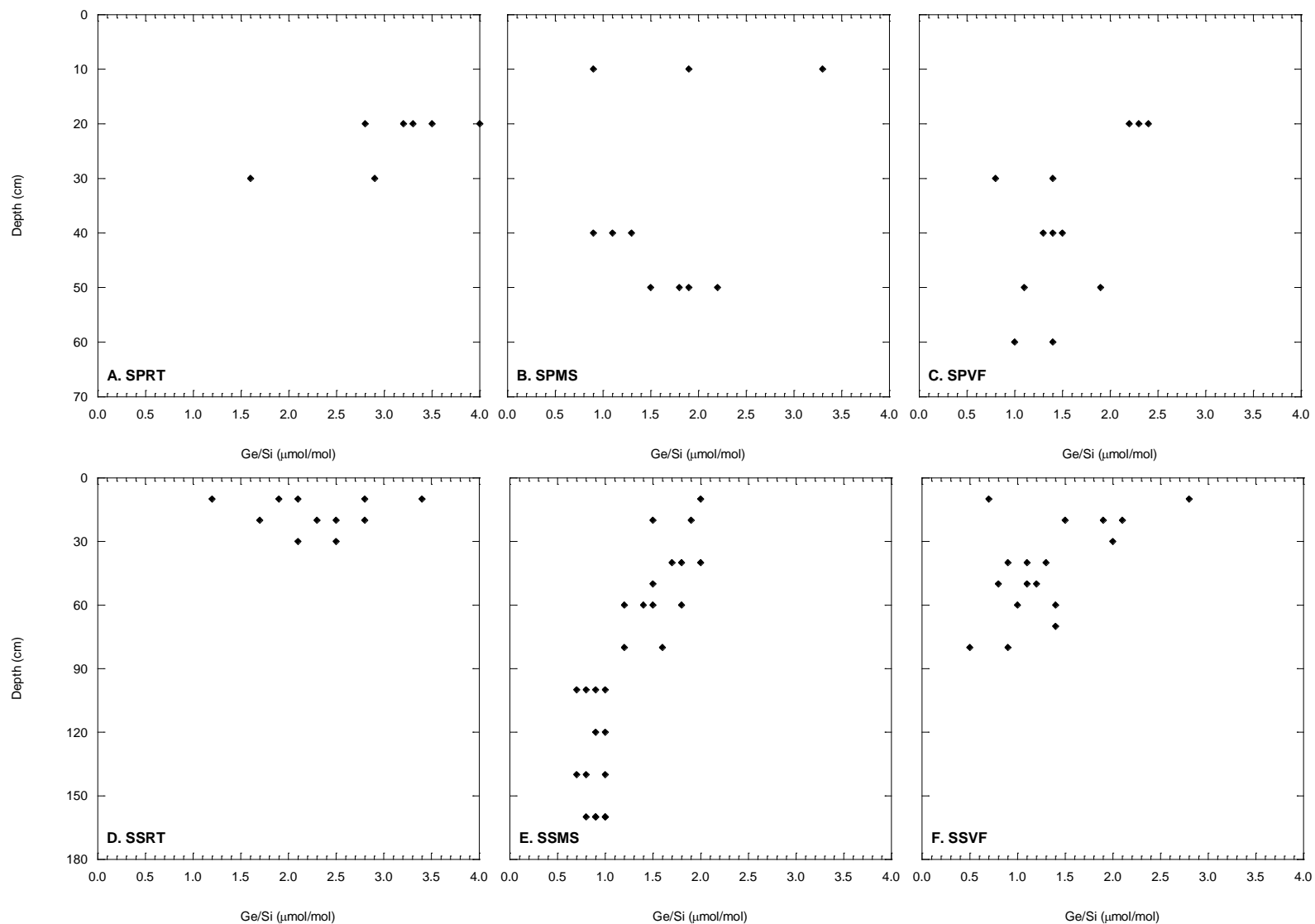


Figure 3.4 Ge/Si ratios for soil porewaters as a function of depth at southern planar ridge top (SPRT) (A), mid slope (SPMS) (B), and valley floor (SPVF) (C) locations and at south swale ridge top (SSRT) (D), mid slope (SSMS) (E), and valley floor (SSVF) (F) locations.

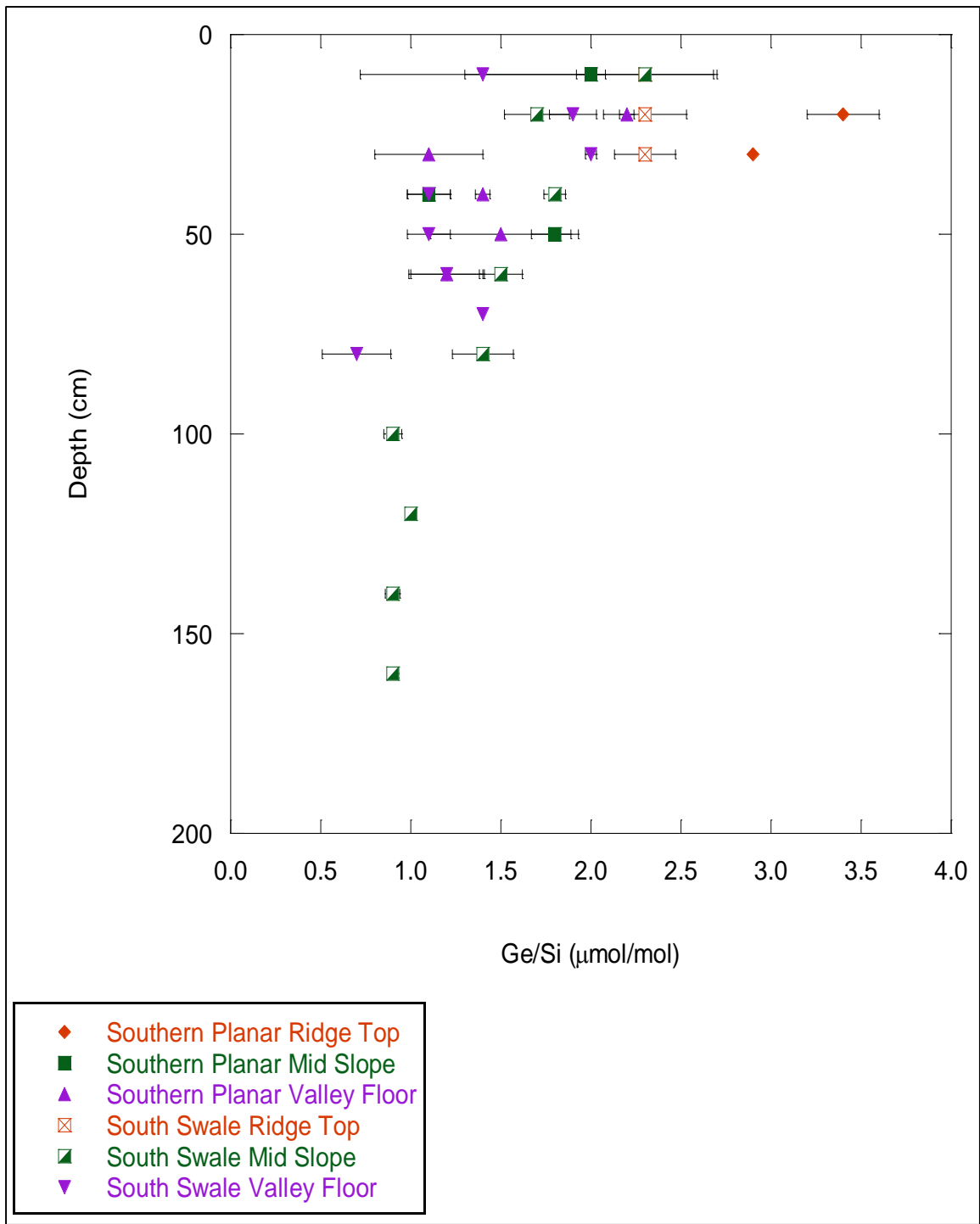


Figure 3.5 Depth versus Ge/Si ratio for southern planar and south swale ridge top, mid slope, and valley floor soil porewaters with error bars shown for average values.

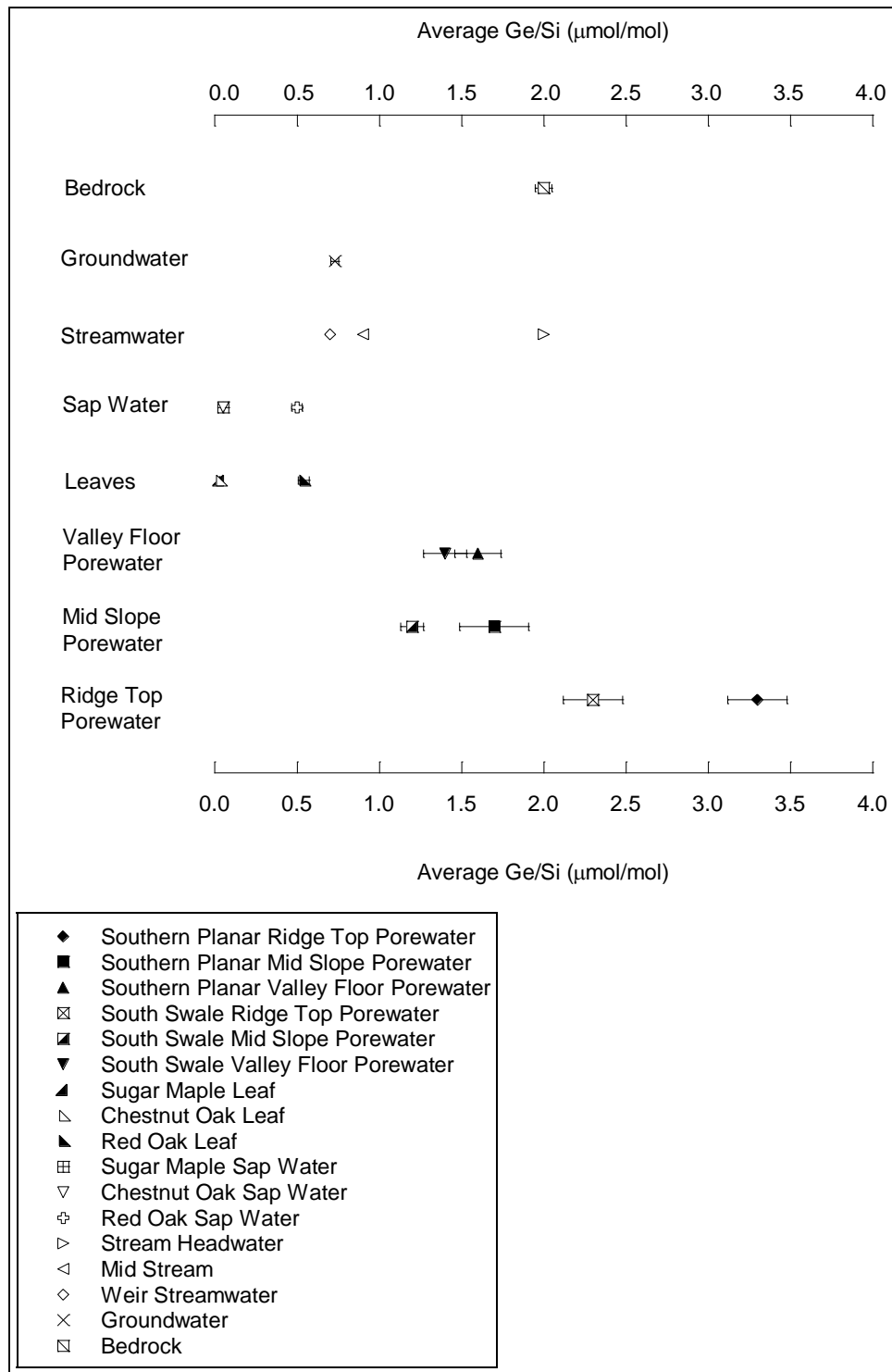


Figure 3.6 Average Ge/Si ratios for southern planar and south swale ridge top, mid slope, and valley floor soil porewaters, sugar maple, chestnut oak, and red oak leaves and sap waters, and streamwaters, groundwaters, and bedrock with error bars shown. Note that average Ge/Si ratios for sugar maple leaves and sap waters overlap with those for chestnut oak leaves and sap waters and that average Ge/Si ratios for leaves collected in 2013 are shown on the figure.

As shown in Table 3.4 in and in Figures 3.7 and 3.8, monthly changes in silicon concentration were more dramatic for porewaters sampled from the southern planar location than for porewaters sampled from the south swale location. The largest monthly differences in silicon concentration were observed for southern planar mid slope, valley floor, and ridge top porewaters from June to July where average silicon concentrations increased by 65, 45, and 30 μM , respectively (Table 3.4). Overall, silicon concentrations decreased from May to June and increased from June to July for southern planar ridge top and valley floor porewaters (Table 3.4, Figure 3.7). Increases in silicon concentration were observed over the course of the growing season for mid slope porewaters sampled at southern planar and south swale locations and for valley floor porewaters sampled at the south swale location (Table 3.4, Figures 3.7 and 3.8). The average silicon concentration for porewaters at the south swale ridge top location remained constant at a value of 110 μM for all months sampled (Table 3.4, Figure 3.8). Average silicon concentrations for southern planar mid slope and south swale valley floor porewaters were shown to overlap in June (Table 3.4). At first glance, these observations would seem to indicate that silicon uptake processes for plants at the catchment are largely passive (e.g. no change in monthly soil porewater silicon concentration) or rejective (e.g. monthly increases in soil porewater silicon concentration). However, silicon concentrations were significantly higher, while Ge/Si ratios were considerably lower in sap waters and leaves compared to shallow soil porewaters (Tables 3.3, 3.8, 3.11, 3.20 and Figures 3.6 and 3.24). Calculated fractionation factors where $K_{\text{Ge/Si}} \ll 1$ for all species suggest strong preferential discrimination against germanium. As noted by Sparks et al. (2010), such large partitioning between silicon and germanium is better explained by active, plant-mediated transport mechanisms which are highly specific (Clarkson, 1993, White, 2001) than by passive molecular diffusion processes or energetic differences

between amorphous SiO_2 and GeO_2 (Pokrovski and Schott, 1998). To this end, concurrent monthly increases in germanium concentrations for soil porewaters (Table 3.6) are consistent with the occurrence of active differential plant uptake processes where silicon is selectively taken up by plants at the expense of germanium. Hence, the coexistence of both active and passive silicon uptake mechanisms is hypothesized for plants at the catchment as has been suggested for silicon uptake in grasses by other researchers (Liang et al., 2006; Sparks et al., 2010). Monthly increases in porewater silicon concentration may be due to higher silicon requirements earlier in the growing season to support growth and development processes in young plants (Alexandre et al., 1997; Seyfferth et al., 2013). As such, soil porewater reservoirs will be rapidly depleted in silicon earlier in the season due to enhanced plant uptake processes which are known to preferentially favor silicon over germanium. Furthermore, silicon inputs to porewaters from external biogenic and pedogenic sources in soils are possible. However, this hypothesis cannot be tested at the current time as water-extractable silicon was not obtained from soils at the catchment.

As shown in Table 3.5 and in Figures 3.9 and 3.10, the largest monthly variations in Ge/Si ratio were found for porewaters sampled from southern planar ridge top, south swale ridge top, southern planar mid slope, and south swale valley floor locations where average Ge/Si ratios changed by 0.5, 0.5, 0.3, and 0.7 $\mu\text{M}/\text{M}$, respectively, from May to June and by 0.2, 0.3, 1.1, and 0.6 $\mu\text{M}/\text{M}$, respectively, from June to July. In general, monthly increases in average Ge/Si ratio were found for porewaters corresponding to southern planar ridge top, mid slope, and valley floor locations and to south swale ridge top and mid slope locations (Table 3.5, Figures 3.9 and 3.10). Average Ge/Si ratios were found to decrease from May to June and then increase from June to July for south swale valley floor porewaters (Table 3.5, Figure 3.10). Additionally,

average Ge/Si ratios for southern planar and south swale mid slope and valley floor porewaters were shown to overlap in June (Table 3.5, Figure 3.10).

Observed monthly increases in average Ge/Si ratio for porewaters sampled at the catchment can be attributed to increased fractionation of Ge and Si during plant uptake processes. As mentioned previously, fractionation factors less than one calculated for sugar maple, chestnut oak, and red oak species suggest preferential discrimination against germanium relative to silicon by plants at the catchment. Additionally, as discussed in Chapter 2, levels of evapotranspiration, as inferred from $\delta^{18}\text{O}$ and $\delta^2\text{H}$ values in shallow soil waters underlying sugar maple, chestnut oak, and red oak species (Gregor, unpublished data), were shown to increase over the course of the growing season. Since evapotranspiration is a product of evaporation and plant transpiration and a strong positive relationship exists between transpiration rate and silicon uptake in plants (Jones and Handreck, 1965), increased levels of evapotranspiration will lead to concomitant monthly increases in porewater Ge/Si ratio as plant transpiration processes deplete porewaters in silicon relative to germanium over the course of the growing season. Another explanation for observed monthly increases in porewater Ge/Si ratio is the seasonal change in dissolved silicon source to porewaters, with phytolith dissolution contributing more significantly earlier in the season presumably due to higher levels of precipitation and larger fluxes of water passing through the soil profile. At first glance, this interpretation would seem to conflict with observed monthly increases in silicon concentration for porewaters at the catchment (Figures 3.7 and 3.8) as phytolith dissolution is known to contribute significant quantities of silicon to porewater reservoirs in temperate forested ecosystems (Bartoli, 1983; Garvin, 2006). However, as mentioned previously, high silicon demands by young, developing plants greatly deplete porewater reservoirs of silicon through rapid uptake processes (Alexandre et al., 1997; Seyffert

et al., 2013) preventing the direct observation of silicon release from phytolith dissolution to porewaters early in the season. Further complicating the situation are potential silicon inputs to porewaters from biogenic and pedogenic sources in soils. In the future, water-extractable silicon should be obtained from soils and analyzed to identify the importance of these inputs to soil porewaters at the catchment.

Table 3.4 Seasonal silicon concentrations for soil porewaters sampled from southern planar and south swale ridge top, mid slope, and valley floor locations

Location	May Average [Si] (μM)	June Average [Si] (μM)	July Average [Si] (μM)
Southern Planar Ridge Top	115 \pm 5	104 \pm 9	134 \pm 8
Southern Planar Mid Slope	147 \pm 8	149 \pm 14	214 \pm 37
Southern Planar Valley Floor	134 \pm 13	106 \pm 7	151 \pm 22
South Swale Ridge Top	110 \pm 13	110 \pm 16	110 \pm 16
South Swale Mid Slope	103 \pm 3	108 \pm 2	114 \pm 3
South Swale Valley Floor	146 \pm 8	149 \pm 10	160 \pm 10

Table 3.5 Seasonal Ge/Si ratios for soil porewaters sampled from southern planar and south swale ridge top, mid slope, and valley floor locations.

Location	May Average Ge/Si ($\mu\text{M}/\text{M}$)	June Average Ge/Si ($\mu\text{M}/\text{M}$)	July Average Ge/Si ($\mu\text{M}/\text{M}$)
Southern Planar Ridge Top	2.9 \pm 0.05	3.4 \pm 0.08	3.6 \pm 0.40
Southern Planar Mid Slope	1.3 \pm 0.20	1.6 \pm 0.16	2.7 \pm 0.54
Southern Planar Valley Floor	1.4 \pm 0.23	1.6 \pm 0.17	1.9 \pm 0.25
South Swale Ridge Top	1.8	2.3 \pm 0.26	2.6 \pm 0.10
South Swale Mid Slope	1.0 \pm 0.13	1.2 \pm 0.10	1.2 \pm 0.12
South Swale Valley Floor	1.9	1.2 \pm 0.13	1.8 \pm 0.29

* Error bars are excluded from locations where only one porewater Ge/Si ratio was measured.

Table 3.6 Seasonal germanium concentrations for soil porewaters sampled from southern planar and south swale ridge top, mid slope, and valley floor locations.

Location	May Average [Ge] (pM)	June Average [Ge] (pM)	July Average [Ge] (pM)
Southern Planar Ridge Top	291 ± 30	384 ± 11	445 ± 26
Southern Planar Mid Slope	184 ± 3	222 ± 21	318 ± 30
Southern Planar Valley Floor	168 ± 27	162 ± 19	244 ± 23
South Swale Ridge Top	235	233 ± 17	329 ± 2
South Swale Mid Slope	102 ± 8	130 ± 11	134 ± 12
South Swale Valley Floor	235	155 ± 14	237 ± 27

* Error bars are excluded from locations where only one porewater germanium concentration was measured.

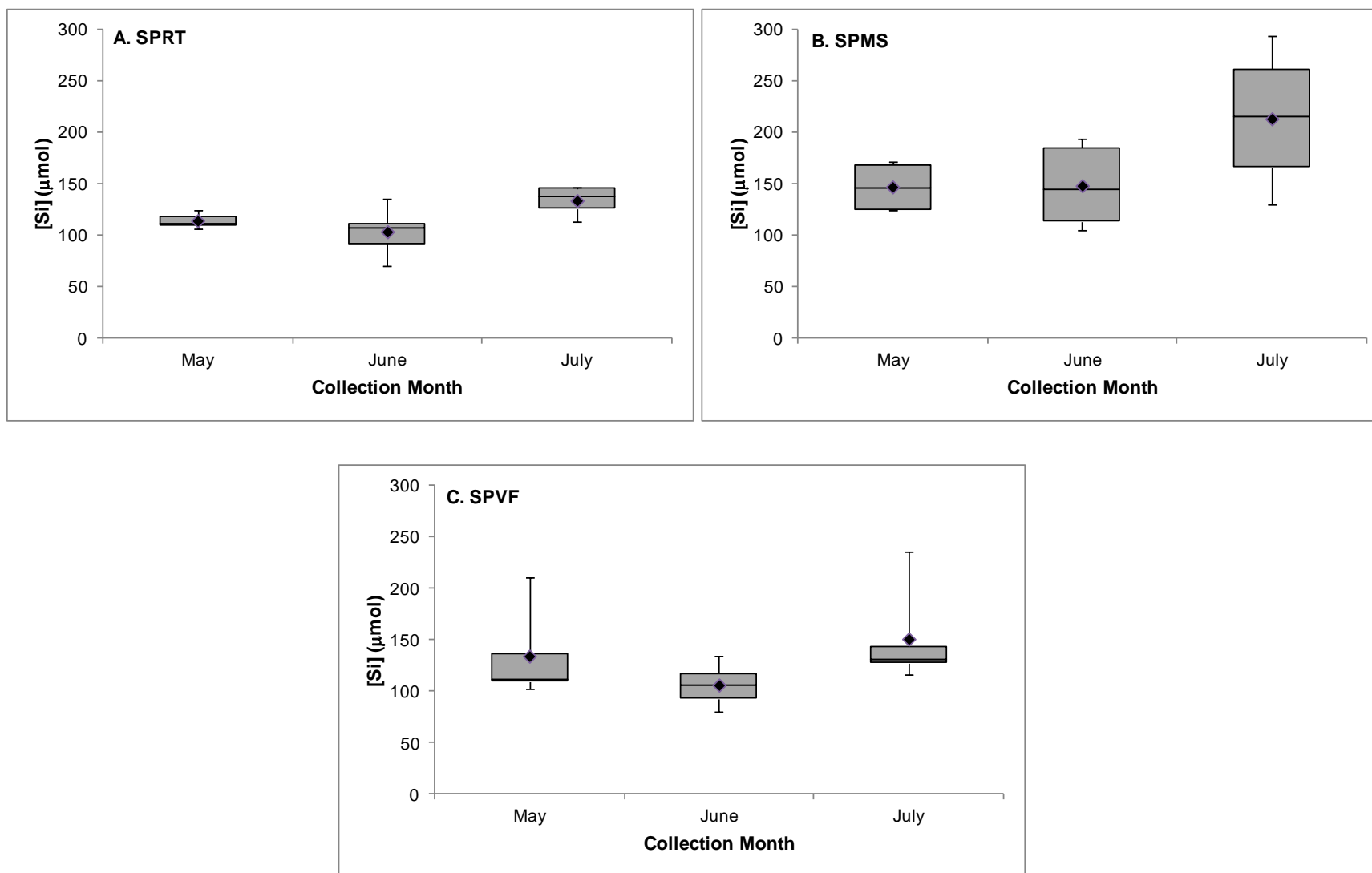


Figure 3.7 Box plots of silicon concentration for southern planar ridge top (SPRT, A), mid slope (SPMS, B), and valley floor (SPVF, C) soil porewaters over the course of the growing season with mean values shown as closed diamonds.

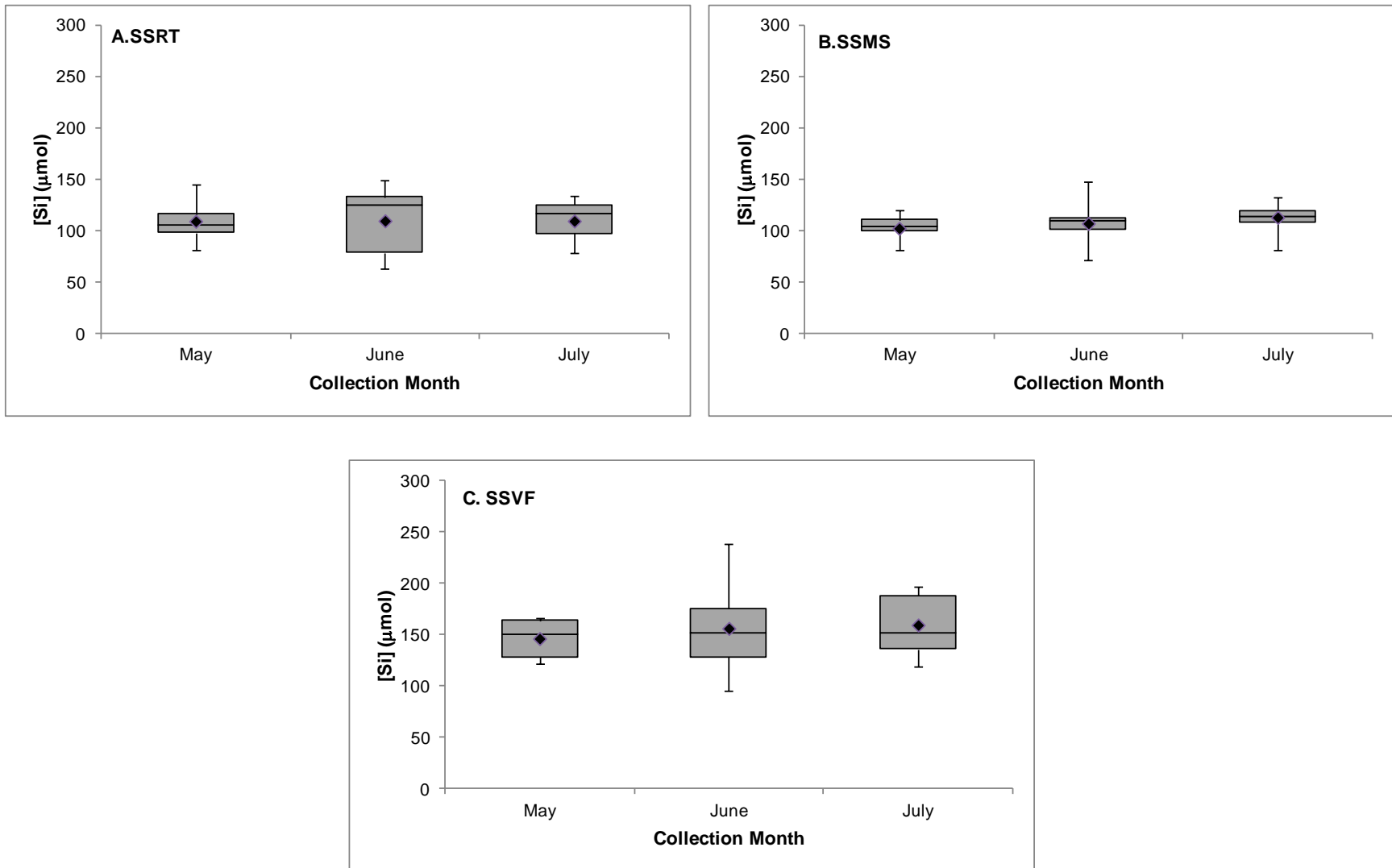


Figure 3.8 Box plots of silicon concentration for south swale ridge top (SSRT, A), mid slope (SSMS, B), and valley floor (SSVF, C) soil porewaters over the course of the growing season with mean values shown as closed diamonds.

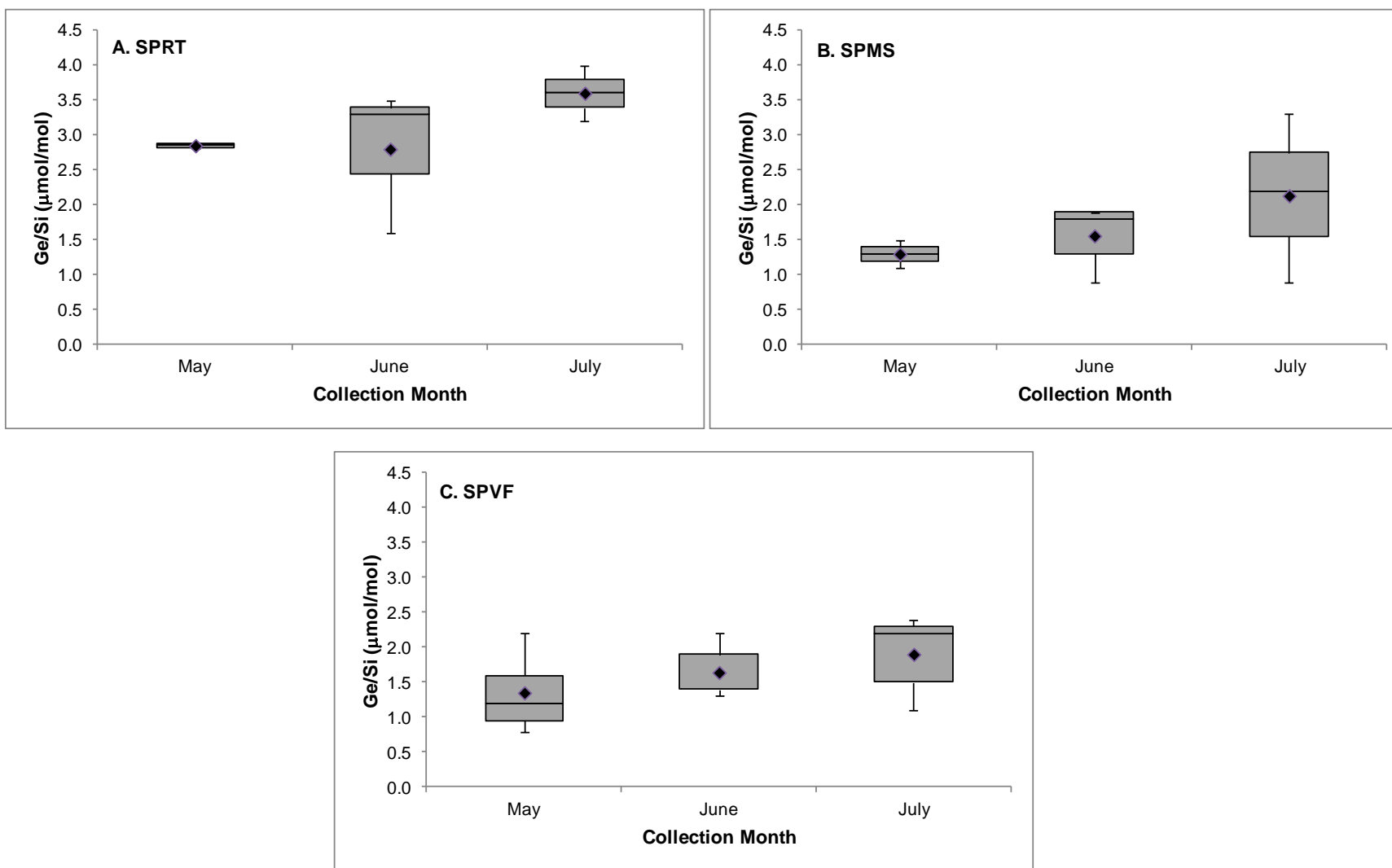


Figure 3.9 Box plots of Ge/Si ratio for southern planar ridge top (SPRT, A), mid slope (SPMS, B), and valley floor (SPVF, C) soil porewaters over the course of the growing season with mean values shown as closed diamonds.

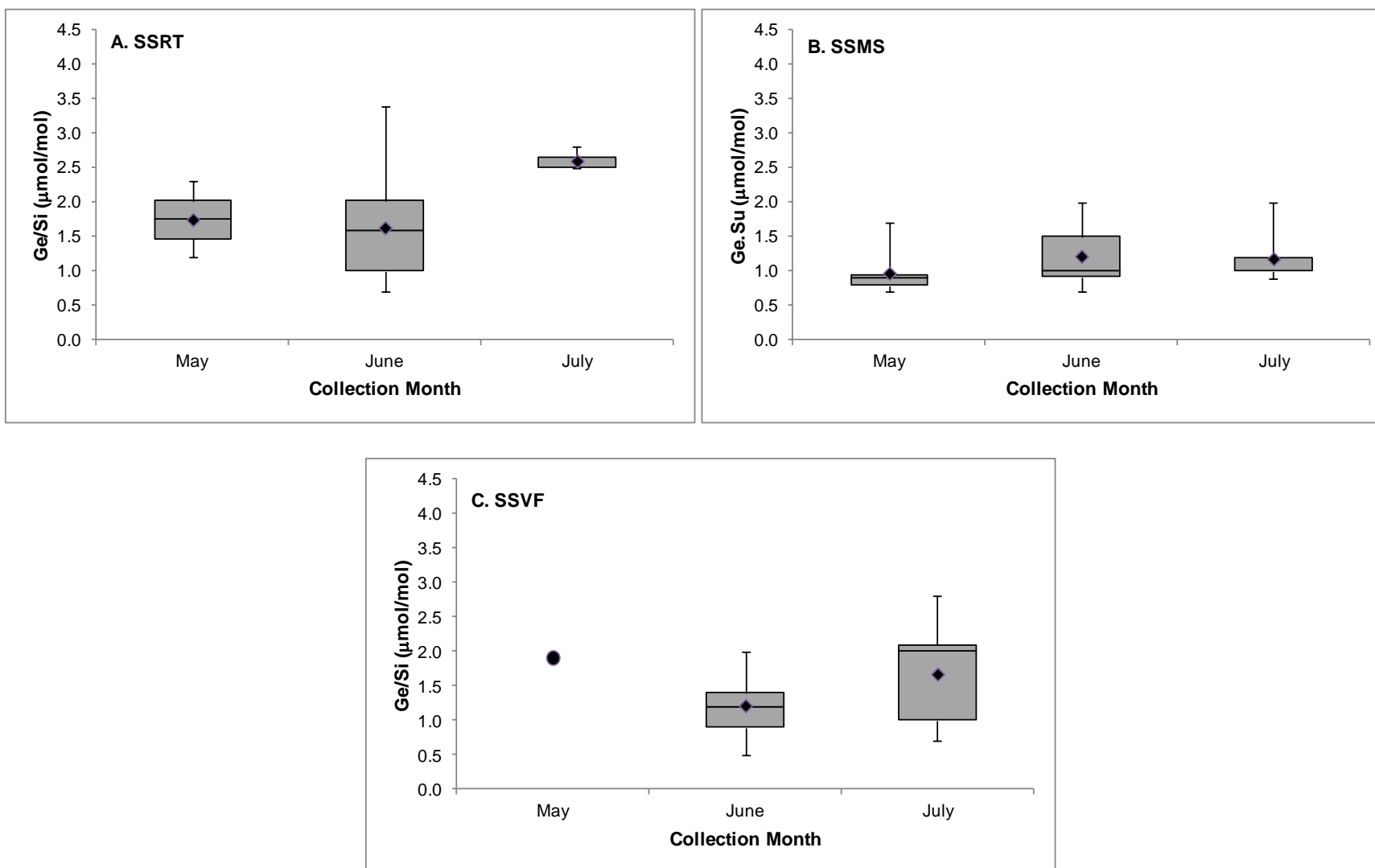


Figure 3.10 Box plots of Ge/Si ratio for south swale ridge top (SSRT, A), mid slope (SSMS, B), and valley floor (SSVF, C) soil porewaters over the course of the growing season with mean values shown as closed diamonds. The Ge/Si ratio measured for a single south swale valley floor porewater collected in May is represented as a closed circle.

3.2 Leaves

Silicon concentrations for sugar maple, chestnut oak, and red oak leaves collected at mid slope positions in northeastern, northwestern, southwestern, and southeastern quadrants of the catchment from June to September of 2013 ranged from 1.04 to 2.53, 0.30 to 1.50, and 0.07 to 0.55 mg/g dry leaf (Table 3.7) respectively, with average values of 1.72 ± 0.07 , 1.00 ± 0.07 , and 0.20 ± 0.02 mg/g dry leaf (Table 3.8), respectively. For sugar maple leaves collected at ridge top, mid slope, and valley floor positions in the northeastern quadrant of the catchment from June to September of 2011, silicon concentrations ranged from 2.38 to 3.03, 1.31 to 2.83, and 2.04 to 2.69 mg/g dry leaf (Table 3.9), respectively, with average values of 2.71 ± 0.33 , 2.05 ± 0.15 , and 2.32 ± 0.09 mg/g dry leaf (Table 3.10), respectively. Chestnut oak leaves sampled from ridge top, mid slope, and valley floor positions in the northeastern quadrant of the catchment from June to September of 2011 had silicon concentrations ranging from 0.59 to 1.86, 1.05 to 2.06, and 0.56 to 1.46 mg/g dry leaf (Table 3.9), respectively, with average values of 1.20 ± 0.12 , 1.37 ± 0.10 , and 0.99 ± 0.08 mg/g dry leaf (Table 3.10), respectively. Composite average silicon concentrations for sugar maple and chestnut oak leaves sampled from all locations in 2011 were 2.21 ± 0.10 and 1.17 ± 0.06 mg/g dry leaf (Table 3.11), respectively. A single red oak leaf collected from the northeastern quadrant in 2011 was found to have a silicon concentration of 0.20 mg/g dry leaf, consistent with the average value obtained for red oak leaves in 2013 (Tables 3.8 and 3.11). Observed silicon concentrations fall within the range of values reported by Herndon (2012) for leaves derived from the same tree species at comparable locations of the catchment. Higher silicon concentrations present in leaf tissue relative to soil porewaters indicate that leaf phytoliths recycle a considerable amount of silicon to soil reservoirs every autumn during leaf fall, particularly those pertaining to sugar maple and chestnut oak species.

While calcium and strontium transport are believed to be largely mediated by passive apoplastic pathways (Clarkson, 1984; White, 2001), recent studies have implicated active symplastic pathways as important transport mechanisms of silicic and germanic acid molecules in plants (Mitani and Ma, 2005; Ma and Yamaji, 2006; Ma et al., 2007; Yamaji et al., 2008; Sparks et al., 2010). To this end, studies have identified aquaporin type influx (e.g. transport from external solution to roots) and efflux (e.g. transport from roots to xylem) transporter genes, *Lsi1* and *Lsi2*, respectively, which are responsible for the transcellular transport of small, uncharged molecules such as water and glycerol in grasses (Mitani and Ma, 2005; Ma and Yamaji, 2006; Ma et al., 2007). Localization of silicon and germanium in grasses has been identified on the proximal side of the cell wall of endodermal cells (Sparks et al., 2010) where *Lsi2* efflux transporter genes are known to reside (Mitani and Ma, 2005; Ma and Yamaji, 2006; Ma et al., 2007). This implies that active symplastic transport mechanisms, mediated by aquaporin type transporter genes, are likely transporting small, uncharged silicic and germanic acid molecules in plants. As an active transport mechanism, the symplastic pathway enables plants to control the rate and selectivity of elements transported through the shoot (Clarkson, 1993; White, 2001). In this way, transport is a plant-controlled process where the plant will expend energy to utilize silicon for a specific purpose. Interestingly, significant differential uptake of silicon relative to germanium was observed for leaves and sap waters at the catchment (Tables 3.7, 3.9 and 3.19, Figure 3.6) which is consistent with findings for plants in other studies (Derry et al., 2005; Garvin, 2006; Blecker et al., 2007; Delvigne et al., 2009; Sparks et al., 2010). As described by Sparks et al. (2010), such large partitioning between silicon and germanium observed in all studies for higher vascular plants to date is best explained by active, plant-mediated transport mechanisms which are highly specific (Clarkson, 1993, White, 2001) rather

than by molecular diffusion processes or energetic differences between amorphous SiO_2 and GeO_2 (Pokrovski and Schott, 1998). However, the importance of passive silicon transport processes should not be overlooked, since a strong positive correlation was observed between transpiration rate and silicon concentration in leaves at the catchment (Figure 3.11) using sap fluxes as proxies for levels of tree transpiration (Granier et al., 1996; Oren et al., 1999; Ewers and Oren, 2000; Pataki and Oren, 2003). Specifically, greater sap fluxes correspond to higher silicon concentrations in sugar maple relative to oak species (Tables 3.8 and 3.11, Figure 3.11). Furthermore, as discussed previously, relatively stable silicon concentrations observed in soil porewaters during the growing season (Table 3.4, Figures 3.7 and 3.8) suggest passive transport mechanisms of silicon (and by inference, germanium) in plants at the catchment. Based on these observations, both active and passive transport mechanisms of silicic and germanic acid molecules are possible in plants at the catchment. The relative importance of each for individual tree species is beyond the scope of this project and requires future research.

Overall, silicon concentrations were higher for leaves sampled from maple species than for those sampled from oak species (Tables 3.8 and 3.11). As shown in Figure 3.11, a strong positive relationship was observed between silicon concentration and tree transpiration as inferred from sap flux data (Meinzer et al., 2013) which is consistent with findings from other studies (Jones and Handreck, 1965). Hence, higher silicon concentrations in maple relative to oak leaves may be due to their higher levels of tree transpiration. Within oak species, average chestnut oak leaf silicon concentrations collected from 2011 and 2013 were found to be 6 and 5 times larger than those observed in red oak leaves, respectively (Tables 3.8 and 3.11). Although higher fractionation factors and Ge/Si ratios in red oak leaves and sap waters suggest less discrimination against germanium relative to silicon during uptake, xylem sapwater silicon

concentrations were only 1.3 times smaller in red oak compared to chestnut oak species (Table 3.20, Figure 3.3). Additionally, sap fluxes were found to be only 1.5 times smaller in red oak relative to chestnut oak trees (Figure 3.11). Thus, the significant discrepancy in leaf silicon concentration between chestnut oak and red oak species cannot be explained by differences in root uptake of silicon or tree transpiration alone. Recently, Yamaji et al. (2008) identified *Lsi6*, an aquaporin transporter gene in roots and shoots of grasses implicated in the transport of silicic acid from the xylem to leaf mesophyll cells. Immobilization of *Lsi6* in cells of root tips as a defense mechanism against stress or suppression of *Lsi6* will alter symplastic transport pathways of silicon from the xylem to leaf mesophyll cells and thus, the distribution of silicon in leaf tissues (Yamaji et al., 2008). Greater incorporation of silicon into leaf tissue by smaller chestnut oak trees, as has been previously noted for nitrogen (Reich et al, 2004), may also be responsible for the higher observed leaf silicon concentrations in chestnut oak relative to red oak trees. Although both hypotheses are seemingly plausible, future research is necessary to adequately evaluate the observed variation in silicon concentration between oak species at the catchment.

Table 3.7 Silicon and germanium elemental concentrations and Ge/Si ratios for chestnut oak (QUPR), red oak (QURU), and sugar maple (ACSA) leaves sampled at mid slope positions in northeastern (NE), northwestern (NW), southeastern (SE), and southwestern (SW) locations of the catchment from June to September of 2013

Sample Date	Sample ID	Species Code	Si (mg/g dry leaf)	Ge (pM/kg)	Ge/Si (μM/M)
6/11/2013	SW 1164	ACSA	1.67	129	0.01
6/11/2013	NW 121	QUPR	0.54	nm	nm
6/12/2013	SE DOWNHILL	ACSA	1.04	243	0.03
6/12/2013	SE UPHILL	ACSA	1.47	189	0.01
6/12/2013	SW 1073	ACSA	1.56	152	0.01
6/12/2013	SE 1266	QUPR	0.30	nm	nm
6/12/2013	SW 1080	QUPR	0.30	nm	nm
6/12/2013	SW 1077	QURU	0.07	493	0.80

6/13/2013	NE 620	ACSA	1.45	nm	nm
6/13/2013	NE 622	QUPR	0.57	90	0.02
6/13/2013	NE 613	QURU	0.07	396	0.65
7/15/2013	NW 121	QUPR	0.98	289	0.03
7/15/2013	NW 102	QURU	0.12	665	0.65
7/15/2013	NW 110	QURU	0.10	672	0.74
7/16/2013	NW 137	ACSA	1.56	583	0.04
7/16/2013	NW UPHILL	ACSA	1.62	939	0.07
7/16/2013	SW 1073	ACSA	1.78	462	0.03
7/16/2013	SW 1164	ACSA	1.89	225	0.01
7/16/2013	SE 1329	QUPR	0.62	148	0.03
7/16/2013	SW 1080	QUPR	0.71	148	0.02
7/16/2013	SW 1170	QUPR	0.80	179	0.02
7/16/2013	SE 1271	QURU	0.13	587	0.51
7/16/2013	SE 1331	QURU	0.12	678	0.65
7/16/2013	SW 1074	QURU	0.14	730	0.60
7/16/2013	SW 1077	QURU	0.14	572	0.46
7/17/2013	NE 620	ACSA	1.55	418	0.03
7/17/2013	NE NO TAG	ACSA	2.18	353	0.02
7/17/2013	SE DOWNHILL	ACSA	1.43	386	0.03
7/17/2013	SE UPHILL	ACSA	1.77	360	0.02
7/17/2013	NE 622	QUPR	1.08	252	0.03
7/17/2013	SE 1266	QUPR	0.80	117	0.02
7/17/2013	NE 613	QURU	0.13	848	0.75
7/17/2013	NE 636	QURU	0.17	977	0.63
8/12/2013	NW 137	ACSA	1.85	531	0.03
8/12/2013	NE DOWNHILL	ACSA	2.53	415	0.02
8/12/2013	SE DOWNHILL	ACSA	1.56	651	0.05
8/12/2013	SE UPHILL	ACSA	1.65	444	0.02
8/12/2013	NE 622	QUPR	1.25	250	0.02
8/12/2013	NE 637	QUPR	1.05	264	0.03
8/12/2013	NW 121	QUPR	1.50	480	0.04
8/12/2013	SE 1329	QUPR	1.36	243	0.02
8/12/2013	NE 636	QURU	0.15	588	0.43
8/12/2013	NW 102	QURU	0.17	1047	0.69
8/12/2013	SE 1331	QURU	0.19	617	0.36
8/13/2013	SW 1073	ACSA	2.35	262	0.01
8/13/2013	SW 1164	ACSA	1.85	409	0.02
8/13/2013	SE 1266	QUPR	1.14	267	0.03
8/13/2013	SW 1080	QUPR	0.87	200	0.03
8/13/2013	SW 1170	QUPR	1.32	313	0.03

8/13/2013	NE 613	QURU	0.21	617	0.33
8/13/2013	NW 110	QURU	0.20	nm	nm
8/13/2013	SE 1271	QURU	0.24	904	0.43
8/13/2013	SW 1074	QURU	0.13	578	0.42
8/13/2013	SW 1077	QURU	0.19	881	0.51
9/27/2013	NE DOWNHILL	ACSA	1.79	590	0.04
9/27/2013	NW DOWNHILL	ACSA	1.84	674	0.04
9/27/2013	NW UPHILL	ACSA	1.33	652	0.06
9/27/2013	SW 1073	ACSA	1.74	870	0.06
9/27/2013	NE 622	QUPR	1.28	313	0.03
9/27/2013	NE 637	QUPR	1.19	394	0.04
9/27/2013	NW 121	QUPR	1.00	428	0.05
9/27/2013	SE 1266	QUPR	1.23	263	0.01
9/27/2013	SE 1329	QUPR	1.49	294	0.02
9/27/2013	SW 1080	QUPR	1.25	171	0.02
9/27/2013	SW 1170	QUPR	1.30	251	0.02
9/27/2013	NE 613	QURU	0.41	2411	0.67
9/27/2013	NE 636	QURU	0.36	1528	0.47
9/27/2013	NW 102	QURU	0.31	nm	nm
9/27/2013	NW 110	QURU	0.55	nm	nm
9/27/2013	SE 1271	QURU	0.30	1345	0.50
9/27/2013	SW 1074	QURU	0.15	nm	nm
9/27/2013	SW 1077	QURU	0.24	nm	nm

*The 'nm' term refers to leaves where germanium concentrations and Ge/Si ratios were not measured.

Table 3.8 Average silicon concentrations and Ge/Si ratios for sugar maple, chestnut oak, and red oak leaves sampled in 2013

Tree Species	Average [Si] (mg/g dry leaf)	Average Ge/Si ($\mu\text{M}/\text{M}$)	DBH (cm)
Sugar Maple	1.72 ± 0.07	0.03 ± 0.004	29.61
Chestnut Oak	1.00 ± 0.07	0.03 ± 0.002	32.92
Red Oak	0.20 ± 0.02	0.56 ± 0.031	41.73

Table 3.9 Silicon and germanium elemental concentrations and Ge/Si ratios for chestnut oak (QUPR), red oak (QURU), and sugar maple (ACSA) leaves sampled at ridge top (RT), mid slope (MS), and valley floor (VF) positions of the northeastern quadrant of the catchment in 2011

Sample Date	Sample ID	Species Code	Position	Si (mg/g dry leaf)	Ge (pM/kg)	Ge/Si ($\mu\text{M}/\text{M}$)
6/9/2011	AS 356	ACSA	MS	1.68	473	0.04
6/9/2011	QP 230	QUPR	RT	0.59	347	0.08
6/14/2011	AS 2061	ACSA	MS	1.31	223	0.02
6/14/2011	QP 358	QUPR	MS	1.05	318	0.07
6/14/2011	QP 358	QUPR	MS	1.05	305	0.04
6/16/2011	AS 352	ACSA	MS	2.10	820	0.05
6/16/2011	QP 351	QUPR	MS	1.12	726	0.09
6/16/2011	QP 351	QUPR	MS	1.12	517	0.06
6/21/2011	AS Near AS 2063	ACSA	MS	2.72	662	0.03
6/21/2011	AS 2062	ACSA	VF	2.19	393	0.03
6/21/2011	QP 333	QUPR	VF	0.68	414	0.09
6/21/2011	QP 340	QUPR	VF	0.56	248	0.06
6/23/2011	QR 325	QURU	MS	0.20	190	0.13
6/24/2011	AS Near QP 347	ACSA	MS	1.39	272	0.03
6/27/2011	AS Near QP 330	ACSA	VF	2.18	308	0.02
6/29/2011	QP 330	QUPR	VF	0.93	305	0.05
7/6/2011	AS 2059	ACSA	RT	2.38	1430	0.08
7/6/2011	AS 2061	ACSA	MS	2.39	692	0.04
7/6/2011	QP 2060	QUPR	MS	2.06	579	0.08
7/6/2011	QP 393	QUPR	RT	1.12	599	0.07
7/6/2011	QP 394	QUPR	RT	1.49	952	0.09
7/6/2011	QP 396	QUPR	RT	0.69	173	0.03
7/7/2011	AS 2063	ACSA	MS	2.27	720	0.04
7/7/2011	AS 352	ACSA	MS	2.83	757	0.04
7/7/2011	QP 347	QUPR	MS	1.50	376	0.04
7/7/2011	QP 347	QUPR	MS	1.35	444	0.04
7/7/2011	QP 351	QUPR	MS	1.38	303	0.03
7/12/2011	AS 2062	ACSA	VF	2.04	392	0.03
7/12/2011	AS 2064	ACSA	VF	2.22	678	0.04
7/12/2011	AS 2067	ACSA	VF	2.61	171	0.01
7/12/2011	QP 330	QUPR	VF	0.78	388	0.07

7/12/2011	QP 340	QUPR	VF	0.78	475	0.09
7/14/2011	AS 387	ACSA	MS	1.68	479	0.04
7/14/2011	QP 1219	QUPR	VF	1.45	246	0.02
7/14/2011	QP 390	QUPR	VF	1.02	540	0.07
7/19/2011	QP 1219	QUPR	VF	1.09	327	0.04
7/19/2011	QP 230	QUPR	RT	1.07	270	0.02
7/20/2011	QP 230	QUPR	RT	1.60	698	0.06
8/5/2011	QP 330	QUPR	VF	1.06	484	0.06
8/5/2011	QP 394	QUPR	RT	1.12	655	0.08
8/30/2011	AS 352	ACSA	MS	2.32	581	0.04
8/30/2011	AS 356	ACSA	MS	1.86	553	0.04
8/30/2011	QP 2060	QUPR	MS	1.74	953	0.08
8/30/2011	QP 230	QUPR	RT	1.32	335	0.04
8/30/2011	QP 351	QUPR	MS	1.34	832	0.08
9/13/2011	AS 2064	ACSA	VF	2.69	517	0.05
9/13/2011	AS 2065	ACSA	VF	2.32	961	0.06
9/13/2011	QP 330	QUPR	VF	1.06	542	0.07
9/13/2011	QP 332	QUPR	VF	1.01	638	0.09
9/13/2011	QP 394	QUPR	RT	1.86	514	0.04
9/13/2011	QP 396	QUPR	RT	1.12	781	0.10
9/13/2011	QP 1219	QUPR	VF	1.46	272	0.03
9/20/2011	AS 2059	ACSA	RT	3.03	1351	0.06

Table 3.10 Average silicon concentrations for sugar maple and chestnut oak leaves sampled at ridge top, mid slope, and valley floor positions of the northeastern quadrant of the catchment in 2011

Tree Species	Ridge Top Average [Si] (mg/g dry leaf)	Mid Slope Average [Si] (mg/g dry leaf)	Valley Floor Average [Si] (mg/g dry leaf)
Sugar Maple	2.71 ± 0.33	2.05 ± 0.15	2.32 ± 0.09
Chestnut Oak	1.20 ± 0.12	1.37 ± 0.10	0.99 ± 0.08

Table 3.11 Average silicon concentrations and Ge/Si ratios for sugar maple, chestnut oak, and red oak leaves sampled in 2011

Tree Species	Average [Si] (mg/g dry leaf)	Average Ge/Si ($\mu\text{M}/\text{M}$)	DBH (cm)
Sugar Maple	2.21 ± 0.10	0.04 ± 0.004	29.61
Chestnut Oak	1.17 ± 0.06	0.06 ± 0.004	32.92
Red Oak	0.20	0.13	41.73

* Error bars are excluded from tree species where only one leaf silicon concentration or Ge/Si ratio was measured.

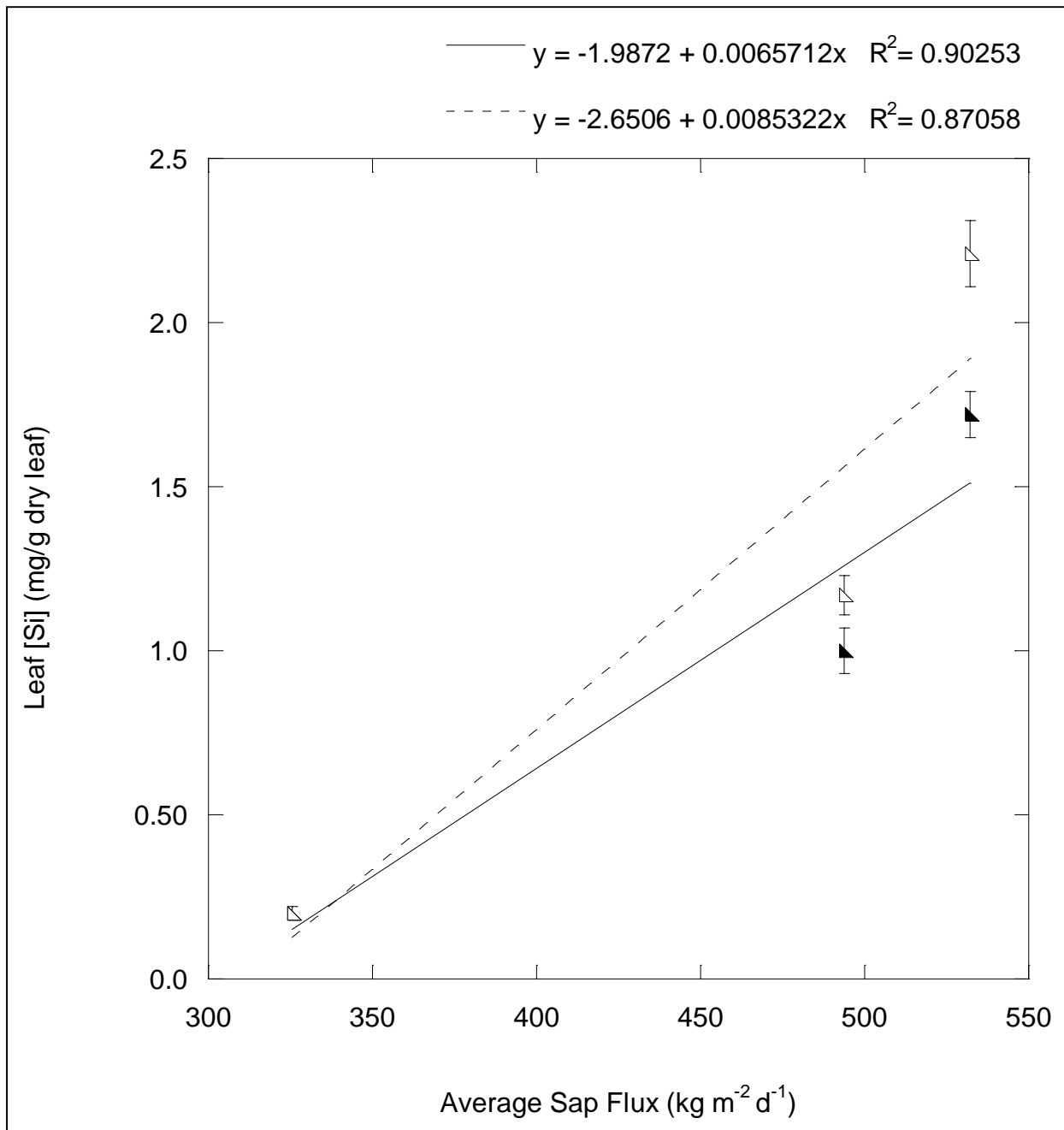


Figure 3.11 Average leaf silicon concentration versus average sap flux for leaves sampled at the catchment. Dashed and solid lines connect average silicon concentrations for leaves sampled in 2011 (open triangles) and 2013 (closed triangles), respectively, with error bars shown for average values. Average sap flux values were determined using information contained within Meinzer et al. (2013).

As shown in Tables 3.8 and 3.11 and in Figure 3.12, an inverse relationship was observed between average silicon concentration and diameter at breast height (DBH) for leaves sampled at mid slope positions in 2011 and 2013. Larger oak trees displayed lower overall leaf silicon concentrations than smaller maple trees. A similar pattern between average silicon concentration and DBH was found by Garvin (2006) for leaves in a similar canopy setting. The higher transpiration rates per unit area mentioned earlier (Figure 3.11), characteristic of smaller trees (Garvin, 2006), and the greater allocation of silicon into leaf tissue by smaller, less mature maple trees, as has previously been noted for nitrogen (Reich et al., 2004), are possible explanations for the higher silicon concentrations in maple relative to oak leaves at the catchment. According to Dawson (1993, 1996) and Garvin (2006), small maple trees with shallow root systems are usually limited to nutrients from shallow porewater reservoirs, while large oak trees with deeper tap roots can acquire nutrients from both shallow porewater and deep porewater/groundwater reservoirs. However, as mentioned in Chapter 2, trees analyzed in this study are hypothesized to be largely acquiring water (and hence, solutes) from shallow soil exchange pool and soil porewater sources. To this end, average xylem stem water $\delta^{18}\text{O}$ values (Gregor, unpublished data) for sugar maple ($\delta^{18}\text{O} = -7.59 \text{ ‰}$) and oak ($\delta^{18}\text{O} = -7.65 \text{ ‰}$) trees were found to more closely resemble underlying shallow soils (Average $\delta^{18}\text{O} = -6.47 \text{ ‰}$ and -6.57 ‰ for shallow soils underlying sugar maple and oak species, respectively, Gregor, unpublished data) than groundwaters (Average $\delta^{18}\text{O} = -8.82 \text{ ‰}$, Thomas, 2013). Hence, observed variation in silicon concentration between smaller maple and larger oak trees is unlikely due to different sources from which these species are acquiring silicon.

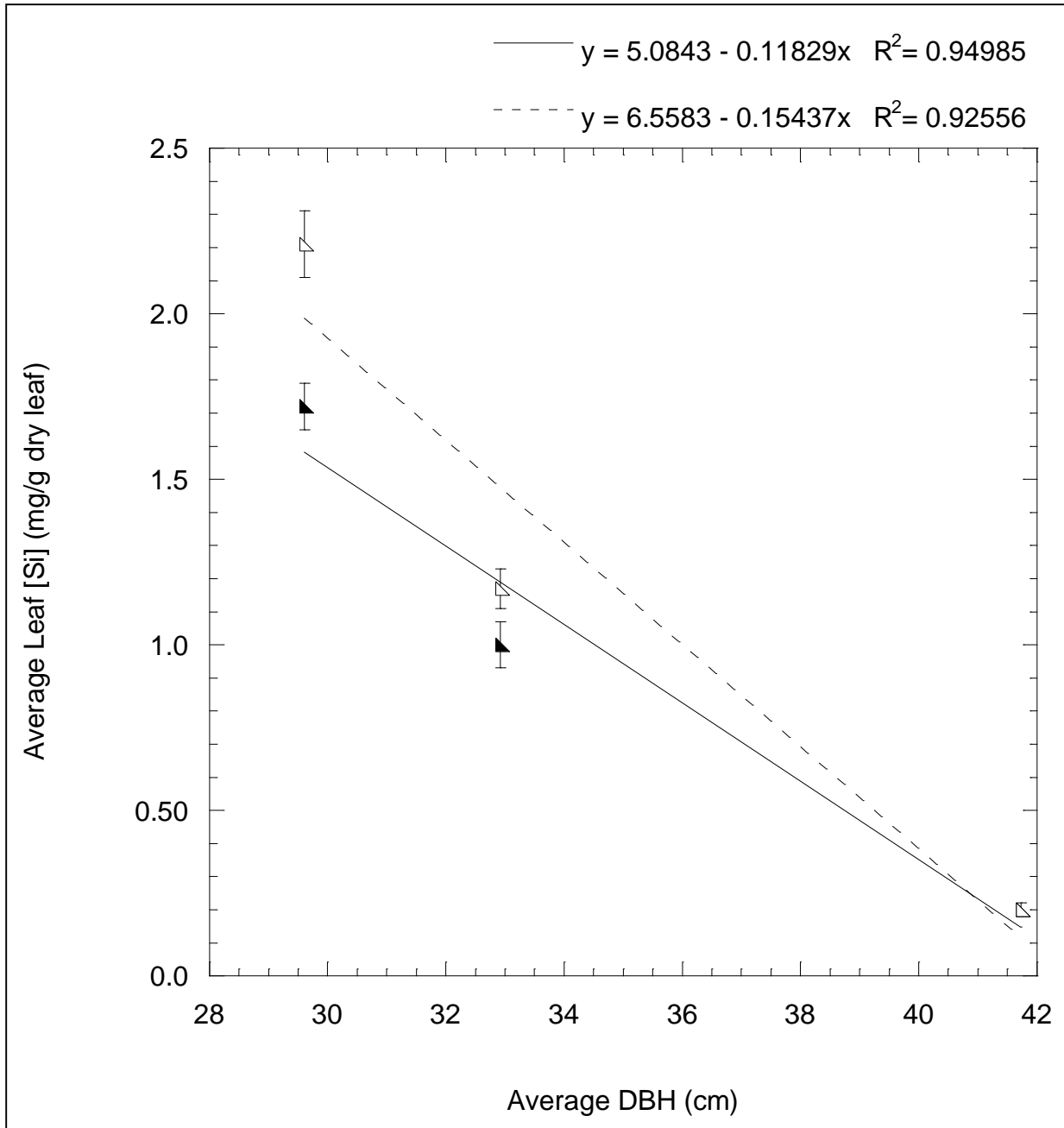


Figure 3.12 Average silicon concentration versus average diameter at breast height (DBH) for leaves sampled at the catchment. Dashed and solid lines connect average silicon concentrations for leaves sampled in 2011 (open triangles) and 2013 (closed triangles), respectively, with error bars shown for average values. Average DBH values were derived from Wubbels (2010).

In 2011, sugar maple and chestnut oak trees sampled at mid slope positions in the northeastern quadrant were shown to accumulate more silicon in leaf tissue than trees sampled from the same species at these locations in 2013 (Figure 3.13). Specifically, average leaf silicon concentrations for sugar maple and chestnut oak tree species were observed to be 0.49 and 0.20 mg/g dry leaf higher over the course of the growing season in 2011 than in 2013, respectively. Such variation may reflect differences in porewater chemistry at Shale Hills between 2011 and 2013. As soil porewaters were not sampled in 2011, this hypothesis cannot be tested at the present time. It should be noted that, although from the same species, leaves sampled in 2011 were derived from different individual trees than those sampled in 2013. Variation in silicon concentrations may simply reflect sampling inconsistencies between 2011 and 2013.

Interestingly, lower calcium concentrations were also found for leaves sampled from the same tree species in the northeastern quadrant in 2011 compared to 2013 (Table 2.9, Figure 2.18). As mentioned in Chapter 2, Ma and Takahashi (1993) and Brackhage et al. (2013) observed a negative correlation between leaf silicon and calcium concentration where silicon accumulation led to lower calcium concentrations in leaf tissue, on average. Hence, competition between calcium and silicon is possible in plants at the catchment where the transport of silicon is presumably favored over calcium due to lower energy demands involving uptake, polymerization, and distribution of silicon relative to calcium on plant membranes and cell wall matrices (Ma and Takahashi, 1993; Brackhage et al., 2013).

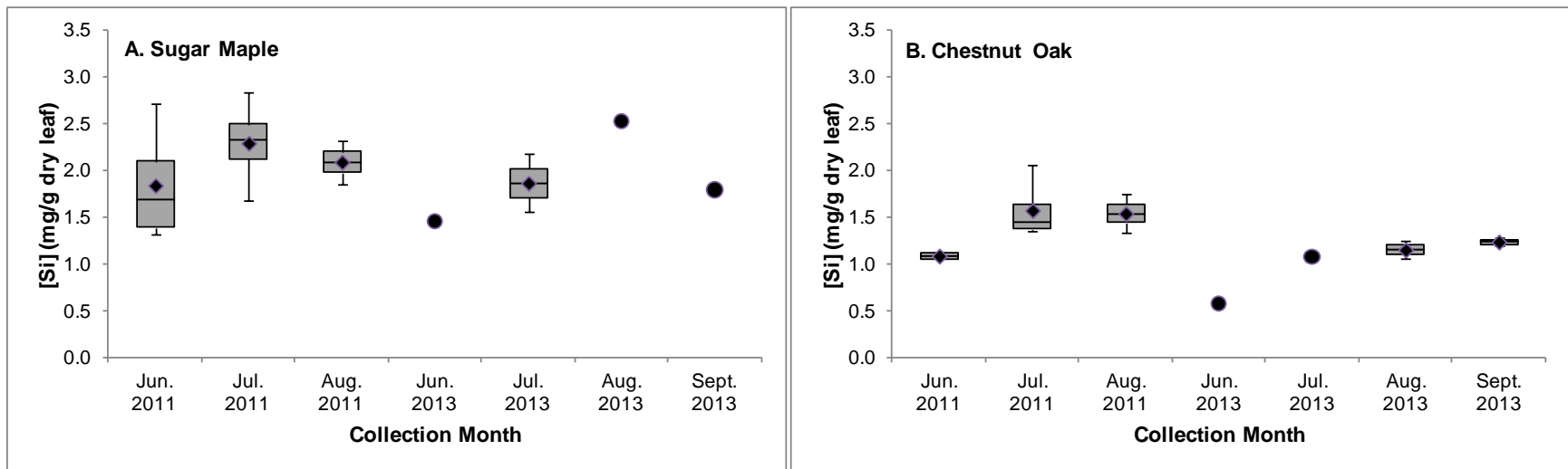


Figure 3.13 Box plots of silicon concentration for sugar maple (A) and chestnut oak (B) leaves sampled at mid slope positions of the northeastern quadrant in June to August of 2011 and in June to September of 2013 with mean values shown as closed diamonds. Single silicon measurements for sugar maple leaves collected in June, August, and September of 2013 and for chestnut oak leaves collected in June and July of 2013 are represented as closed circles.

A wide range of silicon concentrations occurred within each tree species. Seasonality (Tables 3.12 and 3.13, Figures 3.13 to 3.15) as opposed to sampling location (Tables 3.10 and 3.14, Figure 3.16 and 3.17) across the catchment contributed to variation in silicon concentration within each tree species in 2013. For sugar maple leaves sampled in 2013, average silicon concentrations increased from June to July to August before decreasing from August to September. Alternating increasing/decreasing patterns in silicon concentration were observed between June and July, July and August, and August and September for sugar maple leaves sampled in 2011. Oak leaves displayed monthly increases in average silicon concentration in 2011 and 2013. Accumulation of silicon in leaf tissue over the course of the growing season is consistent with findings by other studies for higher plants conducted in similar canopy settings (Garvin, 2006). Garvin (2006) and Carnelli et al. (2001) have attributed these monthly increases to constant inputs from waters transporting silicon to leaves by means of the transpiration pathway. This is reasonable considering silicon's nature as an uncharged molecule (silicic acid, H_4SiO_4) where its translocation in plant tissue is more dependent on the transpiration stream than other chemical species (Jones and Handreck, 1969). Complementing this are enhanced levels of evapotranspiration over the course of the growing season, as inferred from shallow soil water $\delta^{18}\text{O}$ and $\delta^2\text{H}$ values (Gregor, unpublished data), which facilitate transpiration processes, and hence the preferential uptake of silicon over germanium from porewater reservoirs by plants at the catchment. Additionally, silicon concentrations generally increase with leaf age as silicon cannot be remobilized for retranslocation to other plant tissues once deposited in leaves (Tanaka and Park, 1966; Jones and Handreck, 1969; Jarvis, 1987; Marschner, 1995; de Bakker et al., 1999; Ma and Yamaji, 2006). Thus, monthly increases in silicon concentration may be attributed to maturation of leaves over the course of the growing season. Lower silicon levels in sugar

maple leaves sampled in September compared to August of 2013 and in August compared to July of 2011 may be the result of early leaf fall where biogenic silicon is recycled to soil reservoirs. This hypothesis cannot be tested at the current time as dry conditions at the catchment prevented collection of porewaters during these months of the year.

Table 3.12 Seasonal silicon concentrations for sugar maple, chestnut oak, and red oak leaves sampled at mid slope positions in the northeastern, northwestern, southeastern, and southwestern quadrants of the catchment in 2013

Tree Species	June Average [Si] (mg/g dry leaf)	July Average [Si] (mg/g dry leaf)	August Average [Si] (mg/g dry leaf)	September Average [Si] (mg/g dry leaf)
<i>Northeast</i>				
Sugar Maple	1.45	1.87 ± 0.32	2.53	1.79
Chestnut Oak	0.57	1.08	1.15 ± 0.10	1.24 ± 0.05
Red Oak	0.07	0.15 ± 0.02	0.18 ± 0.03	0.39 ± 0.03
<i>Northwest</i>				
Sugar Maple	nm	1.59 ± 0.03	1.85	1.59 ± 0.26
Chestnut Oak	0.54	0.98	1.5	1.0
Red Oak	nm	0.11 ± 0.01	0.19 ± 0.02	0.43 ± 0.12
<i>Southeast</i>				
Sugar Maple	1.26 ± 0.22	1.60 ± 0.17	1.61 ± 0.05	nm
Chestnut Oak	0.30	0.71 ± 0.09	1.25 ± 0.11	1.36 ± 0.13
Red Oak	nm	0.13 ± 0.01	0.22 ± 0.03	0.3
<i>Southwest</i>				
Sugar Maple	1.62 ± 0.06	1.84 ± 0.06	2.10 ± 0.25	1.74
Chestnut Oak	0.30	0.76 ± 0.05	1.10 ± 0.23	1.28 ± 0.03
Red Oak	0.07	0.14 ± 0.00	0.16 ± 0.03	0.20 ± 0.05
<i>All Locations</i>				
Sugar Maple	1.44 ± 0.10	1.73 ± 0.08	2.03 ± 0.20	1.71 ± 0.06
Chestnut Oak	0.43 ± 0.07	0.88 ± 0.09	1.25 ± 0.09	1.22 ± 0.08
Red Oak	0.07 ± 0.00	0.13 ± 0.01	0.19 ± 0.01	0.33 ± 0.05

*The 'nm' term refers to months when silicon concentrations were not measured for a designated leaf sample.

*Error bars are excluded from species where only one leaf was collected during a given month.

Table 3.13 Seasonal silicon concentrations for sugar maple and chestnut oak leaves sampled at ridge top, mid slope, and valley floor positions of the northeastern quadrant in 2011

Tree Species	June Average [Si] (mg/g dry leaf)	July Average [Si] (mg/g dry leaf)	August Average [Si] (mg/g dry leaf)	September Average [Si] (mg/g dry leaf)
<i>Ridge Top</i>				
Sugar Maple	nm	2.38	nm	3.03
Chestnut Oak	0.59	1.19 ± 0.16	1.22 ± 0.10	1.49 ± 0.37
<i>Mid Slope</i>				
Sugar Maple	1.84 ± 0.26	2.29 ± 0.24	2.09 ± 0.23	nm
Chestnut Oak	1.09 ± 0.02	1.57 ± 0.17	1.54 ± 0.20	nm
<i>Valley Floor</i>				
Sugar Maple	2.19 ± 0.01	2.29 ± 0.17	nm	2.51 ± 0.19
Chestnut Oak	0.72 ± 0.11	1.02 ± 0.12	1.06	1.18 ± 0.14
<i>All Locations</i>				
Sugar Maple	2.02 ± 0.18	2.32 ± 0.03	2.09	2.77 ± 0.26
Chestnut Oak	0.80 ± 0.15	1.26 ± 0.16	1.27 ± 0.14	1.34 ± 0.16

*The 'nm' term refers to months when silicon concentrations were not measured for a designated leaf sample.

*Error bars are excluded from species where only one leaf was collected during a given month.

Table 3.14 Average silicon concentrations for sugar maple, chestnut oak, and red oak leaves sampled at mid slope positions in northeastern (NE), northwestern (NW), southeastern (SE), and southwestern (SW) quadrants of the catchment in 2013

Location	Sugar Maple Average [Si] (mg/g dry leaf)	Chestnut Oak Average [Si] (mg/g dry leaf)	Red Oak Average [Si] (mg/g dry leaf)
NE	1.90 ± 0.20	1.07 ± 0.11	0.21 ± 0.05
NW	1.64 ± 0.10	1.01 ± 0.20	0.24 ± 0.07
SE	1.49 ± 0.10	0.99 ± 0.16	0.20 ± 0.03
SW	1.83 ± 0.10	0.94 ± 0.14	0.15 ± 0.02

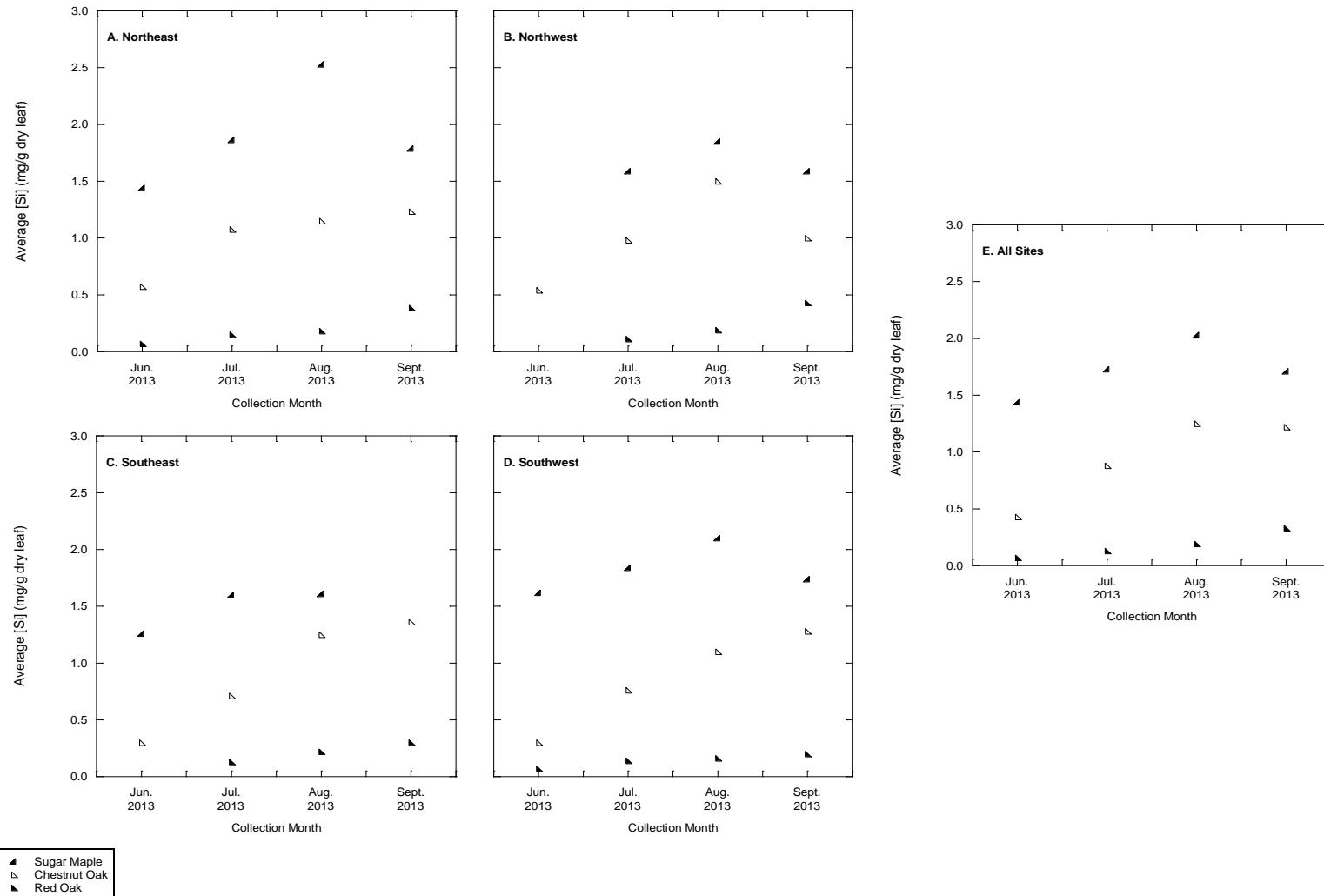


Figure 3.14 Seasonal silicon concentrations for sugar maple, chestnut oak, and red oak leaves sampled in 2013 at mid slope positions in northeastern (A), northwestern (B), southeastern (C), and southwestern (D) quadrants as well as for all quadrants (E) of the catchment.

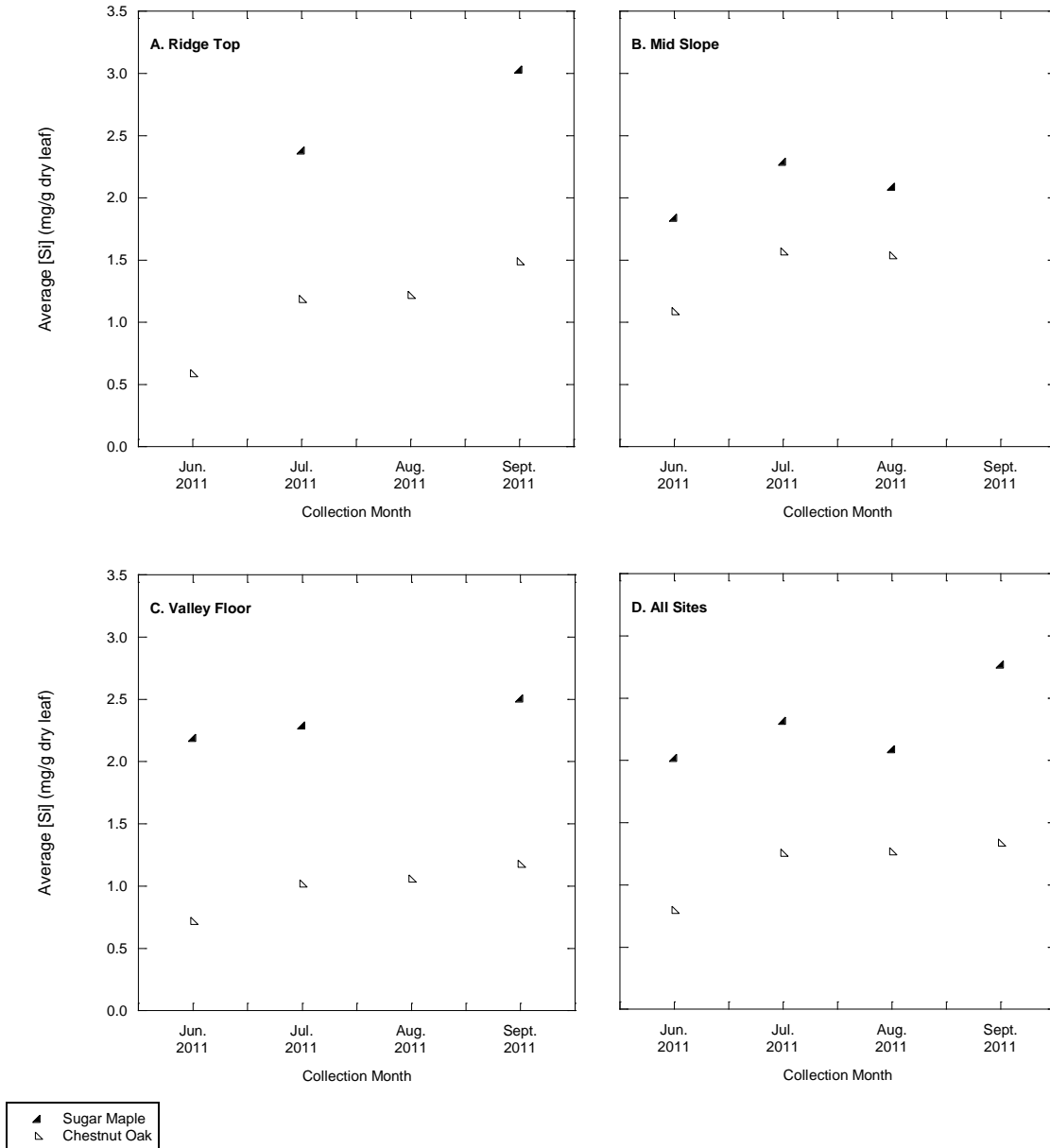


Figure 3.15 Seasonal silicon concentrations for sugar maple and chestnut oak leaves sampled in 2011 at ridge top (A), mid slope (B), and valley floor (C) locations of the northeastern quadrant. Sugar maple and chestnut oak leaf seasonal silicon concentrations for all northeastern positions (D) are also shown.

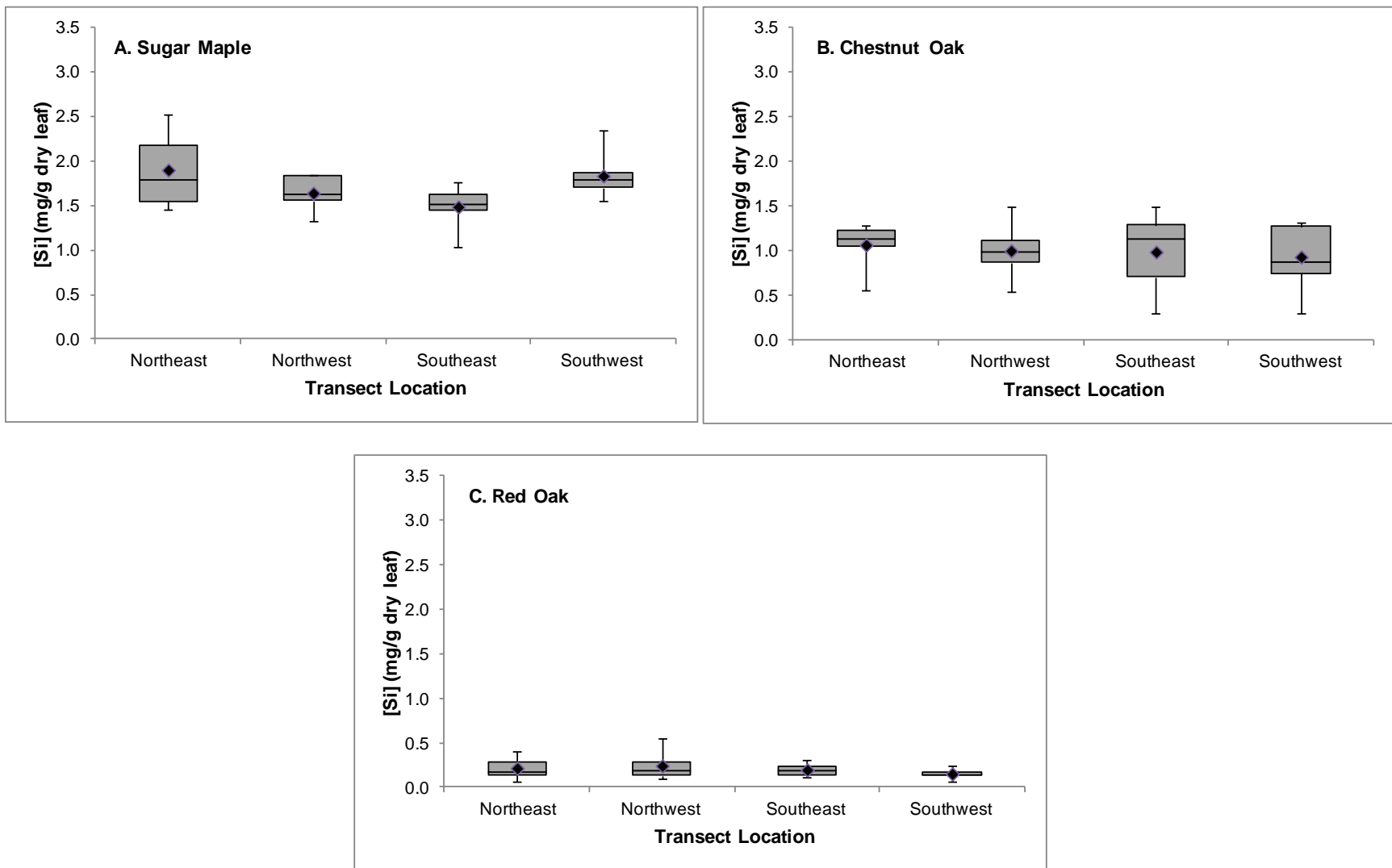


Figure 3.16 Box plots of silicon concentration based on sampling location for sugar maple (A), chestnut oak (B), and red oak (C) leaves sampled at mid slope positions in northeastern, northwestern, southeastern, and southwestern quadrants in 2013 with mean values shown as closed diamonds.

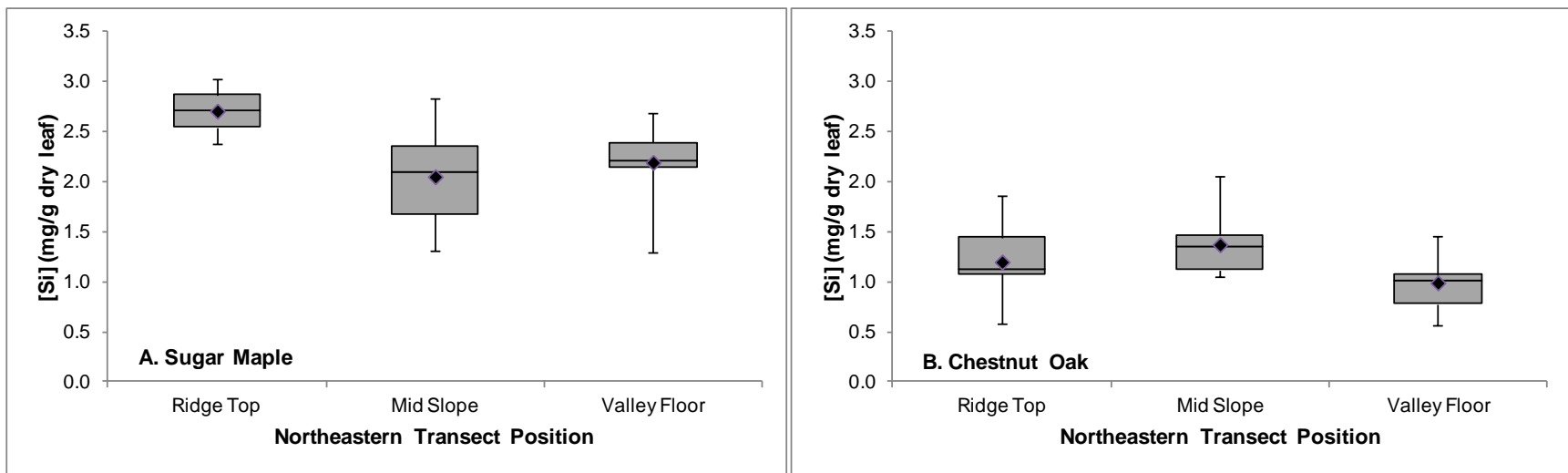


Figure 3.17 Box plots of silicon concentration based on sampling position for sugar maple (A) and chestnut oak (B) leaves sampled at ridge top, mid slope, and valley floor positions of the northeastern quadrant of the catchment in 2011 with mean values shown as closed diamonds.

On the other hand, average silicon concentrations did not change significantly based on sampling location at the catchment. As shown in Table 3.14 and in Figure 3.16, average silicon concentrations for chestnut oak and red oak leaves sampled at mid slope positions in 2013 were rather uniform across the catchment. Based on transect location, slight deviations were observed from average silicon concentrations of 1.00 and 0.20 mg/g dry leaf for chestnut and red oak leaves, respectively. However, sugar maple leaves exhibited greater variability in silicon concentration based on sampling location with leaves sampled at southwestern and northeastern locations shown to accumulate more silicon than corresponding leaves sampled at northwestern and southeastern locations, on average (Table 3.14, Figure 3.16). In studies at Shale Hills, Meinzer et al. (2013) demonstrated that transpiration rates in diffuse-porous maple species were responsive to fluctuations in soil moisture (e.g. isohydric), while ring porous oak species were shown to be relatively unaffected by soil moisture content (e.g. anisohydric) which is consistent with findings from other studies (Abrams, 1990; Tardieu and Simonneau, 1998; Ewers et al., 2007; McDowell, 2011). As depicted in Figure 3.11, leaf silicon concentration was shown to be dependent on levels of tree transpiration according to sap flux estimates (Meinzer et al., 2013) and leaf silicon concentrations for plants at the catchment. Thus, variation in levels of evapotranspiration as a result of the isohydric behavior in diffuse-porous maple species may be contributing to larger differences in silicon concentration for sugar maple leaves based on sampling location. In fact, $\delta^{18}\text{O}$ and $\delta^2\text{H}$ values in shallow soil waters indicated higher levels of evapotranspiration at southwestern locations followed by northeastern, northwestern, and southeastern locations. Specifically, $\delta^{18}\text{O}$ and $\delta^2\text{H}$ values in shallow soil water increased from -6.72 and -51.44 ‰ to -5.96 and -47.55 ‰ to -5.90 and -44.15 ‰ to -5.47 and -42.38 ‰ (Gregor, unpublished data) from southeastern to northwestern to northeastern to southwestern locations,

respectively, with higher values indicating higher levels of evapotranspiration (Hsieh et al., 1998). Indeed, quadrant locations with the highest levels of evapotranspiration, as inferred from shallow soil water $\delta^{18}\text{O}$ and $\delta^2\text{H}$ values (e.g. the southwestern and northeastern quadrants), were observed to have the highest silicon concentrations in sugar maple leaves (Table 3.14, Figure 3.16).

Furthermore, average silicon concentration was shown to vary based on sampling position for sugar maple and chestnut oak leaves sampled at ridge top, mid slope, and valley floor positions of the northeastern quadrant in 2011 (Table 3.10, Figure 3.17). For chestnut oak leaves, average silicon concentration increased slightly from ridge top to mid slope locations and then decreased from mid slope to valley floor locations. Average silicon concentration for sugar maple leaves decreased from ridge top to mid slope locations and then increased slightly from mid slope to valley floor locations. Patterns in silicon concentration observed for sugar maple leaves sampled at various positions of the northeastern quadrant conflict with those observed for shallow porewaters sampled at depths of ≤ 20 cm at the nearby north swale location (Herndon, 2012). According to Herndon (2012), north swale porewater average silicon concentrations increased from ridge top to mid slope locations and then decreased from mid slope to valley floor locations. As mentioned earlier, variation in levels of evapotranspiration as a result of the isohydric behavior in diffuse-porous maple species (Meinzer et al., 2013) may be resulting in the observed discrepancy in silicon concentration between sugar maple leaves and soil porewaters. Furthermore, studies at Shale Hills (Jin et al., 2011b; Takagi and Lin, 2012) have shown that topographic position is an important criterion in determining soil moisture content where increases in soil moisture are observed downslope as soils thicken. Considering fluctuations in tree transpiration occur at different sampling locations as a result of variability in soil moisture

content, spatial patterns in silicon concentration for sugar maple leaves need not necessarily reflect those for soil porewaters.

Sugar maple leaf Ge/Si ratios ranged from 0.06 to 0.08, 0.02 to 0.05, and 0.01 to 0.06 $\mu\text{M}/\text{M}$ (Table 3.9), respectively, with average values of 0.07 ± 0.010 , 0.04 ± 0.002 , and 0.03 ± 0.006 $\mu\text{M}/\text{M}$ (Table 3.15) at ridge top, mid slope, and valley floor locations of the northeastern quadrant in 2011, respectively. For chestnut oak leaves collected at ridge top, mid slope, and valley floor locations in the northeastern quadrant of the catchment in 2011, Ge/Si ratios ranged from 0.02 to 0.10, 0.03 to 0.09, and 0.02 to 0.09 $\mu\text{M}/\text{M}$ (Table 3.9), respectively, with an average value of 0.06 ± 0.01 $\mu\text{M}/\text{M}$ (Table 3.15) determined for all locations sampled. Collectively, Ge/Si ratios for sugar maple and chestnut oak leaves sampled from all locations were 0.04 ± 0.004 and 0.06 ± 0.004 $\mu\text{M}/\text{M}$, respectively (Table 3.11). Additionally, a Ge/Si ratio of 0.13 $\mu\text{M}/\text{M}$ was obtained for a single red oak leaf collected at a mid slope location in the northeastern quadrant of the catchment in 2011 (Tables 3.9 and 3.11). Average Ge/Si ratios for sugar maple, chestnut oak, and red oak leaves sampled at mid slope positions in all quadrants of the catchment in 2013 ranged from 0.01 to 0.07, 0.01 to 0.05, and 0.33 to 0.80 $\mu\text{M}/\text{M}$ (Table 3.7), respectively, with average values of 0.03 ± 0.004 , 0.03 ± 0.002 , and 0.56 ± 0.031 $\mu\text{M}/\text{M}$ (Table 3.8, Figure 3.6), respectively.

Leaf Ge/Si ratios at Shale Hills fall within the range of values reported by Garvin (2006) for sugar maple species in a comparable deciduous canopy setting in Vermont. Significantly lower average leaf Ge/Si ratios compared to porewaters, groundwaters, and streamwaters were found for all tree species. To this end, fractionation factors were calculated via Equation 9 using Ge/Si ratios for leaves and shallow soil porewaters (at depths of ≤ 20 cm) collected in southern quadrants of the catchment. Fractionation factors were found to be less than one for all species

suggesting discrimination against germanium relative to silicon in plants at the catchment. Specifically, red oak leaves in southwestern and southeastern quadrants were shown to have higher average fractionation factors (0.28 and 0.25, respectively) and discriminate to a lesser degree against germanium than sugar maple (0.01 and 0.01, respectively) and chestnut oak (0.01 and 0.01, respectively) leaves. High silicon concentrations and low Ge/Si ratios for leaves studied at Shale Hills agree with observations for leaf phytoliths collected from a wide range of vascular plant species throughout the United States including in Hawaii (Derry et al., 2005), Kansas (Blecker, 2005), and Vermont (Garvin, 2006). Thus, recycling of these phytoliths into soil reservoirs should produce a low Ge/Si, high silicon source for porewaters and streamwaters at the catchment.

Average Ge/Si ratios were slightly lower for sugar maple and chestnut oak leaves sampled at mid slope positions of the northeastern quadrant in 2013 than in 2011 (Tables 3.15 and 3.16). As shown in Tables 3.7 and 3.9, lower germanium and silicon concentrations were also observed for sugar maple and chestnut oak leaves sampled at mid slope positions in the northeastern quadrant in 2013 compared to 2011. Specifically, average germanium concentrations were found to be 1.2 and 1.9 times smaller, while average silicon concentrations were found to be 1.2 and 1.1 times smaller for sugar maple and chestnut oak leaves, respectively. Comparisons in Ge/Si ratio between red oak leaves collected in 2011 and 2013 cannot be made as only a single red oak leaf was collected in 2011. As mentioned earlier, this may be due to sampling inconsistencies between 2011 and 2013. In the case of silicon concentration, reduced competition between silicon and calcium during plant transport processes is possible as a result of less calcium present in leaf tissue in 2011 relative to 2013 (Table 2.9, Figure 2.18) which would increase silicon (and by inference, germanium) concentrations in leaves sampled in 2011.

For both years, red oak leaves were found to have higher Ge/Si ratios than leaves derived from sugar maple and chestnut oak species whose Ge/Si ratios closely resembled one another (Tables 3.8 and 3.11). For leaves where both silicon and germanium concentrations were measured in 2013 (Table 3.7), average germanium concentrations were 1.9 and 3.4 times larger, while average silicon concentrations were 9.8 and 6.1 times smaller in red oak compared to sugar maple and chestnut oak species, respectively. As mentioned previously, observed discrepancy in silicon concentration between red oaks and the other species may be due to possible immobilization or suppression of the *Lsi6* gene implicated in the transport of silicon from the xylem to leaf mesophyll cells (Yamaji et al., 2008). In the case of germanium, fractionation factors between 25 and 28 times larger than sugar maple and chestnut oak species suggest significantly less discrimination against germanium for red oak species. Proportionally higher average silicon and germanium concentrations in sugar maple leaves compared to chestnut oak leaves resulted in their relatively similar Ge/Si ratios. Specifically, sugar maple leaf silicon and germanium concentrations were found to be 1.6 and 1.8 times greater than those in chestnut oak leaves sampled in 2013, respectively (Table 3.7). Furthermore, in 2011, silicon and germanium concentrations were observed to be 2.1 and 1.7 times greater in sugar maple compared to those in chestnut oak leaves, respectively (Table 3.9). For all species, silicon and germanium concentrations were significantly higher in leaves than in sap waters (Tables 3.7, 3.8, 3.9, 3.11, 3.19, and 3.20). To this end, silicic acid is known to be concentrated in the shoot through transpiration and polymerization processes before being transported to leaf tissues (Ma and Takahashi, 2002; Ma and Yamaji, 2006).

Table 3.15 Average Ge/Si ratios for sugar maple and chestnut oak leaves sampled at ridge top, mid slope, and valley floor positions of the northeastern quadrant in 2011

Tree Species	Ridge Top Average Ge/Si ($\mu\text{M}/\text{M}$)	Mid Slope Average Ge/Si ($\mu\text{M}/\text{M}$)	Valley Floor Average Ge/Si ($\mu\text{M}/\text{M}$)
Sugar Maple	0.07 ± 0.010	0.04 ± 0.002	0.03 ± 0.006
Chestnut Oak	0.06 ± 0.007	0.06 ± 0.009	0.06 ± 0.007

Table 3.16 Average Ge/Si ratios for sugar maple, chestnut oak, and red oak leaves sampled at mid slope positions in northeastern (NE), northwestern (NW), southeastern (SE), and southwestern (SW) quadrants of the catchment in 2013

Location	Sugar Maple Average Ge/Si ($\mu\text{M}/\text{M}$)	Chestnut Oak Average Ge/Si ($\mu\text{M}/\text{M}$)	Red Oak Average Ge/Si ($\mu\text{M}/\text{M}$)
NE	0.03 ± 0.005	0.03 ± 0.003	0.56 ± 0.058
NW	0.05 ± 0.007	0.04 ± 0.006	0.69 ± 0.026
SE	0.03 ± 0.006	0.02 ± 0.003	0.49 ± 0.048
SW	0.02 ± 0.007	0.02 ± 0.002	0.56 ± 0.068

In the northeastern quadrant of the catchment in 2011, sugar maple leaf Ge/Si ratios were observed to decrease from ridge top to mid slope to valley floor locations, while chestnut oak leaf Ge/Si ratios remained constant at a value of $0.06 \mu\text{M}/\text{M}$ for all positions sampled (Table 3.15, Figure 3.18). As shown in Table 3.15 and in Figure 3.18, variation in average leaf Ge/Si ratio was minimal between sugar maple and chestnut oak species sampled in 2011 at similar positions with differences ranging from 0.01 to $0.03 \mu\text{M}/\text{M}$. For leaves sampled from all tree species in 2013, average Ge/Si ratio remained rather uniform across the catchment despite differences in sampling location with ratios observed to be only slightly higher or lower than the average value determined for all quadrants (Table 3.16, Figure 3.19). Specifically, differences in average Ge/Si ratio based on transect location were highest in red oak leaves (range: 0.07 to $0.19 \mu\text{M}/\text{M}$) followed by sugar maple (range 0.01 to $0.04 \mu\text{M}/\text{M}$) and chestnut oak leaves (range: 0.01

to 0.02 $\mu\text{M}/\text{M}$) (Table 3.16, Figure 3.19). Leaves derived from northwestern locations displayed the highest average Ge/Si ratio for all tree species consistent with the higher germanium concentrations found in leaves collected from this quadrant of the catchment (Table 3.16). Higher average Ge/Si ratios for sugar maple leaves in the southeastern quadrant relative to the southwestern quadrant (Table 3.16, Figure 3.19) conform to patterns observed for mid slope shallow porewaters in these quadrants of the catchment (Table 3.3). However, average chestnut oak leaf Ge/Si ratios were found to be identical at southeastern and southwestern locations, while the average Ge/Si ratio for southwestern red oak leaves was higher than the ratio observed for leaves in the southeastern quadrant. As mentioned previously, spatial patterns in Ge/Si ratio for leaves should not necessarily reflect those for soil porewaters. Differential uptake processes preferentially discriminating against germanium relative to silicon are variable based on sampling location (Tables 3.15 and 3.16, Figures 3.18 and 3.19) or collection month (Tables 3.17 and 3.18, Figures 3.20 and 3.21). Furthermore, differences in tree transpiration processes, known to concentrate silicon in sap waters relative to soil porewaters (Hull, 2004; Mitani and Ma, 2005; Garvin, 2006), could result in deviation from spatial patterns in Ge/Si ratio observed for soil porewaters.

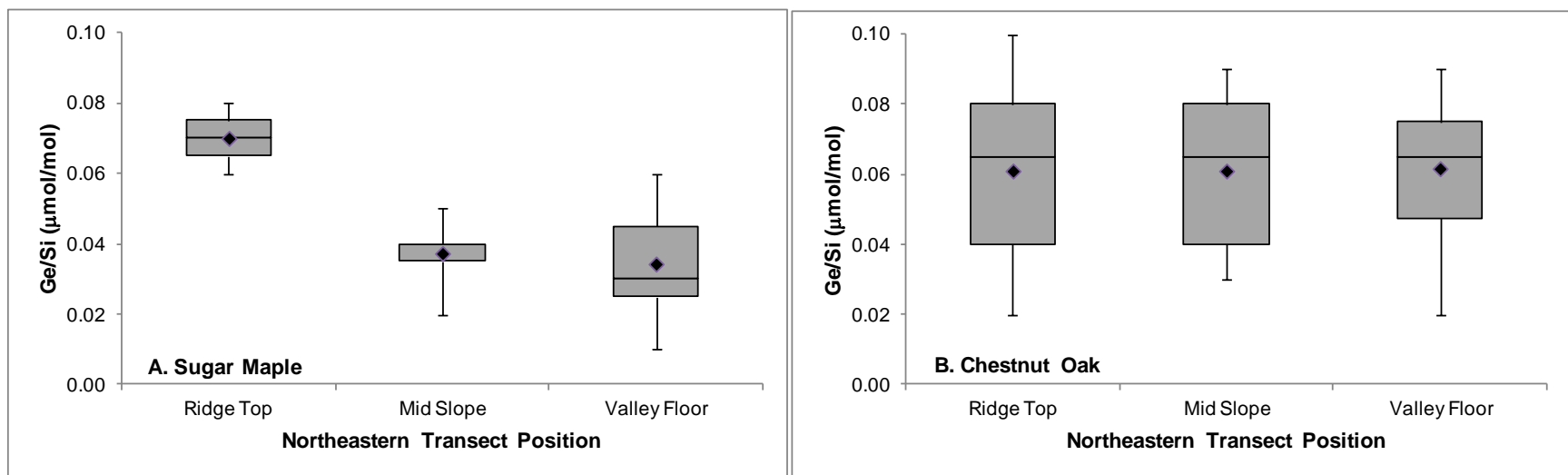


Figure 3.18 Box plots of Ge/Si ratio based on sampling position for sugar maple (A) and chestnut oak (B) leaves sampled at ridge top, mid slope, and valley floor positions of the northeastern quadrant of the catchment in 2011 with mean values shown as closed diamonds.

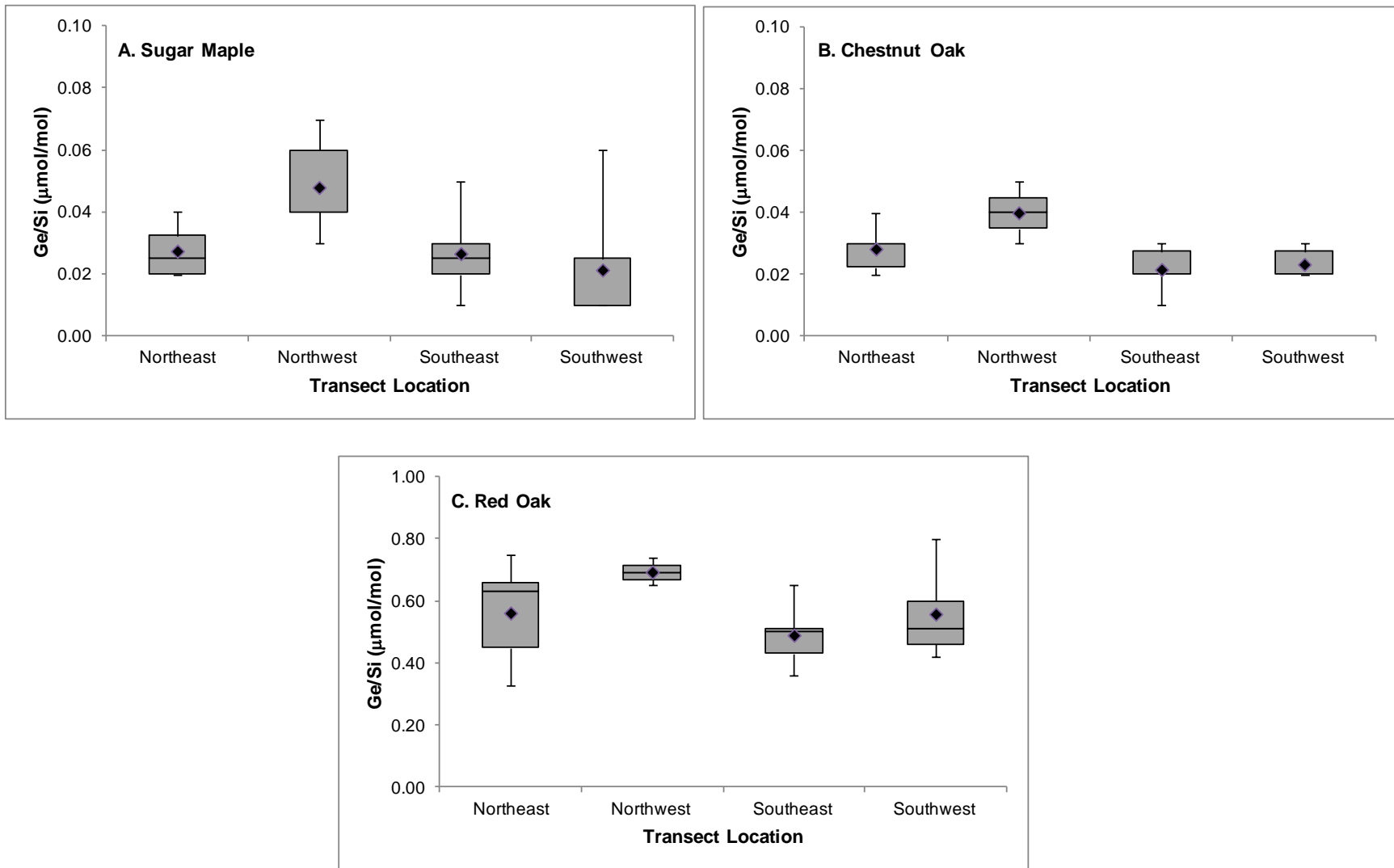


Figure 3.19 Box plots of Ge/Si ratio based on sampling location for sugar maple (A), chestnut oak (B), and red oak (C) leaves sampled at mid slope positions in northeastern, northwestern, southeastern, and southwestern quadrants in 2013 with mean values shown as closed diamonds.

Negligible temporal variation in average Ge/Si ratio occurred for tree species over the course of the growing season in 2011 (Table 3.17, Figure 3.20). On average, leaves sampled from sugar maple trees displayed greater monthly differences in average Ge/Si ratio than leaves sampled from chestnut oak trees. As was observed in silicon concentration, average sugar maple leaf Ge/Si ratio displayed an alternating increasing/decreasing pattern from June to July, July to August, and August to September (Table 3.17, Figure 3.20). Modest decreases in average Ge/Si ratio were noted for chestnut oak leaves from June to July with reported average leaf Ge/Si ratios for August and September found to be identical to the June value (Table 3.17, Figure 3.20). Germanium concentrations were not measured for porewaters in the northeastern quadrant in 2011 so comparisons cannot be made between porewaters and leaf Ge/Si ratios for this quadrant at the current time. In 2013, an alternating increasing/decreasing trend was observed in average leaf Ge/Si ratio from June to July, July to August, and August to September for sugar maple species (Table 3.18, Figure 3.21). For chestnut oak species, average leaf Ge/Si ratio increased from June to July, remaining at the July value in August and September (Table 3.18, Figure 3.21). As was observed in 2011, sugar maple leaves displayed greater monthly differences in Ge/Si ratio over the course of the growing season than chestnut oak leaves. However, red oak leaves exhibited greater temporal variability in Ge/Si ratio than either sugar maple or chestnut oak leaves. Specifically, rather significant decreases were observed from June to August, while the average September Ge/Si ratio was found to be only slightly higher than the August value (Table 3.18).

As mentioned previously, Meinzer et al. (2013) noted isohydric and anisohydric behavior in diffuse-porous maple species and ring-porous oak species at the catchment, respectively. In the case of the former, fluctuations in soil moisture content directly affect

transpiration levels. As such, the silicon (and by inference, germanium) flux to the xylem is highly influenced by transpiration levels as suggested by the strong positive relationship between transpiration rate and leaf silicon concentration based on sap fluxes and silicon concentrations in leaves at the catchment (Figure 3.11). Thus, spatio-temporal variations in Ge/Si ratio are expected to be larger for sugar maple species whose transpiration rates vary as a result of differences in soil moisture content which, in of itself, is subject to fluctuate based on sampling location (e.g. planar versus convergent topography) or collection month (e.g. variable temperatures and levels of precipitation) (Takagi and Lin, 2012). Indeed, spatial differences in silicon concentration for sugar maple leaves (Table 3.14, Figure 3.16) were attributed to differences in evapotranspiration as inferred from shallow soil water $\delta^{18}\text{O}$ and $\delta^2\text{H}$ values (Gregor, unpublished data). Reasons for such large spatio-temporal variations in Ge/Si ratio for anisohydric red oak species remain unclear and require future research.

Table 3.17 Seasonal Ge/Si ratios for sugar maple and chestnut oak leaves sampled at ridge top, mid slope, and valley floor positions of the northeastern quadrant in 2011

Tree Species	June Average Ge/Si ($\mu\text{M}/\text{M}$)	July Average Ge/Si ($\mu\text{M}/\text{M}$)	August Average Ge/Si ($\mu\text{M}/\text{M}$)	September Average Ge/Si ($\mu\text{M}/\text{M}$)
<i>Ridge Top</i>				
Sugar Maple	Nm	0.08	nm	0.06
Chestnut Oak	0.08	0.05 ± 0.013	0.06 ± 0.020	0.07 ± 0.030
<i>Mid Slope</i>				
Sugar Maple	0.03 ± 0.005	0.04 ± 0.000	0.04 ± 0.000	nm
Chestnut Oak	0.07 ± 0.010	0.05 ± 0.011	0.08 ± 0.000	nm
<i>Valley Floor</i>				
Sugar Maple	0.03 ± 0.005	0.03 ± 0.009	nm	0.06 ± 0.005
Chestnut Oak	0.07 ± 0.012	0.06 ± 0.012	0.06	0.06 ± 0.018
<i>All Locations</i>				
Sugar Maple	0.03 ± 0.000	0.05 ± 0.015	0.04	0.06 ± 0.000
Chestnut Oak	0.07 ± 0.003	0.05 ± 0.003	0.07 ± 0.007	0.07 ± 0.005

*The 'nm' term refers to months when Ge/Si ratios were not measured for a designated leaf sample.

*Error bars are excluded from species where only one leaf was collected during a given month.

Table 3.18 Seasonal Ge/Si ratios for sugar maple, chestnut oak, and red oak leaves sampled at mid slope positions in northeastern (NE), northwestern (NW), southeastern (SE), and southwestern (SW) quadrants of the catchment in 2013

Tree Species	June Average Ge/Si ($\mu\text{M}/\text{M}$)	July Average Ge/Si ($\mu\text{M}/\text{M}$)	August Average Ge/Si ($\mu\text{M}/\text{M}$)	September Average Ge/Si ($\mu\text{M}/\text{M}$)
<i>Northeast</i>				
Sugar Maple	nm	0.03 \pm 0.005	0.02	0.04
Chestnut Oak	0.02	0.03	0.03 \pm 0.005	0.04 \pm 0.005
Red Oak	0.65	0.69 \pm 0.060	0.38 \pm 0.050	0.57 \pm 0.100
<i>Northwest</i>				
Sugar Maple	nm	0.06 \pm 0.015	0.03	0.05 \pm 0.010
Chestnut Oak	nm	0.03	0.04	0.05
Red Oak	nm	0.70 \pm 0.045	0.69	nm
<i>Southeast</i>				
Sugar Maple	0.02 \pm 0.010	0.03 \pm 0.005	0.04 \pm 0.015	nm
Chestnut Oak	nm	0.03 \pm 0.005	0.03 \pm 0.005	0.02 \pm 0.005
Red Oak	nm	0.58 \pm 0.070	0.40 \pm 0.035	0.50
<i>Southwest</i>				
Sugar Maple	0.01 \pm 0.000	0.02 \pm 0.010	0.02 \pm 0.005	0.06
Chestnut Oak	nm	0.02 \pm 0.000	0.03 \pm 0.000	0.02 \pm 0.000
Red Oak	0.80	0.53 \pm 0.070	0.47 \pm 0.045	nm
<i>All Locations</i>				
Sugar Maple	0.02 \pm 0.005	0.04 \pm 0.009	0.03 \pm 0.005	0.05 \pm 0.006
Chestnut Oak	0.02	0.03 \pm 0.003	0.03 \pm 0.003	0.03 \pm 0.008
Red Oak	0.73 \pm 0.075	0.63 \pm 0.042	0.49 \pm 0.071	0.54 \pm 0.035

*The 'nm' term refers to months when Ge/Si ratios were not measured for a designated leaf sample.

*Error bars are excluded from species where only one leaf was collected during a given month.

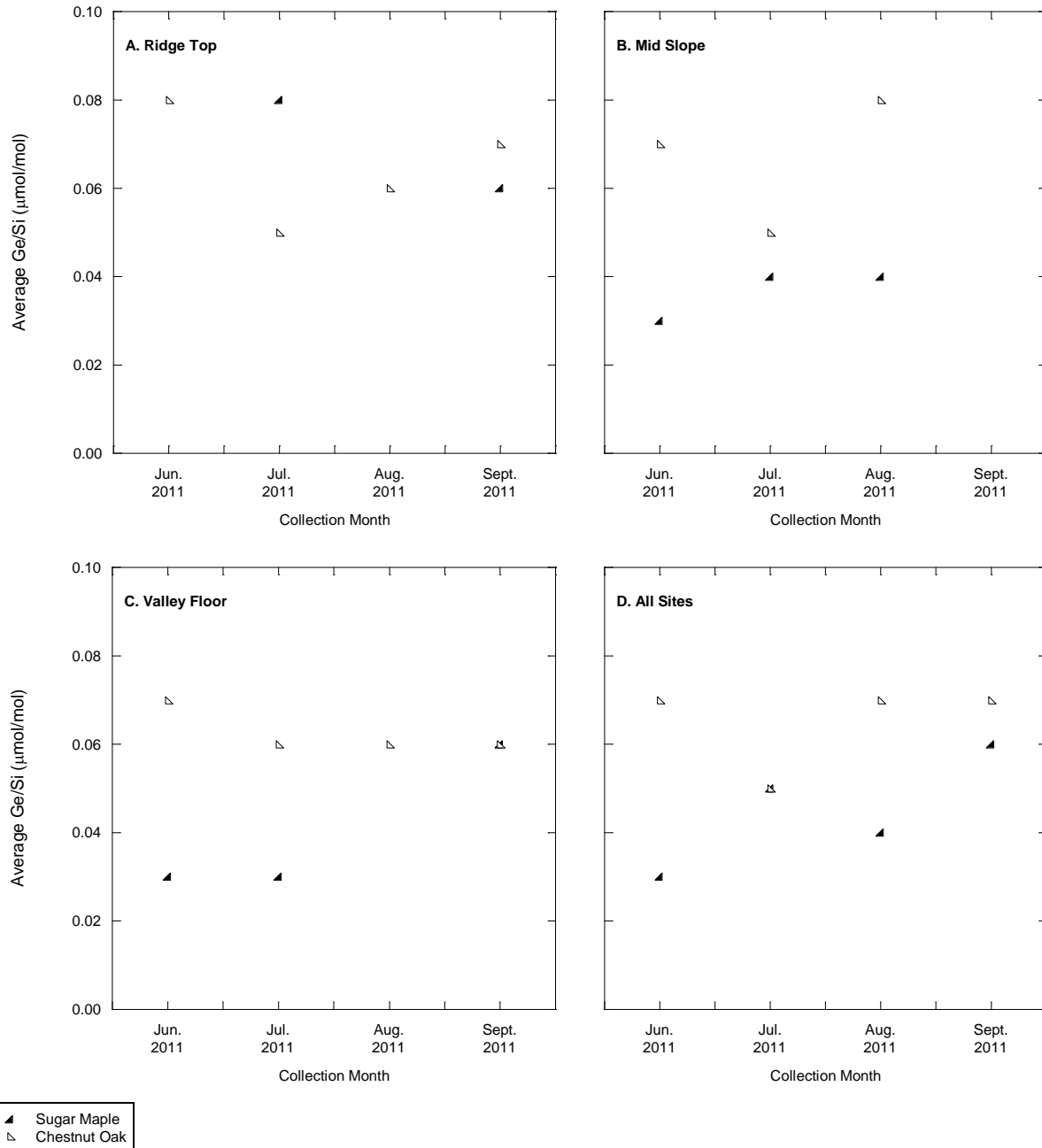


Figure 3.20 Seasonal Ge/Si ratios for sugar maple and chestnut oak leaves sampled in 2011 at ridge top (A), mid slope (B), and valley floor (C) positions of the northeastern quadrant. Sugar maple and chestnut oak leaf seasonal Ge/Si ratios for all northeastern positions (D) are also shown.

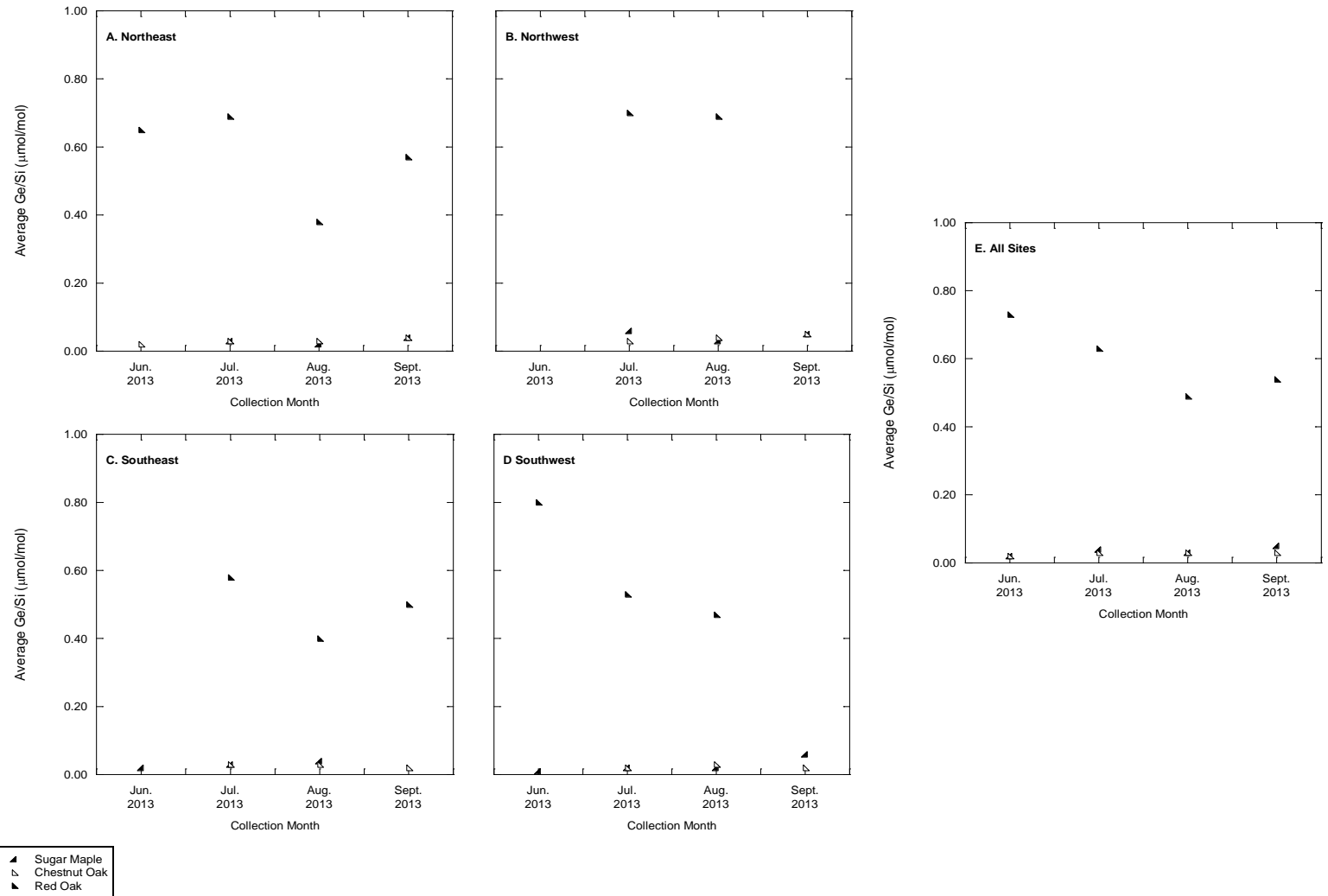


Figure 3.21 Seasonal Ge/Si ratios for sugar maple, chestnut oak, and red oak leaves sampled in 2013 at mid slope positions in northeastern (A), northwestern (B), southeastern (C), and southwestern (D) quadrants as well as for all quadrants (E) of the catchment.

3.3 Sap Waters

Silicon concentrations for sugar maple, chestnut oak, and red oak sap waters collected at mid slope positions in northeastern, northwestern, southwestern, and southeastern quadrants of the catchment from June to September of 2013 ranged from 221 to 1193, 446 to 896, and 300 to 733 μM (Table 3.19), respectively, with average values of 567 ± 55 , 639 ± 27 , and 496 ± 22 μM (Table 3.20, Figure 3.3), respectively. Sap water silicon concentrations were rather homogeneous across tree species. In fact, the sap water sugar maple average silicon concentration of 567 μM was nearly identical to the composite average determined for both oak species of 568 μM . Within oak species, however, silicon concentrations for chestnut oak sap waters were moderately larger than those found for red oak sap waters (Table 3.20). Relatively uniform silicon concentrations in sap waters sampled from different species at the catchment imply similar silicon uptake mechanisms in plants at the catchment. To this end, spatio-temporal patterns in leaf and sap water silicon concentration and Ge/Si ratio (Tables 3.10, 3.12 to 3.18, 3.21 to 3.24, Figures 3.14 to 3.23) suggest the coexistence of active and passive silicon transport mechanisms for plants at the catchment. Minimal variation in average sap water silicon concentration between maple and oak trees implies that levels of leaf transpiration must be greater for maple compared to oak species as silicon concentrations in maple leaves were moderately higher than those observed in oak leaves (Tables 3.8 and 3.11). Indeed, Meinzer et al. (2013) found higher transpiration rates and sap fluxes in maple relative to oak species at the catchment.

For sap waters where both silicon and germanium concentrations were measured (Table 3.19), average sugar maple, chestnut oak, and red oak sap water silicon concentrations were 3.0, 3.6, and 2.6 times larger than those in shallow soil porewaters (depth ≤ 20 cm, Table 3.3) sampled at mid slope positions in the southwestern quadrant, respectively. Additionally, average

sugar maple, chestnut oak, and red oak sap water silicon concentrations were 8.2, 7.0, and 4.4 times larger than those determined for shallow soil porewaters sampled at mid slope positions in the southeastern quadrant, respectively (Tables 3.3 and 3.19). On the contrary, germanium concentrations in sugar maple and chestnut oak sap waters were 18 and 8.4 times smaller than those in southwestern soil porewaters, respectively, and 4.5 and 5.0 times smaller than southeastern soil porewaters, respectively (Tables 3.3 and 3.19). Interestingly, germanium concentrations in red oak sap waters were found to be relatively similar to those in shallow soil porewaters in both quadrants (Tables 3.3 and 3.19). As silicon and germanium concentrations in sugar maple and chestnut oak sap waters were shown to be considerably higher and lower, respectively, than source porewaters, differential uptake of silicon relative to germanium is likely for these species at the catchment. However, this was not observed to be the case for red oak sap waters as silicon concentrations in red oak sap waters were higher yet germanium concentrations were comparable to those in source porewaters.

Higher concentrations of silicon in sap waters compared to source porewaters are consistent with other studies performed for similar tree species in a deciduous canopy setting (Hull, 2004; Garvin, 2006). The authors attributed increased levels of silicon observed in sap waters to tree transpiration which, in effect, concentrates levels of silicon in sap water. However, it should be noted that other studies (Casey et al., 2003; Sparks et al., 2010) have implicated active differential plant uptake processes, where silicon is selectively taken up by the plant at the expense of germanium, for the observed discrepancy in silicon concentration between sap waters and porewaters. As mentioned previously, this explanation is only appropriate for sugar maple and chestnut oak species at the catchment.

Table 3.19 Silicon and germanium elemental concentrations and Ge/Si ratios for sap waters collected from chestnut oak (QUPR), red oak (QURU), and sugar maple (ACSA) trees at mid slope positions in northeastern (NE), northwestern (NW), southeastern (SE), and southwestern (SW) locations of the catchment

Sample Date	Sample ID	Species Code	Si (μM/kg)	Ge (pM/kg)	Ge/Si (μM/M)
7/16/2013	NE 620	ACSA	510	nm	nm
7/16/2013	NE NOTAG	ACSA	701	25	0.04
7/16/2013	NW 137	ACSA	676	nm	nm
7/16/2013	NW Uphill	ACSA	621	nm	nm
7/16/2013	NW Uphill	ACSA	612	nm	nm
7/16/2013	NW 121	QUPR	563	28	0.05
7/16/2013	SW 1080	QUPR	530	nm	nm
7/16/2013	SW 1170	QUPR	493	nm	nm
7/16/2013	SW 1164	ACSA	792	9	0.01
7/16/2013	NW 102	QURU	420	286	0.68
7/16/2013	NW 110	QURU	559	nm	nm
7/16/2013	SE 1271	QURU	433	238	0.55
7/16/2013	SE 1331	QURU	541	nm	nm
7/16/2013	SE UPHILL	ACSA	767	53	0.07
7/16/2013	SW 1074	QURU	321	204	0.64
7/16/2013	SW 1077	QURU	546	305	0.56
7/17/2013	SE Downhill	ACSA	626	nm	nm
7/17/2013	SW 1073	ACSA	665	nm	nm
7/17/2013	NE 622	QUPR	533	nm	nm
7/17/2013	NE 637	QUPR	624	nm	nm
7/17/2013	SE 1266	QUPR	647	nm	nm
7/17/2013	NE 613	QURU	424	329	0.78
7/17/2013	NE 636	QURU	455	nm	nm
8/12/2013	NW 137	ACSA	567	22	0.04
8/12/2013	SE Uphill	ACSA	1193	53	0.04
8/12/2013	NE 622	QUPR	637	22	0.03
8/12/2013	NE 637	QUPR	773	33	0.04
8/12/2013	NW 121	QUPR	611	25	0.04
8/12/2013	SW 1170	QUPR	624	32	0.05
8/12/2013	NE 613	QURU	641	242	0.38
8/12/2013	NE 636	QURU	605	265	0.44
8/12/2013	NW 102	QURU	490	nm	nm
8/12/2013	SE 1271	QURU	595	278	0.47

8/12/2013	SE 1331	QURU	548	208	0.38
8/13/2013	SE 1266	QUPR	896	54	0.06
8/13/2013	SW 1080	QUPR	639	45	0.07
8/13/2013	NW 110	QURU	497	206	0.41
8/13/2013	SW 1074	QURU	405	178	0.44
9/27/2013	SW 1074	QURU	455	140	0.31
9/27/2013	SW 1164	ACSA	224	20	0.09
9/27/2013	NE 622	QUPR	446	nm	nm
9/27/2013	NE 637	QUPR	680	40	0.06
9/27/2013	NW 121	QUPR	705	36	0.05
9/27/2013	SE 1266	QUPR	792	48	0.06
9/27/2013	SE 1329	QUPR	816	43	0.05
9/27/2013	SW 1080	QUPR	489	6	0.01
9/27/2013	SW 1170	QUPR	649	42	0.06
9/27/2013	NE 613	QURU	546	392	0.72
9/27/2013	NE 636	QURU	407	212	0.52
9/27/2013	NW 102	QURU	504	237	0.47
9/27/2013	NW 110	QURU	733	236	0.32
9/27/2013	SE 1271	QURU	494	261	0.53
9/27/2013	SE 1331	QURU	548	235	0.43
9/28/2013	NE DOWNHILL	ACSA	395	nm	nm
9/28/2013	NE UPHILL	ACSA	414	nm	nm
9/28/2013	NW DOWNHILL	ACSA	416	nm	nm
9/28/2013	NW UPHILL	ACSA	221	nm	nm
9/28/2013	SE DOWNHILL	ACSA	326	nm	nm
9/28/2013	SW 1073	ACSA	481	nm	nm

*The 'nm' term refers to sap water samples where germanium concentrations and Ge/Si ratios were not measured

Table 3.20 Average silicon concentrations and Ge/Si ratios for sap waters collected in 2013 from chestnut oak (QUPR), red oak (QURU), and sugar maple (ACSA) trees located at mid slope positions in northeastern (NE), northwestern (NW), southeastern (SE), and southwestern (SW) locations of the catchment

Tree Species	Average [Si] (μM)	Average Ge/Si ($\mu\text{M}/\text{M}$)
Sugar Maple	567 ± 55	0.05 ± 0.011
Chestnut Oak	639 ± 28	0.05 ± 0.004
Red Oak	496 ± 22	0.50 ± 0.032

A wide range of silicon concentrations were found for sap waters from all tree species (Table 3.19), likely reflecting differences in sampling location and seasonality (Table 3.21 and 3.22, Figures 3.22 and 3.23). For sugar maple sap waters, southeastern locations displayed considerably higher average silicon concentrations than those for sap waters sampled at southwestern, northwestern, and northeastern locations. Additionally, average chestnut oak sap water silicon concentrations were noticeably greater for southeastern locations compared to northwestern, northeastern, and southwestern locations. Only modest differences in silicon concentration were observed across quadrant locations for red oak sap waters with northwestern and northeastern locations shown to have higher silicon concentrations than southeastern and southwestern locations, on average. Variation in tree transpiration processes, known to concentrate silicon in sap waters (Hull, 2004; Mitani and Ma, 2005; Garvin, 2006), may be resulting in the observed discrepancy in sap water silicon concentration based on sampling location. In the case of sugar maple species, differences in soil moisture have been shown to directly affect levels of tree transpiration across locations of the catchment (Meinzer et al., 2013). Interestingly, Takagi and Lin (2012) noted higher levels of near surface soil moisture in convergent relative to planar locations of the catchment. Indeed, higher levels of silicon were noted in sugar maple sap waters derived from swale (e.g. eastern) relative to planar (e.g. western)

locations in the southern quadrant of the catchment (Table 3.21, Figure 3.22). Average silicon concentrations were found to increase from July to August and then decrease from August to September for sap waters collected from all three tree species studied at the catchment, with monthly variations shown to be greater for sap waters derived from sugar maple species (Table 3.22, Figure 3.23). As mentioned previously, Meinzer et al. (2013) demonstrated that transpiration rates in ring-porous oak species are relatively unaffected by changes in soil moisture over the course of the growing season, while diffuse-porous sugar maple species are responsive to variation in soil moisture content. Therefore, fluctuations in soil moisture, due to differences in temperature or precipitation levels, may be resulting in more dramatic temporal variability in evapotranspiration levels and hence, silicon concentrations for sap waters derived from sugar maple relative to oak species.

Table 3.21 Average silicon concentrations for sugar maple, chestnut oak, and red oak sap waters sampled at mid slope positions in northeastern (NE), northwestern (NW), southeastern (SE), and southwestern (SW) quadrants of the catchment in 2013

Location	Sugar Maple Average [Si] (μM)	Chestnut Oak Average [Si] (μM)	Red Oak Average [Si] (μM)
NE	505 \pm 70	616 \pm 47	513 \pm 40
NW	519 \pm 70	627 \pm 42	534 \pm 44
SE	728 \pm 180	788 \pm 52	485 \pm 43
SW	540 \pm 123	571 \pm 30	432 \pm 47

Table 3.22 Seasonal silicon concentrations for sugar maple, chestnut oak, and red oak sap waters sampled at mid slope positions in northeastern (NE), northwestern (NW), southeastern (SE), and southwestern (SW) quadrants of the catchment in 2013

Tree Species	July Average [Si] (μM)	August Average [Si] (μM)	September Average [Si] (μM)
Sugar Maple	647 ± 27	850 ± 183	354 ± 38
Chestnut Oak	565 ± 24	697 ± 47	654 ± 53
Red Oak	462 ± 29	540 ± 31	439 ± 69

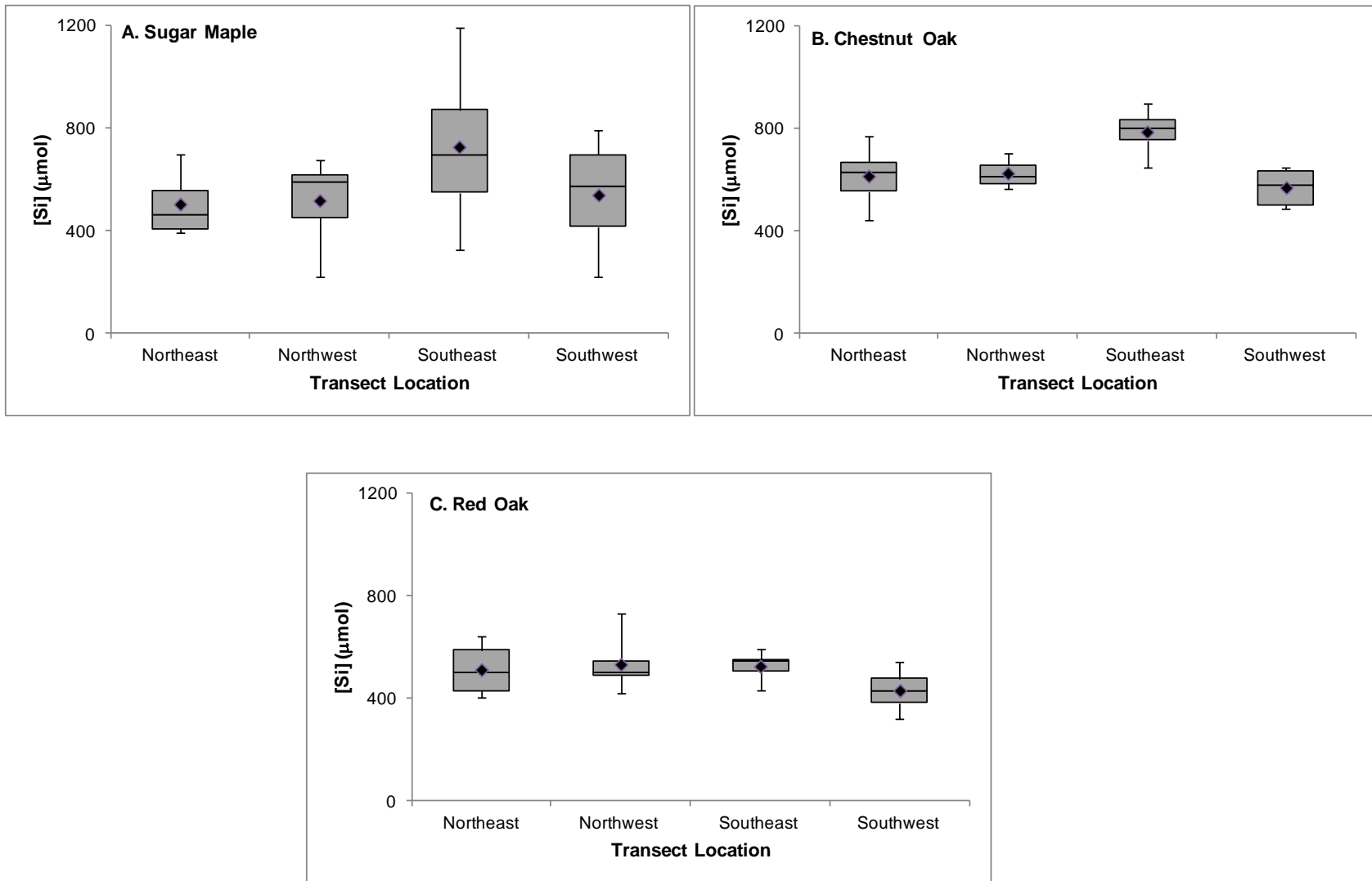


Figure 3.22 Box plots of silicon concentration based on sampling location for sugar maple (A), chestnut oak (B), and red oak (C) sap waters sampled from trees at mid slope positions in northeastern, northwestern, southeastern, and southwestern quadrants of the catchment with mean values shown as closed diamonds

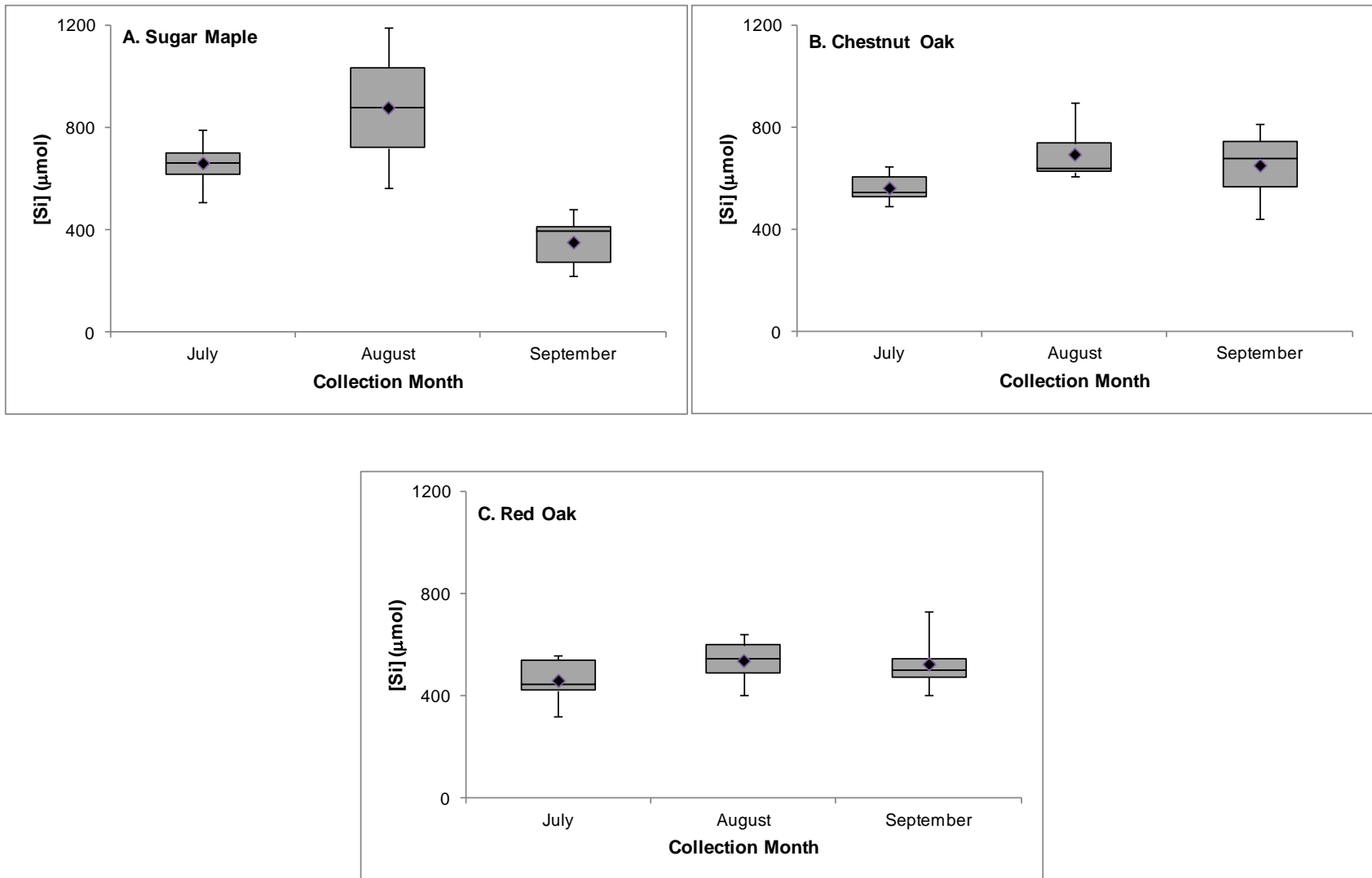


Figure 3.23 Box plots of seasonal silicon concentration for sugar maple (A), chestnut oak (B), and red oak (C) sap waters sampled from trees at mid slope positions in northeastern, northwestern, southeastern, and southwestern quadrants of the catchment with mean values shown as closed diamonds.

Ge/Si ratios for sugar maple, chestnut oak, and red oak sap waters collected at mid slope positions in northeastern, northwestern, southwestern, and southeastern quadrants of the catchment from June to September of 2013 ranged from 0.01 to 0.09, 0.01 to 0.07, and 0.31 to 0.78 $\mu\text{M}/\text{M}$ (Table 3.19), respectively, with average values of 0.05 ± 0.011 , 0.05 ± 0.004 , and 0.50 ± 0.032 $\mu\text{M}/\text{M}$ (Table 3.20), respectively. Average Ge/Si ratios for sap waters derived from sugar maple species fall within the range of values reported by Garvin (2006) at the Sleepers River Watershed in Vermont. To my knowledge, this is the first study to date to document Ge/Si ratios for sap waters collected from oak species.

As was observed for leaves, significantly higher Ge/Si ratios were found for sap waters derived from red oak relative to sugar maple and chestnut oak species. For sap waters where both silicon and germanium concentrations were measured (Table 3.19), silicon concentrations were only 1.4 and 0.7 times smaller, while germanium concentrations were 8.2 and 7.1 times larger for red oak species relative to sugar maple and chestnut oak species, respectively. Average Ge/Si ratios for sap waters collected from sugar maple and chestnut oak species were found to be identical as average silicon (Avg. $[\text{Si}]_{\text{Sugar Maple}} = 707$ μM and Avg. $[\text{Si}]_{\text{Chestnut Oak}} = 683$ μM) and germanium (Avg. $[\text{Ge}]_{\text{Sugar Maple}} = 30$ pM and Avg. $[\text{Ge}]_{\text{Chestnut Oak}} = 34$ pM) concentrations were relatively similar between species. Fractionation factors were calculated through Equation 9 using Ge/Si ratios for sapwaters (Table 3.19) and shallow soil porewaters (at depths of ≤ 20 cm, Table 3.3) collected in southern quadrants of the catchment. Fractionation factors less than one calculated for all species suggest discrimination against germanium relative to silicon in plants at the catchment. Specifically, red oak sap waters in southwestern and southeastern quadrants were shown to have higher fractionation factors (0.31 and 0.24, respectively) and discriminate to a lesser degree against germanium than sugar maple (0.02 and 0.03, respectively) and chestnut oak

(0.03 and 0.03, respectively) sap waters. As mentioned previously, significantly higher and lower silicon and germanium concentrations relative to source porewaters, respectively, in sugar maple and chestnut oak sap waters suggest differential uptake of silicon over germanium in these species at the catchment. This, however, was not observed to be the case for red oak sap waters where germanium concentrations were similar to, yet silicon concentrations were higher than those found in source porewaters.

On average, Ge/Si ratios for sap waters were found to correspond more closely to leaves than soil porewaters (Figures 3.6 and 3.24). This contrasts with patterns observed in Ca/Sr ratio where sap water Ca/Sr ratios were found to better resemble soil porewaters than leaves (Tables 2.1, 2.2, 2.16, and 2.17 and Figure 2.8). Minimal differences between leaf and sap water Ge/Si ratios suggest that partitioning between germanium and silicon occurs in the transport from the endodermal cell layer (and casparian strip) to the xylem stream either during plant uptake or soon thereafter. Regardless, Ge/Si fractionation must precede phytolith formation. These findings are in agreement with those presented by Garvin (2006), Blecker et al. (2007), and Delvigne et al. (2009) where Ge/Si ratios for stem xylem water derived from sugar maple trees, grasses, bananas, and horsetails were found to be in close agreement to those determined for leaves. Previous authors have interpreted this as Ge/Si fractionation during plant uptake (Garvin, 2006; Blecker et al., 2007) or germanium sequestration in root tissues as a plant defense mechanism against germanium toxicity (Delvigne et al., 2009). However, it should be noted that these observations contrast with findings by Rains et al. (2006) and Nikolic et al (2007) where silicon and germanium were found to be incorporated by the same pathway into the plant. The authors attributed this to the root's inability in distinguishing germanium from silicon during uptake. Observed discrepancy between findings at Shale Hills and these studies are unclear and

require future research.

Compared to leaves, sap water Ge/Si ratios displayed greater spatial homogeneity based on sampling location across the catchment (Tables 3.16 and 3.23). As shown in Table 3.23, spatial variation in sap water Ge/Si ratio was minimal with differences ranging from 0.00 to 0.02 $\mu\text{M}/\text{M}$ for sugar maple and chestnut oak species and from 0.00 to 0.10 $\mu\text{M}/\text{M}$ for red oak species. Specifically, sap waters derived from sugar maple and chestnut oak trees in northern quadrants had slightly lower Ge/Si ratios than those in southern quadrants with red oak sap waters displaying a trend opposite to this. Lower Ge/Si ratios are consistent with modestly lower average germanium concentrations in sap waters at these locations; however, sap water silicon concentrations were not observed to be higher in locations possessing lower Ge/Si ratios, on average (Table 3.19). Temporal patterns in Ge/Si ratio were not assessed due to insufficient sap water data collected from identical trees on a monthly basis.

Table 3.23 Average Ge/Si ratios for sugar maple, chestnut oak, and red oak sap waters sampled at mid slope positions in northeastern (NE), northwestern (NW), southeastern (SE), and southwestern (SW) quadrants of the catchment in 2013

Location	Sugar Maple Average Ge/Si ($\mu\text{M}/\text{M}$)	Chestnut Oak Average Ge/Si ($\mu\text{M}/\text{M}$)	Red Oak Average Ge/Si ($\mu\text{M}/\text{M}$)
NE	0.04	0.04 ± 0.009	0.57 ± 0.078
NW	0.04	0.05 ± 0.003	0.47 ± 0.076
SE	0.06	0.06 ± 0.003	0.47 ± 0.031
SW	0.05	0.05 ± 0.013	0.49 ± 0.072

* Error bars are excluded from tree species where only one sap water Ge/Si ratio was measured at a designated location

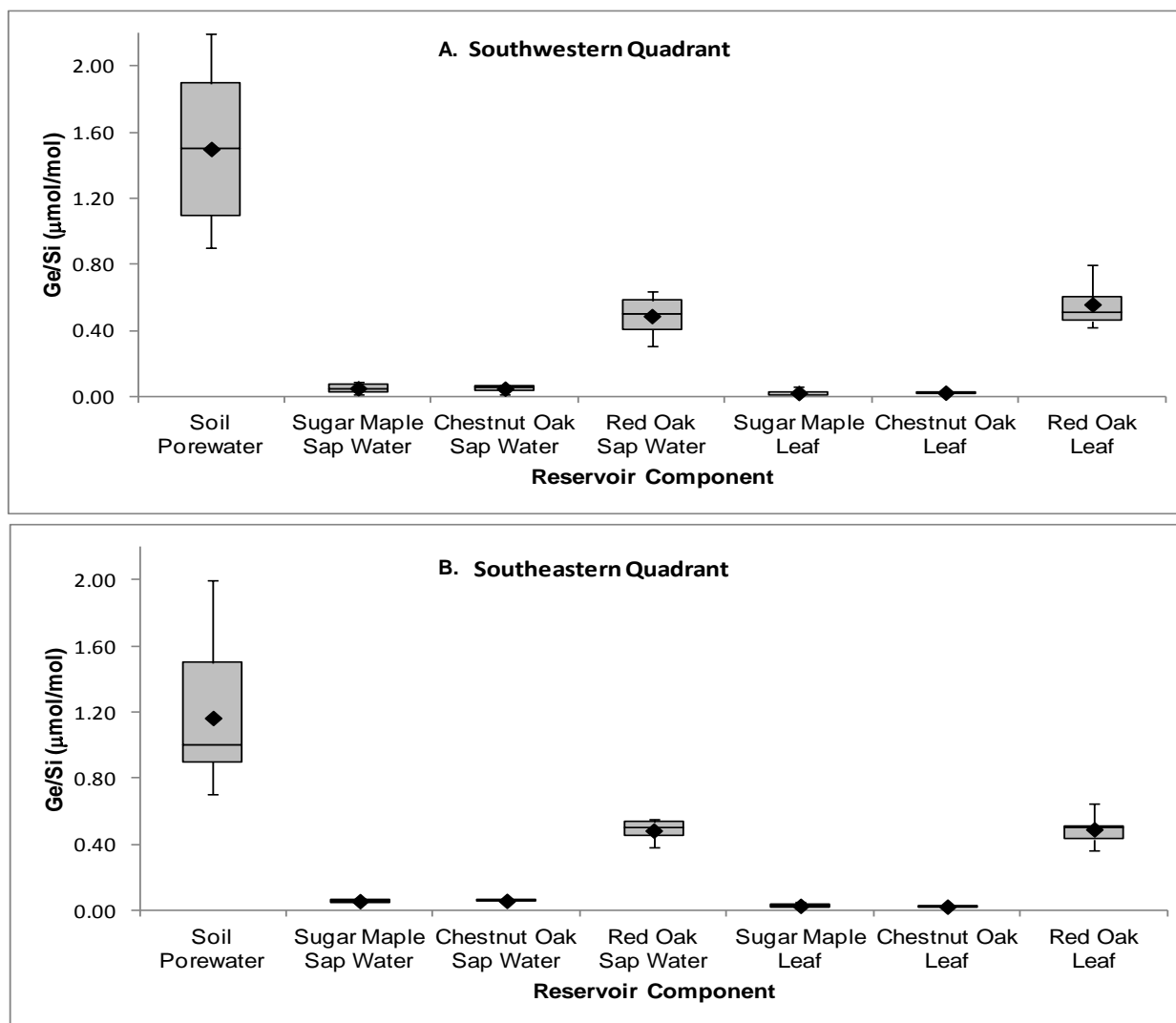


Figure 3.24 Box plots of Ge/Si ratio for soil porewaters and sugar maple, chestnut oak, and red oak sapwaters and leaves collected from mid slope positions of the southwestern (A) and southeastern (B) quadrants with mean values shown as closed diamonds.

3.4 Groundwaters and Streamwaters

Silicon concentrations of 112 and 169 μM were measured for groundwaters sampled at shallow (91 cm) and deep (849 cm) boreholes, respectively (Table 3.24, Figure 3.25). Silicon concentrations were also determined for groundwaters sampled from wells at depths of 230, 276, and 478 cm and found to be 127, 118, and 114 μM , respectively (Table 3.24, Figure 3.25). An average silicon concentration of 128 ± 11 μM was obtained for groundwaters sampled from both locations (Figure 3.3). Interestingly, silicon concentrations at deep depths (≥ 40 cm) of the southern planar valley floor location (Average [Si] = 114 μM) corresponded reasonably well to silicon concentrations of nearby shallow groundwaters at CZMW 1 (Average [Si] = 112 μM), indicating a possible groundwater source of silicon to southern planar valley floor porewaters. This corroborates observations of groundwater recharge to valley floor porewaters as suggested in Chapter 2 as well as by other researchers at the catchment (Lin, 2006; Jin et al., 2010, 2011b; Brantley et al., 2013; Thomas, 2013). As shown in Figure 3.3, groundwater silicon concentrations were relatively similar to those observed in soil porewaters and streamwaters but were considerably lower than those determined for sap waters derived from maple and oak trees. As mentioned previously, increased levels of silicon in sap waters relative to the other waters may be related to tree transpiration processes (Hull, 2004; Mitani and Ma, 2005; Garvin, 2006) or differential plant uptake processes (Casey et al., 2003; Sparks et al., 2010).

With the exception of the CZMW 6 groundwater collected from the deepest depth, silicon concentrations in borehole and well groundwaters were found to be rather similar despite differences in sampling location or depth ([Si] Range: 112 to 127 μM , Table 3.24 and Figure 3.25). Based on in situ observations (Jin et al., 2010, 2011b; Brantley et al., 2013), groundwaters are hypothesized to exist in fractured bedrock at the catchment. Borehole and well groundwaters,

excluding the sample derived from the CZMW 6 borehole, are located in upper fractured layer of the shale. In the uppermost 700 cm under the valley floor, fluid flow is rather significant in porous, relatively fractured bedrock where weathering is intensive and residence times are shorter (Jin et al., 2011a). Furthermore, neutron scattering studies at the catchment (Jin et al., 2011a) have indicated that bedrock chips collected beneath the upper fractured layer are relatively impermeable and low in porosity. As a consequence, diffusion dominates transport processes with solute concentrations in bedrock between fractures assumed to have long residence times. Thus, elevated silicon concentrations in deep groundwaters below the upper fractured layer are likely resulting from greater water-rock interaction over longer residence times as implied from relatively uniform $\delta^{18}\text{O}$ and $\delta^2\text{H}$ values in deep groundwaters at the catchment (Thomas, 2013).

Ge/Si ratios of 0.70 and 0.75 $\mu\text{M}/\text{M}$ were also observed for groundwaters sampled from Wells 13 and 11 at depths of 276 and 478 cm, respectively (Table 3.24, Figure 3.26). An average Ge/Si ratio of 0.73 $\mu\text{M}/\text{M}$ was obtained for groundwaters sampled from both locations (Figure 3.6). Groundwater Ge/Si ratios are most likely reflecting primary weathering of silicate minerals. As mentioned earlier, preferential sequestration of germanium in secondary clay minerals will lower Ge/Si ratios in solution relative to values determined for unweathered bedrock (Table 3.25) (Murnane and Stallard, 1990; Froelich et al., 1992; Kurtz et al., 2002; Scribner et al., 2006). Ge/Si ratios were observed to be rather similar between groundwaters at Wells 11 and 13 with silicon and germanium concentrations slightly lower and higher, respectively, in groundwaters from Well 11 than those from Well 13 (Table 3.24). Considering groundwaters sampled from Wells 11 and 13 are located within the upper fractured layer where porosities, weathering rates, and water residence times are similar, comparable germanium and silicon

concentrations in groundwaters sampled from these locations seem reasonable (Jin et al., 2011a). Interestingly, Ge/Si ratios in groundwaters were consistent with values determined for streamwaters at the weir location (Table 3.24 and Figure 3.26), suggestive of a possible groundwater source to weir streamwaters. This agrees with findings in this study as well as other studies at the catchment (Lin, 2006; Jin et al., 2011b) which implicate groundwaters to be a significant source of solutes to streamwaters at the weir location.

Silicon concentrations of 128, 127, and 126 μM were measured for streamwaters sampled from weir, mid stream, and stream headwater positions of a first-order catchment stream, respectively (Table 3.24, Figure 3.25). An average silicon concentration of $127 \pm 0.6 \mu\text{M}$ was determined for streamwaters sampled from all locations (Figure 3.3). Jin et al. (2010) noted that silicon in streamwaters at the catchment originates from illite and chlorite mineral dissolution processes which incorporate silicon into soluble loads. As mentioned previously, silicon can also be lost from soils through formation of secondary mineral particles (e.g. secondary kaolinites or Si-oxyhydroxides) which accumulate at valley floor locations of the catchment (Jin et al., 2010).

As shown in Figure 3.25, streamwater silicon concentrations were rather uniform across the catchment despite differences in sampling location. This contrasts with patterns observed for other elements (e.g. Ca, Sr (Table 2.22), and Mg (Jin et al., 2011)) where streamwater elemental concentrations were found to significantly increase from stream headwater to weir locations. According to field observations, the stream headwater position is ephemeral and only flows during the early spring and fall as a result of snowmelt and rainstorms, respectively (Lin, 2006; Jin et al., 2011b). Additionally, dissolved silicon in precipitation is present in insignificant quantities (Bartoli, 1983). As a consequence, silicon contributions to stream headwaters are likely due to porewater flushing by infiltrating precipitation. On the contrary, weir streamwaters

flow a larger proportion of the year due to greater influxes of groundwaters to streamwaters at this location (Jin et al., 2011b). The average groundwater silicon concentration (Avg. [Si] = 128 μM) was shown to be remarkably similar to the value observed for soil porewaters in the southern quadrant of the catchment (Avg. [Si] = 130 μM). Thus, if groundwater is largely supplying silicon to streamwaters at the weir location and porewaters are the source of silicon for stream headwaters (where mid streamwaters integrate silicon concentrations from both locations), silicon concentrations in streamwaters should not vary appreciably based on sampling location.

Ge/Si ratios of 0.73, 0.90, and 1.98 $\mu\text{M}/\text{M}$ were obtained for streamwaters corresponding to weir, mid stream, and stream headwater locations, respectively (Table 3.24, Figure 3.26). As displayed in Figure 3.26, Ge/Si ratios were observed to increase from weir to mid stream to stream headwater positions. While weir and mid streamwaters predictably displayed lower Ge/Si ratios than unweathered bedrock, stream headwaters displayed a ratio similar to the average value for unweathered bedrock (Table 3.25, Figure 3.6). However, the Ge/Si ratio in stream headwaters also corresponded reasonably well to those determined for shallow southern quadrant valley floor porewaters (Table 3.3). As mentioned previously, the stream headwater position is transient and flows only during snowmelt and rainstorms. Hence, the high Ge/Si ratio is likely due to flushing of germanium enriched soil porewaters into the headwater position by infiltrating precipitation. Incidentally, average groundwater silicon and germanium concentrations and Ge/Si ratios were found to be identical to values determined for weir streamwaters. This is consistent with strontium isotope and Ca/Sr ratios (Table 2.22) and calcium (Table 2.22), strontium (Table 2.22), silicon (Table 3.24), and germanium (Table 3.24) elemental concentrations which suggest that groundwater is an important source of solutes to the weir location. The Ge/Si ratio and

germanium concentration for mid streamwaters more closely resembled weir streamwaters and groundwaters than stream headwaters and soil porewaters, illustrating the importance of silicon and germanium influences by groundwaters to streamwaters at this location.

Table 3.24 Silicon and germanium elemental concentrations and Ge/Si ratios for groundwaters and streamwaters

Sample Date	Sample ID	Depth to water from top of casing (cm)	Si (µM/kg)	Ge (pM/kg)	Ge/Si (µM/M)
10/08/2013	CZMW 1	91	112	nm	nm
10/08/2013	CZMW 6	849	169	nm	nm
10/08/2013	Well 8	230	127	nm	nm
10/08/2013	Well 11	478	114	86	0.75
10/08/2013	Well 13	276	118	79	0.70
10/08/2013	Weir	0	128	93	0.73
	Streamwater				
10/08/2013	Mid Stream	0	127	111	0.90
10/08/2013	Stream	0	126	249	1.98
	Headwater				

*The 'nm' term refers to samples where germanium concentrations and Ge/Si ratios were not measured

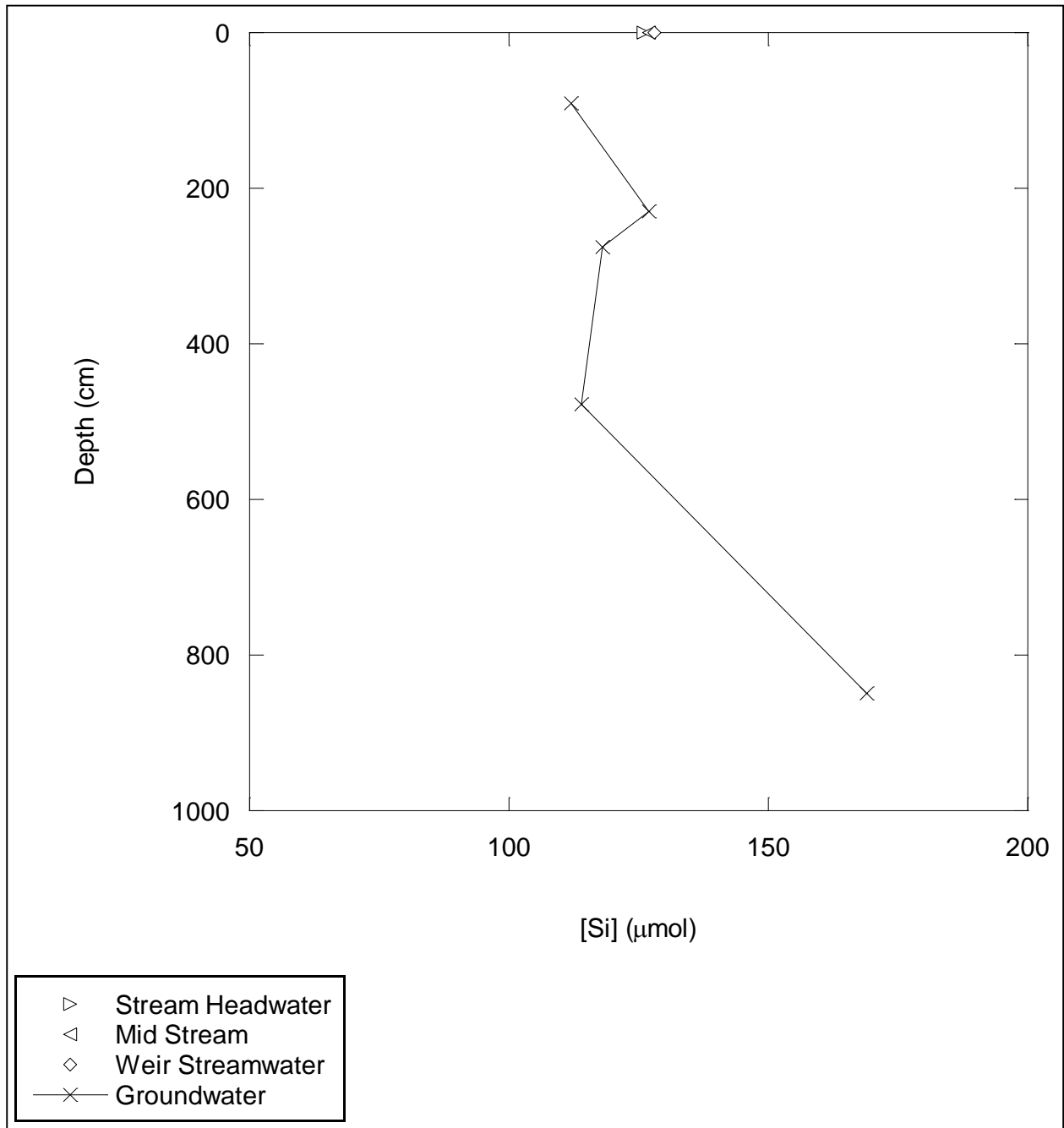


Figure 3.25 Depth versus silicon concentration for groundwaters and streamwaters.

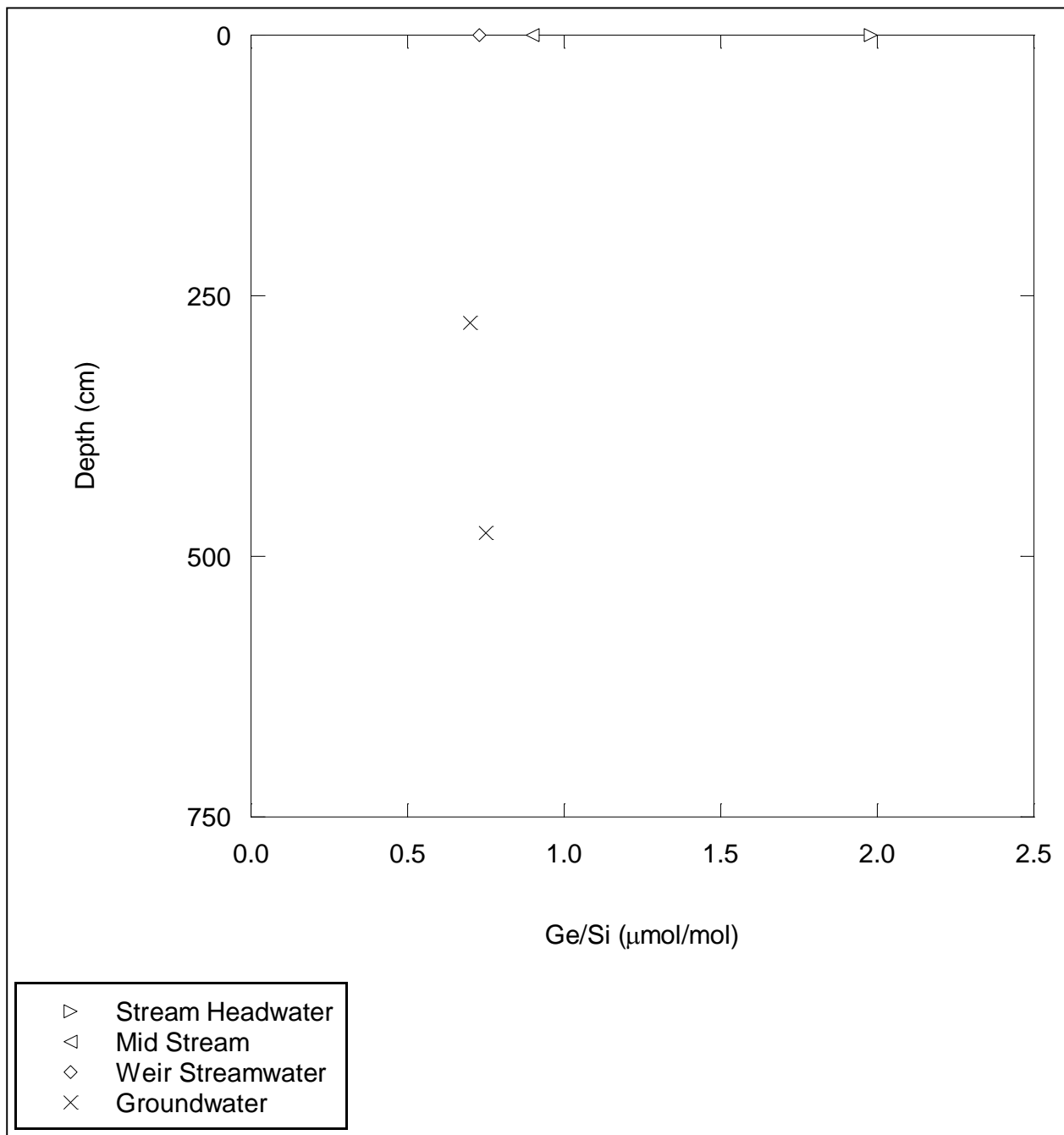


Figure 3.26 Depth versus Ge/Si ratio for groundwaters and streamwaters.

3.5 Drill Core

As shown in Table 3.25, Ge/Si ratios for DC 3 drill core samples collected near the stream's weir ranged from 1.77 to 2.09 $\mu\text{M}/\text{M}$ with an average value of $2.00 \pm 0.06 \mu\text{M}/\text{M}$. These values fall within the range of values reported for Cody Shale (Ge/Si range: 1.8 to 2.2 $\mu\text{M}/\text{M}$, Mortlock and Froelich, 1987; L. Derry, personal communication, July 14, 2014). No discernible pattern was observed between Ge/Si ratio and depth for DC 3 valley floor drill core samples. With the exception of the drill core sample collected at the 1296 cm depth (DC 3-42-43), Ge/Si ratios were found to be rather uniform despite differences in sampling depth (Figure 3.27). Kuntz et al. (2011) noted that fluid flow in DC 3 shale chips was greater in the uppermost 600-700 cm layer under the valley floor presumably due to fractured, high porosity shale present there. Low natural gamma ray emissions (Kuntz et al., 2011) and losses of magnesium, potassium, and silicon in elemental profiles (Brantley et al., 2013) suggest that clay depletion (e.g. illites and chlorites) is significant in the uppermost 600-700 cm layer of the DC 3 valley floor drill core. Interestingly, the onset of feldspar weathering at the valley floor is hypothesized to occur between 600 and 700 cm whereby increases in porosity in the upper fractured layer are likely related to loss of base cations and particles from feldspar dissolution processes (Jin et al., 2010, 2011a; Brantley et al., 2013). However, beneath the 600 or 700 cm layer, flow pathways are confined to more widely spaced fractures which inhibit fluid flow and clay mineral dissolution processes resulting in additions of magnesium, potassium, and silicon in elemental profiles (Brantley et al., 2013). Hence, the higher Ge/Si ratios for drill core samples collected in the uppermost fractured layer (DC-3-4-5 to DC-3-22-23) relative to the one sampled at a depth below this layer (DC-3-42-43).

Table 3.25 Ge/Si ratios for DC 3 valley floor drill core samples and the Cody Shale standard

Sample Date	Sample ID	Depth (cm)	Ge/Si ($\mu\text{M}/\text{M}$)
5/21/2014	DC-3-4-5	137	2.09
5/21/2014	DC-3-5-6	168	1.99
5/21/2014	DC-3-8-9	259	1.99
5/21/2014	DC 3-21-22	655	2.12
5/21/2014	DC 3-22-23	686	2.04
5/21/2014	DC 3-42-43	1296	1.77
n/a	Cody Shale	n/a	1.98

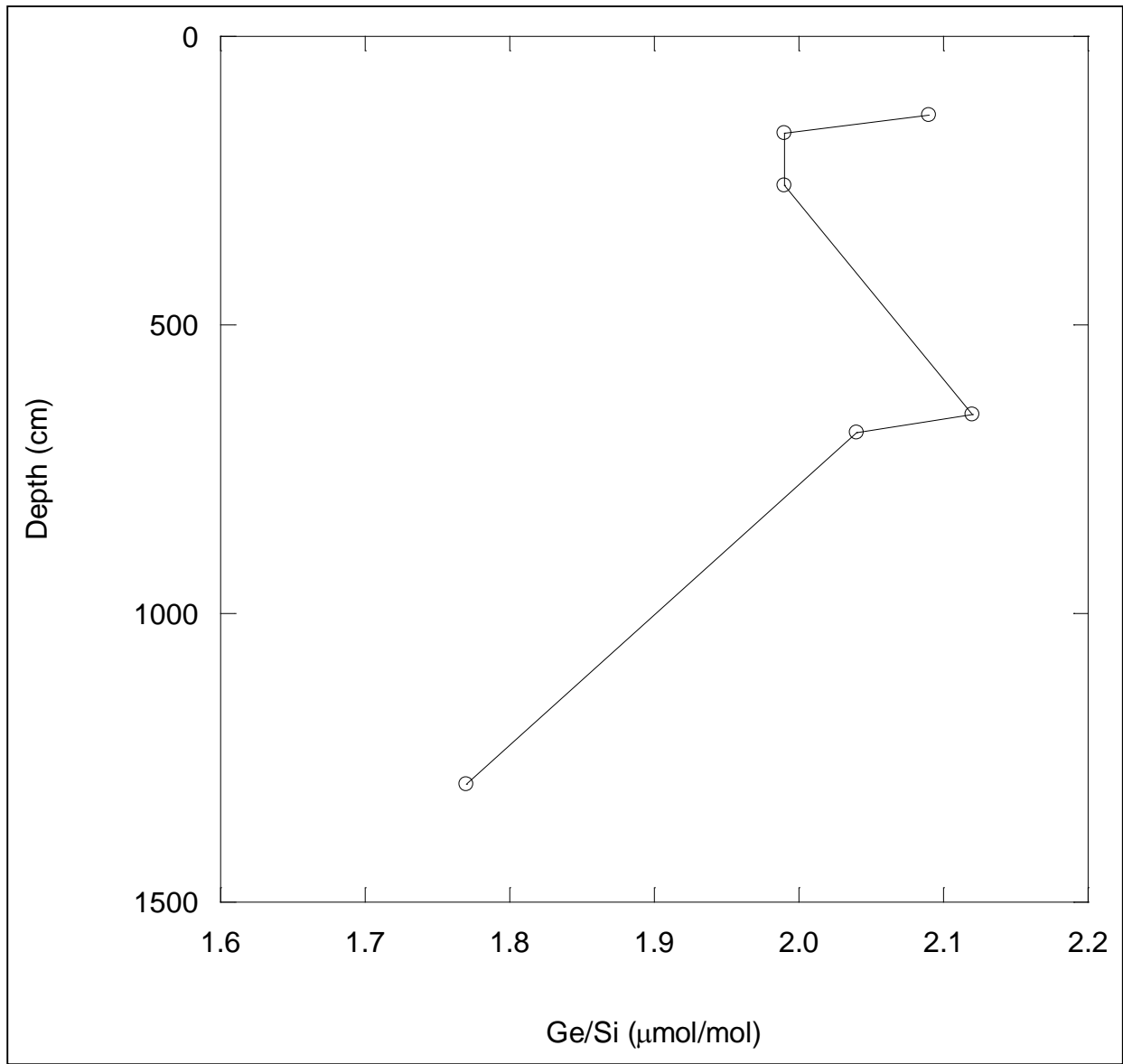


Figure 3.27 Ge/Si ratio versus depth for DC 3 valley floor drill core samples.

4. Conclusions

4.1 Soil porewaters

Ridge top porewaters displayed relatively low silicon concentrations and high Ge/Si ratios, while the reverse was observed for porewaters sampled at valley floor locations. Rapid downslope transport processes may be responsible for reducing residence times and hence, silicon concentrations in soil porewaters at ridge top relative to valley floor locations. Furthermore, these processes transfer silicon inputs in the form of solutes from both ridge top and mid slope locations to valley floor locations. Biogeochemical processes may also be responsible for enriching or depleting silicon and germanium concentrations in soil porewaters at the catchment. Preferential adsorption of germanium relative to silicon onto iron and aluminum hydroxides may be enriching porewaters in silicon at valley floor locations where iron and aluminum particles are known to accumulate. Furthermore, average silicon concentrations in porewaters at ridge top locations where regolith is thinner will be more heavily weighted toward shallow soil horizons and porewaters which are strongly influenced by plant activities at the surface. As plants in the study were shown to discriminate against germanium relative to silicon, lower average silicon concentrations and higher Ge/Si ratios in porewaters derived from ridge top relative to valley floor locations seem reasonable. Generally, southern planar soil porewaters had higher silicon concentrations (with the exception of the valley floor location) and Ge/Si ratios than those sampled from south swale locations. Steeper topography enhances lateral subsurface flow activities at swale relative to planar locations and may be reducing residence times for solutes present in porewaters at the swale location.

Silicon concentrations and Ge/Si ratios were observed to vary according to sampling depth, generally in an unpredictable fashion. Decreases in silicon concentration with depth

conform to observations of lower silicon concentrations in elemental profiles of soils as a function of depth. Conversely, leaching of organic acids from litterfall in upper soil horizons lowers pH and increases DOC in shallow porewaters to facilitate mineral and phytolith dissolution processes in these horizons. This may be resulting in the relatively high silicon concentrations observed in shallow porewaters. Complementing this is the observation of greater kaolinite abundances in upper horizons of the soil profile which may indicate greater interaction of dissolved biogenic silicon in porewaters with aluminum and iron oxides present in soils at the catchment. Depth dependent patterns in silicon are also consistent with observed preferential flow pathways. Specifically, low flow zones between A-B horizons of the soil profile have greater solute concentrations than high flow zones at A-B and B-C horizon interfaces because of enhanced weathering and longer mineral-water contact times present there. Accumulation of groundwater at valley floor locations of the catchment and the formation of perched water tables promotes rapid fluid flushing of soil porewaters with dilute precipitation inputs along both vertical and lateral preferential flow paths. Hence, the erratic “zig-zag” patterns in silicon concentration observed for valley floor exchangeable soils and soil porewaters.

Ge/Si ratios were highest in porewaters sampled from the shallowest depths at all southern planar locations and the south swale mid slope location. Possible explanations for high Ge/Si ratios in shallow porewaters are the formation of complexes between germanium and dissolved organic matter (DOM) or plant uptake processes where silicon is preferentially extracted from porewater reservoirs to a greater degree than germanium. Although germanium enriched disordered kaolinite was observed to be in its highest abundance in ridge top soils sampled from the shallowest horizons, addition of germanium to soil porewaters by dissolution of secondary kaolinites is unlikely at the catchment since no significant correlation was observed

between Ge/Si and Al/Si ratios in porewaters as would be expected if solutes were released into porewater solutions from dissolution of secondary aluminosilicates. Furthermore, kaolinite exists in its stable secondary phase in temperate regions such as Shale Hills.

Albeit minimal, monthly changes in silicon concentration were more evident for porewaters sampled from the southern planar location than for porewaters sampled from the south swale location. Overall, silicon concentrations decreased from May to June and increased from June to July for southern planar ridge top and valley floor porewaters. Increases in silicon concentration were observed over the course of the growing season for mid slope porewaters sampled at southern planar and south swale locations and for valley floor porewaters sampled at the south swale location, while the average silicon concentration for porewaters at the south swale ridge top location remained constant for all months sampled. Plant uptake processes may be responsible for monthly increases in silicon concentration as younger, less mature plants rapidly deplete porewater reservoirs of silicon for growth and developmental purposes early in the growing season. Relatively stable silicon concentrations in porewaters during the growing season suggest passive silicon uptake by plants at the catchment.

In general, monthly increases in average Ge/Si ratio were found for porewaters corresponding to southern planar ridge top, mid slope, and valley floor locations and to south swale ridge top and mid slope locations. Observed monthly increases in average Ge/Si ratio for porewaters sampled at the catchment may be attributed to the increased fractionation of Ge and Si by plant uptake processes over the course of the growing season. To this end, increased levels of evapotranspiration will lead to concomitant increases in plant transpiration and hence, silicon uptake by plants from porewater reservoirs. Another explanation for observed monthly increases in porewater Ge/Si ratio is the seasonal change in dissolved silicon source to porewaters with

phytolith dissolution processes contributing more significantly earlier in the season presumably due to higher levels of precipitation and larger fluxes of water passing through the soil profile.

4.2 Leaves

Both active and passive transport mechanisms of silicic and germanic acid molecules are possible in plants at the catchment. Considerable partitioning between silicon and germanium observed in leaf and sap waters suggests active, plant-mediated transport mechanisms which are highly specific, while relatively stable porewater silicon concentrations during the growing season and a strong positive correlation between transpiration rate and leaf silicon concentration imply passive transport mechanisms. Higher leaf silicon concentrations were observed in maple relative to oak species. Differences in transpiration rates, tree size, and effectiveness of transporter genes in allocating silicon to leaf tissues may be resulting in differences in leaf silicon concentration between tree species. Specifically, sap flux estimated transpiration rates, found to closely correlate with leaf silicon levels, were higher for smaller maple relative to larger oak trees. Furthermore, studies on grasses have shown that immobilization or suppression of an aquaporin type transporter gene alters transport pathways of silicon from the xylem to leaf mesophyll cells and hence, the distribution of silicon in leaves.

Yearly, spatial, and seasonal variations in silicon concentration were observed for leaves at the catchment. Specifically, sugar maple and chestnut oak trees were shown to accumulate more silicon and less calcium in leaf tissue in 2011 than trees sampled from the same species at these locations in 2013. A negative correlation between leaf silicon and calcium concentration implies competition during transport of these chemical species in plants and is consistent with other studies. To this end, silicon transport is suggested to be favored over calcium transport due to lower energy demands involving uptake, polymerization, and distribution of silicon relative to

calcium on plant membranes and cell wall matrices. However, these differences may simply reflect sampling inconsistencies as leaves collected in 2011, although from the same species, were derived from different individual trees than those sampled in 2013. Seasonality as opposed to sampling location across the catchment contributed to variation in silicon concentration within each tree species. Generally, accumulation of silicon in leaf tissue was observed over the course of the growing season and is consistent with findings in other studies. Monthly increases in leaf silicon concentration may be due to constant inputs of waters carrying silicon to leaves by means of the transpiration pathway, enhanced levels of evapotranspiration over the course of the growing season, or the maturation of leaves where silicon accumulates in older tissues as a consequence of silicon's inability to be remobilized for retranslocation to other plant tissues once deposited in leaves. On the other hand, average silicon concentrations did not change significantly based on sampling location at the catchment. Slight deviations were observed from average silicon concentrations for oak leaves, while maple leaves exhibited greater variability in silicon concentration based on sampling location. Furthermore, silicon concentrations in oak leaves were found to correspond to spatial patterns for porewaters while those in maple leaves did not. These observations are likely due to isohydric and anisohydric behavior in diffuse-porous maple species and ring-porous oak species, respectively. In the case of the former, fluctuations in soil moisture content are shown to affect transpiration levels and hence, silicon concentrations in leaf tissues.

Significantly lower average leaf Ge/Si ratios found for all tree species compared to porewaters, groundwaters, and streamwaters indicate that partitioning between silicon and germanium occurs in leaves. This agrees with findings for leaf phytoliths sampled from a wide range of vascular plant species throughout the United States. Fractionation factors less than one

calculated for all species suggest discrimination against germanium relative to silicon in plants at the catchment. Interestingly, red oak leaves were shown to have higher Ge/Si ratios and fractionation factors and discriminate to a lesser degree against germanium than sugar maple and chestnut oak leaves. On the other hand, Ge/Si ratios and fractionation factors were found to be relatively similar between sugar maple and chestnut oak leaves. Silicon and germanium concentrations were significantly higher in leaves than in sap waters, consistent with transpiration and polymerization processes which concentrate silicic acid in the shoot before it is subsequently transported to leaves. For leaves from all tree species, spatio-temporal patterns in Ge/Si ratio were relatively constant with leaves derived from red oak species displaying the greatest variability followed by sugar maple and chestnut oak species. As mentioned previously, diffuse-porous maple species are isohydric and more susceptible to spatial and temporal fluctuations in soil moisture content which will affect both transpiration levels and leaf silicon concentrations. Reasons for such large spatio-temporal variations in Ge/Si ratio for anisohydric red oak species are unclear and require future research.

4.3 Sap waters

Sap water silicon concentrations were rather homogeneous across tree species which contrasts with patterns observed for leaves where maple species were shown to have higher leaf silicon concentrations than oak species. This implies similar mechanisms of silicon uptake yet different levels of tree transpiration in plants as suggested by other studies at the catchment. Sap water silicon concentrations were significantly higher than those observed in porewaters, groundwaters, and streamwaters where tree transpiration or active differential plant uptake processes are implicated in concentrating silicon in sap waters. Active differential plant uptake of silicon relative to germanium is likely in sugar maple and chestnut oak species as germanium

and silicon concentrations in sap waters were shown to be significantly lower and higher than those in source porewaters, respectively. Although silicon concentrations were found to be higher, germanium concentrations in red oak sap waters were observed to be comparable to source porewaters. Thus, active differential plant uptake processes are less likely for red oak species at the catchment with higher silicon concentrations being a product of tree transpiration rather than active differential plant uptake processes.

Sap water Ge/Si ratios were significantly lower than soil porewaters and closely resembled those in paired leaf samples which contrasts with patterns observed in Ca/Sr ratio. This suggests that partitioning between germanium and silicon occurs in transport from the endodermal cell layer (and casparian strip) to the xylem stream either during plant uptake or soon thereafter. Either way, Ge/Si fractionation must precede phytolith formation which is consistent with findings for higher vascular plants studied in a wide range of ecosystems. Fractionation factors for all species were observed to be less than one suggestive of discrimination against germanium relative to silicon in plants at the catchment. Sap water Ge/Si ratios and fractionation factors were found to be higher for red oak relative to sugar maple and chestnut oak species indicating less discrimination for this species against germanium.

Spatio-temporal variations in silicon concentration were observed to be greater for sugar maple relative to oak species at the catchment and largely reflective of differences in tree transpiration. Other studies have demonstrated that transpiration rates in ring-porous oak species are relatively unaffected by changes in soil moisture over the course of the growing season, while diffuse-porous sugar maple species are rather responsive to variation in soil moisture content. Hence, spatio-temporal changes should be larger for sugar maple species as a result of fluctuations in soil moisture content present at different sampling locations as a result of

topographical or temporal variability. In the case of Ge/Si ratios, spatial differences were minimal with sugar maple and chestnut oak sap waters collected in northern quadrants displaying slightly lower Ge/Si ratios than those in southern quadrants and vice versa for red oak sap waters. Although germanium concentrations were lower, silicon concentrations were not necessarily higher in locations displaying lower Ge/Si ratios for all tree species.

4.4 Groundwaters and Streamwaters

Groundwater silicon concentrations fell within the range of values observed for soil porewaters and streamwaters but were significantly lower than those found for sap waters. Interestingly, silicon concentrations at deep depths of the southern planar valley floor location were nearly identical to those found for nearby groundwaters at CZMW 1 indicating a potential groundwater source of silicon to southern planar valley floor porewaters. Furthermore, silicon concentration was shown to increase with depth for groundwaters sampled at borehole locations and decrease with depth for groundwaters sampled at wells. Deep groundwater (CZMW 6) had the highest silicon concentration presumably due to more extensive water-rock interaction from longer residence times. Groundwater Ge/Si ratios were relatively uniform between sites and found to be lower than values determined for unweathered shale where groundwater ratios are hypothesized to be reflecting primary weathering of silicate minerals. As was observed for silicon concentration, groundwater Ge/Si ratios were comparable to those observed for streamwaters at the weir location suggesting that groundwater is an important source of solutes to this location.

Streamwater silicon concentrations were rather uniform across the catchment despite differences in sampling location which contrasts with patterns observed for other elements (e.g. Ca, Sr, Mg) where streamwater elemental concentrations were found to increase from stream

headwater to weir locations. Considering that the stream headwater location receives water exclusively through precipitation, either in the form of snowmelt or from rainstorms, and that dissolved silicon in precipitation is known to be present in insignificant quantities, silicon contributions to stream headwaters are likely due to porewater flushing by infiltrating precipitation. On the other hand, weir streamwaters flow a larger proportion of the year due to greater influxes of groundwaters to streamwaters at this location. Incidentally, the average groundwater silicon concentration was shown to be remarkably similar to the composite average value for porewaters from all locations. Thus, if groundwater is largely supplying silicon to streamwaters at the weir location and porewaters are the source of silicon for stream headwaters (where mid streamwaters integrate silicon concentrations from both locations), silicon concentrations in streamwaters should not vary considerably based on sampling location. While weir and mid streamwaters predictably displayed lower Ge/Si ratios than unweathered bedrock, stream headwaters displayed a ratio similar to the average value for unweathered bedrock. However, the Ge/Si ratio in stream headwaters also corresponded reasonably well to those determined for shallow southern quadrant valley floor porewaters. Hence, the high Ge/Si ratio may be due to flushing of germanium enriched porewaters into the headwater position by infiltrating precipitation as suggested for silicon concentration. Interestingly, average groundwater silicon and germanium concentrations and Ge/Si ratios were found to be identical to values determined for weir streamwaters. This corroborates observations presented in Chapter 2 and by other researchers' findings at the catchment which suggest significant groundwater influxes to streamwaters at the weir location. The Ge/Si ratio and germanium concentration for mid streamwaters more closely resembled weir streamwaters and groundwaters than stream headwaters and soil porewaters, illustrating the importance of silicon and germanium influences

by groundwaters to streamwaters at this location.

4.5 Drill Core

Ge/Si ratios for DC 3 drill core samples collected near the stream's weir were consistent with those reported for shale. Ge/Si ratios were found to be rather uniform despite differences in sampling depth; however, the Ge/Si ratio of the drill core sample collected from the deepest depth was somewhat lower than those reported for other samples. This was attributed to enhanced clay dissolution processes from increased porosity present in the uppermost fractured layer above 700 cm, as has been hypothesized by other researchers as a result of the onset of feldspar weathering at this depth of the valley floor. On the other hand, below this layer, flow pathways are confined to more widely spaced fractures whose isolation from each other inhibit fluid flow and restrict clay mineral dissolution processes. Hence, the higher silicon concentration and lower Ge/Si ratio for drill cores sampled at deep relative to shallow depths.

5. References

Abrams, M., 1990, Adaptations and responses to drought in *Quercus* species of North America: *Tree Physiology*, v. 7, 227-238.

Alexandre, A., Meunier, J., Colin, F., and Koud, J., 1997, Plant impact on the biogeochemical cycle of silicon and related weathering processes: *Geochimica et Cosmochimica Acta*, v. 61, p. 677-682.

Anders, A., Sletten, R., Derry, L., and Hallet, B., 2003, Germanium/silicon ratios in the Copper River Basin, Alaska: Weathering and partitioning in periglacial versus glacial environments: *Journal of Geophysical Research*, v. 108.

Andrews, D., Lin, H., Zhu, Q., Jin, L., and Brantley, S., 2011, Hot spots and hot moments of dissolved organic carbon export and soil organic carbon storage in the Shale Hills catchment: *Vadose Zone Journal*, v. 10, p. 943–954.

Barman, A., Varadachari, C., and Ghosh, K., 1992, Weathering of silicate minerals by organic acids. I. Nature of cation solubilisation: *Geoderma*, v. 53, p. 45-63.

Bartoli, F., 1983, The biogeochemical cycle of silica in two temperate forest ecosystems: *Environmental Biogeochemistry Ecological Bulletins*, v. 35, p. 469-476.

Bernstein, L., 1985, Germanium geochemistry and mineralogy: *Geochimica et Cosmochimica Acta*, v. 49, p. 2409-2422.

Blecker, S., 2005, Silica biogeochemistry across a grassland climosequence: Dissertation, Colorado State University, 147 p.

Blecker, S., King, S., Derry, L., Chadwick, O., Ippolito, J., and Kelly, E., 2007, The ratio of germanium to silicon in plant phytoliths: quantification of biological discrimination under controlled experimental conditions: *Biogeochemistry*, v. 86, p. 189-199.

Brackhage, C., Schaller, J., Baucker, E., and Dudel, E., 2013, Silicon availability affects the stoichiometry and content of calcium and micro nutrients in the leaves of common reed: *Silicon*, v. 5, p. 199-204.

Brantley, S., Holleran, M., Jin, L., and Bazilevskaya, E., 2013, Probing deep weathering in the Shale Hills Critical Zone Observatory, Pennsylvania (USA): the hypothesis of nested chemical

reaction fronts in the subsurface: *Earth Surface Processes and Landforms*, v. 38, p. 1280-1298.

Carnelli, A., Madella, M., and Theurillat, J., 2001, Biogenic silica production in selected alpine plant species and plant communities: *Annals of Botany*, v. 87, p. 425-434.

Casey, W., Kinrade, S., Knight, C., Rains, D., and Epstein, E., 2003, Aqueous silicate complexes in wheat, *Triticum Aestivum L.*: *Plant Cell and Environment*, v. 27, p. 51-54.

Clarkson, D., 1984, Calcium transport between tissues and its distribution in the plant: *Plant, Cell and Environment*, v. 7, p. 449-456.

Clarkson, D., 1993, Roots and the delivery of solutes to the xylem: *Philosophical Transactions of the Royal Society of London Series B*, v. 341, p. 5-17.

Cocker, K., Evans, D., and Hodson, M., 1998, The amelioration of aluminum toxicity by silicon in higher plants: solution chemistry or an in planta mechanism?: *Physiologia Plantarum*, v. 104, p. 608-614.

Cornelis, J., Delvaux, B., Cardinal, D., Andre, L., Ranger, J., and Opfergelt, S., 2010, Tracing mechanisms controlling the release of dissolved silicon in forest soil solutions using Si isotopes and Ge/Si ratios: *Geochimica et Cosmochimica Acta*, v. 74, p. 3913-3924.

Cornelis, J., Titeux, H., Ranger, J., and Delvaux, B., 2011, Identification and distribution of the readily soluble silicon pool in a temperate forest soil below three distinct tree species: *Plant Soil*, v. 342, p. 369-378.

Dawson, T., 1993, Hydraulic lift and water use by plants: implications for water balance, performance, plant-plant interactions: *Oecologia*, v. 95, p. 565-574.

Dawson, T., 1996, Determining water use by trees and forests from isotopic, energy, balance, and transpiration analyses: the roles of trees size and hydraulic lift: *Tree Physiology*, v. 16, p. 263-272.

de Bakker, N., Hemminga, M., and Van Soelen, J., 1999, The relationship between silicon availability, and growth and silicon concentration of the salt marsh halophyte *Spartina anglica*: *Plant and Soil*, v. 215, p. 19-27.

Delvigne, C., Opfergelt, S., Cardinal, D., Delvaux, B., and Andre, L., 2009, Distinct silicon and

germanium pathways in the soil-plant system: Evidence from banana and horsetail: *Journal of Geophysical Research*, v. 114, p. 1-11.

Derry, L., Kurtz, A., Ziegler, K., and Chadwick, O., 2005, Biological control of terrestrial silica cycling and export fluxes to watersheds: *Nature*, v. 433, p. 728-731.

Derry, L., Pett-Ridge, J., Kurtz, A., and Troester, J., 2006, Ge/Si and $^{87}\text{Sr}/^{86}\text{Sr}$ tracers of weathering reactions and hydrologic pathways in a tropical granitoid system: *Journal of Geochemical Exploration*, v. 88, p. 271-274.

Doucet, F., Schneider, C., and Bones, S., 2001, The formation of hydroxyaluminosilicates of geochemical and biological significance: *Geochimica et Cosmochimica Acta*, v. 65, p. 2461-2467.

Drever, J., 1994, The effect of land plants on weathering rates of silicate minerals: *Geochimica et Cosmochimica Acta*, v. 58, p. 2325-2332.

Epstein, E., 1994, The anomaly of silicon in plant biology: *Proceedings of the National Academy of Science, USA*, v. 91, p. 11-17.

Epstein, E., 1999, Silicon: *Annual Review of Plant Physiology and Molecular Biology*, v. 50, p. 641-664.

Evans, M., Derry, L., and France-Lanord, C., 2004, Geothermal fluxes of alkalinity in the Narayani river system of central Nepal: *Geochemistry, Geophysics, Geosystems*, v. 5, no. 8.

Ewers, B., and Oren, 2000, Analyses of assumptions and errors in the calculation of conductance from sap flux measurements: *Tree Physiology*, v. 20, p. 579-589.

Ewers, B., Mackay, D., and Samanta, S., 2007, Interannual consistency in canopy stomatal conductance control of leaf water potential across seven tree species: *Tree Physiology*, v. 27, p. 11-24.

Farmer, V., Delbos, E., and Miller, J., 2004, The role of phytolith formation and dissolution in controlling concentrations of silica in soil solutions and streams: *Geoderma*, v. 127, p. 71-79.

Fauteux, F., Remus-Borel, W., Menzies, J., and Belanger, R., 2005, Silicon and plant disease resistance against pathogenic fungi: *FEMS Microbiology Letters*, v. 249, p. 1-6.

Froelich, P., Blanc, V., Mortlock, R., Chillrud, S., Dustan, W., Udomkit, A., and Peng, T., 1992, River fluxes of dissolved silica to the ocean were higher during the glacial: Ge/Si in diatoms, rivers, and oceans: *Paleoceanography*, v. 7, p. 739-768.

Garvin, C., 2006, An exploratory study of the terrestrial biogeochemical silicon cycle at a forested watershed in northern Vermont: Master's Thesis, 128 p.

Gerard, F., Mayer, K., Hodson, M., and Ranger, J., 2008, Modeling the biogeochemical cycle of silicon in soils: application to a temperate forest ecosystem: *Geochimica et Cosmochimica Acta*, v. 72, p. 741-758.

Goldschmidt, V., 1958, *Geochemistry*, Oxford University Press: London.

Graham, R., Daniels, R., and Buol, S., 1990, Soil-geomorphic relations on the Blue Ridge front: I. Regolith types and slope processes: *Soil Science Society of America Journal*, v. 54, p. 1362-1367.

Graham, C., and Lin, H., 2011, Controls and frequency of preferential flow occurrence: A 175-event analysis: *Vadose Zone Journal*, v. 10, p. 816-831.

Granier, A., Biron, P., Kostner, B., Gay, L., and Najjar, G., 1996, Comparisons of xylem sap flow and water vapour flux at the stand level and derivation of canopy conductance for Scots pine: *Theoretical and Applied Climatology*, v. 53, p. 115-122.

Herndon, E., 2012, Biogeochemistry of manganese contamination in a temperate forested watershed: Dissertation, The Pennsylvania State University, 290 p.

Hsieh, J., Chadwick, O., Kelly, E., and Savin, S., 1998, Oxygen isotopic composition of soil water: Quantifying evaporation and transpiration: *Geoderma*, v. 82, p.269-293.

Hull, R., 2004, Scientists start to recognize silicon's beneficial effects: *Turfgrass Trends*, v. 60, p. 69-70.

Jarvis, S., 1987, The uptake and transport of silicon by perennial ryegrass and wheat: *Plant and Soil*, v. 97, p. 429-437.

Jin, L., Hamilton, S., and Walter, L., 2008, Mineral weathering rates in glacial drift soils (SW Michigan, USA): new constraints from seasonal sampling of waters and gases at soil monoliths:

Chemical Geology, v. 249, p. 129-154.

Jin L., Ravella R., Ketchum B., Bierman P. R., Heaney P., White T., and Brantley S. L., 2010, Mineral weathering and elemental transport during hillslope evolution at the Susquehanna/Shale Hills Critical Zone Observatory: *Geochimica et Cosmochimica Acta*, v. 74, p. 3669–3691.

Jin, L., Rother, G., Cole, D., Mildner, D., Duffy, C., and Brantley, S., 2011a, Characterization of deep weathering and nanoporosity development in shale – A neutron study: *American Mineralogist*, v. 96, p. 498-512.

Jin L., Andrews, D., Holmes, G., Lin, H., and Brantley, S., 2011b, Opening the “Black Box”: Water Chemistry Reveals Hydrological Controls on Weathering in the Susquehanna Shale Hills Critical Zone Observatory: *Vadose Zone Journal*, v. 10, p. p. 928-942.

Jin L., and Brantley S. L. , 2011, Soil chemistry and shale weathering on a hillslope influenced by convergent hydrologic flow regime at the Susquehanna/Shale Hills Critical Zone Observatory: *Applied Geochemistry*, v. 26, p. S51–S56.

Jones, L., and Handreck, K., 1965, Studies of silica in the oat plant. III. Uptake of silica from soils by plant: *Plant and Soil*, v. 23, p. 79-96.

Jones, L., and Handreck, K., 1969, Uptake of silica by *trifolium incarnatum* in relation to the concentration in the external solution and to transpiration: *Plant and Soil*, v. 30, p. 71-80.

Kelly, E., Chadwick, O., and Hilinski, T., 1998, The effects of plants on mineral weathering: *Biogeochemistry*, v. 42, p. 21-53.

Kump, L., Brantley, S., and Arthur, M., 2000, Chemical weathering, atmospheric CO₂, and climate: *Annual Review of Earth and Planetary Sciences*, v. 28, p. 611-667.

Kuntz, B., Rubin, S., Berkowitz, B., and Singha, K., 2011, Quantifying solute transport at the Shale Hills Critical Zone Observatory: *Vadose Zone Journal*, v. 10, p. 843–857.

Kurtz, A., 2000, Germanium/silicon and trace element geochemistry of silicate weathering and mineral aerosol deposition: Dissertation, Cornell University, 186 p.

Kurtz, A., Derry, L., and Chadwick, O., 2002, Germanium-silicon fractionation in the weathering environment: *Geochimica et Cosmochimica Acta*, v. 66, p. 1525-1537.

Kurtz, A., and Derry, L., 2004, Tracing silicate weathering and terrestrial silica cycling with Ge/Si ratios, *in* Wanty, R. and Seal, R., eds., *Proceeding of the 11th International Symposium on Water Rock Interaction: The Netherlands*, p. 833-836.

Kurtz, A., Lugolobi, F., and Salvucci, G., 2011, Germanium-silicon as a flow path tracer: Application to the Rio Icaecos watershed: *Water Resources Research*, v. 47, p. 1-16.

Liang, Y., Hua, H., Zhu, Y., Zhang, Z., and Cheng, C., 2006, Importance of plant species and external silica concentrations to active silicon uptake and transport: *New Phytologist*, v. 172, p. 63-72.

Lin, H., 2006, Temporal stability of soil moisture spatial pattern and subsurface preferential flow pathways in the Shale Hills catchment: *Vadose Zone Journal*, v. 5, p. 317-340.

Lin, H., Kogelmann, W., Walker, C., and Bruns, M., 2006, Soil moisture patterns in a forested catchment: A hydropedological perspective: *Geoderma*, v. 131, p. 345–368.

Lin H., and Zhou X., 2008, Evidence of subsurface preferential flow using soil hydrologic monitoring in the Shale Hills catchment: *European Journal of Soil Science*, v. 59, p. 34–49.

Lucas, Y., Luizao, F., Chauvel, A., Rouiller, J., and Nahon, D., 1993, The relation between biological activity of the rain forest and mineral composition of soils: *Science*, v. 260, p. 521-523.

Lucas, Y., 2001, The role of plants in controlling rates and products of weathering: importance of biological pumping: *Annual Review of Earth and Planetary Sciences*, v. 29, p. 135-163.

Lugolobi, F., Kurtz, A., and Derry, L., 2010, Germanium-silicon fractionation in a tropical, granitic weathering environment: *Geochimica et Cosmochimica Acta*, v. 74, p. 1294-1308.

Ma, J., and Takahashi, E., 1990, Effect of silicon on the growth and phosphorous uptake of rice: *Plant and Soil*, v. 126, p. 115-119.

Ma, J., and Takahashi, E., 1993, Interaction between calcium and silicon in water-cultured rice plants: *Plant and Soil*, v. 148, p. 107-113.

Ma, J., and Takahashi, E., 2002, *Soil, Fertilizer, and Plant Silicon Research in Japan*, Elsevier, The Netherlands.

Ma, J., and Yamaji, N., 2006, Silicon uptake and accumulation in higher plants: Trends in Plant Science, v. 11, p. 392-397.

Ma, J., Yamaji, N., Mitani, N., Tamai, K., Konishi, S., Fujiwara, T., Katsuhara, M., and Yano, M., 2007, An efflux transporter of silicon in rice: Nature, v. 448, p. 209-212.

Marschner, H., 1995, Mineral Nutrition of Higher Plants, 2nd Edition: Academic Press, London.

Martin, F., Ildefonse, P., Hazemann, J., Petit, S., Grauby, O., and Decarreau, A., 1996, Random distribution of Ge and Si in synthetic talc: an EXAFS and FTIR study: European Journal of Mineralogy, v. 8, p. 289-299.

McDowell, N., 2011, Mechanisms linking drought, hydraulics, carbon metabolism, and vegetation mortality: Plant Physiology, v. 155, p. 1051-059.

Meinzer, F., Woodruff, D., Eissenstat, D., Lin, H., Adams, T., and McCulloh, K., 2013, Above- and belowground controls on water use by trees of different wood types in an eastern US deciduous forest: Tree Physiology, v. 33, p. 345-356.

Meunier, J., Colin, F., and Alarcon, C., 1999, Biogenic silica storage in soils: Geology, v. 27, p. 835-838.

Mitani, N., and Ma, J., 2005, Uptake system of silicon in different plant species: Journal of Experimental Botany, v. 56, p. 1255-1261.

Mortlock, R., and Froelich, P., 1987, Continental weathering of germanium: Ge/Si in the global river discharge: Geochimica et Cosmochimica Acta, v. 51, p. 2075-2082.

Mortlock, R., and Froelich, P., 1996, Determination of germanium by isotope dilution-hydride generation inductively coupled plasma mass spectrometry: Analytica Chimica Acta, v. 332, p. 277-284.

Murnane, R., and Stallard, R., 1990, Germanium and silicon in rivers of the Orinoco drainage basin: Nature, v. 344, p. 749-752.

Nikolic, M., Nikolic, N., Liang, Y., Kirkby, E., and Romheld, V., 2007, Germanium-68 as an adequate tracer for silicon transport in plants. Characterization of silicon uptake in different crop species: Plant Physiology, v. 143, p. 495-503.

- Norris, A., and Hackney, C., 1999, Silica content of a mesohaline marsh in North Carolina: *Estuarine Coastal and Shelf Science*, v. 49, p. 595-601.
- Opfergelt, S., Cardinal, D., Andre, L., Delvigne, C., Bremond, L., and Delvaux, B., 2010, Variations of $\delta^{30}\text{Si}$ and Ge/Si with weathering and biogenic input in tropical basaltic ash soils under monoculture: *Geochimica et Cosmochimica Acta*, v. 74, p. 225-240.
- Oren, R., Phillips, N., Ewers, B., Pataki, D., and Megonigal, J., 1999, Sap-flux-scaled transpiration responses to light, vapor pressure deficit, and leaf area reduction in a flooded *Taxodium distichum* forest: *Tree Physiology*, v. 19, p. 337-347.
- Pataki, D., and Oren, R., 2003, Species difference in stomatal control of water loss at the canopy scale in a mature bottomland deciduous forest: *Advances in Water Resources*, v. 26, p. 1267-1278.
- Pokrovski, G., and Schott, J., 1998, Experimental study of the complexation of silicon and germanium with aqueous organic species: implications for germanium and silicon transport and Ge/Si ratio in natural waters: *Geochimica et Cosmochimica Acta*, v. 62, p. 3413-3428.
- Pokrovsky, O., Pokrovski, G., Schott, J., and Galy, A., 2006, Experimental study of germanium adsorption on goethite and germanium coprecipitation with iron hydroxide: X-ray absorption fine structure and macroscopic characterization: *Geochimica et Cosmochimica Acta*, v. 70, p. 3325-3341.
- Pokrovsky, O., Galy, A., Schott, J., Pokrovski, G., and Mantoura, S., 2014, Germanium isotope fractionation during Ge adsorption on goethite and its coprecipitation with Fe oxy(hydr)oxides: *Geochimica et Cosmochimica Acta*, v. 131, p. 138-149.
- Puerner, N., Siegel, M., and Siegel, B., 1990, The experimental phytotoxicology of germanium in relation to silicon: *Water, Air, and Soil Pollution*, v. 49, p. 187-195.
- Rains, D., Epstein, E., Zasoski, R., and Aslam, M., 2006, Active silicon uptake by wheat: *Plant and Soil*, v. 280, p. 223-228.
- Raven, J., 1983, The transport and function of silicon in plants: *Biological Reviews*, v. 58, p. 179-207.
- Raven, J., 2003, Cycling silicon – the role of accumulation in plants: *New Phytologist*, v. 158, p. 419-421.

Reich, A., Holbrook, N., and Ewel, J., 2004, Developmental and physiological correlates of leaf size in *Hyeronima alchorneoides* (Euphorbiaceae): American Journal of Botany, v. 91, p. 582-589.

Runge, F., 1999, The opal phytolith inventory of soils in central Africa: quantities, shapes, classification, and spectra: Review of Paleobotany and Palynology, v. 107, p. 23-53.

Scribner, A., Kurtz, A., and Chadwick, O., 2006, Germanium sequestration by soil: Targeting the roles of secondary clays and Fe-oxyhydroxides: Earth and Planetary Science Letters, v. 243, p. 760-770.

Seyfferth, A., Kocar, B., Lee, J., and Fendorf, S., 2013, Seasonal dynamics of dissolved silicon in rice cropping system after straw incorporation: Geochimica et Cosmochimica Acta, v. 123, p. 120-133.

Shannon, R., 1976, Revised effective ionic radii and systematic studies of interatomic distances in halides and chalcogenides: Acta Crystallographica Section A, v. 32, p. 751-767.

Sparks, J., Chandra, S., Derry, L., Parthasarathy, M. Daugherty, C., and Griffin, R., 2010, Subcellular localization of silicon and germanium in grass root and leaf tissues by SIMS: evidence for differential and active transport: Biogeochemistry, v. 104, p. 237-249.

Struyf, E., Van Damme, S., Gribsholt, B., Bal, K., Beauchard, O., Middelburg, J., and Meire, P., 2007, Phragmites australis and silica cycling in tidal wetlands: Aquatic Botany, v. 87, p. 134-140.

Takagi, K., and Lin, H., 2012, Changing controls of soil moisture spatial organization in the Shale Hills Catchment: Geoderma, v. 173-174, p. 289-302.

Takahashi, E., Ma, F., and Miyake, F., 1990, The possibility of silicon as an essential element for higher plants: Comments on Agricultural and Food Chemistry, v. 2, p. 99-122.

Tanaka, A., and Park, Y., 1966, Significance of the absorption and distribution of silica in the growth of the rice plant: Soil Science and Plant Nutrition, v. 12, p. 191-196.

Tardieu, F., and Simonneau, T., 1998, Variability among species of stomatal control under fluctuating soil water status and evaporative demand: modeling isohydric and anisohydric behaviors: Journal of Experimental Botany, v. 49, p. 419-432.

Thomas, E., 2013, Spatial and temporal patterns of water stable isotope compositions at the Susquehanna-Shale Hills Critical Zone Observatory: Master's Thesis, The Pennsylvania State University, 104 p.

White, P., 2001, The pathways of calcium movement to the xylem: *Journal of Experimental Botany*, v. 52, p. 891-899.

White, A., Schulz, M., Vivit, D., Bullen, T., Fitzpatrick, J., 2012, The impact of biotic/abiotic interfaces in mineral nutrient cycling: A study of soils of the Santa Cruz chronosequence, California: *Geochimica et Cosmochimica Acta*, v. 77, p. 62-85.

Yamaji, N., Mitani, N., and Ma, J., 2008, A transporter regulating silicon distribution in rice shoots: *Plant Cell*, v. 20, p. 1381-1389.

Zhang, J, Lin, H., and Doolittle, J., 2014, Soil layering and preferential flow impacts on seasonal changes of GPR signals in two contrasting soils: *Geoderma*, v. 213, p. 560-569.

CHAPTER FOUR

SUMMARY OF COMPLETED WORK AND POTENTIAL FUTURE WORK AT THE SUSQUEHANNA SHALE HILLS CRITICAL ZONE OBERVATORY

1. Introduction

The first part of this chapter outlines the major conclusions of this study based on information presented in Chapters Two and Three. Specifically, the effects of hydrology, biology, mineralogy, and topography on the availability and distribution of calcium, strontium, silicon, and germanium in various reservoir components of the Susquehanna Shale Hills Critical Zone Observatory (SSHCZO) are discussed in detail. Furthermore, facets of drill core chemistry at the catchment are expounded upon. As is the case for any study, sampling, time, and budget constraints limit the scale and scope of questions that can be reasonably addressed for a field site. To this end, the second part of this chapter offers recommendations for potential future work at the catchment.

2. Summary of Completed Work

By combining elemental concentrations with strontium isotope and elemental ratios, this study identified possible sources of calcium, strontium, silicon, and germanium in exchangeable soils, soil porewaters, leaves, sap waters, groundwaters, and streamwaters at the catchment. Hydrological (preferential flow pathways), topographical (hillslope geometry), biological (plant preferential uptake), and mineralogical (dominant weathering inputs) controls on spatio-temporal patterns were identified and found to vary in importance based on the reservoir component or chemical species analyzed. Summary figures depicting strontium isotope and Ca/Sr ratios are included in Chapter Two (Figures 2.2 and 2.8) while those pertaining to silicon concentrations

and Ge/Si ratios can be found in Chapter Three (Figures 3.3 and 3.6). Combined profiles of depth versus strontium isotope and Ge/Si ratios are shown at the end of the chapter for soil porewaters (Figures 4.1 and 4.2)

Spatial patterns in chemistry for soils and soil porewaters are shown to be affected by hydrology, topography, biology, and mineralogy. Based on sampling location, rapid lateral subsurface flow processes (Graham et al., 1990; Graham and Lin, 2011; Lin, 2006; Jin et al., 2011a, 2011b; Jin and Brantley, 2011) reduce residence times and dilute chemical concentrations in soils and soil porewaters upslope. However, these processes also transfer more radiogenic silicate weathering products in the form of cations (e.g. Ca^{2+} , Sr^{2+}) and uncharged molecules (e.g. H_4SiO_4 and H_4GeO_4) downslope. Biology, mineralogy, and topography are also shown to influence spatial patterns for soils and soil porewaters at the catchment. Specifically, enrichment of valley floor soil porewaters in silicon may be due to preferential adsorption of germanium relative to silicon onto iron and aluminum hydroxides present at valley floor locations where iron and aluminum particles are known to accumulate (Jin et al., 2010). Furthermore, in thin soil profiles at ridge top locations, silicon concentrations in porewaters are more heavily influenced by plant uptake activities at the surface which preferentially discriminate against germanium relative to silicon (Tables 3.1, 3.7, 3.9, and 3.19, Figure 3.6). Additionally, in the case of strontium isotope compositions, Ca/Sr ratios, and calcium and strontium concentrations, effects of lateral subsurface flow processes are obscured by inputs from a dominant, less radiogenic, carbonate source to exchangeable soils and soil porewaters at valley floor locations (Tables 2.1 and 2.3, Figures 2.2 and 2.8). Moreover, differences in hillslope geometry impact $^{87}\text{Sr}/^{86}\text{Sr}$ ratios and proportions of strontium derived from silicate weathering, where higher values are observed for planar ridge top exchangeable soils and soil porewaters compared to those sampled at mid

slope locations. Specifically, one dimensional vertical flow at the relatively flat planar ridge top confines precipitation inputs largely in the soil profile or in underlying fractured shale, while two dimensional lateral flow at the planar mid slope location carries precipitation inputs, along with weathering products, downslope from mid slope to valley floor locations. Convergent versus planar topography (Figure 1.2) also influences elemental concentrations and elemental and strontium isotope ratios for soil porewaters in the southern quadrant. In particular, steeper topography, combined with sparser vegetation cover at the swale's ridge, facilitates downslope movement of water along a series of connected macropores through lateral subsurface flow pathways which reduce residence times for chemical species in porewaters at the swale location. Hence, calcium and strontium concentrations (with the exception of the mid slope location), silicon (with the exception of the valley floor location) and germanium concentrations, and Ca/Sr and Ge/Si ratios are elevated in porewaters derived from planar relative to swale locations (Tables 2.1 and 2.2, 3.1 to 3.3, Figures 2.8, 3.3, and 3.6). However, swale locations are found to have more radiogenic isotope compositions and derive greater proportions of strontium from silicate weathering sources than planar locations (Tables 2.1 and 2.2, Figures 2.2 to 2.4). To this end, wetter soils combined with reduced vegetation cover at swale locations (Figure 1.3) enable the increased incidence for percolation of infiltrating precipitation into the soil profile or in underlying shale to initiate subsurface weathering processes. In the case of southern quadrant valley floor porewaters, the planar location is also located closer to the less radiogenic carbonate source near the stream's weir (DC 3) than the swale location (Figure 1.2).

For all locations, organic horizons and shallow soil porewaters are found to have less radiogenic isotope compositions and derive greater proportions of strontium from atmospheric sources (Figures 2.2 to 2.4 and 4.1 and 4.2). Both hydrological and biological processes may be

responsible for these observations. At the surface, weathering products are either transported downslope through lateral flow or translocated downward from shallow to deep horizons through vertical flow. Furthermore, inputs from less radiogenic litterfall may be responsible for lower strontium isotope compositions in organic horizons and shallow soil porewaters. Depth dependent patterns in elemental concentrations and elemental ratios (Tables 2.6 and 3.3, Figures 2.6 to 2.7, 3.1 and 3.2 Figures 4.1 and 4.2) are consistent with observed preferential flow pathways. Specifically, low flow zones between A-B horizons of the soil profile have greater solute concentrations than high flow zones at A-B and B-C horizon interfaces because of enhanced weathering and longer mineral-water contact times present there. Accumulation of groundwater at valley floor locations of the catchment and the formation of perched water tables enables rapid fluid flushing of soil porewaters with dilute precipitation inputs along both vertical and lateral preferential flow paths. Hence, the erratic “zig-zag” patterns observed for valley floor exchangeable soils and soil porewaters. Interestingly, Ge/Si ratios are found to be highest in porewaters sampled from the shallowest depths at all southern planar locations and the south swale mid slope location (Table 3.3, Figures 4.1 and 4.2). Mineralogical processes such as the formation of complexes between germanium and dissolved organic matter (DOM) (Pokrovski and Schott, 1998; Pokrovsky et al., 2006) or biological processes such as plant uptake where silicon is preferentially extracted from porewater reservoirs to a greater degree than germanium may be resulting in the high Ge/Si ratios observed in shallow porewaters.

Albeit minimal, temporal variation exists in Ge/Si and Ca/Sr ratios for porewaters sampled at all locations of the southern quadrant (Tables 2.7, 2.8 and 3.4 to 3.6, Figures 2.10 to 2.12 and 3.7 to 3.10). Temporal variations are largely controlled by biological processes. Specifically, observed monthly decreases in Ca/Sr ratio and increases in Ge/Si ratio for soil

porewaters may be related to increased fractionation of Ca and Sr and of Ge and Si by plant uptake processes over the course of the growing season. Indeed, fractionation factors for maple and oak leaves are calculated to be less than one lending support for preferential discrimination against strontium relative to calcium and germanium relative to silicon in plants at the catchment. Furthermore, observed monthly decreases in Ca/Sr ratio and increases in Ge/Si ratio may be due to higher levels of evapotranspiration present at the catchment over the growing season which will enhance plant transpiration processes and hence, plant uptake of calcium and silicon at the expense of strontium and germanium, respectively, from soil and porewater reservoirs.

Spatial patterns in chemistry for leaves and sap waters (Tables 2.11 to 2.13, 2.18, 2.19, 3.10, 3.14 to 3.16, 3.21, and 3.23, Figures 2.16, 2.17, 2.22, 2.23, 3.16 to 3.19, 3.22, and 3.24) are controlled by biological, hydrological, and topographical processes. Furthermore, the plant transport mechanism (e.g. passive versus active) for a chemical species is important in determining whether or not spatial patterns in leaf and sap water chemistry will adhere to those observed for exchangeable soils and soil porewaters which, as discussed earlier, are shown to be highly influenced by hydrological and topographical processes. However, mineralogical processes (e.g. silicate versus carbonate weathering) are not considered to be important since leaves and sap waters are largely acquiring water (and hence, solutes) from shallow soil exchange pool and soil porewater sources. At shallow depths, soils and soil porewaters are shown to be relatively unaffected by carbonate dissolution processes which initiate at deep depths of the catchment (~2200 cm and ~200 cm at ridge top and valley floor positions) (Jin et al., 2010; Brantley et al., 2013). In the case of calcium (and by inference, strontium), apoplastic passive transport mechanisms through the xylem are hypothesized, since there appears to be

limited competition between calcium and strontium for transport to the shoot (Figure 2.22). Consequently, Ca/Sr ratios in sap waters are found to correspond closely to those in source porewaters (Figures 2.8 and 2.22). In the case of silicic (and by inference, germanic) acid, a coexistence of passive and active transport mechanisms either through apoplastic or symplastic pathways is hypothesized. Specifically, the significant partitioning between silicon and germanium observed in both leaves and sap waters (Tables 3.8, 3.11, and 3.20, Figures 3.6 and 3.24) suggests an active, plant-mediated transport mechanism which is highly specific (Sparks et al., 2010), while relatively stable soil porewater silicon concentrations during the growing season (Table 3.4, Figures 3.7 and 3.8) and a strong positive correlation between transpiration rate and silicon concentration (Figure 3.11) imply a passive transport mechanism. Deviation from spatial patterns observed for soils and soil porewaters is hypothesized to be due to 1) the occurrence of active differential plant uptake processes, known to preferentially discriminate against germanium relative to silicon, to variable degrees based on sampling location and 2) differences in transpiration rates as a result of fluctuations in soil moisture content according to sampling location, particularly for sugar maple species (Meinzer et al., 2013). To this end, spatial patterns for Ca/Sr and strontium isotope ratio are found to more closely correspond to those observed for exchangeable soils and soil porewaters than silicon concentration and Ge/Si ratio for leaves and sap waters at the catchment.

As was observed for exchangeable soils and soil porewaters, temporal variation in leaf and sap water chemistry (Tables 2.14, 2.15, 2.20, 2.21, 3.12, 3.13, 3.17, 3.18, and 3.22, Figures 2.19, 2.20, 2.24, 2.25, 3.14, 3.15, 3.20, 3.21, and 3.23) is modest over the course of the growing season and largely a product of biological processes. In particular, elemental concentrations are observed to generally accumulate in leaf tissue for all tree species over the course of the growing

season (Figures 2.21, 3.14, and 3.15). Studies at the catchment indicate that transpiration rates in anisohydric, ring-porous oak species are relatively unaffected by changes in soil moisture over the course of the growing season, while isohydric, diffuse-porous sugar maple species are quite responsive to soil moisture conditions (Meinzer et al., 2013). Both calcium (and by inference, strontium) and silicon (and by inference, germanium) fluxes to the xylem through passive mechanisms are highly influenced by transpiration rates (Jones and Handreck, 1965; Clarkson, 1984). Considering that levels of evapotranspiration, as inferred from $\delta^{18}\text{O}$ and $\delta^2\text{H}$ values in shallow soil waters underlying sugar maple, chestnut oak, and red oak species (Gregor, unpublished data), are shown to differ over the course of the growing season, monthly changes in leaf and sap water Ca/Sr and Ge/Si ratios seem reasonable for species whose transpiration rates are responsive to variations in soil moisture content. Other possibilities for observed monthly changes in leaf and/or sap water Ca/Sr, Ge/Si, and/or $^{87}\text{Sr}/^{86}\text{Sr}$ ratios are 1) the maturation of leaves over the course of the growing season which inhibits the formation of a sink from which apoplastic binding locations can release calcium bound in xylem walls to increase calcium concentrations and Ca/Sr ratios in sap waters later in the season (Clarkson, 1984), 2) a switch in solute acquisition by plants from “mobile” to “immobile” soil waters held in larger and smaller soil pores, respectively, over shorter and longer residence times, respectively (Brooks et al., 2010) to increase $^{87}\text{Sr}/^{86}\text{Sr}$ ratios, elemental ratios, and elemental concentrations in leaves and sap waters and 3) tapping of deep water sources by trees as the growing season progresses (Gaines, unpublished data) to either increase or decrease $^{87}\text{Sr}/^{86}\text{Sr}$ ratios, elemental ratios, and elemental concentrations in leaves and sap waters depending on whether the source is more radiogenic, silicate weathering dominated deep porewaters or less radiogenic, carbonate affected groundwaters. On another note, sugar maple and chestnut oak trees are shown to accumulate

more silicon and less calcium in leaf tissue in 2011 than trees sampled from the same species at these locations in 2013 (Tables 3.8 and 3.11, Figure 2.18). A negative correlation between leaf silicon and calcium concentration implies competition during transport of these chemical species in plants and is consistent with other studies. To this end, silicon transport is suggested to be favored over calcium transport due to lower energy demands involving uptake, polymerization, and distribution of silicon relative to calcium on plant membranes and cell wall matrices (Ma and Takahashi, 1993; Brackhage et al., 2013). However, these differences may simply reflect sampling inconsistencies as leaves collected in 2011, although from the same species, were derived from different individual trees than those sampled in 2013.

Mineralogical processes are largely controlling groundwater chemistry at the catchment. Consistent with observations of low strontium isotope ratios, high calcium (Table 2.22), strontium (Table 2.22), and magnesium (Jin et al., 2011b) concentrations, and high pH values (Table 2.22), mixing calculations indicate that significant proportions of strontium (and by inference, calcium) are derived from carbonate weathering sources in groundwaters (Figure 2.28). Furthermore, high Ca/Sr ratios are observed for carbonate affected groundwaters (Table 2.22) where differences in the composition of carbonates and in dissolved CO₂ concentrations in groundwaters are hypothesized to be contributing to observed variation in Ca/Sr ratio with depth. Groundwater Ge/Si ratios are relatively uniform between sites and found to be lower than values determined for unweathered shale (Tables 3.24 and 3.25, Figure 3.6). In this way, Ge/Si ratios in groundwaters are hypothesized to be reflecting primary weathering of silicate minerals as this process is known to preferentially sequester germanium in secondary clay minerals (Murnane and Stallard, 1990; Froelich et al., 1992; Kurtz et al., 2002; Scribner et al., 2006). Furthermore, deep groundwaters, existing in relatively impermeable and low porosity shale beneath the upper

fractured layer (e.g. CZMW 6 groundwaters below 700 cm) under diffusion dominated transport regimes (Jin et al., 2011a), are found to have high silicon concentrations due to water-rock interactions over long residence times (Table 3.24).

Streamwater chemistry is shown to be strongly influenced by both mineralogical and hydrological processes. For streamwaters, proportions of strontium derived from carbonate weathering sources increase from stream headwater to mid stream to weir locations (Figure 2.28). Accordingly, concomitant decreases in strontium isotope ratio (Table 2.22), increases in calcium (Table 2.22), strontium (Table 2.22), and magnesium concentrations (Jin et al., 2011b), and increases in pH value (Table 2.22) are observed for streamwaters in the progression sequence from stream headwater to mid stream to weir locations of the catchment. In streamwaters, lower proportions of strontium derived from silicate weathering relative to atmospheric sources are consistent with the slow kinetics of clay dissolution at the catchment (Jin et al., 2010). Additionally, high proportions of atmospherically derived strontium in stream headwaters agree with field observations which indicate the occurrence of stream flow exclusively during snowmelt and rainstorms in early spring and fall, respectively, at this location (Jin et al., 2011b). On the contrary, weir streamwaters flow a larger proportion of the year, where relatively high proportions of strontium derived from carbonate weathering suggest larger influxes of carbonate affected groundwaters to streamwaters at this location (Jin et al., 2011b). Located at the midpoint of weir streamwaters and stream headwaters, strontium derived from carbonate weathering, silicate weathering, and atmospheric sources in mid streamwaters represent roughly a 50:50 mixture of proportions determined for streamwaters at weir and stream headwater locations according to mixing calculations. In contrast, streamwater silicon concentrations are rather uniform across the catchment despite differences in sampling location.

Considering that the stream headwater location receives water exclusively through precipitation, either in the form of snowmelt or from rainstorms, and that dissolved silicon in precipitation is known to be present in insignificant quantities, silicon contributions to stream headwaters are largely influenced by hydrological flushing of porewaters by infiltrating precipitation. On the other hand, as mentioned previously, weir streamwaters are likely receiving influxes of groundwaters. Incidentally, the average groundwater silicon concentration is shown to be remarkably similar to the composite average value for porewaters from all locations (Tables 3.2 and 3.24, Figure 3.3). Thus, if groundwater is largely supplying silicon to streamwaters at the weir location and porewaters are the source of silicon for stream headwaters (where mid streamwaters integrate silicon concentrations from both locations), silicon concentrations in streamwaters should not vary appreciably based on sampling location. While weir and mid streamwaters predictably display lower Ge/Si ratios than unweathered bedrock, the stream headwater ratio is similar to the average value for unweathered bedrock (Tables 3.24 and 3.25, Figure 3.6). However, the Ge/Si ratio in stream headwaters also correspond reasonably well to those determined for shallow southern quadrant valley floor porewaters (Tables 3.3 and 3.24, Figure 3.6). Hence, the high Ge/Si ratio may be due to flushing of germanium enriched porewaters into the headwater position by infiltrating precipitation as suggested earlier for silicon concentration. Relatively similar strontium isotope, Ca/Sr and Ge/Si ratios and calcium, strontium, silicon, and germanium elemental concentrations between groundwaters and weir streamwaters provide strong, converging lines of evidence implicating groundwater as an important source of chemical species to the weir location (Tables 2.22 and 3.24, Figures 2.2, 2.8, 3.3, and 3.6). Similarly, observations of significantly lower strontium isotope ratios, higher Ca/Sr ratios, and lower Ge/Si ratios observed for valley floor porewaters compared to those sampled at

ridge top and mid slope locations suggest recharge by groundwaters to valley floor porewaters at the catchment (Tables 2.1, 2.2, 2.6, and 3.1 to 3.3, Figures 2.2, 2.8, and 3.6).

Based on strontium isotope ratios (Table 2.23 and Figure 2.30) and findings by other researchers (Jin et al., 2010, 2011a, 2014; Brantley et al., 2013), carbonates at the ridge top are hypothesized to be ankerite, while those at the valley floor are likely a mixture of ankerite and calcite. Generally, $^{87}\text{Sr}/^{86}\text{Sr}$ isotope ratios in carbonates at the catchment exceed the value expected for ocean water (Hess et al., 1986). As such, carbonates at the catchment are hypothesized to be diagenetic with strontium isotope compositions influenced by meteoric pore fluids exposed to more radiogenic Rb bearing shales and clay silicates. In this way, diagenetic carbonates of two generations with distinctive mineralogies and strontium isotope ratios are present at Shale Hills due to the heterogeneous lithology of the Rose Hill formation (Flueckinger, 1969) where carbonate layers at the ridge and valley are likely coming from different strata. Lower $^{87}\text{Sr}/^{86}\text{Sr}$ ratios in “weathered shale” relative to shale are hypothesized to be from leaching of less radiogenic strontium from plagioclase feldspar dissolution processes at interlayer and adsorption sites of clay minerals. Variation in Ca/Sr ratio for drill core samples with depth (Table 2.23, Figure 2.32) may be due to variations in carbonate composition or degrees of CO_2 acquisition and CO_2 degassing as these processes lead to the dissolution and precipitation of carbonates at the catchment, respectively (Jin et al., 2011b). The rate of carbonate propagation well exceeds those estimated for regolith production and erosion by other researchers (Jin et al., 2010; Ma et al., 2010) and is consistent with the greater depth inferred for the carbonate weathering front at the catchment (Brantley et al., 2013). However, different timescales used in calculations may be resulting in the observed discrepancy between rates of carbonate propagation and those determined for regolith production and erosion.

Strontium isotope ratios for silicate fractions of drill core samples are shown to be rather similar between ridge top and valley locations (Table 2.24, Figure 2.30) and fall within the range of values reported for shales in the area (Whitney and Hurley, 1964). Heterogeneity in the composition of the Rose Hill shale (Lynch, 1976) or differences in porosity (Jin et al., 2011a) may be responsible for the observed spatial variability in $^{87}\text{Sr}/^{86}\text{Sr}$ ratio for drill core samples collected from both locations. Considering that “weathered shale” is found to be less radiogenic than unweathered shale (Figure 2.2), increased porosity is hypothesized to be decreasing strontium isotope ratios in silicate fractions of drill core samples. As was observed in $^{87}\text{Sr}/^{86}\text{Sr}$ ratio, minimal variation in Ca/Sr ratio occurs between silicate fractions of drill core samples (Table 2.24, Figure 2.32) collected from ridge top and valley floor locations where differences in Ca/Sr ratio are likely due to differences in porosity.

Ge/Si ratios for valley drill core samples (Table 3.25, Figure 3.27) are consistent with those reported for shale (Mortlock and Froelich, 1987). Ge/Si ratios are found to be rather uniform despite differences in sampling depth; however, the Ge/Si ratio of the drill core sample collected from the deepest depth is somewhat lower than those reported for other samples. This is attributed to enhanced clay dissolution processes present from increased porosity in the uppermost fractured layer above 700 cm, as has been hypothesized by other researchers as a result of the onset of feldspar weathering at this depth of the valley floor (Brantley et al., 2013). On the other hand, below this layer, flow pathways are confined to more widely spaced fractures whose isolation from each other inhibit fluid flow and restrict clay mineral dissolution processes (Brantley et al., 2013). Hence, the higher silicon concentration and lower Ge/Si ratio for drill cores sampled at deep relative to shallow depths.

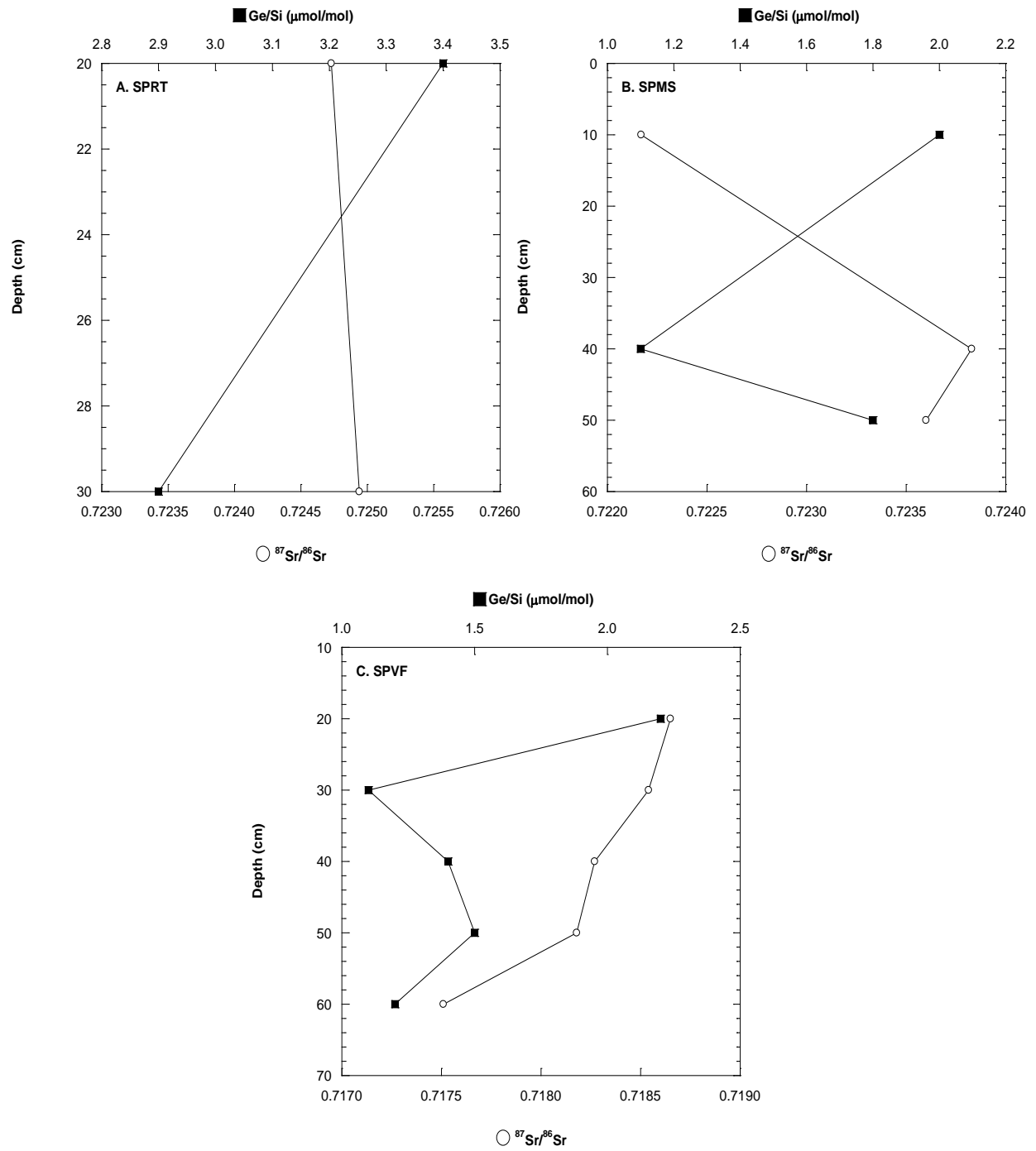


Figure 4.1 Combined profiles of depth versus Ge/Si and $^{87}\text{Sr}/^{86}\text{Sr}$ ratios for southern planar (SP) ridge top (RT), mid slope (MS), and valley floor (VF) soil porewaters.

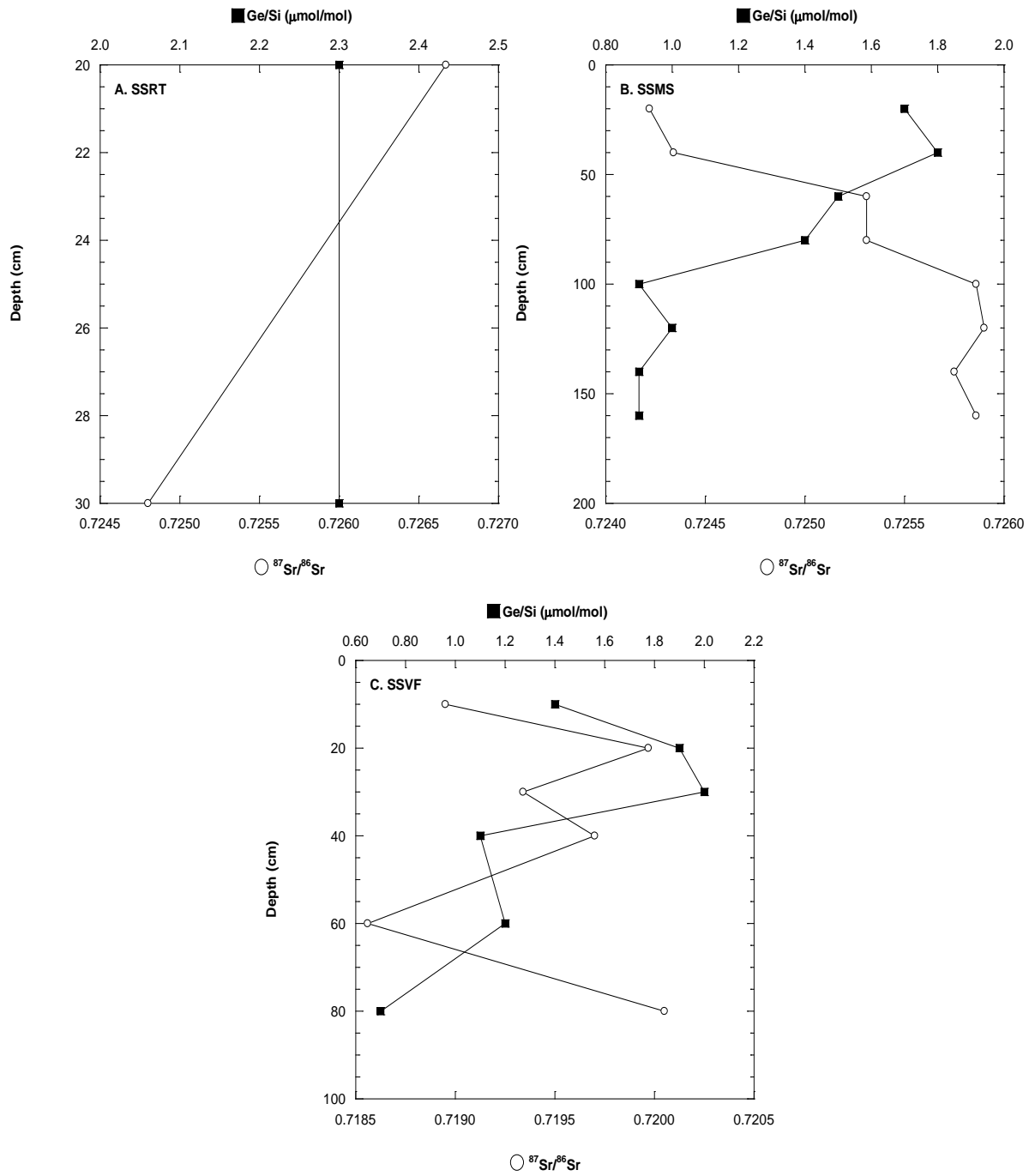


Figure 4.2 Combined profiles of depth versus Ge/Si and $^{87}\text{Sr}/^{86}\text{Sr}$ ratios for south swale (SS) ridge top (RT), mid slope (MS), and valley floor (VF) soil porewaters.

3. Potential Future Work

Although this study was quite comprehensive, future research is necessary to better constrain biogeochemical processes relating to source and cycling of calcium, strontium, silicon, and germanium at the Susquehanna Shale Hills Critical Zone Observatory (SSHCZO). One topic that requires additional research is the site of elemental partitioning in plants at the catchment.

Using Ca/Sr and Ge/Si ratios of leaves and soil porewaters, this study confirmed that discrimination against strontium and germanium does, indeed, occur in plants where significantly higher Ca/Sr (Chapter 2) and lower Ge/Si (Chapter 3) ratios were observed in leaves relative to soil porewaters. Furthermore, minimal discrepancy between leaf and sap water Ge/Si ratios suggests that partitioning between germanium and silicon precedes phytolith formation and occurs in the transport from the endodermal cell layer (and casparian strip) to the xylem stream either during plant uptake or soon thereafter. In the case of calcium and strontium, sap water Ca/Sr ratios more closely resembled those in soil porewaters than those in leaves. However, elemental partitioning is occurring at a point further along the transpiration stream as indicated by observations of higher Ca/Sr ratios in leaves relative to source porewaters. In either case, future research is necessary to identify the exact site of elemental partitioning between calcium and strontium and between silicon and germanium in plants at the catchment.

Compilation of major and trace element data for plant roots, wood, and bark and for litterfall and throughfall will be required to adequately address this question in future studies at the SSHCZO.

Another topic that was not fully addressed in this study is the transport of cations (e.g. Ca^{2+} and Sr^{2+}) and uncharged molecules (e.g. H_4SiO_4 and H_4GeO_4) across roots to the xylem in plants at the catchment. In the case of calcium (and by inference, strontium), passive transport is likely (White, 2001; White and Broadley, 2003); however, the question remains as to whether

transport is occurring through the symplast of endodermal cells or entirely through the apoplast. Information presented in this study suggests apoplastic transport to the xylem as there appears to be limited competition between calcium and strontium for transport to the shoot. On the other hand, such competition would be expected from the symplastic pathway where cation transporters on cell membranes are highly selective (White, 2001; White and Broadley, 2003). To this end, Ca/Sr ratios in sap waters were found to correspond closely to those in source porewaters. However, this interpretation conflicts with the traditional view that calcium transport to the xylem occurs predominately through symplastic pathways in endodermal cells (Marschner, 1995). In the case of silicic (and by inference, germanic) acid, the coexistence of passive and active transport mechanisms either through apoplastic or symplastic pathways is hypothesized. Specifically, significantly higher silicon concentrations and lower Ge/Si ratios in leaves and sap waters relative to source porewaters and calculated fractionation factors where $K_{Ge/Si} \ll 1$ for all species seem to imply strong preferential discrimination against germanium in plants at the catchment which is better explained by highly specific, active, plant-mediated transport mechanisms than by passive molecular diffusion processes or energetic differences between amorphous SiO_2 or GeO_2 (Sparks et al., 2010). However, relatively stable silicon concentrations in porewaters during the growing season (Table 3.4, Figures 3.7 and 3.8) and a strong positive correlation between transpiration rate and silicon concentration in leaves (Figure 3.11) seem to suggest a passive transport mechanism for silicon (and by inference, germanium). Further complicating the situation is whether these active or passive transport mechanisms are occurring through apoplastic or symplastic pathways. Indeed, the relative importance of active and passive transport processes in the transport of cations and uncharged molecules through apoplastic and symplastic pathways in individual species is unknown and requires future biochemical, genomic,

molecular biological, and physiological research on the topic.

Unfortunately, several questions remain unaddressed due to sampling limitations. Limited collection of streamwater samples prevented the use of geochemical hydrograph separations (Wels et al., 1991; Derry et al., 2006; Garvin, 2006; Kurtz et al., 2011) to delineate sources of solutes and uncharged molecules in streamwaters under variable discharge regimes. Specifically, during a precipitation event, elemental concentrations and strontium isotope and elemental ratios should be measured and plotted against stream discharge in hysteresis diagrams to document changes in streamwater source under varying levels of discharge (e.g. base flow versus shallow subsurface storm flow). Additionally, spatial patterns in soil and porewater chemistry can be more fully elucidated through the collection of planar and swale soils and soil porewaters in the northern quadrant and swale soils in the southern quadrant. Furthermore, leaves and sap waters from hemlock, hickory, and pine species should be collected to better understand differences in chemistry and differential uptake processes in plants at the catchment. Additionally, water-extractable silicon should be obtained from soils and analyzed to identify biogenic and pedogenic silicon inputs to soil porewaters. Moreover, reservoir components should be collected during both wet and dry seasons to reasonably assess temporal trends in chemistry at the catchment on an annual basis.

Biogeochemical models are oftentimes used to facilitate the understanding of elemental feedback processes within ecosystems. Sampled data can be extrapolated across longer time scales and broader spatial extents through biogeochemical models to enable discussion of larger scientific questions. Recently, the terrestrial biogeochemical cycle of calcium has been studied to address questions related to the susceptibility of ecosystems to acid deposition (Miller et al., 1993; Bailey et al., 1996; Capo et al., 1998; Pett-Ridge et al., 2009). The terrestrial

biogeochemical cycle of silicon has also been an ongoing topic in literature (Alexandre et al., 1997; Meunier et al., 1999; Carnelli et al., 2001; Lucas, 2001; Sommer et al., 2006; Street-Perrott et al., 2008; Cornelis et al., 2010) due to its role in mediating atmospheric carbon dioxide levels through weathering of silicate minerals. Unfortunately, due to sampling limitations, this study was unable to incorporate biogeochemical models quantifying calcium and silicon fluxes for various reservoirs at the SSHCZO. One reason is that reservoir components were collected at different times of the year (e.g. soils, streamwaters, and groundwaters during the fall; soil porewaters, leaves, and sapwaters during the summer) when conditions at the catchment vary considerably. Additionally, exclusive sampling of soil porewaters from the southern quadrant of the catchment, soils from the southern planar transect, and leaves and sap waters from three tree species proscribed the formulation of holistic models of biogeochemical processes at the catchment. Furthermore, lack of major element, isotope, and trace element data for litterfall, throughfall, and root, bark, and wood biomass at the catchment precluded attempts to adequately model calcium and silicon cycling at the watershed. Thus, attempts to develop steady state and time dependent biogeochemical models were hampered by numerous sampling limitations. In the future, a more coherent sampling methodology needs to be adopted where collaborators confer with all interested parties on achieving realistic research goals and expectations based on sampling, time, and budget limitations. To this end, where samples are taken in successive years, such samples should be taken in an identical manner both as to locations and from identical plants. In summary, several research opportunities are available to improve the understanding of biogeochemical processes involving calcium, strontium, silicon, and germanium at the SSHCZO. The recommendations listed above for potential projects address a small subset of possible questions and, no doubt, additional topics will arise from future investigations.

4. References

- Alexandre, A., Meunier, J., Colin, F., and Koud, J., 1997, Plant impact on the biogeochemical cycle of silicon and related weathering processes: *Geochimica et Cosmochimica Acta*, v. 61, p. 677-682.
- Bailey, S., Hornbeck, J., Driscoll, C., and Gaudette, H., 1996, Calcium inputs and transport in a base-poor forest system as interpreted by Sr isotopes: *Water Resources Research*, v. 32, p. 707-719.
- Brackhage, C., Schaller, J., Baucker, E., and Dudel, E., 2013, Silicon availability affects the stoichiometry and content of calcium and micro nutrients in the leaves of common reed: *Silicon*, v. 5, p. 199-204.
- Brantley, S., Holleran, M., Jin, L., and Bazilevskaya, E., 2013, Probing deep weathering in the Shale Hills Critical Zone Observatory, Pennsylvania (USA): the hypothesis of nested chemical reaction fronts in the subsurface: *Earth Surface Processes and Landforms*, v. 38, p. 1280-1298.
- Brooks, J., Barnard, H., Coulombe, R., and McDonnell, J., 2009, Ecohydrologic separation of water between trees and streams in a Mediterranean climate: *Nature Geoscience*, v. 3, p. 100-104.
- Capo, R., Stewart, B., and Chadwick, O., 1998, Strontium isotopes as tracers of ecosystem processes: theory and methods: *Geoderma*, v. 82, p. 197-225.
- Carnelli, A., Madella, M., and Theurillat, J., 2001, Biogenic silica production in selected alpine plant species and plant communities: *Annals of Botany*, v. 87, p. 425-434.
- Clarkson, D., 1984, Calcium transport between tissues and its distribution in the plant: *Plant, Cell and Environment*, v. 7, p. 449-456.
- Cornelis, J., Delvaux, B., Cardinal, D., Andre, L., Ranger, J., and Opfergelt, S., 2010, Tracing mechanisms controlling the release of dissolved silicon in forest soil solutions using Si isotopes and Ge/Si ratios: *Geochimica et Cosmochimica Acta*, v. 74, p. 3913-3924.
- Derry, L., Pett-Ridge, J., Kurtz, A., and Troester, J., 2006, Ge/Si and $^{87}\text{Sr}/^{86}\text{Sr}$ tracers of weathering reactions and hydrologic pathways in a tropical granitoid system: *Journal of Geochemical Exploration*, v. 88, p. 271-274.

Flueckinger, L., 1969, Report 176, Geology of a portion of the Allensville Quadrangle, Centre and Huntingdon Counties, Pennsylvania: Bureau of Topographic and Geologic Survey, Commonwealth of Pennsylvania State Planning Board: Harrisburg, PA.

Froelich, P., Blanc, V., Mortlock, R., Chillrud, S., Dustan, W., Udomkit, A., and Peng, T., 1992, River fluxes of dissolved silica to the ocean were higher during the glacial: Ge/Si in diatoms, rivers, and oceans: *Paleoceanography*, v. 7, p. 739-768.

Garvin, C., 2006, An exploratory study of the terrestrial biogeochemical silicon cycle at a forested watershed in northern Vermont: Master's Thesis, 128 p.

Graham, R., Daniels, R., and Buol, S., 1990, Soil-geomorphic relations on the Blue Ridge front: I. Regolith types and slope processes: *Soil Science Society of America Journal*, v. 54, p. 1362-1367.

Graham, C., and Lin, H., 2011, Controls and frequency of preferential flow occurrence: A 175-event analysis: *Vadose Zone Journal*, v. 10, p. 816-831.

Hess, J., Bender, M., and Schilling, J., 1986, Evolution of the ratio of strontium-87 to strontium-86 in seawater from Cretaceous to present: *Science*, v. 231, p. 979-984.

Jin L., Ravella, R., Ketchum, B., Bierman, P., Heaney, P., White, T., and Brantley, S., 2010, Mineral weathering and elemental transport during hillslope evolution at the Susquehanna/Shale Hills Critical Zone Observatory: *Geochimica et Cosmochimica Acta*, v. 74, p. 3669-3691.

Jin, L., Rother, G., Cole, D., Mildner, D., Duffy, C., and Brantley, S., 2011a, Characterization of deep weathering and nanoporosity development in shale – A neutron study: *American Mineralogist*, v. 96, p. 498-512.

Jin L., Andrews, D., Holmes, G., Lin, H., and Brantley, S., 2011b, Opening the “Black Box”: Water Chemistry Reveals Hydrological Controls on Weathering in the Susquehanna Shale Hills Critical Zone Observatory: *Vadose Zone Journal*, v. 10, p. 928-942.

Jin, L., Ogrinc, N., Yesavage, T., Hasenmueller, E., Ma, L., Sullivan, P., Kaye, J., Duffy, C., Brantley, S., 2014, The CO₂ consumption potential during gray shale weathering: Insights from the evolution of carbon isotopes in the Susquehanna Shale Hills critical zone observatory: *Geochimica et Cosmochimica Acta*, v. 142, p. 260-280.

Jin L., and Brantley S. , 2011, Soil chemistry and shale weathering on a hillslope influenced by convergent hydrologic flow regime at the Susquehanna/Shale Hills Critical Zone Observatory: *Applied Geochemistry*, v. 26, p. S51–S56.

Jones, L., and Handreck, K., 1965, Studies of silica in the oat plant. III. Uptake of silica from soils by plant: *Plant and Soil*, v. 23, p. 79-96.

Kurtz, A., Derry, L., and Chadwick, O., 2002, Germanium-silicon fractionation in the weathering environment: *Geochimica et Cosmochimica Acta*, v. 66, p. 1525-1537.

Kurtz, A., Lugolobi, F., and Salvucci, G., 2011, Germanium-silicon as a flow path tracer: Application to the Rio Icacos watershed: *Water Resources Research*, v. 47, p. 1-16.

Lin, H., 2006, Temporal stability of soil moisture spatial pattern and subsurface preferential flow pathways in the Shale Hills catchment: *Vadose Zone Journal*, v. 5, p. 317-340.

Lucas, Y., Luizao, F., Chauvel, A., Rouiller, J., and Nahon, D., 1993, The relation between biological activity of the rain forest and mineral composition of soils: *Science*, v. 260, p. 521-523.

Lynch, J., 1976, Effects of antecedent soil moisture on storm hydrographs: Dissertation, The Pennsylvania State University, 141 p.

Ma, J., and Takahashi, E., 1993, Interaction between calcium and silicon in water-cultured rice plants: *Plant and Soil*, v. 148, p. 107-113.

Ma, L., Chabaux, F., Pelt, E., Blaes, E., Jin, L., and Brantley, S., 2010, Regolith production rates calculated with uranium-series isotopes at Susquehanna/Shale Hills Critical Zone Observatory: *Earth and Planetary Science Letters*, v. 297, p. 211-225.

Marschner, H., 1995, *Mineral Nutrition of Higher Plants*, 2nd Edition: Academic Press, London.

Marschner, P., 2012, *Mineral Nutrition of Higher Plants*, 3rd Edition: Academic Press, London.

Meinzer, F., Woodruff, D., Eissenstat, D., Lin, H., Adams, T., and McCulloh, K., 2013, Above- and belowground controls on water use by trees of different wood types in an eastern US deciduous forest: *Tree Physiology*, v. 33, p. 345-356.

Meunier, J., Colin, F., and Alarcon, C., 1999, Biogenic silica storage in soils: *Geology*, v. 27, p. 835-838.

Miller, E., Blum, J., and Friedland, A., 1993, Determination of soil exchangeable cation loss and weathering rates using Sr isotopes: *Nature*, v. 362, p. 438-441.

Mortlock, R., and Froelich, P., 1987, Continental weathering of germanium: Ge/Si in the global river discharge: *Geochimica et Cosmochimica Acta*, v. 51, p. 2075-2082.

Murnane, R., and Stallard, R., 1990, Germanium and silicon in rivers of the Orinoco drainage basin: *Nature*, v. 344, p. 749-752.

Pett-Ridge, J., Derry, L., and Barrows, J., 2009, Ca/Sr and $^{87}\text{Sr}/^{86}\text{Sr}$ ratios as tracers of Ca and Sr cycling in the Rio Icacos watershed, Luquillo Mountains, Puerto Rico: *Chemical Geology*, v. 267, p. 32-45.

Pokrovski, G., and Schott, J., 1998, Experimental study of the complexation of silicon and germanium with aqueous organic species: implications for germanium and silicon transport and Ge/Si ratio in natural waters: *Geochimica et Cosmochimica Acta*, v. 62, p. 3413-3428.

Pokrovsky, O., Pokrovski, G., Schott, J., and Galy, A., 2006, Experimental study of germanium adsorption on goethite and germanium coprecipitation with iron hydroxide: X-ray absorption fine structure and macroscopic characterization: *Geochimica et Cosmochimica Acta*, v. 70, p. 3325-3341.

Scribner, A., Kurtz, A., and Chadwick, O., 2006, Germanium sequestration by soil: Targeting the roles of secondary clays and Fe-oxyhydroxides: *Earth and Planetary Science Letters*, v. 243, p. 760-770.

Sommer, M., Kaczorek, D., Kuzyakov, Y., and Breuer, J., 2006, Silicon Pools and fluxes in soils and landscapes – a review: *Journal of Plant Nutrition and Soil Science*, v. 169, p. 310-329.

Sparks, J., Chandra, S., Derry, L., Parthasarathy, M., Daugherty, C., and Griffin, R., 2010, Subcellular localization of silicon and germanium in grass root and leaf tissues by SIMS: evidence for differential and active transport: *Biogeochemistry*, v. 104, p. 237-249.

Street-Perrott, F., and Barker, P., 2008, Biogenic silica: a neglected component of the coupled global continental biogeochemical cycles of carbon and silicon: *Earth Surface Processes and Landforms*, v. 33, p. 1436-1457.

Wels, C., Cornett, R., and Lazerte, B., 1991, Hydrograph separation: A comparison of geochemical and isotopic tracers: *Journal of Hydrology*, v. 122, p. 253-274.

White, P., 2001, The pathways of calcium movement to the xylem: *Journal of Experimental Botany*, v. 52, p. 891-899.

White, P., Whitting, S., Baker, A., and Broadley, M., 2002, Does zinc move apoplastically to the xylem in roots of *Thlaspi caerulescens*?: *New Phytologist*, v. 153, p. 199-211.

White, P., and Broadley, M., 2003, Calcium in plants: *Annals of Botany*, v. 92, p. 487-511.

Whitney, P., and Hurley, P., 1964, The problem of inherited radiogenic strontium in sedimentary age determinations: *Geochimica et Cosmochimica Acta*, v. 28, p. 425-436.

APPENDIX

SUPPLEMENTARY DATA TABLES

Table A.1 Elemental concentrations and Ca/Sr ratios for soil porewaters sampled at the catchment

Sampling Date	Sample ID	Depth (cm)	[Sr] ($\mu\text{M/L}$)	[Ca] ($\mu\text{M/L}$)	[Si] ($\mu\text{M/L}$)	Ca/Sr (molar)
5/17/2013	SPVF	40	0.21	74	108	354
5/17/2013	SPVF	60	0.25	78	113	317
5/17/2013	SPVF	30	0.25	89	209	356
5/17/2013	SPVF	30	0.26	92	210	359
5/17/2013	SPVF	60	0.24	78	111	318
5/17/2013	SPVF	30	0.26	92	211	361
5/17/2013	SPVF	40	0.20	70	103	346
5/17/2013	SPVF	40	0.20	70	102	347
5/17/2013	SPMS	40	0.14	50	170	363
5/17/2013	SPMS	50	0.16	62	124	380
5/17/2013	SSMS	100	0.23	62	103	274
5/17/2013	SSMS	40	0.18	38	82	212
5/17/2013	SPMS	50	0.17	64	126	383
5/17/2013	SPVF	20	0.16	58	111	371
5/17/2013	SPVF	20	0.16	58	111	359
5/17/2013	SSMS	100	0.23	64	104	281
5/17/2013	SPVF	60	0.25	81	112	328
5/17/2013	SPMS	40	0.14	52	168	377
5/17/2013	SPMS	50	0.17	63	126	381
5/17/2013	SPVF	20	0.16	63	111	400
5/17/2013	SSMS	40	0.18	44	82	247
5/17/2013	SSMS	40	0.18	41	84	229
5/17/2013	SSMS	40	0.14	52	171	373
5/24/2013	SSMS	100	0.23	61	112	268
5/24/2013	SSMS	160	0.25	75	106	297
5/24/2013	SSMS	40	0.18	38	99	208
5/24/2013	SPRT	20	0.18	58	112	329
5/24/2013	SSMS	120	0.23	60	102	257
5/24/2013	SSRT	10	0.10	20	107	210
5/24/2013	SSRT	30	0.12	30	82	244
5/24/2013	SSRT	10	0.09	19	104	202
5/24/2013	SPRT	20	0.16	48	107	298

5/24/2013	SSVF	20	0.16	92	122	563
5/24/2013	SSVF	30	0.14	36	138	252
5/24/2013	SSMS	140	0.23	61	104	263
5/24/2013	SPRT	30	0.19	66	124	344
5/24/2013	SSMS	120	0.24	64	111	265
5/24/2013	SPMS	10	0.06	16	147	261
5/24/2013	SSVF	30	0.15	40	166	269
5/24/2013	SSMS	80	0.20	50	112	251
5/30/2013	SSMS	140	0.23	62	111	264
5/30/2013	SSVF	40	0.23	57	164	247
5/30/2013	SSRT	20	0.07	16	146	219
5/30/2013	SSMS	120	0.24	70	110	289
5/30/2013	SSMS	160	0.23	62	105	266
5/30/2013	SSVF	20	0.13	48	126	358
5/30/2013	SSMS	100	0.22	58	120	263
5/30/2013	SSVF	80	0.08	14	163	171
6/5/2013	SSMS	120	0.23	62	112	270
6/5/2013	SSMS	160	0.24	65	108	270
6/5/2013	SSMS	100	0.23	60	116	268
6/5/2013	SSMS	140	0.23	63	112	277
6/11/2013	SSMS	120	0.23	61	109	271
6/11/2013	SSMS	40	0.17	35	108	203
6/11/2013	SSMS	140	0.24	65	111	269
6/11/2013	SPRT	20	0.13	40	136	311
6/11/2013	SSMS	100	0.23	60	118	265
6/11/2013	SSMS	160	0.23	62	107	270
6/11/2013	SSMS	40	0.17	36	113	215
6/12/2013	SSRT	20	0.08	13	149	155
6/12/2013	SPRT	20	0.15	48	111	324
6/12/2013	SSMS	160	0.23	65	108	278
6/12/2013	SSVF	10	0.12	63	230	534
6/12/2013	SSVF	40	0.24	65	177	266
6/12/2013	SSMS	20	0.10	21	111	219
6/12/2013	SSMS	10	0.07	23	148	324
6/12/2013	SPRT	30	0.12	41	89	342
6/12/2013	SSMS	80	0.21	52	113	249
6/12/2013	SSMS	60	0.20	48	111	240
6/12/2013	SSMS	140	0.24	64	116	266
6/12/2013	SSVF	20	0.15	54	129	355
6/12/2013	SSMS	100	0.21	57	118	264
6/12/2013	SSMS	80	0.21	51	120	237

6/12/2013	SPMS	50	0.14	48	121	341
6/12/2013	SSMS	120	0.22	60	113	273
6/12/2013	SPMS	10	0.06	15	168	242
6/12/2013	SSRT	10	0.09	20	133	224
6/12/2013	SSVF	10	0.08	37	148	456
6/12/2013	SSMS	40	0.17	33	91	198
6/12/2013	SSVF	60	0.11	28	147	251
6/12/2013	SPMS	60	0.11	40	194	357
6/21/2013	SSVF	40	0.21	47	176	222
6/21/2013	SPMS	40	0.13	40	194	319
6/21/2013	SPMS	50	0.13	45	107	346
6/21/2013	SSRT	10	0.07	13	126	191
6/21/2013	SSVF	50	0.20	80	152	408
6/21/2013	SPVF	40	0.12	41	135	335
6/21/2013	SSVF	80	0.07	11	154	162
6/21/2013	SSMS	160	0.22	52	100	239
6/21/2013	SSMS	40	0.16	58	105	375
6/21/2013	SPRT	20	0.10	28	112	270
6/28/2013	SSVF	80	0.07	13	127	173
6/28/2013	SSVF	90	0.13	30	239	237
6/28/2013	SSVF	60	0.12	27	106	232
6/28/2013	SSVF	70	0.10	16	96	168
6/28/2013	SPVF	50	0.12	26	122	227
6/28/2013	SPVF	40	0.16	49	93	303
6/28/2013	SPVF	60	0.20	58	93	287
6/28/2013	SPVF	30	0.14	44	102	307
6/28/2013	SPVF	20	0.12	36	81	302
6/28/2013	SPMS	10	0.05	11	106	238
6/28/2013	SPMS	50	0.15	48	116	321
6/28/2013	SPMS	40	0.13	39	183	313
6/28/2013	SPRT	30	0.12	35	71	291
6/28/2013	SPRT	20	0.13	35	104	270
6/28/2013	SSRT	20	0.04	5	64	123
6/28/2013	SSRT	10	0.06	10	64	174
6/28/2013	SSMS	60	0.17	35	89	204
6/28/2013	SSMS	80	0.17	36	93	213
6/28/2013	SSVF	40	0.17	36	109	208
6/28/2013	SSVF	50	0.15	37	114	249
6/28/2013	SSVF	10	0.06	24	158	399
6/28/2013	SSVF	20	0.10	34	100	333
6/28/2013	SSMS	160	0.18	42	94	235

6/28/2013	SSMS	20	0.08	18	111	241
6/28/2013	SSMS	40	0.13	24	72	184
6/28/2013	SSMS	120	0.19	44	93	228
6/28/2013	SSMS	100	0.19	46	102	236
6/28/2013	SSRT	10	0.08	23	80	278
7/12/2013	SSVF	10	0.10	43	195	441
7/12/2013	SSVF	50	0.15	36	181	238
7/12/2013	SSVF	20	0.15	45	119	302
7/12/2013	SSVF	30	0.12	26	152	222
7/12/2013	SPVF	30	0.20	65	236	319
7/12/2013	SPVF	20	0.17	52	117	311
7/12/2013	SPMS	40	0.15	48	251	312
7/12/2013	SPMS	10	0.05	11	179	221
7/12/2013	SPRT	10	0.10	27	131	261
7/12/2013	SPRT	20	0.13	36	113	272
7/12/2013	SPRT	30	0.12	40	147	322
7/12/2013	SSRT	10	0.07	12	117	170
7/12/2013	SSRT	30	0.10	22	79	218
7/12/2013	SSMS	20	0.09	23	110	266
7/12/2013	SSVF	10	0.06	23	127	403
7/12/2013	SSVF	30	0.13	32	152	249
7/12/2013	SSVF	60	0.12	34	150	281
7/12/2013	SSVF	40	0.22	45	191	206
7/12/2013	SPVF	40	0.19	57	128	305
7/12/2013	SSMS	120	0.20	48	115	237
7/12/2013	SSMS	160	0.20	48	105	234
7/12/2013	SSMS	60	0.18	37	114	209
7/12/2013	SSMS	40	0.14	26	105	181
7/12/2013	SSMS	140	0.21	50	114	238
7/12/2013	SSMS	100	0.20	47	127	236
7/12/2013	SSRT	20	0.07	8	134	113
7/18/2013	SPVF	20	0.13	38	131	301
7/18/2013	SPMS	50	0.13	42	130	319
7/18/2013	SPMS	40	0.16	51	294	321
7/18/2013	SPRT	20	0.10	27	145	267
7/18/2013	SSVF	20	0.14	38	132	279
7/18/2013	SPVF	40	0.16	55	144	347
7/18/2013	SSMS	160	0.20	48	108	234
7/18/2013	SSMS	140	0.20	49	123	240
7/18/2013	SSVF	50	0.15	49	197	321
7/18/2013	SSMS	120	0.20	49	121	246

7/18/2013	SSMS	40	0.12	27	118	230
7/18/2013	SSMS	100	0.18	44	133	241
7/18/2013	SSMS	20	0.06	13	118	202
7/18/2013	SSMS	140	0.15	37	81	240

Table A.2 Elemental concentrations and Ca/Sr ratios for 2013 leaves sampled at the catchment

Sample Date	Sample ID	Species Code	[Ca] (mg/g dry leaf)	[Sr] (mg/g dry leaf)	[Si] (mg/g dry leaf)	Ca/Sr (molar)
6/11/2013	NW 121	QUPR	13.96	0.02	0.54	1611
6/12/2013	SW 1080	QUPR	9.02	0.01	0.30	1267
6/12/2013	SW 1077	QURU	9.04	0.01	0.07	1284
6/12/2013	SW 1073	ACSA	9.96	0.03	1.56	681
6/12/2013	SE 1266	QUPR	4.82	0.01	0.30	1234
	SE					
6/12/2013	DOWNHILL	ACSA	6.26	0.02	1.04	611
6/12/2013	SE UPHILL	ACSA	6.54	0.02	1.47	579
6/13/2013	NE 620	ACSA	10.07	0.04	1.45	528
6/13/2013	NE 622	QUPR	10.96	0.02	0.57	1082
6/13/2013	NE 613	QURU	5.69	0.01	0.07	1021
7/15/2013	NW 121	QUPR	15.87	0.02	0.98	1489
7/15/2013	NW 110	QURU	8.39	0.01	0.10	1414
7/15/2013	NW 102	QURU	11.60	0.02	0.12	1532
7/16/2013	SE 1329	QUPR	11.02	0.02	0.62	1256
7/16/2013	NW 137	ACSA	10.37	0.03	1.56	728
7/16/2013	SW 1164	ACSA	13.29	0.05	1.89	575
7/16/2013	SE 1271	QURU	6.86	0.01	0.13	1427
7/16/2013	SW 1073	ACSA	16.28	0.05	1.78	671
7/16/2013	SW 1077	QURU	9.71	0.01	0.14	1297
7/16/2013	SW 1074	QURU	10.21	0.01	0.14	1458
7/16/2013	SW 1170	QUPR	9.63	0.02	0.80	1181
7/16/2013	SE 1331	QURU	9.44	0.02	0.12	1007
7/16/2013	NW UPHILL	ACSA	13.42	0.04	1.62	647
7/16/2013	SW 1080	QUPR	11.03	0.02	0.71	1381
7/17/2013	NE 636	QURU	14.63	0.03	0.17	1004
7/17/2013	SE 1266	QUPR	9.21	0.01	0.80	1311
7/17/2013	NE 620	ACSA	10.07	0.04	1.55	530
7/17/2013	NE 613	QURU	12.86	0.02	0.13	1074
	SE					
7/17/2013	DOWNHILL	ACSA	5.92	0.02	1.43	527
7/17/2013	NE NO TAG	ACSA	9.34	0.03	2.18	565

7/17/2013	NE 622	QUPR	11.34	0.02	1.08	988
7/17/2013	SE UPHILL	ACSA	10.30	0.04	1.77	488
8/12/2013	SE 1331	QURU	8.36	0.01	0.19	1339
	SE					
8/12/2013	DOWNHILL	ACSA	6.88	0.03	1.56	536
8/12/2013	SE 1329	QUPR	7.50	0.02	1.36	1089
8/12/2013	NW 137	ACSA	9.83	0.03	1.85	756
8/12/2013	SE UPHILL	ACSA	9.92	0.04	1.65	544
8/12/2013	NW 102	QURU	11.00	0.01	0.17	1667
8/12/2013	NE 622	QUPR	9.85	0.02	1.25	1168
8/12/2013	NE 637	QUPR	10.11	0.02	1.05	1203
8/12/2013	NE 636	QURU	13.65	0.03	0.19	1037
8/12/2013	NW UPHILL	ACSA	14.50	0.05	1.29	642
8/12/2013	NW 121		19.88	0.03	1.12	1403
8/12/2013	SE 1329	QUPR	7.65	0.02	1.10	991
8/13/2013	NE 613	QURU	10.29	0.02	0.21	1187
8/13/2013	SW 1074	QURU	10.35	0.01	0.13	1531
8/13/2013	SE 1266	QUPR	8.87	0.02	1.14	1221
8/13/2013	SW 1077	QURU	7.86	0.01	0.19	1162
8/13/2013	SE 1271	QURU	7.85	0.01	0.24	1548
8/13/2013	NW 110	QURU	9.98	0.01	0.20	1636
8/13/2013	SW 1080	QUPR	7.96	0.01	0.87	1545
8/13/2013	SW 1170	QUPR	10.82	0.02	1.32	1272
8/13/2013	SW 1073	ACSA	14.42	0.05	1.68	583
8/13/2013	SW 1164	ACSA	14.19	0.05	1.61	570
9/27/2013	SE 1331	QURU	8.23	0.02	0.26	1036
9/27/2013	SW 1080	QUPR	10.27	0.02	1.25	1301
9/27/2013	NE 622	QUPR	11.46	0.02	1.28	1091
9/27/2013	NW 102	QURU	8.14	0.01	0.31	1799
9/27/2013	SW 1074	QURU	9.21	0.01	0.15	1585
9/27/2013	NE 637	QUPR	10.04	0.02	1.19	1361
9/27/2013	NW 110	QURU	10.16	0.01	0.55	1551
9/27/2013	NE 613	QURU	10.33	0.01	0.41	1786
9/27/2013	SE 1266	QUPR	11.61	0.02	1.23	1348
	NW					
9/27/2013	DOWNHILL	ACSA	11.56	0.03	1.84	741
9/27/2013	NE 636	QURU	15.63	0.03	0.43	971
9/27/2013	NW UPHILL	ACSA	17.58	0.06	1.15	623
9/27/2013	SW 1077	QURU	13.82	0.02	0.27	1325
9/27/2013	SE 1271	QURU	14.23	0.03	0.33	1081
9/27/2013	NE	ACSA	20.88	0.08	1.74	555

DOWNHILL

9/27/2013	SW 1073	ACSA	19.39	0.06	1.55	606
9/27/2013	SW 1170	QUPR	13.76	0.02	1.09	1198
9/27/2013	NW 121	QUPR	20.05	0.03	0.79	1308
9/27/2013	SE 1329	QUPR	13.74	0.02	1.15	1303

Table A.3 Elemental concentrations and Ca/Sr ratios for 2011 leaves sampled at the catchment where $^{87}\text{Sr}/^{86}\text{Sr}$ ratios were not measured.

Sample Date	Sample ID	Species Code	Sr (mg/g dry leaf)	Ca (mg/g dry leaf)	Ca/Sr
6/9/2011	AS 437	ACSA	0.06	16.76	594
6/9/2011	QP 230	QUPR	0.02	8.91	972
6/9/2011	QP 437	QUPR	0.05	7.07	300
6/14/2011	AS 2061	ACSA	0.03	4.93	300
6/14/2011	QP 358	QUPR	0.03	7.82	614
6/16/2011	AS 352	ACSA	0.06	6.44	204
6/16/2011	QP 351	QUPR	0.03	2.67	200
6/16/2011	QP 351	QUPR	0.02	5.04	614
6/21/2011	QP 333	QUPR	0.01	7.25	1066
6/21/2011	QP 340	QUPR	0.01	4.93	964
7/6/2011	AS 2059	ACSA	0.07	8.74	236
7/6/2011	AS 2066	ACSA	0.04	12.47	640
7/6/2011	QP 2060	QUPR	0.04	11.59	626
7/6/2011	QP 393	QUPR	0.01	7.66	1126
7/6/2011	QP 394	QUPR	0.02	7.17	806
7/6/2011	QP 396	QUPR	0.01	9.99	1328
7/6/2011	QP 396	QUPR	0.02	7.96	958
7/6/2011	QP 437	QUPR	0.02	7.36	710
7/7/2011	AS 332	ACSA	0.01	4.89	928
7/7/2011	QP 347	QUPR	0.02	15.31	1242
7/7/2011	QP 351	QUPR	0.04	6.25	332
7/12/2011	AS 2065	ACSA	0.09	9.96	228
7/12/2011	QP 330	QUPR	0.01	9.93	1598
7/14/2011	AS 387	ACSA	0.08	9.39	254
7/14/2011	QP 1219	QUPR	0.01	3.45	1002
7/19/2011	QP 230	QUPR	0.03	6.42	434
8/5/2011	QP 330	QUPR	0.01	7.21	990
8/5/2011	QP 394	QUPR	0.01	7.08	1294
8/30/2011	QP 2060	QUPR	0.02	3.64	336
8/30/2011	QP 230	QUPR	0.03	8.52	536
8/30/2011	QP 351	QUPR	0.02	9.61	1054

8/30/2011	QP 358	QUPR	0.04	8.11	410
9/13/2011	AS 2066	ACSA	0.07	13.32	378
9/13/2011	QP 332	QUPR	0.01	4.05	580
9/13/2011	QP 394	QUPR	0.03	5.31	368
9/13/2011	QP 396	QUPR	0.03	9.50	756

Table A.4 Elemental concentrations and Ca/Sr ratios for sap waters sampled at the catchment

Sample Date	Sample ID	Species Code	[Sr] ($\mu\text{M/L}$)	[Ca] ($\mu\text{M/L}$)	[Si] ($\mu\text{M/L}$)	Ca/Sr (molar)
7/16/2013	NE 620	ACSA	1.42	380	510	267
7/16/2013	NE NOTAG	ACSA	1.25	363	701	291
7/16/2013	NW 137	ACSA	1.59	325	676	205
7/16/2013	NW Uphill	ACSA	1.61	428	621	266
7/16/2013	NW Uphill	ACSA	1.58	452	612	287
7/16/2013	NW 121	QUPR	0.92	479	563	521
7/16/2013	SW 1080	QUPR	2.03	618	530	305
7/16/2013	SW 1170	QUPR	1.32	480	493	363
7/16/2013	NW 102	QURU	1.11	589	420	530
7/16/2013	NW 110	QURU	1.54	1555	559	1010
7/16/2013	SE 1271	QURU	1.51	945	433	625
7/16/2013	SE 1331	QURU	1.98	458	541	231
7/16/2013	SE UPHILL	ACSA	1.90	409	767	215
7/16/2013	SW 1074	QURU	1.76	468	321	266
7/16/2013	SW 1077	QURU	2.63	714	546	271
7/17/2013	SE Downhill	ACSA	1.21	389	626	321
7/17/2013	SW 1073	ACSA	2.19	507	665	231
7/17/2013	NE 622	QUPR	1.35	310	533	229
7/17/2013	NE 637	QUPR	1.21	612	624	504
7/17/2013	SE 1266	QUPR	2.41	1560	647	648
7/17/2013	NE 613	QURU	1.76	447	424	254
7/17/2013	NE 636	QURU	2.43	603	455	248
8/12/2013	NW 137	ACSA	2.25	985	567	438
8/12/2013	SE Uphill	ACSA	4.23	801	1193	189
8/12/2013	NE 622	QUPR	1.63	639	637	392
8/12/2013	NE 637	QUPR	2.01	561	773	280
8/12/2013	NW 121	QUPR	1.93	1437	611	747
8/12/2013	SW 1170	QUPR	1.65	355	624	215
8/12/2013	NE 613	QURU	3.82	838	641	219
8/12/2013	NE 636	QURU	2.23	685	605	308
8/12/2013	NW 102	QURU	1.45	1363	490	941

8/12/2013	SE 1271	QURU	1.13	280	595	248
8/12/2013	SE 1331	QURU	2.68	1523	548	568
8/13/2013	SE 1266	QUPR	2.28	1620	896	710
8/13/2013	SW 1080	QUPR	1.73	667	639	386
8/13/2013	NW 110	QURU	2.54	2166	497	854
8/13/2013	SW 1074	QURU	2.19	1425	405	651
9/27/2013	SW 1074	QURU	2.37	612	455	259
9/27/2013	SW 1164	ACSA	0.31	190	224	609
9/27/2013	NE 622	QUPR	0.88	448	446	508
9/27/2013	NE 637	QUPR	2.40	1632	680	679
9/27/2013	NW 121	QUPR	1.38	527	705	382
9/27/2013	SE 1266	QUPR	2.87	897	792	312
9/27/2013	SE 1329	QUPR	3.94	1009	816	256
9/27/2013	SW 1080	QUPR	5.63	2039	489	362
9/27/2013	SW 1170	QUPR	1.82	527	649	290
9/27/2013	NE 613	QURU	2.89	671	546	232
9/27/2013	NE 636	QURU	4.54	1006	407	221
9/27/2013	NW 102	QURU	1.04	271	504	262
9/27/2013	NW 110	QURU	3.22	896	733	278
9/27/2013	SE 1271	QURU	1.68	513	494	305
9/27/2013	SE 1331	QURU	3.31	1209	548	365
	NE					
9/28/2013	DOWNHILL	ACSA	0.48	255	395	533
9/28/2013	NE UPHILL	ACSA	0.66	400	414	607
	NW					
9/28/2013	DOWNHILL	ACSA	3.65	2559	416	702
9/28/2013	NW UPHILL	ACSA	0.66	400	221	607
9/28/2013	SE DOWNHILL	ACSA	0.26	116	326	448
9/28/2013	SW 1073	ACSA	1.17	555	481	476
